

Electrochemistry of immobilized hemes and heme proteins

Citation for published version (APA):

Groot, de, M. T. (2007). *Electrochemistry of immobilized hemes and heme proteins*. [Phd Thesis 1 (Research TU/e / Graduation TU/e), Chemical Engineering and Chemistry]. Technische Universiteit Eindhoven.
<https://doi.org/10.6100/IR626249>

DOI:

[10.6100/IR626249](https://doi.org/10.6100/IR626249)

Document status and date:

Published: 01/01/2007

Document Version:

Publisher's PDF, also known as Version of Record (includes final page, issue and volume numbers)

Please check the document version of this publication:

- A submitted manuscript is the version of the article upon submission and before peer-review. There can be important differences between the submitted version and the official published version of record. People interested in the research are advised to contact the author for the final version of the publication, or visit the DOI to the publisher's website.
- The final author version and the galley proof are versions of the publication after peer review.
- The final published version features the final layout of the paper including the volume, issue and page numbers.

[Link to publication](#)

General rights

Copyright and moral rights for the publications made accessible in the public portal are retained by the authors and/or other copyright owners and it is a condition of accessing publications that users recognise and abide by the legal requirements associated with these rights.

- Users may download and print one copy of any publication from the public portal for the purpose of private study or research.
- You may not further distribute the material or use it for any profit-making activity or commercial gain
- You may freely distribute the URL identifying the publication in the public portal.

If the publication is distributed under the terms of Article 25fa of the Dutch Copyright Act, indicated by the "Taverne" license above, please follow below link for the End User Agreement:

www.tue.nl/taverne

Take down policy

If you believe that this document breaches copyright please contact us at:

openaccess@tue.nl

providing details and we will investigate your claim.

Electrochemistry of Immobilized Hemes and Heme Proteins

PROEFSCHRIFT

ter verkrijging van de graad van doctor aan de
Technische Universiteit Eindhoven, op gezag van de
Rector Magnificus, prof.dr.ir. C.J. van Duijn, voor een
commissie aangewezen door het College voor
Promoties in het openbaar te verdedigen
op donderdag 14 juni 2007 om 16.00 uur

door

Matheus Theodorus de Groot

geboren te Deurne

Dit proefschrift is goedgekeurd door de promotoren:

prof.dr. M.T.M. Koper
en
prof.dr. R.A. van Santen

Copromotor:
dr. M. Merkx

A catalogue record is available from the Library Eindhoven University of Technology

ISBN: 978-90-386-0985-0

Copyright © 2007 by Matheus T. de Groot

The work described in this thesis has been carried out at the Schuit Institute of Catalysis within the Laboratory of Inorganic Chemistry and Catalysis, Eindhoven University of Technology and the Leiden Institute of Chemistry, Leiden University, The Netherlands. Financial support has been supplied by the National Research School Combination Catalysis (NRSC-C).

Design cover: Thijs de Groot and Paul Verspaget
Printed at the Universiteitsdrukkerij, Eindhoven University of Technology

*Life is not measured by the number of breaths you take,
but by the number of moments that take your breath away.*

Contents

Chapter 1	Introduction	1
Chapter 2	Electrochemical reduction of NO by hemin adsorbed at pyrolytic graphite	11
Chapter 3	Heme release in myoglobin-DDAB films and its role in electrochemical NO reduction	33
	A. Heme release in myoglobin-DDAB films and its role in electrochemical NO reduction	35
	B. Additional evidence for heme release in myoglobin-DDAB films on pyrolytic graphite	61
Chapter 4	Heme release and adsorption in layer-by-layer assemblies of polystyrenesulfonate and myoglobin on pyrolytic graphite	73
Chapter 5	Electron transfer and ligand binding to cytochrome <i>c'</i> immobilized on self-assembled monolayers	85
Chapter 6	Reorganization of immobilized horse and yeast cytochrome <i>c</i> induced by pH changes or nitric oxide binding	109
Chapter 7	Redox transitions of chromium, manganese, iron, cobalt and nickel protoporphyrins in aqueous solution	131
Chapter 8	Conclusions and future prospects	161
Summary		165
Samenvatting		168
List of publications		170
Curriculum vitae		171
Dankwoord		172

Chapter 1

Introduction

1.1 The search for better catalysts

Catalysts are of great value to mankind, since they enable reactions that would otherwise not occur or would occur at a very slow rate. The best-known example of a catalyst is the catalytic converter located in the exhaust of a car. It converts toxic gases such as carbon monoxide (CO), nitric oxide (NO) and nitrogen dioxide (NO₂), which are formed in the car engine, into the relatively harmless gases nitrogen (N₂) and carbon dioxide (CO₂). In this way the catalytic converter contributes to the improvement of the air quality in urban areas, which in turn has a positive influence on public health. The catalytic converter consists of a support with small metal particles, on which the reaction occurs in three steps (Figure 1.1). Firstly, the toxic gas molecules are adsorbed on the metal particles, next the reaction occurs, and finally the molecules are desorbed from the particles. The metal particles play an important role in the reaction, but they are not consumed. Therefore, the metal particles can in principle be used to convert an infinite number of toxic molecules and do not have to be replaced over the lifetime of a car. Without the metal particles the reaction would either not occur or occur at a very slow rate. This is the essence of every catalyst, which is defined as a substance that increases the rate of a reaction without being consumed. Although less known to the general public, catalysts are being used in many other processes. These include oil refinery, production of fertilizers, production of plastics and the production of drugs.

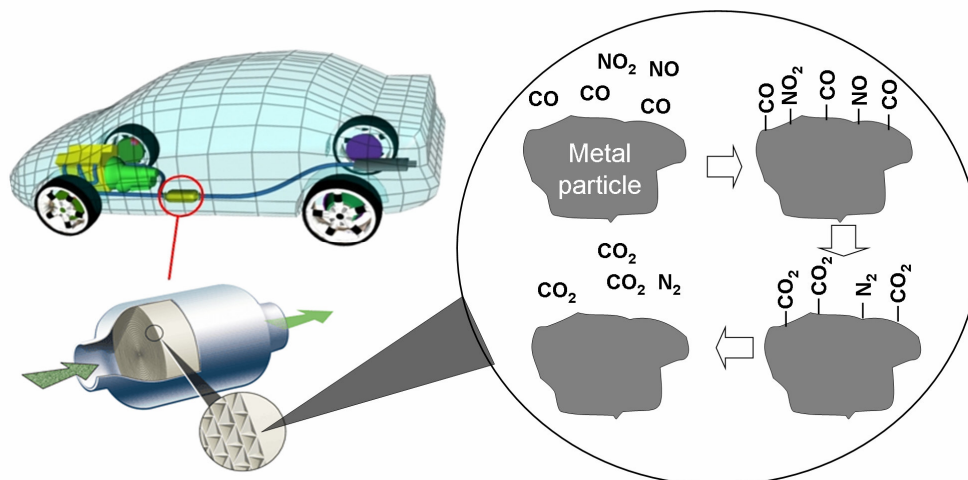


Figure 1.1 *The catalytic converter in a car. The figure depicts its location (top left), its macroscopic shape (bottom left) and a schematic representation of the reactions that occur on the small metal particles of the catalytic converter (right).*

Catalysis is big business, as reflected in the fact that the global catalyst market is worth \$ 210 billion annually.¹ Finding the right catalyst for an industrial process can determine whether such a process is economically feasible. Therefore, there is a continuous search for better and cheaper catalysts to improve the competitiveness of chemical processes. When considering the use of a catalyst for a particular reaction, one has to take into account the following important properties:

- **Activity.** This corresponds to the rate of the reaction that occurs on the catalyst. Ideally, a catalyst should be very active, which means that only a small amount of catalyst is needed to convert many molecules in a relatively short time.
- **Selectivity.** The selectivity of a catalyst indicates what products are formed in the reaction. In many chemical reactions more than one product can be formed and normally only one of the products is desired. Selectivity is of particular importance in the drug industry, where one reaction product might be a good drug and another product might be toxic.
- **Stability.** This relates to the lifetime of a catalyst. Ideally, a catalyst should be able to catalyze an endless number of reactions, but in practice the catalyst becomes inactive after a certain time. The lifetime of a catalyst depends on its specific properties, but also on the temperature and pressure of the reaction.
- **Ease of separation.** This corresponds to the ease of separation of the catalyst from the final reaction products. Catalysts that are dissolved in solutions are more difficult to separate compared to catalysts immobilized on a support, such as the catalyst used in a car.
- **Cost.** Many industrial catalysts are made of relatively expensive noble metals, such as platinum and palladium. These metals generally determine the overall cost price of a catalyst. Replacing these metals by cheaper materials with similar catalytic properties, can improve the economic competitiveness of a process.

1.2 Nature's catalysts

Catalysts also play an important role in many natural processes. These natural catalysts are called enzymes and are found in every living cell. Enzymes catalyze a wide variety of reactions that enable vital biological processes such as respiration, processing of food, building of organs and photosynthesis. Most enzymes are proteins, which are complex organic molecules made of amino acids. The catalytic reaction occurs at a particular place in the enzyme, the so-called active site. At this place the reacting molecules interact with the enzyme. As an example the enzyme cytochrome *c* oxidase is depicted in Figure 1.2. This enzyme catalyzes the reaction of oxygen to water and is part of the respiration process. Apart from the enzyme's amino acids, the active site of cytochrome *c* oxidase has incorporated iron and copper atoms, which play an important role in the reaction. Therefore cytochrome *c* oxidase is a so-called metalloenzyme.

Similar to the industrial catalysts enzymes increase the rate of a reaction without being consumed. However, compared to industrial catalysts enzymes show very high activity and selectivity, meaning that they are able to make the desired product at a very high rate without producing any byproducts. This is the result of millions of years of evolution. On the other hand, most enzymes are less stable than industrial catalysts. As a result of this they stop catalyzing the reaction after a certain amount of time, which is called deactivation. The lifetime of the enzyme depends on the conditions under which they work. In nature deactivated enzymes are automatically replaced by new enzymes.

The high activity and selectivity of enzymes has always encouraged mankind to use them as catalysts in industrial processes. An ancient example of such a biocatalytic process is the brewing of beer, in which the conversion of sugar to alcohol is catalyzed by yeast. Yeast is a microorganism and the enzymes in this microorganism catalyze the reaction. Nevertheless, the use of enzymes in industrial processes has been rather limited until now. They are used mainly in applications where selectivity is of the utmost importance such as the production of drugs. The main reasons for their limited use are their low stability and the costs involved in separating them from the reaction products. Therefore they are generally less economical than manmade catalysts.

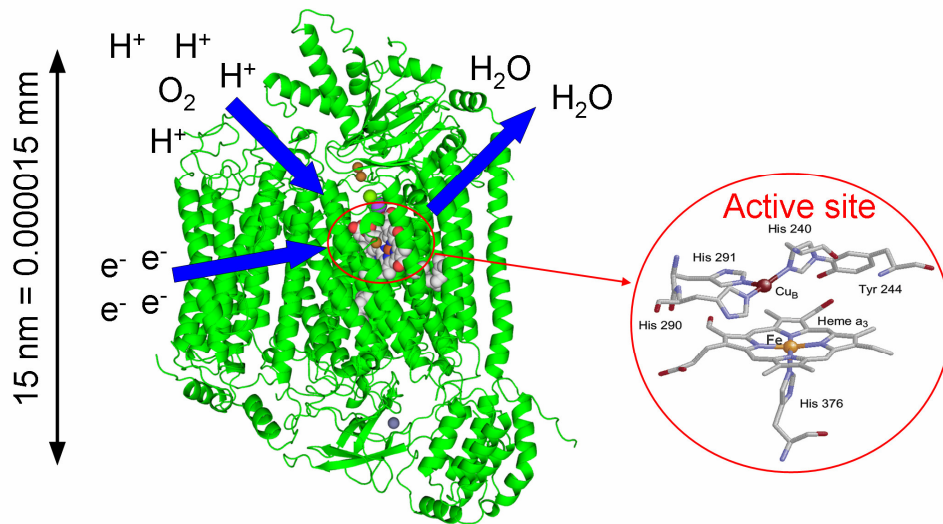


Figure 1.2 Cartoon representation of the enzyme cytochrome *c* oxidase and its active site. This enzyme catalyzes the reduction of oxygen to water and is part of the respiration cycle.

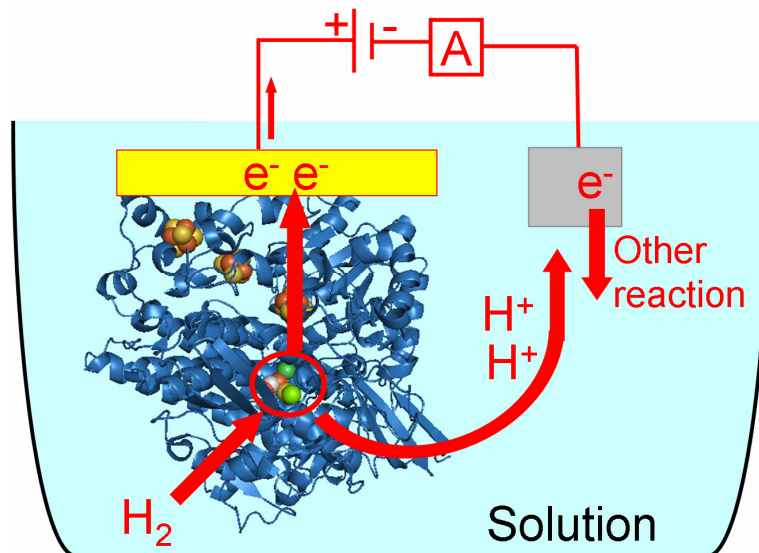


Figure 1.3 Schematic representation of an enzyme immobilized on a conducting support with a connected external circuit. The active site of the enzyme is indicated by a red circle. The external circuit connects the enzymatic reaction to another reaction that consumes the electrons. The depicted enzyme is a hydrogenase, which catalyzes the reaction of hydrogen to protons. In the external circuit a voltage source, which can be used to switch the reaction on and off, and a current measurement, which can be used as a detection method in a biosensor, have been incorporated.

1.3 Immobilization of enzymes

One possibility to tackle the disadvantages of using enzymes in industrial processes is attachment of the enzymes to a support (Figure 1.3). This so-called immobilization enables an easy separation of the products from the catalyst, since the enzyme is not in solution. Once the enzyme has been deactivated, replacement of the catalyst can easily be achieved by replacing the obsolete support (e.g. a grid) with a new support loaded with active enzymes. In case the catalyzed reaction is a redox reaction, immobilization on a conducting support has an additional advantage. Redox reactions are reactions that involve a number of electrons. Examples are the reduction of oxygen catalyzed by cytochrome *c* oxidase depicted in Figure 1.2 and the oxidation of hydrogen, as depicted in Figure 1.3. Enzymes that catalyze redox reactions are called redox enzymes. In order for the redox enzyme to function electrons have to be transported to or from the enzyme. Natural processes make use of so-called electron donors and acceptors, which are relatively large molecules. These molecules are expensive and it is generally not economically feasible to use them in industrial processes. However, if the enzyme is immobilized on a conducting support, this support can function as an electron source or drain, removing the need to use electron donors and acceptors. The support with the immobilized enzyme has to be coupled to another reaction via an external circuit. This other reaction can consume or release the electrons and in this way close the electronic circuit. An example is given in Figure 1.3, in which the electrons released in the hydrogen oxidation are taken up by the electrode surface and released in another reaction.

Research into the immobilization of enzymes on conducting supports is also valuable for the development of biosensors. Biosensors are sensors that can monitor the concentrations of toxic or vital molecules in our environment and in our body. If one of the concentrations is outside the desired range, the biosensor should raise an alarm, to which people can then respond. An example is the glucose biosensor, which is used by diabetics to monitor their blood sugar levels. Biosensors have to be sensitive, which means that they should be able to detect molecules at low concentrations, and specific, which means that they should only respond to one particular molecule out of many molecules present in the human body. As enzymes are generally sensitive and specific towards the binding of their reacting molecules, they are particularly suitable for use in biosensors. However, an enzyme alone is not a biosensor. It is necessary that the binding of the enzyme with the molecule to be detected is translated into a measurable external signal. This can be done by immobilizing redox enzymes on conducting surfaces. Once the enzyme binds and reacts with the molecule to be detected, electrons are exchanged with the conducting surface. This current can be detected with the use of an external circuit (Figure 1.3).

In order to successfully immobilize an enzyme on a surface certain challenges have to be overcome. Firstly, immobilization should not result in structural changes to the enzyme, since this could affect the selectivity and activity of the enzyme. However, in

order to immobilize an enzyme on a surface, interactions between the enzyme and the surface are needed. These interactions can affect the structure and function of the enzyme. Therefore, immobilization should be carried out using relatively mild interactions that are sufficient to retain the enzyme on the surface, but that do not affect the enzyme's structure. Secondly, in case a redox enzyme is immobilized on a conducting surface, direct electron transfer between the surface and the active site of the enzyme is a prerequisite. Whether electron transfer to the surface occurs, depends on the distance between the surface and the active site of the enzyme. The maximum distance the electrons can jump is about two nanometer.^{2,3} If the distance is longer, electron transfer will not occur. Since the diameter of an enzyme is generally significantly larger than two nanometer, the enzyme should be immobilized on the surface in such a way that the active site is relatively close to the surface.

1.4 Bio-inspired catalysts

Another possibility to tackle the disadvantages of using enzymes in industrial processes is to make use of bio-inspired catalysts. These catalysts are synthetic complexes designed based on the structure of the active site of the enzyme, which catalyzes the desired reaction. An example is given in Figure 1.4, which shows a synthetic complex for the active site of cytochrome *c* oxidase (Figure 1.2).⁴ The advantage of these synthetic catalysts is that they are potentially more stable than enzymes and can therefore be used at higher temperatures and pressures. Additionally, immobilization of these complexes on surfaces is much easier than in the case of enzymes. However, the complexes remain models, and therefore their catalytic properties are not the same as the properties of the enzymes. Since enzymes have evolved over millions of years, it is unlikely that the properties of the model complexes will be as good as the properties of the enzymes. Another issue regarding the model complexes is their synthesis, which can be very expensive. Whether model complexes can replace existing catalysts in industrial processes depends on whether they can outperform existing catalysts with regard to activity, selectivity or cost.

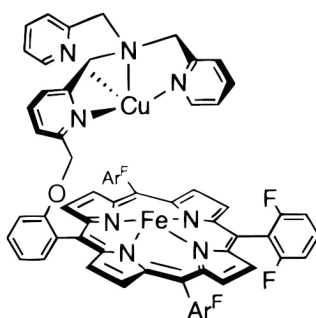


Figure 1.4 A synthetic model complex for the active site of cytochrome *c* oxidase.⁴

A class of reactions that seems particularly suitable for the investigation of catalysis by model complexes is the interconversion of nitrogen containing molecules (Figure 1.5). Some of the depicted reactions are part of large-scale industrial processes, such as the synthesis of nylon (NH_3 to NH_2OH) and the cleaning of ground water (NO_3^- to N_2). For these industrial applications highly selective catalysts resulting in minimal byproduct formation are preferred. The noble metal catalysts used do date do not display the desired selectivities and are expensive. Model complexes might provide an increased selectivity at lower cost. The design of the model complexes can be based on the structures of the active sites of the enzymes that are involved in the conversion of nitrogen compounds, which are indicated in Figure 1.5.

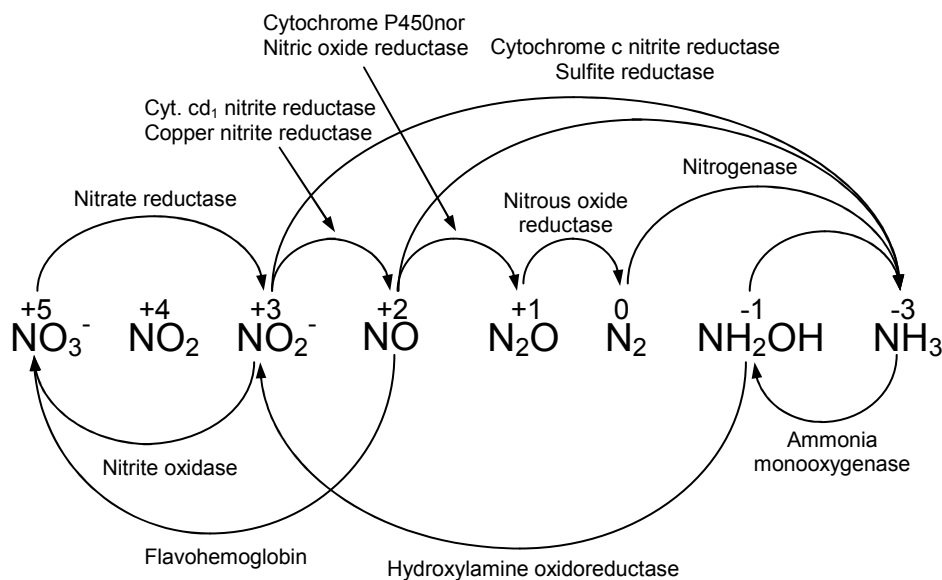


Figure 1.5 Overview of the most important nitrogen containing molecules. The enzymes that catalyze the redox reactions from one molecule to another have been indicated in the figure. The numbers above the molecules indicate the oxidation state of nitrogen.

1.5 Heme proteins and enzymes

In this thesis we focus on immobilization methods and model complexes for one particular class of proteins and enzymes, namely the heme proteins. In their active site heme proteins and enzymes have an embedded heme group (Figure 1.6), which consists of an iron atom inside an organic ring. The best-known heme protein is hemoglobin, which facilitates oxygen transport through the human body. However, there are many other heme proteins, which perform a wide variety of functions, including oxygen reduction (cytochrome *c* oxidase, Figure 1.2) and electron transport (cytochrome *c*). The particular function of a heme protein depends on the particular way, in which the heme group is embedded in the active site of the protein. Some examples are shown in Figure

1.6 and Figure 1.2. Not all heme proteins are enzymes, since proteins are only enzymes if they catalyze a reaction. For example, cytochrome *c* oxidase is an enzyme, since it reduces oxygen to water, but hemoglobin is not, since it only transports oxygen.

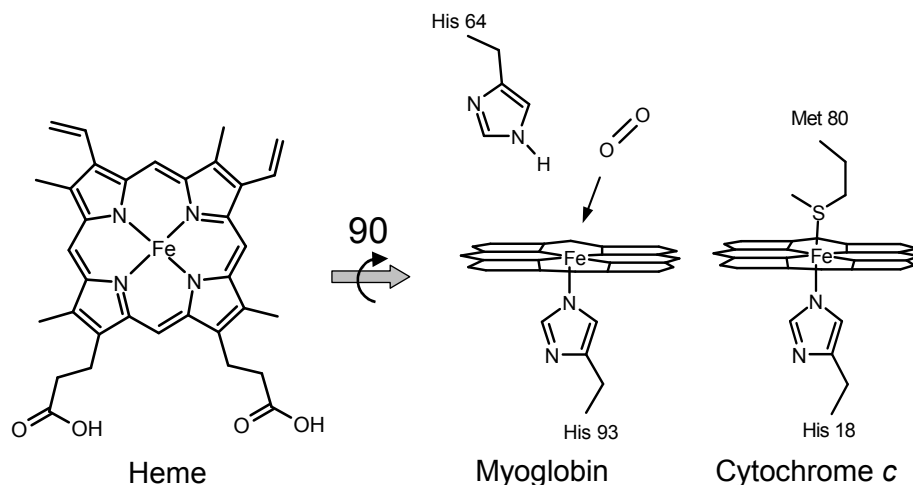


Figure 1.6 The structure of a heme group (left) and the coordination of heme groups in the proteins myoglobin and cytochrome *c* (right). The view of the heme groups in the proteins is side-on, which means that they are tilted 90° compared to the heme structure on the left. The depicted amino acids (His and Met) determine the properties of the protein. Myoglobin is an oxygen storage protein and cytochrome *c* is an electron transfer protein.

1.6 Scope of this thesis

In the first part of this thesis (Chapter 2 and part of Chapter 3A) we investigate a bio-inspired catalytic reaction, namely electrochemical nitric oxide (NO) reduction by immobilized heme groups. A heme group can be regarded as a simple model complex for the active site of NO reducing heme enzymes. The goal of this part of the thesis is to compare NO reduction by immobilized heme groups to NO reduction by NO reducing enzymes and metal catalysts. The focus of the chapters is especially on determining the selectivity of the reaction, since the reaction can result in the formation of more than one product (Figure 1.5), namely nitrous oxide (N_2O), nitrogen (N_2), hydroxylamine (NH_2OH) and ammonia (NH_3). This also makes the reaction of industrial relevance, since hydroxylamine is a raw material in the nylon production and is synthesized from nitric oxide. In Chapter 2 and part of Chapter 3A we determine the mechanisms by which immobilized heme groups reduce NO and also determine how these mechanisms are influenced by pH, potential and the way in which the heme group are immobilized. The difference between chapter 2 and chapter 3A is in the way in which the heme groups are immobilized. Chapter 2 discusses adsorbed heme groups on graphite, whereas

Chapter 3A discusses heme groups incorporated in a surfactant (detergent) film on graphite.

In the second part of this thesis (Chapter 3 to 6) different immobilization methods for heme proteins and enzymes on conducting surfaces are investigated. The goals of these chapters are to understand to what extent the particular immobilization method affects the properties of the protein, to understand the electron transfer between the active site of the protein and the electrode, and to understand how the protein is adsorbed on the electrode. These goals are achieved by studying the electrochemical properties of the immobilized proteins and comparing these to the properties of the proteins in solution. The conclusions not only teach us whether a particular immobilization method is suitable, but also provide insights that should make it easier to immobilize other proteins and enzymes in the future. In the different chapters a number of immobilization methods are discussed, all of which are commonly employed protein immobilization methods.⁵ The first discussed methods are incorporation in a surfactant film on pyrolytic graphite (Chapter 3A and 3B) and incorporation in a layer-by-layer assembly on pyrolytic graphite (Chapter 4). Our results show that these methods can induce the release of heme from heme proteins, and therefore these methods are unsuitable for protein immobilization. The other discussed method is immobilization via electrostatic interactions on a self-assembled monolayer on gold (Chapter 5 and 6). It is already known that this is a good immobilization method for the protein cytochrome *c*, but so far it has not been used to immobilize other heme proteins. In Chapter 5 we investigate the immobilization of the more complex protein cytochrome *c'* and study its orientation and electron transfer properties. In Chapter 6 we investigate the influence of pH and ligand binding on the electron transfer properties and orientation of immobilized horse and yeast cytochrome *c*. Catalysis using immobilized enzymes is not discussed within these chapters. The reason for this absence is that it is desirable to first obtain a good understanding of the interactions between relatively small proteins and conducting surfaces, before moving to enzymes that are generally larger and therefore more difficult to immobilize and study.

Since this thesis deals with heme groups and heme proteins, it is desirable to obtain a more fundamental understanding of the chemical and catalytic properties of a heme group. This is the aim of the last part of this thesis (Chapter 7), in which heme is compared to molecules that resemble heme, but that have chromium, manganese, cobalt or nickel instead of iron in the center of the molecule. The comparison is made based on both experiments and theoretical calculations.

1.7 Experimental approach

In this thesis we have mainly employed electrochemical techniques to investigate the immobilized heme groups and heme proteins. These techniques are particularly useful in the investigation of redox reactions, since the activity of a reaction is directly related to the current measured. Also, from the dependence of current on potential it is possible to determine the reaction mechanisms. In case of the immobilized proteins, the electrochemical techniques allow us to determine whether electrons are able to move

from the electrode surface to the active site of the immobilized protein. They also enable us to indirectly determine whether the immobilization process affects the properties of the protein, as we can deduce from protein specific properties. Obviously, the techniques also have their limitations. Therefore we have sometimes made use of other techniques, such as mass spectroscopy, UV/vis spectroscopy and density functional theory (DFT) calculations.

1.8 References

1. Abelson, P. H., *Science* **2000**, *288*, 269.
2. Langen, R.; Chang, I. J.; Germanas, J. P.; Richards, J. H.; Winkler, J. R.; Gray, H. B., *Science* **1995**, *268*, 1733.
3. Moser, C. C.; Keske, J. M.; Warncke, K.; Farid, R. S.; Dutton, P. L., *Nature* **1992**, *355*, 796.
4. Kim, E.; Chufan, E. E.; Kamaraj, K.; Karlin, K. D., *Chem. Rev.* **2004**, *104*, 1077.
5. Armstrong, F. A.; Wilson, G. S., *Electrochim. Acta* **2000**, *45*, 2623.

Chapter 2

Electrochemical reduction of NO by hemin adsorbed at pyrolytic graphite*

Abstract: *The mechanism of the electrochemical reduction of nitric oxide (NO) by hemin adsorbed at pyrolytic graphite was investigated. The selectivity of NO reduction was probed by combining the Rotating Ring Disk Electrode (RRDE) technique with a newly developed technique called On-Line Electrochemical Mass Spectroscopy (OLEMS). These techniques show that NO reduction by adsorbed heme groups results in production of hydroxylamine (NH₂OH) with almost 100% selectivity at low potentials. Small amounts of nitrous oxide (N₂O) were only observed at higher potentials. The rate determining step in NO reduction most likely consists of an electrochemical equilibrium involving a proton transfer, as can be derived from the Tafel slope value of 62 mV/dec and the pH dependence of -42 mV/pH. The almost 100% selectivity towards NH₂OH distinguishes this system both from NO reduction on bare metal electrodes, which often yields NH₃, and from biological NO reduction in cytochrome P450_{nor}, which yields N₂O exclusively.*

* The contents of this chapter have been published: de Groot, M.T.; Merkx, M.; Wonders, A.H.; Koper, M.T.M., *J. Am. Chem. Soc.* **2005**, *127*, 7579-7586

2.1 Introduction

Reduction of nitric oxide (NO) to nitrous oxide (N₂O) is a key step in denitrification, the five-electron reduction of NO₃⁻ to N₂ that is used by many microorganisms to respire anaerobically and gain energy for cell growth.^{1,2} Enzymes involved in NO reduction direct the selectivity of this reaction towards N₂O (fungal cytochrome P450nor) and circumvent reduction to NH₂OH and NH₃, products that are observed in NO reduction on transition metals such as platinum^{3,4} and palladium.⁵ Understanding what controls the selectivity of NO reduction is not only interesting from a fundamental point of view, but such knowledge may also be applied to develop new catalysts for the removal of pollutants from exhaust gases, the purification of ground water or the more efficient production of NH₂OH, which is a raw material in nylon production.⁶

The mechanism of electrocatalytic reduction of NO by transition metals and adsorbed inorganic complexes has been extensively studied. On transition metals like Pt^{3,4} and Pd⁵ it was found that the mechanism and the selectivity of the NO reduction depend on the kind of metal used and on the applied potential. In general, N₂O and N₂ are formed at positive potentials, while NH₂OH and NH₃ are formed at more negative potentials. Electrochemical NO reduction on adsorbed inorganic complexes such as iron-phthalocyanine,⁶ cobalt-phthalocyanine,⁷ vitamin B12,⁸ Prussian blue⁹ and a cobalt porphyrin¹⁰ primarily leads to the formation of NH₂OH and NH₃, with the actual selectivity depending on the specific system studied and the applied potential.

Biological NO reduction catalyzed by NO reductases such as cytochrome P450nor results in the selective formation of N₂O. This enzyme is found in the denitrifying fungus *Fusarium oxysperum*¹¹ and contains one heme group as cofactor. Reduction of NO by cytochrome P450nor^{12,13} occurs by binding of NO to the heme group, which is followed by a direct hydride transfer from NADH to the heme group^{14,15} leading to the formation of an Fe^{II}-HNO adduct. The Fe^{II}-HNO adduct reacts with another NO molecule to form N₂O exclusively. Interestingly, a similar Fe^{II}-HNO intermediate has been proposed for the 6-electron reduction of nitrite to NH₃ by the enzyme cytochrome c' nitrite reductase. In contrast to cytochrome P450nor, in this multiheme enzyme (5 hemes per protein) the Fe^{II}-HNO is further reduced to hydroxylamine and finally dehydrated to form ammonia.¹⁶

In order to understand the factors that govern activity and selectivity in NO reduction by enzymes and inorganic systems, it would be interesting to study the behavior of NO reducing enzymes or their cofactors that are directly adsorbed on electrodes. In these systems the oxidation state of the cofactor can be controlled directly by the potential applied to the electrode,^{17,18} which is very helpful in gaining mechanistic understanding of NO reduction. Unfortunately, until now no successful immobilization of P450nor has been achieved, but immobilization has been reported for other heme proteins such as myoglobin and hemoglobin.¹⁹⁻²² Although these heme proteins are not NO reductases, they are capable of electrochemically reducing NO when they are immobilized. N₂O was reported as the major product of electrochemical NO reduction by myoglobin,²³ hemoglobin²⁴ and cytochrome P450 CYP119²⁵ as was shown by analysis of the head gas

above the solution with a mass spectrometer.^{23,25} Analysis of the solution after NO reduction showed that NH_2OH and NH_3 were not formed in NO reduction by immobilized myoglobin.²³ In general, the mechanisms proposed for electrochemical NO reduction by immobilized myoglobin, hemoglobin and cytochrome P450 CYP119 resemble the NO reduction mechanism for cytochrome P450nor, the only difference being that electrons for the NO reduction are not provided by NADH, but by the electrode.

To provide an intermediate system between NO reduction on bare metal electrodes and enzymes immobilized on electrodes, we decided to study the electrochemical NO reduction by adsorbed heme groups (iron protoporphyrin IX). This system combines the cofactor used by enzymatic systems with the direct electronic contact between the electroactive group and the electrode typical of an (inorganic) electrochemical system. Heme groups are known to adsorb rapidly on graphite surfaces and their electrochemical and spectroscopic properties on these surfaces have been studied extensively.²⁶⁻³⁶ They form an ordered structure²⁶ in which the heme groups are slightly tilted²⁷ and catalytic reactivity has been reported towards oxygen,^{28,29} hydrogen peroxide,^{29,30} organohalides,³¹ nitrite^{32,33} and NO.³³⁻³⁶ Previous papers on NO reduction by heme adsorbed on graphite mainly focused on the development of a biosensor, however, and did not address the mechanism and the selectivity of the NO reduction. Given the importance of selectivity issues in NO reduction we have applied two techniques that are able to directly determine the selectivity of the NO reduction: On-line Electrochemical Mass Spectrometry (OLEMS) and the Rotating Ring Disk Electrode (RRDE). OLEMS is a new technique recently developed in our laboratory that is able to measure gases formed at an immersed electrode. It resembles Differential Electrochemical Mass Spectrometry (DEMS),³⁷ but has the advantage that it can be applied to electrodes of any shape and any material. OLEMS can be used very effectively in NO reduction to follow the formation of N_2O and N_2 as well as the consumption of NO, whereas the RRDE can detect the formation of NH_2OH . These techniques have a short response time, a low detection limit, are generally not influenced by reactions in solution, and can give quantitative information. Therefore they are more effective than ex-situ determinations such as sampling of the head gas or analysis of the solution, techniques that have high detection limits and can be influenced by homogeneous reactions.

2.2 Experimental Procedures

Materials. Hemin (Fluka, 98%) was used as received. All other chemicals were p.a. grade (Merck). Pyrolytic graphite (Carbone-Lorraine) was fabricated into home-made rotating ring-disk electrodes.^{38,39} The geometric surface area of the electrodes was 0.5 cm^2 . Buffer solutions were prepared with sodium acetate (pH 4-6), sodium dihydrogen phosphate monohydrate (pH 2-3, 6-8, 11-12) or boric acid (pH 9-10) combined with concentrated solutions of hydrochloric acid or caustic soda and Millipore MilliQ water (resistivity $>18.2 \text{ M}\Omega \text{ cm}$). The concentration of the buffer was 0.5 M in experiments involving NO or NH_2OH reduction and 0.1 M in all other experiments. Prior to entering the electrochemical cell nitric oxide 2.5 (Linde AG) was bubbled through two washing

flasks filled with a 3 M KOH solution, a procedure that was found to be important in order to remove NO_2 .^{3,38} Purging the solution with NO for 10 minutes resulted in a saturated NO solution, which corresponds to a concentration of 2 mM as can be calculated from Henry's law constant of $2.0 \times 10^{-3} \text{ mol atm}^{-1}$ at 21°C .⁴⁰

Electrochemical Apparatus and Procedures. An Autolab PGstat 20 potentiostat was used for cyclic voltammetry. A homemade three-electrode cell consisting of a platinum flag counter electrode, a Hg|Hg₂SO₄ or Ag|AgCl reference electrode, and a rotating ring disk electrode were used. All potentials in this chapter are relative to the standard calomel electrode (SCE). The rotating ring disk electrode consisted of a pyrolytic graphite (PG) disk and a Pt ring. Experiments with rotation were conducted using a Motomatic[®] motor generator. All solutions were deaerated by purging with argon for 10 minutes. All electrochemical experiments were performed at room temperature ($21 \pm 2^\circ\text{C}$).

Immobilization of hemin. A 0.5 mM hemin solution was prepared by dissolving 1.6 mg hemin in 5 ml of a 0.01 M pH 10 buffer solution, since hemin only dissolves in alkaline solution. Prior to use, the PG electrodes were abraded using 40 μm Al₂O₃ sandpaper and ultrasonicated in Millipore MilliQ water for 5 minutes. The electrode was dried in a N₂ stream for 10 seconds. The electrode was immersed in the hemin solution for 10 minutes to saturate the surface with hemin,^{41,42} after which the electrode was rinsed with water.

Rotating Ring Disk Electrode (RRDE) experiments. Rotating Ring Disk Electrodes were constructed as described previously^{38,39} and have a collection efficiency of 0.27 ± 0.03 . Prior to the measurements, the Pt ring was abraded together with the PG disk on 40 μm Al₂O₃ sandpaper and was also immersed in the 0.5 mM hemin solution. Subsequently the Pt ring was cleaned by electro-polishing: alternately a potential in the hydrogen evolution region (-0.8 V vs. SCE) and a potential in the oxygen evolution region (1.5 V vs. SCE) were applied for 5 seconds, which was repeated 25 times.

On-Line Electrochemical Mass Spectrometry (OLEMS). OLEMS measurements were performed on a Balzers Prisma QMS 200 mass spectrometer. The connection between the mass spectrometer and the cell was established through a steel capillary connected to a glass tube onto which a porous Teflon tip was attached. This tip was placed at approximately 10 μm from the PG-heme electrode surface as shown by the photograph in Figure 2.1. Details of the setup have been published elsewhere.⁴³ The electrode could not be rotated and hence NO was continuously bubbled through solution to enhance NO mass transfer. Baseline values measured in a solution without NO were subtracted in NO reduction experiments.

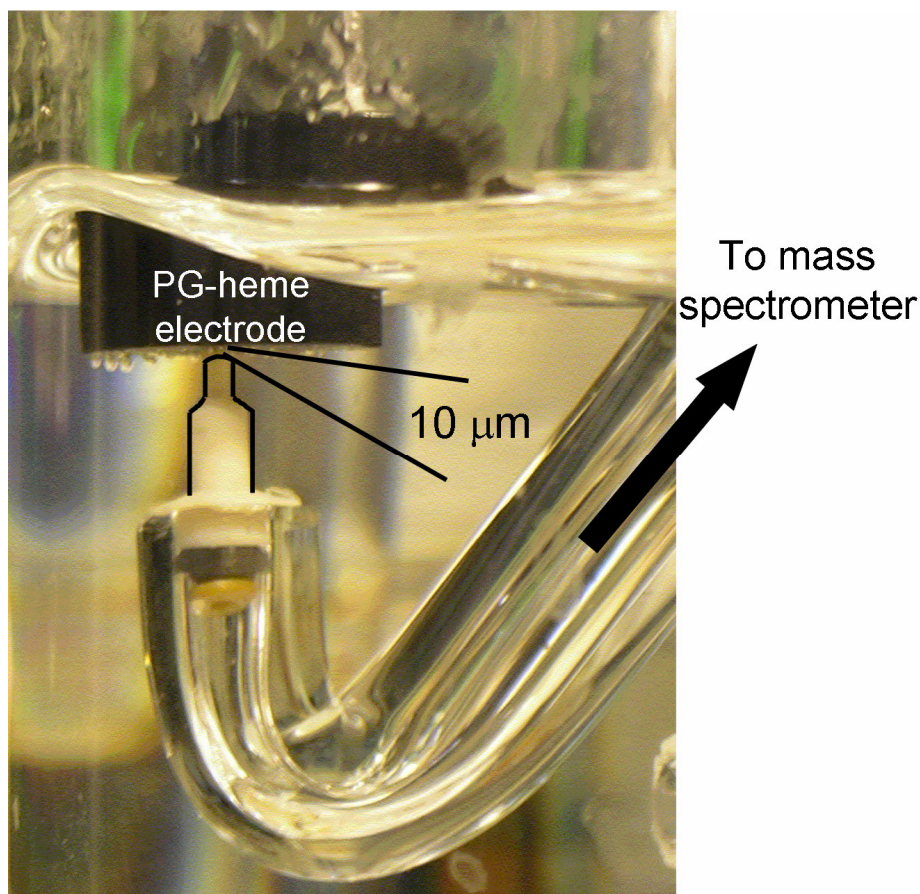


Figure 2.1 Photograph of OLEMS setup: a porous teflon tip is in close contact ($d \sim 10 \mu\text{m}$) to the PG-heme electrode.

2.3 Results

Prior to studying electrochemical NO reduction, we investigated the electrochemical properties of adsorbed heme groups on pyrolytic graphite. Figure 2.2a shows a voltammogram of a freshly prepared PG-heme electrode. The observed redox couple corresponds to the $\text{Fe}^{\text{III}}/\text{Fe}^{\text{II}}$ couple of the adsorbed heme groups. The redox couple has a midpoint potential $E_m = -0.42 \text{ V}$ vs. SCE, which is the same as values of E_m previously reported for heme adsorbed on gold⁴⁴ and highly ordered pyrolytic graphite (HOPG).²⁷ E_m is not dependent on the pH of the solution below pH 4, but shows a dependence of -59 mV/pH above pH 5 (Figure S2.1, which can be found at the end of this chapter). This dependence can be ascribed to a proton transfer accompanying the electron transfer of the $\text{Fe}^{\text{III}}/\text{Fe}^{\text{II}}$ couple, possibly due to a ligand change from H_2O to OH^- upon oxidation of the iron center.^{29,44} A linear relation between the current density J_p and the scan rate ν was observed (Figure S2.2), which indicates that the voltammetric response is due to a surface-confined species. Electron transfer between the graphite and the adsorbed heme

groups is fast, since the cathodic and anodic peak potentials do not depend on the scan rate v for scan rates up to 10 V/s. As can be calculated from Laviron's theory⁴⁵ this is in line with the previously obtained electron transfer rate of $4.9 \times 10^3 \text{ s}^{-1}$.^{27,46} The amount of adsorbed hemin that can be calculated from the anodic peak charge is $1.5 \times 10^{-10} \text{ mol cm}^{-2}$. This is higher than for hemin adsorbed on HOPG (7.7×10^{-11}),^{27,46} which can be explained by the roughness of the pyrolytic graphite used.

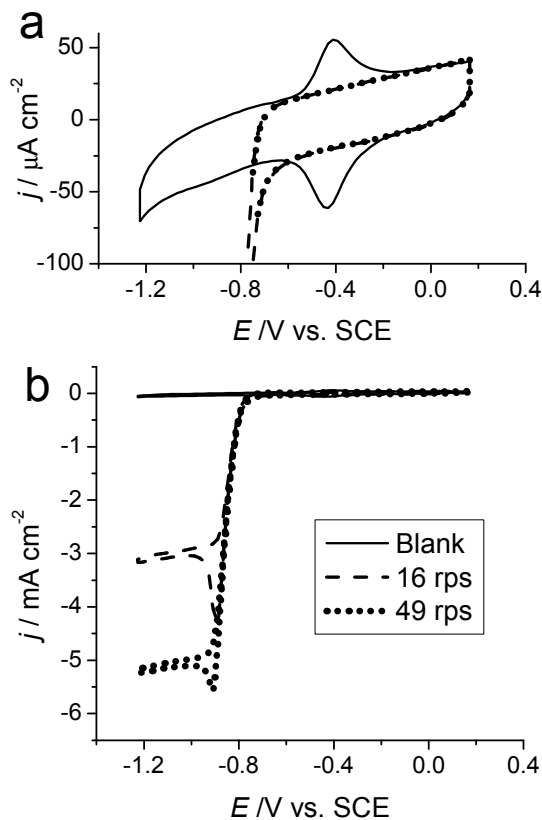


Figure 2.2 Cyclic voltammograms of a hemin-modified PG electrode in an NO free (—) and in a saturated NO solution at 16 rps (- - -) and 49 rps (.....). Note that (a) and (b) have different current scales. Buffer: 0.5 M phosphate, pH 7; scan rate = 500 mV/s.

Upon saturation of the solution with NO a new reduction wave is observed starting at potentials around -0.75 V vs. SCE (Figure 2.2b), which can be assigned to NO reduction by the adsorbed heme groups. Below -0.9 V vs. SCE the reaction rate of this reaction is limited by NO mass transfer, as can be deduced from the fact that the observed current is strongly dependent on the rotation rate of the electrode. It is important to note that the observed reduction waves are not influenced by nitrite, which is often observed in concentrated NO solutions. PG-heme electrodes are only able to reduce nitrite at low pH^{32,33} and are unable to do so at pH 7 (Figure S2.3). Another effect of the saturation of

the solution with NO is the disappearance of the Fe^{III}/Fe^{II} couple from voltammetry (Figure 2.2a). This can be explained by NO binding to the heme group, which affects the reduction potentials of the Fe^{III}/Fe^{II} couple. Both the Fe^{III} and the Fe^{II} state of the heme can bind NO.^{47,48}

The selectivity of the electrochemical NO reduction, which is the main focus of this chapter, cannot be directly derived from a voltammogram such as Figure 2.2. Therefore, voltammetry was combined with On-Line Electrochemical Mass Spectroscopy (OLEMS) and the Rotating Ring Disk Electrode (RRDE), techniques that can determine selectivity *in situ*. The OLEMS results are displayed in Figure 2.3, which shows the voltammetric response as well as the ion current intensities for $m/z = 30$ (NO) and $m/z = 44$ (N₂O) for electrochemical NO reduction. The observed voltammetric response is similar to NO reduction in other voltammetric experiments (Figure 2.2), even though the electrode could not be rotated. As soon as NO reduction occurred (around -0.8 V), a sharp decrease in the ion current intensity for $m/z = 30$ was observed, indicating that NO is consumed. A small increase in the ion current intensity for $m/z = 44$ was also observed, indicating the formation of a small amount of N₂O. However, contrary to the consumption of NO, the formation of N₂O was only observed at the start of the NO reduction and was not observed during continuous NO reduction at lower potentials. As was shown previously, the OLEMS setup is able to detect the formation of very small amounts of N₂O and since the cell is purged with argon, CO₂ from air does not interfere with N₂O detection.⁴³ This is also evidenced by the small amount of CO₂ that can be detected during methanol oxidation on a platinum single-crystal electrode,⁴³ and by the very small amounts of N₂O measured during hydroxylamine oxidation on a polycrystalline platinum electrode utilizing a similar DEMS setup, in complete accordance with results from independent FTIR measurements.⁴⁹ As the sensitivities for NO and N₂O are similar in the mass spectrometer, the relatively small N₂O signal that is observed implies that N₂O is only a minor byproduct at the start of the NO reduction. N₂ ($m/z = 28$), another possible product of NO reduction by PG-heme, was never observed in our OLEMS experiments, indicating that the main reaction product of the NO reduction is either NH₂OH or NH₃. These products are difficult to observe with OLEMS, because they are not gaseous and their fragmentation products have ion current intensities close to those of water.

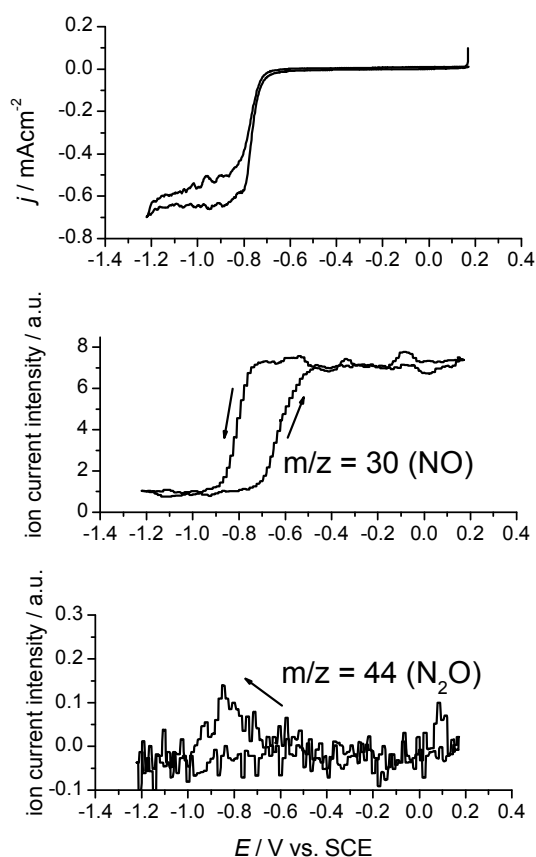


Figure 2.3 OLEMS measurements of adsorbed hemin in saturated NO solution. Top: cyclic voltammogram of adsorbed hemin. Middle: ion current intensity for $m/z = 30$ (NO) measured in the mass spectrometer as a function of potential. Bottom: ion current intensity for $m/z = 44$ (N_2O) measured in the mass spectrometer as a function of potential. Measurements were done in 0.5 M phosphate, pH 7.0 under continuous NO bubbling through the solution using a scan rate of 10 mV/s.

RRDE⁵⁰ was employed to detect the possible formation of NH_2OH and NH_3 . For the ring to be used for selectivity measurements, the voltammetric responses of the possible products (NH_2OH and NH_3) and of the reactant (NO) on Pt have to be known. Therefore cyclic voltammetry was performed with NO, NH_2OH and NH_3 in solution (Figure 2.4). NH_3 could not be oxidized within our potential window, which agrees with previous observations that ammonia oxidation on Pt only occurs in alkaline solution.⁵¹ NH_2OH exhibits an oxidation wave starting at 0 V vs. SCE and NO exhibits a reduction wave starting at 0 V vs. SCE. The fact that reduction of NH_2OH occurs at much lower potentials and that oxidation of NO occurs at much higher potentials, allows for a straightforward distinction between NO and NH_2OH on the Pt ring.

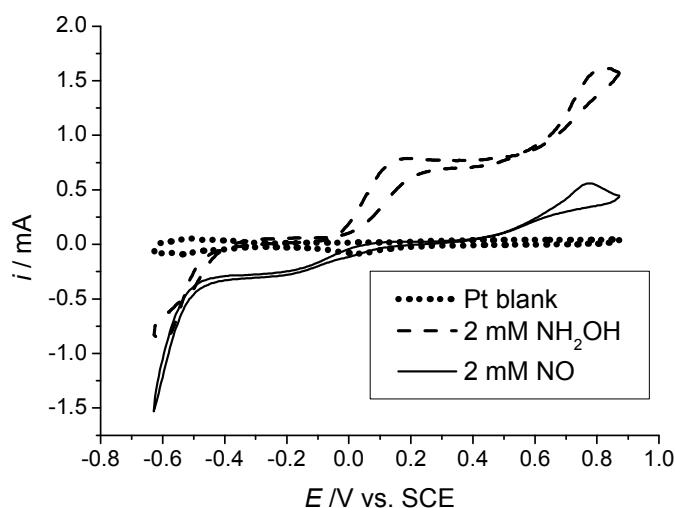


Figure 2.4 Cyclic voltammograms of a Pt-ring in the absence (.....), and in the presence of 2 mM NO (—) or 1 mM $(\text{NH}_3\text{OH})_2\text{SO}_4$ (- - -). Buffer: 0.5 M phosphate, pH 7.0; scan rate = 50 mV/s; 16 rps.

Figure 2.5 shows the voltammetric response of the Pt ring during NO reduction on the PG-heme disk as compared to the voltammetric response of the Pt ring in saturated NO solution without NO reduction on the disk. When NO is reduced on the disk (at $E_{\text{disk}} = -0.9$ V, $i_{\text{disk}} = -1.5$ mA) a decrease of approximately 0.14 mA was observed in the NO reduction wave on the ring. On the Pt ring NO is reduced via a one electron process to N_2O^3 at potentials between -0.2 V and -0.4 V vs. SCE. Assuming that NO is reduced to NH_2OH on the disk, the observed decrease in current of 0.14 mA corresponds to a collection efficiency of 0.28, which is in agreement with the collection efficiency of 0.27 ± 0.03 previously reported for this electrode.^{38,39} This also confirms that N_2O is not the main product of NO reduction on the disk, since this would imply an unrealistically low collection efficiency of only 0.09. The decrease in the NO reduction wave is accompanied by an increase of ca. 0.21 mA at potentials above 0 V. Comparison of Figure 2.4 and 2.5 suggests that this increase is due to the oxidation of NH_2OH , implying that NH_2OH is formed as a product on the PG-heme disk. It is difficult to determine quantitatively from these measurements whether NO reduction is 100% selective towards NH_2OH , since for this we need to know the number of electrons transferred in NH_2OH oxidation on the Pt ring. However, the oxidation of NH_2OH on Pt in neutral media is known to result in the formation of more than one product (NO , N_2O , N_2)⁵²⁻⁵⁴ and therefore this number can range between 1 and 3. In our case, assuming that NH_2OH is the only product of NO reduction on the disk, the increase in current of 0.21 mA corresponds to a calculated number of electrons of approximately 1.5. This is plausible and suggests that NH_2OH on the ring is oxidized to a combination of N_2 and N_2O .

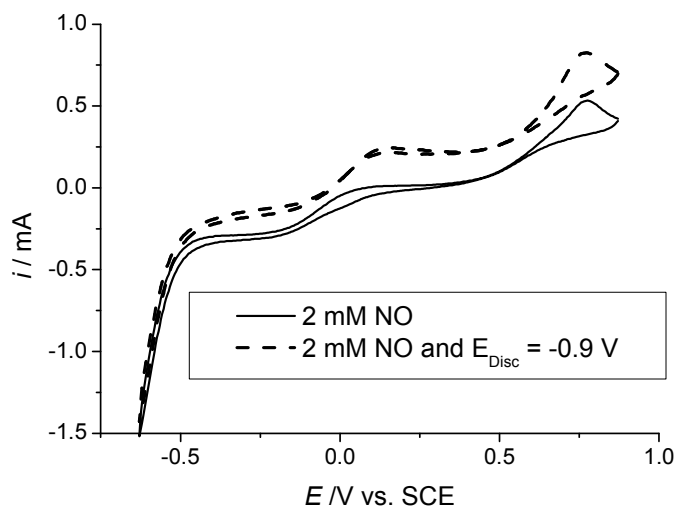


Figure 2.5 Cyclic voltammograms of Pt-ring in saturated NO (2 mM) solution (—) and in saturated NO solution with a potential of -0.9 V (---) applied to the PG-heme disk. Buffer: 0.5 M phosphate, pH 7.0; scan rate = 50 mV/s; 16 rps. The recorded current on the disk was -1.5 mA.

OLEMS and RRDE strongly suggest that NH_2OH is the main reaction product of NO reduction at a PG-heme electrode and this can be confirmed by indirect but quantitative evidence from voltammetry. One such experiment is comparing NO reduction on a PG-heme electrode to NO reduction on a Pt electrode constructed in exactly the same way, such that both electrode geometries exhibit the same NO mass transfer behavior. It is known that NO reduction on Pt leads to N_2O as the only product at potentials between -0.2 V and -0.4 V vs. SCE³ and that the reaction rate is limited by NO mass transfer. On a PG-heme disk NO mass transfer also limits the NO reduction at potentials below -0.9 V. Both mass transfer limited currents are compared in Figure 2.6. On the Pt-disk a current of 1.63 mA cm^{-2} was observed, whereas on the PG-heme disk a current of 4.92 mA cm^{-2} was observed, which is almost exactly three times the mass transfer limited current observed on Pt. Since the reduction of NO to N_2O on Pt corresponds to a one-electron transfer, the reduction on the PG-heme disk must correspond to a three-electron transfer. This implies that NO is reduced to NH_2OH and the selectivity is very close to 100%.

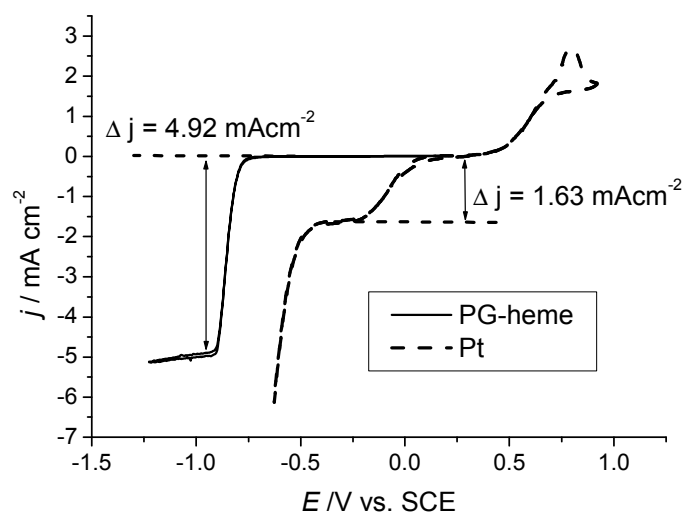


Figure 2.6 Cyclic voltammograms of adsorbed hemin on PG (—) and Pt (- -) in saturated NO solution. Electrodes have the same geometry. Buffer: 0.5 M phosphate, pH 7.0; scan rate = 50 mV/s; 49 rps.

Calculation of the number of electrons transferred in a so-called NO “stripping” experiment also confirms the almost 100% selective formation of NH_2OH . Such an experiment is performed by reducing the $\text{Fe}^{\text{II}}\text{-NO}$ adduct of the adsorbed heme groups without NO present in solution. The $\text{Fe}^{\text{II}}\text{-NO}$ adduct was formed by performing continuous NO reduction on the PG-heme electrode for a short time (5 seconds) and transporting it to a buffer solution without NO. The $\text{Fe}^{\text{II}}\text{-NO}$ adduct formed is stable in aerobic buffer solution for at least 10 minutes. The first two voltammetric scans recorded after transfer to the NO free buffer solution, are shown in Figure 2.7. A reduction peak is observed in the first scan, which coincides with the reduction peak for continuous NO reduction (Figure 2.2). After this reduction peak the $\text{Fe}^{\text{III}}/\text{Fe}^{\text{II}}$ couple reappears and in the second scan no NO reduction peak is observed. The area under the reduction peak corresponds to a charge equivalent to 5.4×10^{-10} mol cm^{-2} . From the $\text{Fe}^{\text{III}}/\text{Fe}^{\text{II}}$ couple a heme coverage of 1.8×10^{-10} mol cm^{-2} can be calculated. The ratio of $\sim 3:1$ again indicates that three electrons are transferred per heme group, implying that NH_2OH is the main reaction product. The fact that the NO stripping peak coincides with the continuous NO reduction wave suggests similar mechanisms for continuous NO reduction and the NO stripping experiment.

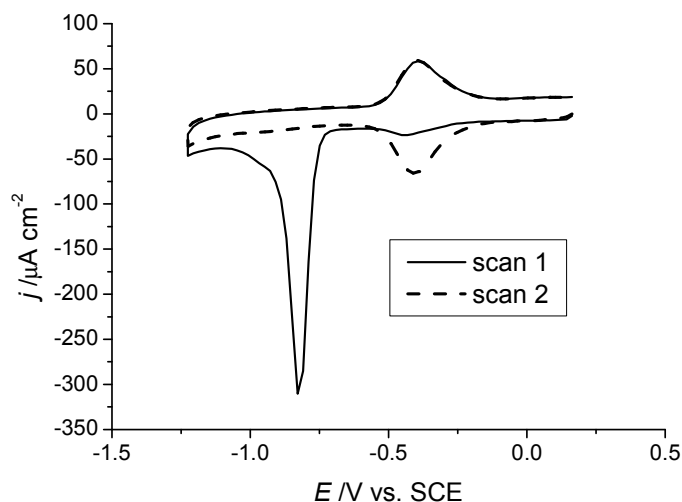


Figure 2.7 *NO stripping voltammetry of adsorbed hemin. Scan 1 (—) and scan 2 (- - -). Buffer: 0.5 M phosphate buffer, pH 7.0; scan rate = 500 mV/s.*

The observation that the selectivity of NO reduction on PG-heme towards NH_2OH is very close to 100% suggests that the heme group is not able to break the N-O bond in NH_2OH . We investigated NH_2OH reduction by PG-heme, which showed that NH_2OH could be reduced by PG-heme (Figure S2.3), but that the rate is much slower than NO reduction. This indicates that breaking the N-O bond is indeed difficult although not impossible.

The fact that NH_2OH and not N_2O is the main product of the electrochemical NO reduction by PG-heme prompts a more detailed study of the reduction mechanism. To this end, we constructed Koutecky-Levich and Tafel plots⁵⁰ from the voltammetric RDE experiments to provide information about the rate determining step in the mechanism and the possible involvement of reaction equilibria (Figure 2.8 and 2.12). We also investigated pH dependence. Data for the Koutecky-Levich plots can be obtained by performing chronoamperometric measurements at different rotation rates at potentials between -0.7 V and -0.9 V. At these potentials, the reaction rate is determined by both reaction kinetics and NO mass transfer. A Tafel plot was constructed from the kinetically limiting currents at different potentials, which were determined by extrapolating the Koutecky-Levich plots to infinite rotation rate, i.e. $\omega^{-1/2} \rightarrow 0$. Kinetically limiting currents could only be determined for potentials of -0.81 V and higher, since accurate determination at more negative potentials is hampered by non-linear Koutecky-Levich plots, which are probably related to saturation of the heme groups by NO. At full saturation, the current will not increase with higher rotation rate ($\omega^{-1/2} \rightarrow 0$). The rotation rate at which the nonlinearity sets in depends on the applied potential, since reduction of the heme-NO adduct becomes faster with decreasing potential. At high potentials (> -0.8 V) the heme group is almost saturated for all rotation rates, which makes it relatively

straightforward to extrapolate the kinetically limiting current. At lower potentials nonlinear Koutecky-Levich plots are observed, indicating that the heme groups become saturated with increasing rotation rate.

The slope determined from the Tafel plot (Figure 2.9) is 62 mV/dec, which can be interpreted in terms of a mechanism in which an electrochemical equilibrium is followed by a chemical rate-determining step (EC-mechanism).⁵⁵ The slope of the Tafel plot does not depend on the pH of the solution, indicating that the rate-determining step does not change with pH. Since the kinetically limiting current is directly related to the turnover number (number of reacted molecules per reactive center per second), the exponential relation between the kinetically limiting current and the potential in the Tafel plot implies that the turnover number depends exponentially on potential.

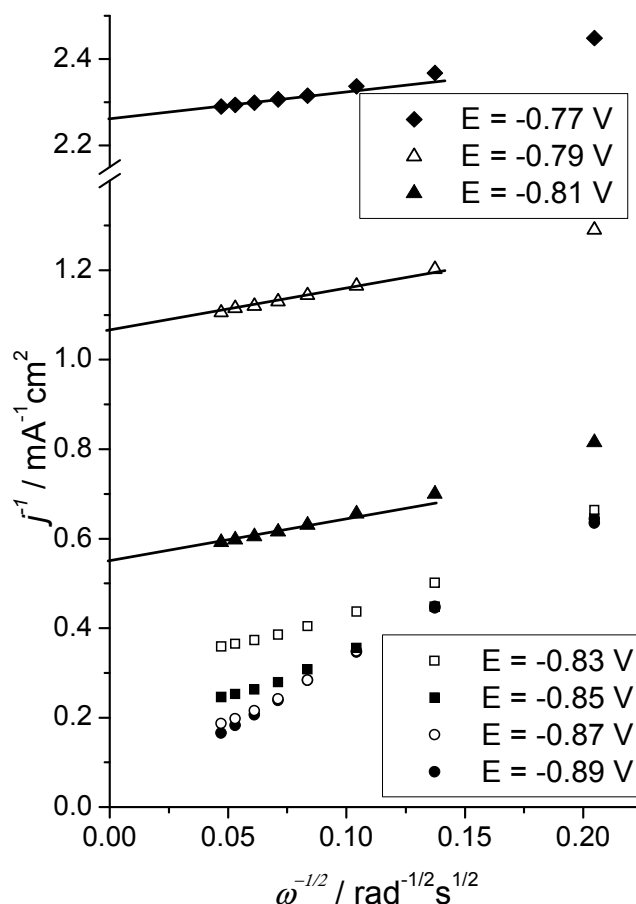


Figure 2.8 Koutecky-Levich plots of adsorbed hemin in saturated NO solution at $E = -0.77\text{ V}$ (\blacklozenge), $E = -0.79\text{ V}$ (\triangle), $E = -0.81\text{ V}$ (\blacktriangle), $E = -0.83\text{ V}$ (\square), $E = -0.85\text{ V}$ (\blacksquare), $E = -0.87\text{ V}$ (\circ), $E = -0.89\text{ V}$ (\bullet). Buffer: 0.5 M phosphate buffer, pH 7.0. Kinetically limiting currents were determined by drawing a line through the four points with the highest rotation rates and extrapolating to the j^{-1} -axis as indicated in figure.

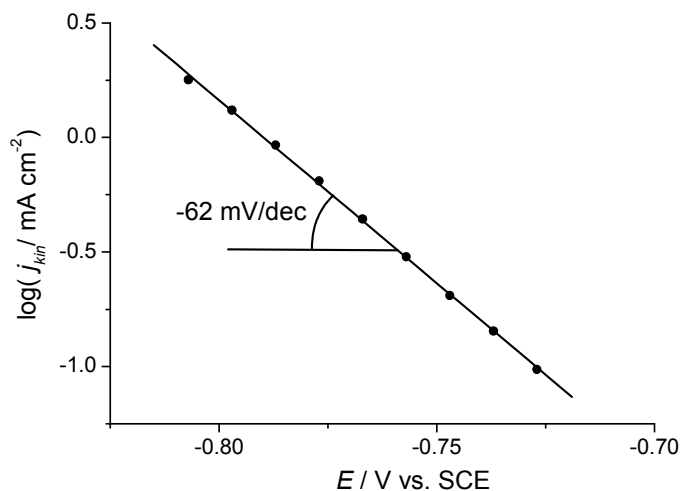


Figure 2.9 Tafel plot of adsorbed hemin in saturated NO solution. Buffer: 0.5 M phosphate, pH 7.0.

The pH dependence of the NO reduction was determined by plotting the potential at which a steady state current of 0.6 mA cm^{-2} was measured versus the pH of the solution (Figure 2.10). This value of 0.6 mA cm^{-2} was chosen as it is relatively small compared to the current observed when the reaction is completely limited by NO mass transfer (3 mA cm^{-2}) so that the influence of different diffusion parameters in the different buffer solutions was avoided. In contrast to the Tafel slope, the NO reduction rate is pH dependent indicating that proton transfer plays an important role in the rate-determining step of the reaction. Surprisingly, however, the observed slope of -42 mV/pH significantly differs from the value of -59 mV/pH that is expected for one proton transfer per electron transfer.

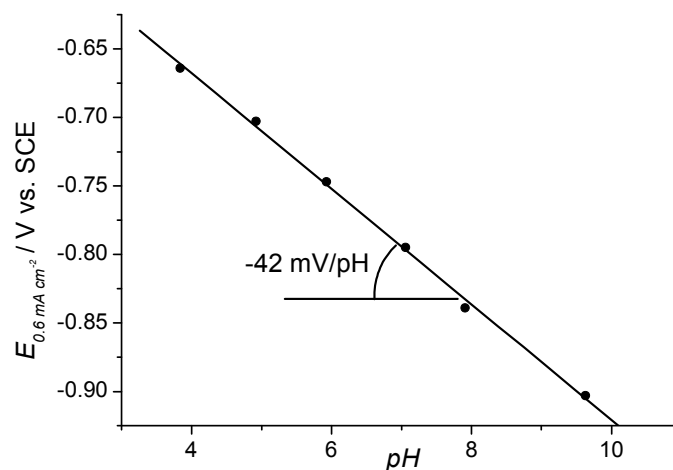
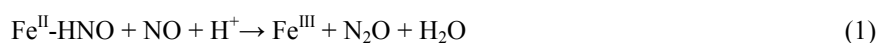


Figure 2.10 Potential at which a steady state current of 0.6 mA cm^{-2} is measured as a function of pH in saturated NO solution. Buffer: 0.5 M acetate, phosphate or borate; 16 rps .

2.4 Discussion

Electrochemical NO reduction by adsorbed heme groups results in the formation of NH_2OH as the main product. This can be concluded from (i) the OLEMS measurements that did not show the formation of significant amounts of N_2O and N_2 , (ii) the RRDE experiments that showed the oxidation of NH_2OH on the Pt ring, (iii) the comparison to NO reduction on Pt that showed that three electrons are consumed in the NO reduction on the PG-heme electrode, and (iv) the stripping experiments that also showed that three electrons are involved in the reduction of heme-bonded NO.

N_2O was observed as a minor product in the OLEMS experiment. This suggests that there are two competing pathways for NO reduction, one leading to the formation of NH_2OH and one leading to the formation of N_2O . The mechanism by which the N_2O is formed is probably similar to the mechanism previously reported for NO reduction by immobilized myoglobin and hemoglobin: it proceeds via a $\text{Fe}^{\text{II}}\text{-HNO}$ adduct, which has been observed for myoglobin in solution,^{12,56,57} and subsequently reacts with NO to form N_2O (Reaction 1).



The main reaction pathway in our system, however, leads to the formation of NH_2OH and hence occurs via another mechanism. The Tafel slope of 62 mV/dec and the pH dependence of -42 mV/pH suggest an EC mechanism i.e. an electrochemical equilibrium

followed by a chemical step, combined with a proton transfer. On the basis of this information we postulate a mechanism for the NH_2OH formation (Reactions 2-4). The first two steps are identical to the mechanism in which N_2O is formed and also result in the formation of an $\text{Fe}^{\text{II}}\text{-HNO}$ intermediate. Subsequently, the $\text{Fe}^{\text{II}}\text{-HNO}$ adducts reacts further to NH_2OH (Reaction 4). Note that reaction 4 is an *overall* reaction – in the EC mechanism the rate-determining step is chemical and should not involve electron transfer. It would be premature to speculate on the nature of the chemical step and how the involvement of proton transfer could lead to the unusual pH dependence.



This mechanism suggests that the $\text{Fe}^{\text{II}}\text{-HNO}$ adduct is the branching point between the pathway leading to N_2O and the pathway leading to NH_2OH . This raises the question why our system favors the pathway to NH_2OH and other systems such as NO reduction by cytochrome P450nor favor the pathway to N_2O . This question is difficult to answer, since most likely there are a number of factors that can influence the preference for one or the other pathway. These probably include the residues surrounding the heme group, the mode of electron transfer to the heme group, the way in which a second NO molecule can bind to the active site and the pH of the solution.

A comparison to enzymatic NO reduction shows that the way in which the electrons are provided to the catalytic centre of the enzyme can have a profound influence on selectivity. The reason that NO reduction catalyzed by cytochrome P450nor leads to N_2O and not NH_2OH may be tentatively related to the fact that the electron donor NADH can only provide two electrons. The transfer of more electrons from a second NADH is unlikely, since only one NADH can bind close to the heme.⁵⁸ This implies that NH_2OH formation is impeded due to lack of electrons and therefore the $\text{Fe}^{\text{II}}\text{-HNO}$ can only react to N_2O . Interestingly, the nitrite reduction by cytochrome *c'* nitrite reductase also proceeds via a $\text{Fe}^{\text{II}}\text{-HNO}$ intermediate, which reacts via NH_2OH to NH_3 ,¹⁶ showing that reduction of the $\text{Fe}^{\text{II}}\text{-HNO}$ adduct to NH_2OH by an enzyme is possible. Cytochrome *c'* nitrite reductase has 5 heme groups that can provide more electrons and further reduction of the $\text{Fe}^{\text{II}}\text{-HNO}$ adduct is therefore not impeded by a limited availability of electrons. However, sufficient availability of electrons does not necessarily imply that NH_2OH is the reaction product. NO reduction by immobilized heme proteins results in the formation of N_2O , even though further reduction of the $\text{Fe}^{\text{II}}\text{-HNO}$ adduct should be possible in these systems, since the electrode can provide an unlimited number of electrons. In contrast to NO reduction by adsorbed heme groups the pathway to N_2O is apparently favored over the pathway to NH_2OH . This implies that the specific surroundings of the heme group also have a profound influence on selectivity.

Another important observation from this study is that NH_3 was not observed as a product in NO reduction by adsorbed heme groups. Our experiments show that electrocatalytic reduction of NH_2OH is possible, but it is much slower than NO reduction, which suggests that NO bond breaking by adsorbed heme groups is very sluggish. This is in contrast to transition metals like Pt^{3,4} and Pd,⁵ on which NO reduction has been shown to result in the formation of N_2O , N_2 , NH_2OH and NH_3 depending on both the kind of metal used and the potential applied. Significantly, NO adsorbed on Pt without NO in solution can only be reduced to NH_3 and not to N_2O and NH_2OH .⁵⁹ Interestingly, NH_2OH was also observed as the main product in electrocatalytic reduction of NO by adsorbed iron-phthalocyanine,⁶ which suggests that adsorbed iron complexes are poor catalysts for reducing NO to NH_3 . An explanation could be that N-O bonds can only be broken at significant rates when at least two adjacent adsorption sites are available. This is supported by the fact that NH_3 formation on most metals is only possible if the adsorbed NO has space to tilt to a bridging configuration (as illustrated in Figure 2.11).⁶⁰ Since a heme group has only one iron center such a bridging confirmation cannot be achieved and therefore N-O bond breaking is very sluggish.

The selectivity of NO reduction by adsorbed heme confirms that this is an intermediate system between NO reduction on bare metal electrodes and enzymes, whether immobilized on electrodes or not. Figure 2.11 gives a schematic representation in which NO reduction by cytochrome P450nor, adsorbed heme complexes and metal electrodes are compared.

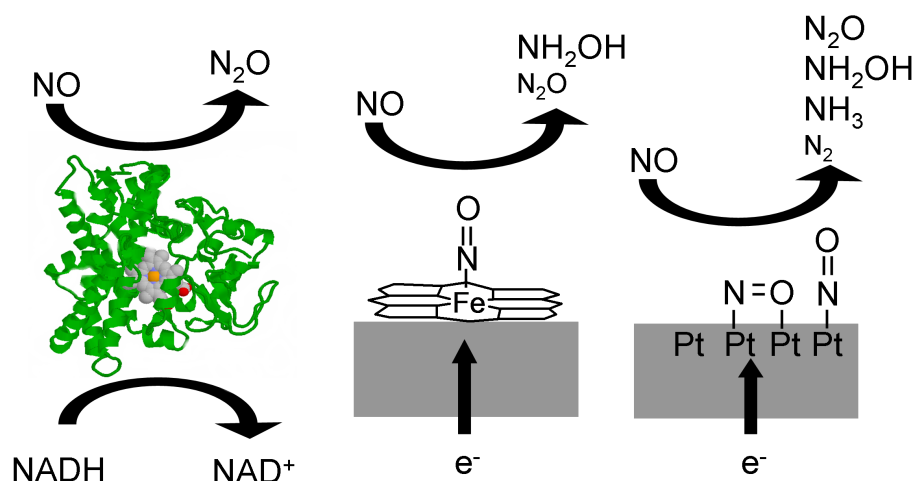


Figure 2.11 Schematic overview of the selectivity of NO reduction by P450nor, adsorbed heme, and metal surfaces.

2.5 Conclusion

We have shown that adsorbed heme groups reduce NO to NH_2OH with a selectivity of almost 100%. A small amount of N_2O was also observed at high potentials, indicating that there is competition between a NO reduction pathway to NH_2OH and a pathway to N_2O . However, the pathway to NH_2OH is clearly favored at low potentials. Adsorbed

heme provides an interesting new system for mechanistic study of NO reduction that can help in obtaining a better understanding of the factors that govern selectivity in both biological NO reduction and inorganic NO reduction.

2.6 Supporting information

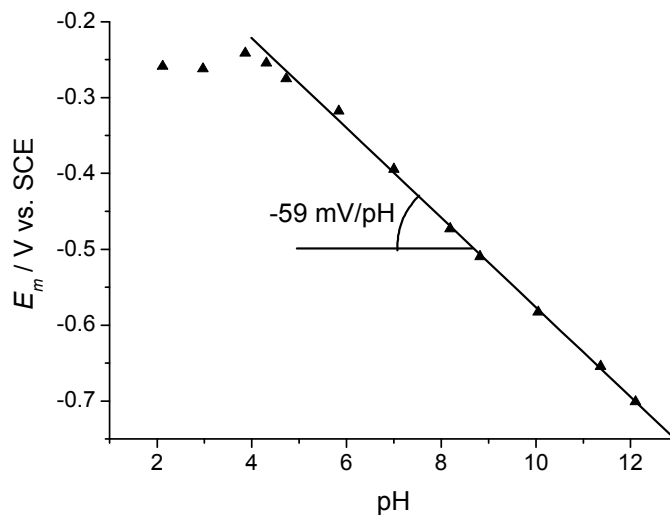


Figure S2.1 Midpoint potentials of adsorbed hemin as a function of pH. Buffer: 0.1 M acetate, phosphate or borate; scan rate = 500 mV/s.

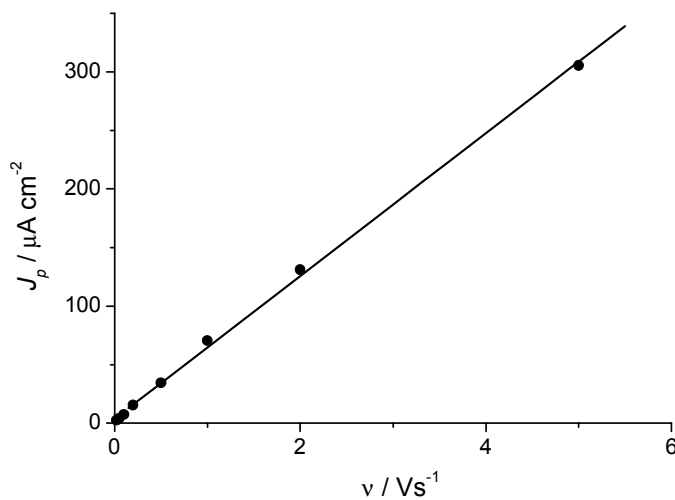


Figure S2.2 Average of absolute cathodic and anodic peak currents of adsorbed hemin as function of scan rate. Buffer: 0.1 M phosphate, 5 M NaCl, pH 7.0.

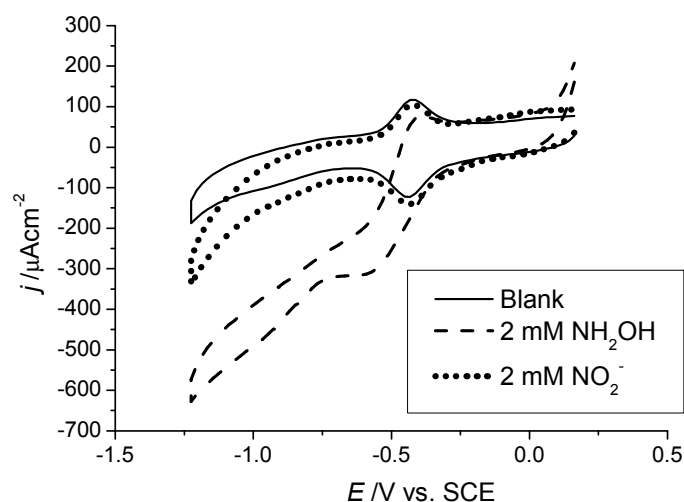


Figure S2.3 Cyclic voltammograms of adsorbed hemin in the absence (—) and presence of 1 mM $(\text{NH}_3\text{OH})_2\text{SO}_4$ (- - -) or 2 mM KNO_2 (.....). Buffer: 0.5M phosphate, pH 7.0; scan rate = 500 mV/s; 16 rps.

2.7 References

1. Averill, B. A., *Chem. Rev.* **1996**, *96*, 2951-2964.
2. Wasser, I. M.; de Vries, S.; Moeenne-Loccoz, P.; Schroeder, I.; Karlin, K. D., *Chem. Rev.* **2002**, *102*, 1201-1234.
3. de Vooy, A. C. A.; Koper, M. T. M.; van Santen, R. A.; van Veen, J. A. R., *Electrochim. Acta* **2001**, *46*, 923-930.
4. Janssen, L. J. J.; Pieterse, M. M. J.; Barendrecht, E., *Electrochim. Acta* **1977**, *22*, 27-30.
5. de Vooy, A. C. A.; Koper, M. T. M.; van Santen, R. A.; van Veen, J. A. R., *J. Catal.* **2001**, *202*, 387-394.
6. Otsuka, K.; Sawada, H.; Yamanaka, I., *J. Electrochem. Soc.* **1996**, *143*, 3491-3497.
7. Ogura, K.; Yamasaki, S., *J. Appl. Electrochem.* **1985**, *15*, 279-84.
8. Vilakazi, S. L.; Nyokong, T., *Electrochim. Acta* **2000**, *46*, 453-461.
9. Pan, K. C.; Chuang, C. S.; Cheng, S. H.; Su, Y. O., *J. Electroanal. Chem.* **2001**, *501*, 160-165.
10. Cheng, S.-H.; Su, Y. O., *Inorg. Chem.* **1994**, *33*, 5847-54.
11. Shoun, H.; Sudo, Y.; Seto, Y.; Beppu, T., *J. Biochem.* **1983**, *94*, 1219-29.
12. Daiber, A.; Nauser, T.; Takaya, N.; Kudo, T.; Weber, P.; Hultschig, C.; Shoun, H.; Ullrich, V., *J. Inorg. Biochem.* **2002**, *88*, 343-352.
13. Obayashi, E.; Tsukamoto, K.; Adachi, S.-i.; Takahashi, S.; Nomura, M.; Iizuka, T.; Shoun, H.; Shiro, Y., *J. Am. Chem. Soc.* **1997**, *119*, 7807-7816.

14. Shimizu, H.; Park, S. Y.; Lee, D. S.; Shoun, H.; Shiro, Y., *J. Inorg. Biochem.* **2000**, *81*, 191-205.
15. Kudo, T.; Takaya, N.; Park, S.-Y.; Shiro, Y.; Shoun, H., *J. Biol. Chem.* **2001**, *276*, 5020-5026.
16. Einsle, O.; Messerschmidt, A.; Huber, R.; Kroneck, P. M. H.; Neese, F., *J. Am. Chem. Soc.* **2002**, *124*, 11737-11745.
17. Armstrong, F. A., *J. Chem. Soc., Dalton. Trans.* **2002**, 661-671.
18. Leger, C.; Elliott, S. J.; Hoke, K. R.; Jeuken, L. J. C.; Jones, A. K.; Armstrong, F. A., *Biochemistry* **2003**, *42*, 8653-8662.
19. Rusling, J. F.; Nassar, A. E. F., *J. Am. Chem. Soc.* **1993**, *115*, 11891-7.
20. Nassar, A.-E. F.; Willis, W. S.; Rusling, J. F., *Anal. Chem.* **1995**, *67*, 2386-92.
21. Nassar, A.-E. F.; Bobbitt, J. M.; Stuart, J. D.; Rusling, J. F., *J. Am. Chem. Soc.* **1995**, *117*, 10986-93.
22. Lu, Z.; Huang, Q.; Rusling, J. F., *J. Electroanal. Chem.* **1997**, *423*, 59-66.
23. Bayachou, M.; Lin, R.; Cho, W.; Farmer, P. J., *J. Am. Chem. Soc.* **1998**, *120*, 9888-9893.
24. Mimica, D.; Zagal, J. H.; Bedioui, F., *Electrochem. Commun.* **2001**, *3*, 435-438.
25. Immoos, C. E.; Chou, J.; Bayachou, M.; Blair, E.; Greaves, J.; Farmer, P. J., *J. Am. Chem. Soc.* **2004**, *126*, 4934-4942.
26. Tao, N. J.; Cardenas, G.; Cunha, F.; Shi, Z., *Langmuir* **1995**, *11*, 4445-8.
27. Sagara, T.; Fukuda, M.; Nakashima, N., *J. Phys. Chem. B.* **1998**, *102*, 521-527.
28. Arifuku, F.; Mori, K.; Muratani, T.; Kurihara, H., *Bull. Chem. Soc. Jpn.* **1992**, *65*, 1491-5.
29. Shigehara, K.; Anson, F. C., *J. Phys. Chem.* **1982**, *86*, 2776-83.
30. Jiang, R.; Dong, S., *Electrochim. Acta* **1990**, *35*, 1227-32.
31. Nakashima, N.; Tokunaga, T.; Owaki, H.; Murakami, H.; Sagara, T., *Colloids Surf. A.* **2000**, *169*, 163-170.
32. Younathan, J. N.; Wood, K. S.; Meyer, T. J., *Inorg. Chem.* **1992**, *31*, 3280-5.
33. Bedioui, F.; Trevin, S.; Albin, V.; Gomez Villegas, M. G.; Devynck, J., *Anal. Chim. Acta* **1997**, *341*, 177-185.
34. Lei, J.; Ju, H.; Ikeda, O., *Electrochim. Acta* **2004**, *49*, 2453-2460.
35. Hayon, J.; Ozer, D.; Rishpon, J.; Bettelheim, A., *J. Chem. Soc., Chem. Commun.* **1994**, 619-620.
36. Bedioui, F.; Bouchier, Y.; Sorel, C.; Devynck, J.; Coche-Guerrente, L.; Deronzier, A.; Moutet, J. C., *Electrochim. Acta* **1993**, *38*, 2485-91.
37. Willsau, J.; Heitbaum, J., *J. Electroanal. Chem.* **1985**, *194*, 27-35.
38. Van der Plas, J. F.; Barendrecht, E., *Rec. Trav. Chim. Pays Bas* **1977**, *96*, 133-6.
39. Van den Brink, F.; Visscher, W.; Barendrecht, E., *J. Electroanal. Chem.* **1983**, *157*, 283-304.
40. Dean, J. A.; *Lange's Handbook of Chemistry*, 14th ed. McGraw-Hill: London, 1992; p 5.6.
41. Brown, A. P.; Koval, C.; Anson, F. C., *J. Electroanal. Chem.* **1976**, *72*, 379-87.

42. Duong, B.; Arechabaleta, R.; Tao, N. J., *J. Electroanal. Chem.* **1998**, *447*, 63-69.
43. Wonders, A. H.; Housmans, T. H. M.; Rosca, V.; Koper, M. T. M., *J. Appl. Electrochem.* **2006**, *36*, 1215-1221.
44. Pilloud, D. L.; Chen, X.; Dutton, P. L.; Moser, C. C., *J. Phys. Chem. B.* **2000**, *104*, 2868-2877.
45. Laviron, E., *J. Electroanal. Chem.* **1979**, *101*, 19-28.
46. Feng, Z. Q.; Sagara, T.; Niki, K., *Anal. Chem.* **1995**, *67*, 3564-70.
47. Hoshino, M.; Ozawa, K.; Seki, H.; Ford, P. C., *J. Am. Chem. Soc.* **1993**, *115*, 9568-75.
48. Hoshino, M.; Maeda, M.; Konishi, R.; Seki, H.; Ford, P. C., *J. Am. Chem. Soc.* **1996**, *118*, 5702-5707.
49. Rosca, V.; Beltramo, G. L.; Koper, M. T. M., *J. Electroanal. Chem.* **2004**, *566*, 53-62.
50. Bard, A. J.; Faulkner, L. R.; *Electrochemical Methods: Fundamentals and Applications*, 2 John Wiley & Sons: New York, 1980, 311-367; p 718 pp.
51. Gerischer, H.; Mauerer, A., *J. Electroanal. Chem.* **1970**, *25*, 421-33.
52. Karabinas, P.; Wolter, O.; Heitbaum, J., *Ber. Bunsen-Ges. Phys. Chem.* **1984**, *88*, 1191-6.
53. Moeller, D.; Heckner, K. H., *Z. Phys. Chem.* **1972**, *251*, 81-102.
54. Davis, D. G., *Anal. Chem.* **1963**, *35*, 764-5.
55. Vetter, K. J.; *Elektrochemische Kinetik*, Springer Verlag: Berlin, 1961; p 302-357.
56. Sulc, F.; Fleischer, E.; Farmer, P. J.; Ma, D.; La Mar, G. N., *J. Biol. Inorg. Chem.* **2003**, *8*, 348-352.
57. Sulc, F.; Immoos, C. E.; Pervitsky, D.; Farmer, P. J., *J. Am. Chem. Soc.* **2004**, *126*, 1096-1101.
58. Park, S.-Y.; Shimizu, H.; Adachi, S.-I.; Nakagawa, A.; Tanaka, I.; Nakahara, K.; Shoun, H.; Obayashi, E.; Nakamura, H.; Iizuka, T.; Shiro, Y., *Nature Struc. Biol.* **1997**, *4*, 827-832.
59. Beltramo, G. L.; Koper, M. T. M., *Langmuir* **2003**, *19*, 8907-8915.
60. Brown, W. A.; King, D. A., *J. Phys. Chem. B.* **2000**, *104*, 2578-2595.

Chapter 3

Heme release in myoglobin- DDAB films and its role in electrochemical NO reduction

This chapter consists of two parts.

*In part A myoglobin-DDAB films and their electrocatalytic behavior in NO reduction are discussed. This was published in J. Am. Chem. Soc. **2005**, 127, 16224-16232. One of the main conclusions of this part is that heme release can occur in myoglobin-DDAB films. This conclusion was challenged by Guto and Rusling in Electrochem. Commun. **2006**, 8, 455-459. They claim that heme release does not occur in myoglobin-DDAB films. As a response to this article and as a further support of the heme release hypothesis part B was written and published in Electrochem. Commun. **2006**, 8, 999-1004.*

Chapter 3A

Heme release in myoglobin- DDAB films and its role in electrochemical NO reduction*

Abstract: Electrochemical nitric oxide (NO) reduction by heme groups incorporated in films of didodecyldimethylammonium bromide (DDAB) on pyrolytic graphite was investigated. It is shown that DDAB most likely induces the release of the heme group from myoglobin and therefore myoglobin-DDAB and heme-DDAB films give the same voltammetric responses. This is confirmed by UV/Vis spectroscopy showing a clear shift in the Soret band of myoglobin in a DDAB solution. The electrochemical NO reduction on a heme-DDAB film at different pH reveals the presence of a pH dependent and a pH independent NO reduction pathway. The selectivity of these pathways is probed by combining the rotating ring disk electrode technique with on-line electrochemical mass spectroscopy showing that the product of the pH independent pathway is N₂O and the product of the pH dependent pathway is NH₂OH. The preference for one or the other pathway seems to depend on whether a proton or a NO molecule is transferred to a Fe^{II}-NO reaction intermediate and is influenced by pH, NO concentration and potential.

* The contents of this chapter have been published: de Groot, M.T.; Merckx, M.; Koper, M.T.M., *J. Am. Chem. Soc.* **2005**, *127*, 16224-16232

3A.1 Introduction

Selective reduction of nitric oxide (NO) is a challenging catalytic problem, since four stable products can be formed: nitrous oxide (N_2O), dinitrogen (N_2), hydroxylamine (NH_2OH) and ammonia (NH_3). Enzymes such as cytochrome P450nor^{1,2} are able to selectively reduce NO to N_2O , without formation of the other possible reduction products. On the other hand, on transition metals such as Pt³⁻⁵ NO reduction often leads to a combination of N_2O , NH_2OH and NH_3 . Understanding the factors that govern selectivity in NO reduction is interesting from both a fundamental and a more applied point-of-view, since developing catalysts that are selective for either one of these products would be valuable.

The study of NO reducing enzymes or their cofactors adsorbed on electrodes can provide important insights in the factors that control selectivity in NO reduction by enzymes and inorganic catalysts. In these systems the oxidation state of the enzyme or its cofactor can be directly controlled by the potential applied to the electrode. In Chapter 2 we have studied NO reduction by heme groups directly adsorbed on pyrolytic graphite (PG)⁶ and monitored its selectivity using a combination of on-line electrochemical mass spectroscopy (OLEMS)⁷ and the rotating ring disk electrode (RRDE) technique. Remarkably, NH_2OH was observed as the main reaction product and N_2O was observed only as a minor byproduct. This is in sharp contrast to the selectivity observed for NO reduction by heme proteins in films of didodecyldimethylammonium bromide (DDAB) on graphite. DDAB films have been employed in the immobilization of many heme proteins, notably myoglobin,⁸⁻²² hemoglobin,²¹⁻²⁶ catalase,²⁷ cytochrome P450cam,²⁸ cytochrome P450 CYP119,²⁹ cytochrome P450st³⁰ and cytochrome P450_{BM3}³¹ and are known to increase the electrochemical response of these proteins compared with bare electrodes. The increased electrochemical response has been ascribed to the fact that proteins are able to diffuse rapidly through the DDAB layer and to the fact that DDAB inhibits the adsorption of macromolecular adsorbates that block electron transfer.^{10,15} Selective N_2O formation has been reported for NO reduction by myoglobin⁸ and cytochrome P450 CYP119²⁹ immobilized in DDAB films. Two NO reduction pathways therefore seem possible for heme based catalysts, one leading to the formation of N_2O and another one leading to the formation of NH_2OH . Which pathway is favored apparently depends on the specific surroundings of the heme group.

In order to resolve the puzzling differences in selectivity between adsorbed heme groups and heme protein-DDAB films, we decided to study the selectivity of electrochemical NO reduction by myoglobin-DDAB and heme-DDAB films as a function of potential and pH. Comparing the voltammetric and catalytic responses of these films we noted to our surprise that no significant differences between the two systems could be discerned. An explanation for this striking similarity could be the DDAB induced release of heme from myoglobin, which would transform the myoglobin-DDAB film into a heme-DDAB film. This is discussed in the first part of this chapter. In the second part of this chapter the selectivity of electrochemical NO reduction by heme-DDAB films as a function of potential and pH is investigated employing both OLEMS

and RRDE. A new mechanism is presented that can explain our present results and is in accordance with previous results obtained with heme-protein DDAB films. This mechanism assumes a pH dependent and a pH independent route that yield NH_2OH and N_2O , respectively, via a common $\text{Fe}^{\text{II}}\text{-NO}^-$ intermediate.

3A.2 Experimental procedures

Materials. Hemin (Fluka, 98%), equine skeletal muscle myoglobin (95%-100%, Aldrich), human hemoglobin (Aldrich), horse heart cytochrome *c* (95%, Fluka), horseradish peroxidase (Fluka) and didodecyldimethylammonium bromide (DDAB, 98%, Aldrich) were all used as received. All other chemicals were p.a. grade (Merck). Pyrolytic graphite (Carbone-Lorraine) was fabricated into homemade rotating ring-disk electrodes.^{32,33} The geometric surface area of the electrodes was 0.5 cm^2 . Buffer solutions were prepared with sodium acetate (pH 4-6), sodium dihydrogen phosphate monohydrate (pH 2-3, 6-8.5, 11-12)) or boric acid (pH 8.5-10) combined with concentrated solutions of hydrochloric acid or caustic soda and Millipore MilliQ water (resistivity $>18.2 \text{ M}\Omega \text{ cm}$). The concentration of the buffer was 0.5 M in experiments involving NO, NH_2OH or NO_2^- reduction and 0.1 M in all other experiments. Prior to entering the electrochemical cell, nitric oxide (purity 2.5, Linde AG) was bubbled through two washing flasks filled with a 3 M KOH solution, a procedure that was found to be important in order to remove NO_2 .^{4,32} Purging the solution with NO for 10 min resulted in a saturated NO solution, which corresponds to a concentration of 2 mM as can be calculated from the Henry's Law constant of $2.0 \times 10^{-3} \text{ mol atm}^{-1}$ at $21 \text{ }^\circ\text{C}$.³⁴

Electrochemical Apparatus and Procedures. An Autolab PGstat 20 potentiostat was used for cyclic voltammetry. A homemade three-electrode cell consisting of a platinum flag counter electrode, a $\text{Hg|Hg}_2\text{SO}_4$ or Ag|AgCl reference electrode, and a rotating ring disk electrode was used. All potentials in this chapter are relative to the standard calomel electrode (SCE). The rotating ring disk electrode consisted of a pyrolytic graphite (PG) disk and a Pt ring. Experiments with rotation were conducted using a Motomatic motor generator. All solutions were deaerated by purging with argon for 10 min. All electrochemical experiments were performed at room temperature ($21 \pm 2 \text{ }^\circ\text{C}$).

Preparation of protein-DDAB and heme-DDAB films. Protein-DDAB and heme-DDAB solutions were prepared by mixing 0.5 mM protein in a 0.01 M acetate solution (pH 5) or 0.5 mM hemin in a 0.01 M borate solution (pH 10) with an equal volume of 0.01 M DDAB in a 0.1 M acetate solution (pH 5). The DDAB suspension was prepared by ultrasonication for 3 hours. Prior to use, the PG electrodes were abraded using $40 \mu\text{m}$ Al_2O_3 sandpaper and ultrasonicated in Millipore MilliQ water for 5 min. The electrode was dried in a N_2 stream for 10 s. Subsequently, $5 \mu\text{l}$ of the heme/protein-DDAB solution was applied to the electrode. The electrode was dried for approximately 15 min in air, after which it was used for electrochemical experiments. Film preparation techniques, which differ from this technique, were also employed to determine their influence on the voltammetric response of the film. The differences of these techniques compared to the

technique described here will be listed in the corresponding figure captions. In some cases myoglobin filtered through an YM30 filter (Amicon, 30000 MW cutoff) was used for these films.

UV/Vis spectroscopy. UV/Vis spectroscopy was performed on a Shimadzu Multispec-1501. Heme-DDAB and protein-DDAB solutions were incubated overnight using the same conditions that were used for preparing the films on PG. To allow accurate absorbance measurements, the solutions were diluted to a heme/protein concentration of 10 μM just before measuring.

Rotating ring-disk electrode (RRDE) experiments. Rotating ring disk electrodes were constructed as described previously^{32,33} and have a collection efficiency of 0.27 ± 0.03 . Prior to the measurements the Pt ring was abraded together with the PG disk on 40 μm Al_2O_3 sandpaper and a protein-DDAB or heme-DDAB film was cast onto it. To remove the film the Pt ring was cleaned by electro-polishing: alternately a potential in the hydrogen evolution region (-0.8 V versus SCE) and a potential in the oxygen evolution region (1.5 V versus SCE) were applied for 5 s, a procedure which was repeated 25 times.

On-line electrochemical mass spectrometry (OLEMS). OLEMS measurements were performed on a Balzers Prisma QMS 200 mass spectrometer. The connection between the mass spectrometer and the cell was established through a steel capillary connected to a glass tube onto which a porous Teflon tip was attached. This tip was placed at approximately 10 μm from the electrode surface. The electrode could not be rotated and hence NO was continuously bubbled through solution to enhance NO mass transfer. Baseline values measured in a solution without NO were subtracted in NO reduction experiments. A more detailed description of the setup has been published elsewhere.^{6,7}

3A.3 Results

Comparison of myoglobin-DDAB and heme-DDAB films. Figure 3A.1 shows the voltammetric responses of a film cast from a myoglobin-DDAB solution and of a film cast from a heme-DDAB solution. The responses of both films resemble each other in the similarity of their peak potentials and their comparable peak sizes, which is surprising considering the differences between a large protein molecule and a small heme group. The results suggest that the peaks in both films are caused by the same species, namely a heme group in a DDAB environment. In the Mb-DDAB film this species could be formed by dissociation of the heme group from myoglobin.

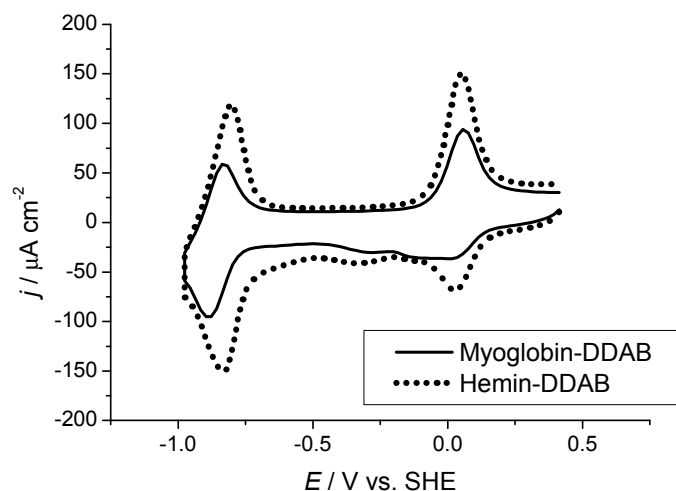


Figure 3A.1 Cyclic voltammogram of a film cast from a solution of myoglobin-DDAB in 0.1 M sodium acetate pH 5 (—) as compared to a film cast from a solution of heme-DDAB in 0.1 M sodium acetate pH 5 (.....). Films were cast on PG and were measured in 0.1 M phosphate, pH 7.0, at a scan rate of 500 mV/s.

No evidence indicating that the similarity of the Mb-DDAB film to the heme-DDAB film is a result of our particular film preparation technique was found. Results reported in the literature on differently prepared Mb-DDAB films^{8,14,21,22,28} show similar peak potentials and peak sizes. To ensure that the film preparation technique does not have a significant effect on the voltammetric response we employed different film preparation techniques with differences in protein purification (Figure S3A.1), salt concentration (Figure 3A.4, below), pH (Figure S3A.2), solution equilibration time (Figure S3A.1) and film drying time. Apart from some differences in peak size, all films yielded a similar voltammetric response, suggesting that none of these parameters has a significant influence on the nature of the Mb-DDAB film.

The peaks in the voltammograms are due to different redox couples of the heme group. The redox couple at $E = -0.21$ V versus SCE corresponds to the $\text{Fe}^{\text{III}}/\text{Fe}^{\text{II}}$ transition of the heme group and the redox couple at $E = -1.12$ V versus SCE has been tentatively assigned to the $\text{Fe}^{\text{II}}/\text{Fe}^{\text{I}}$ transition of the heme group.¹⁴ The $\text{Fe}^{\text{III}}/\text{Fe}^{\text{II}}$ transition is partly irreversible, which could be related to a potential-induced phase transition occurring in the DDAB film, which has been observed with AFM.¹⁷ Interestingly, the transition becomes more reversible with increasing scan rate and at a scan rate of 5 V/s the couple is reversible.

To investigate further the similarities between myoglobin-DDAB and heme-DDAB films, we determined the midpoint potential of the $\text{Fe}^{\text{III}}/\text{Fe}^{\text{II}}$ couple as a function of pH (Figure 3A.2a) and performed electrocatalytic reduction of NO and NO_2^- (Figure 3A.2b-c) on both films. The pH dependence of the midpoint potential is identical for both films

and in agreement with a previous study on myoglobin-DDAB films.¹⁹ Both films also exhibit similar electrocatalytic behavior in both NO and NO₂⁻ reduction.^{16,21} The lower activity in NO₂⁻ reduction for a myoglobin-DDAB film can be explained by the lower heme coverage of a myoglobin-DDAB film as compared to a heme-DDAB film (Figure 3A.1). For NO reduction this lower heme coverage does not significantly affect the catalytic wave, since NO reduction is limited by NO mass transfer. These results confirm that both films are very similar and therefore again strongly suggest that the voltammetric peaks are caused by the same species. Since it is known that DDAB forms vesicles in aqueous solution,¹⁰ this species probably consists of a heme group incorporated in a DDAB vesicle, which can be formed after DDAB induced heme release from the protein.

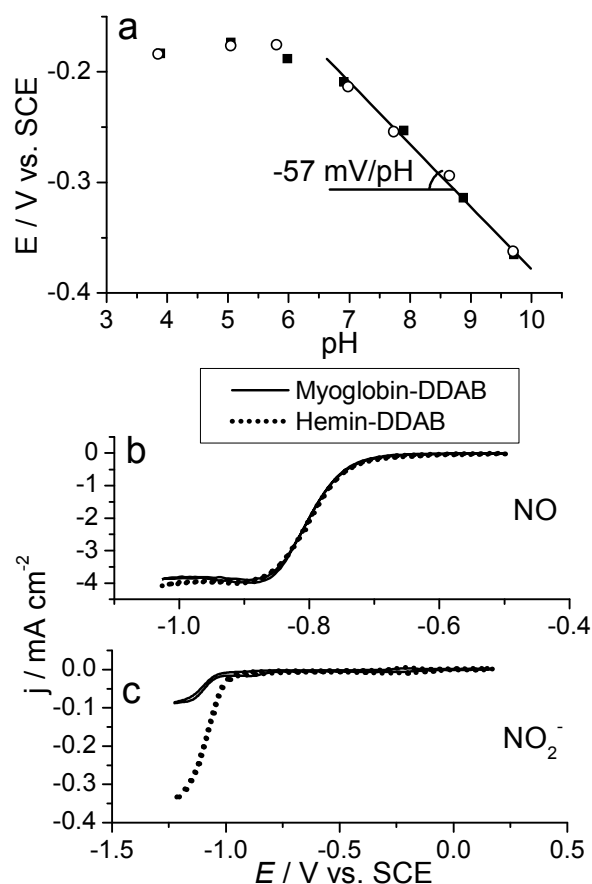


Figure 3A.2 (a): pH dependence of midpoint potentials of redox peaks of a myoglobin-DDAB film (○) as compared to a heme-DDAB film (■). Measurements were performed in 0.1 M acetate (pH 4.0-6.0), phosphate (pH 6.0-8.5) or borate (pH 8.5-10.5) at a scan rate of 500 mV/s. (b) and (c): Cyclic voltammograms of a myoglobin-DDAB film (—) and a heme-DDAB film (·····) in 0.5 M sodium acetate, pH 5.0, saturated with NO (b) and in 2 mM KNO₂ in 0.5 M phosphate, pH 7.0 (c). Measurements were performed at a scan rate of 50 mV/s and a rotation rate of 16 rps.

Spectroscopic evidence for DDAB induced heme release from myoglobin can be obtained by collecting UV/Vis spectra of myoglobin-DDAB and heme-DDAB solutions that were allowed to stand overnight at pH 5. Figure 3A.3 shows that the Soret band of a myoglobin-DDAB solution is decreased and shifted (from 409 to 395 nm) as compared to a myoglobin solution without DDAB. The UV/Vis spectrum of a heme-DDAB solution is similar to the UV/Vis spectrum of a myoglobin-DDAB solution showing the Soret (~395 nm), Q (~569 nm) and CT1 (~600 nm) bands at similar wavelengths, which suggests that the species in both solutions are equivalent. This species most likely is a heme group in a micellar environment, since similar wavelengths were found for the Soret, Q and CT1 bands of heme groups incorporated in cetyltrimethylammonium (CTAB) (400, 576 nm and 600 nm) and Triton X-100 (398, 576 nm and 600 nm) micelles.^{35,36} In the case of DDAB this micellar environment probably does not consist of micelles, but of vesicles.³⁷ These results show that DDAB can induce heme release from myoglobin and therefore support our voltammetric results.

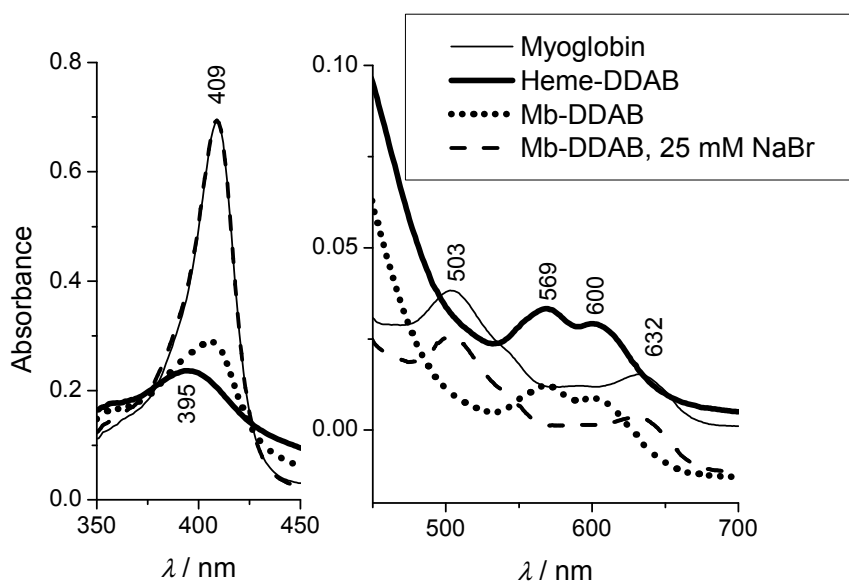


Figure 3A.3 UV/Vis spectra of solutions of myoglobin (—), heme-DDAB (—), myoglobin-DDAB (.....) and myoglobin-DDAB with 25 mM NaBr (- - -) solution after overnight incubation at 4 °C in 0.1 M sodium acetate pH 5.5, 0.25 mM myoglobin/heme, and 5 mM DDAB. Solutions were diluted 1:50 in 0.1 M sodium acetate pH 5.5 immediately before UV/Vis measurement.

Our UV/Vis spectra also show that no shift of the Soret band occurs for a myoglobin-DDAB solution if 25 mM NaBr is present. Apparently the presence of salt prevents the release of heme from myoglobin in solution. This stabilizing effect of salt has also been observed for Mb-DDAB films cast on quartz and glass^{8,13-15,24,27}. Interestingly, the

voltammetric response of a myoglobin-DDAB film on graphite cast from a solution with salt does not significantly differ from a myoglobin-DDAB film on graphite cast from a solution without salt (Figure 3A.4) or a heme-DDAB film on graphite. In our view it is unlikely that native myoglobin and heme give such similar voltammetric peaks in a DDAB film and therefore we think that the graphite surface is able to enhance the DDAB induced release of heme from myoglobin. Unfortunately, we cannot prove this with spectroscopic evidence, since pyrolytic graphite strongly adsorbs light, which makes it difficult to perform UV/Vis or other forms of spectroscopy.

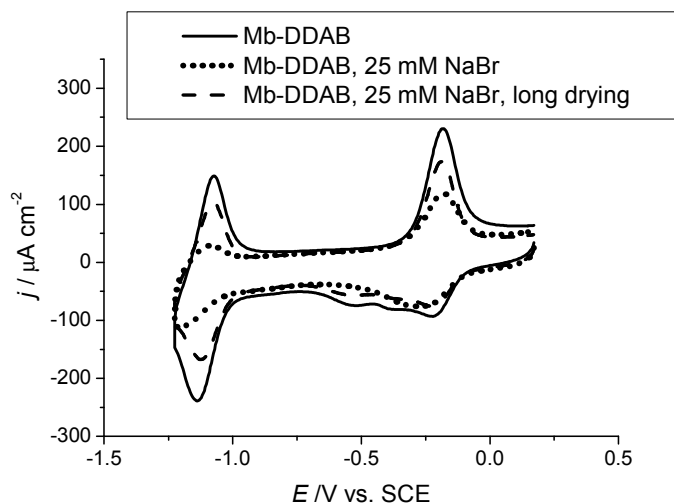


Figure 3A.4 Cyclic voltammograms of myoglobin-DDAB films prepared according to the procedure described in the experimental section (—), prepared using a Mb-DDAB solution of pH 5.5 with 25 mM NaBr (.....) and prepared using a Mb-DDAB solution of pH 5.5 with 25 mM NaBr and slow overnight drying (- - -). Films were cast on PG that was abraded using 40 μm Al_2O_3 sandpaper and were measured in 0.1 M phosphate pH 7.0, at a scan rate of 500 mV/s.

Increasing the pH of the myoglobin-DDAB solution gives an effect similar to the effect of salt. At pH 7 the UV/Vis spectrum of the solution does not exhibit a shift in the Soret band, even in the absence of salt (Figure S3A.2a). This shows that the DDAB induced release of heme also depends on the pH of the solution. Nevertheless, on graphite the voltammetric response of the film is very similar to a heme-DDAB film (Figure S3A.2b), which again suggests that the peaks are caused by heme groups, the release of which is enhanced by the graphite surface. Interestingly, there is a strong influence of film drying time on the height of the peaks. A short drying time results in only small peaks, whereas a long drying time results in peak sizes similar to a film cast from a pH 5 solution. This effect could be explained in terms of a relatively slow process in which graphite enhances the DDAB induced release of heme. Short drying times abruptly abort this process, since the process cannot occur in dry films. This can explain

why a similar effect of drying time was observed for a film cast from a pH 5.5 solution with salt (Figure 3A.4), but was not observed for a film cast from a pH 5.5 solution without salt (for which heme is already released in solution).

In order to investigate whether our findings also apply to other heme proteins, we also studied the voltammetric responses of hemoglobin-DDAB, cytochrome *c*-DDAB and horseradish peroxidase-DDAB films (Figure 3A.5). Voltammetric peaks for the hemoglobin-DDAB film were found at similar potentials as for the myoglobin-DDAB and heme-DDAB films, which suggests that DDAB induced heme release occurs for hemoglobin. For cytochrome *c* and horseradish peroxidase (HRP) the peaks are much smaller. This suggests that DDAB induced heme release does not readily occur for cytochrome *c* and HRP. A plausible reason for this is that the heme group is more tightly bound to the protein in HRP and cytochrome *c* than in myoglobin and hemoglobin.³⁸ UV/Vis spectra for solutions of myoglobin, HRP and cytochrome *c* in the presence of DDAB indeed show that cytochrome *c* and HRP are not affected by DDAB, whereas hemoglobin is (Figure S3A.3).

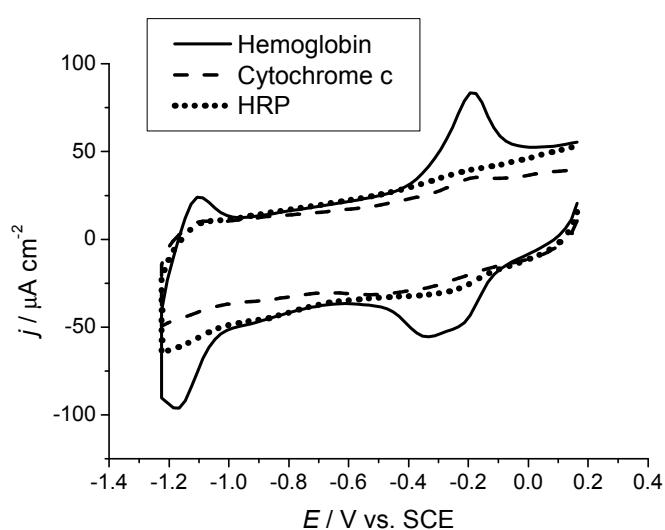


Figure 3A.5 Cyclic voltammograms of a hemoglobin-DDAB film (—), a cytochrome *c*-DDAB film (- -) and a HRP-DDAB film (·····). Films were cast on PG from protein-DDAB acetate solutions of pH 5. Measurements were performed in 0.1 M phosphate, pH 7.0, at a scan rate of 500 mV/s.

NO reduction by heme-DDAB films. Given the similarity in voltammetric response between myoglobin-DDAB and heme-DDAB films, it is remarkable that N_2O formation has previously been reported for NO reduction by myoglobin-DDAB films and NH_2OH formation for NO reduction by heme directly adsorbed to pyrolytic graphite. To understand the influence of the DDAB vesicles on the selectivity, we investigated NO reduction by heme-DDAB films as a function of pH and potential. Figure 3A.6 shows the

NO reduction waves for a heme-DDAB film at different pH's. The data suggest the presence of two NO reduction pathways, which can most clearly be discerned from the measurement performed at pH 10.2. At this pH reduction of NO starts around $E = -0.7$ V versus SCE, after which a plateau is reached between -0.9 V and -1.0 V. A second NO reduction wave starts at $E = -1.05$ V, after which another plateau is reached. These NO reduction waves can be assigned to different pathways of NO reduction, which we will refer to as pathway I and pathway II, respectively. Pathway I starts around $E = -0.7$ V and is pH independent. Pathway II, on the other hand, is clearly pH dependent: at high pHs it is not observed at all and with decreasing pH, it shifts to less negative potentials. Pathway I may therefore be referred to as the pH independent pathway and pathway II as the pH dependent pathway.

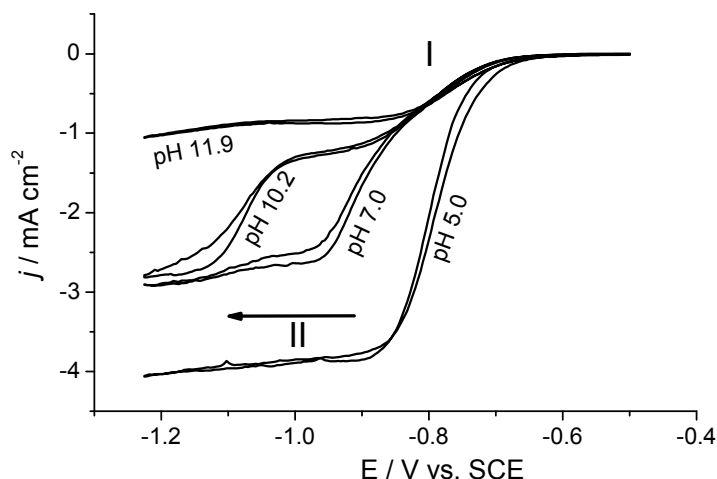


Figure 3A.6 Cyclic voltammograms of a heme-DDAB film in 0.5 M acetate, pH 5.0, 0.5 M phosphate, pH 7.0, 0.5 M borate, pH 10.2 and 0.5 M phosphate, pH 11.9. Measurements were performed in saturated NO solution at a scan rate of 50 mV/s and a rotation rate of 16 rps.

The voltammetry also suggests that the pH independent pathway and the pH dependent pathway have a different selectivity in NO reduction. The dependence of current on rotation rate (Figure S3A.4) shows that the plateau currents are limited by NO mass transfer. The plateau currents for the pH dependent pathway are considerably higher than for the pH independent pathway, which implies that more electrons are involved in the pH dependent pathway than in the pH independent pathway. The small differences between plateau currents at the different pH's can be explained by the dependence of the NO diffusion coefficient on the composition of the buffer solution.

The products of both pathways were determined employing on-line electrochemical mass spectroscopy (OLEMS)⁷ and the rotating ring disk electrode (RRDE),³⁹ techniques that can determine selectivity *in situ*. Since our voltammetric results suggested a strong

influence of pH on the selectivity of NO reduction, OLEMS measurements were performed at different pHs. As was shown previously, the OLEMS setup is able to detect the formation of very small amounts of N_2O and since the cell is purged with argon, CO_2 from air does not interfere with N_2O detection.⁷ Figure 3A.7 shows the ion current intensity for $m/z = 44$ (N_2O) as a function of potential at different pHs. The voltammetric response and the ion current intensity for $m/z = 30$ (NO) that were recorded simultaneously can be found in Figure S3A.5. Even though the electrode could not be rotated, the observed voltammetric response at different pHs is similar to Figure 3A.6. Figure 3A.7 shows that the amount of N_2O produced increases with increasing pH. At pH 5.1 N_2O is only produced at the start of the NO reduction and not during continuous NO reduction at lower potentials. Apparently, at these lower potentials N_2O is not a reaction product. On the other hand, at pH 11.9 N_2O is observed at all potentials. When the pH independent pathway is dominant in voltammetry, N_2O is observed in the OLEMS measurements. When the pH dependent pathway becomes dominant, N_2O is no longer observed. This suggests that N_2O is the product of the pH independent NO reduction pathway. The product of the pH dependent pathway cannot be determined using OLEMS. The formation of N_2 ($m/z = 28$) was not observed and NH_2OH and NH_3 are difficult to observe with OLEMS, because they are not gaseous and their fragmentation products have ion current intensities close to those of water.

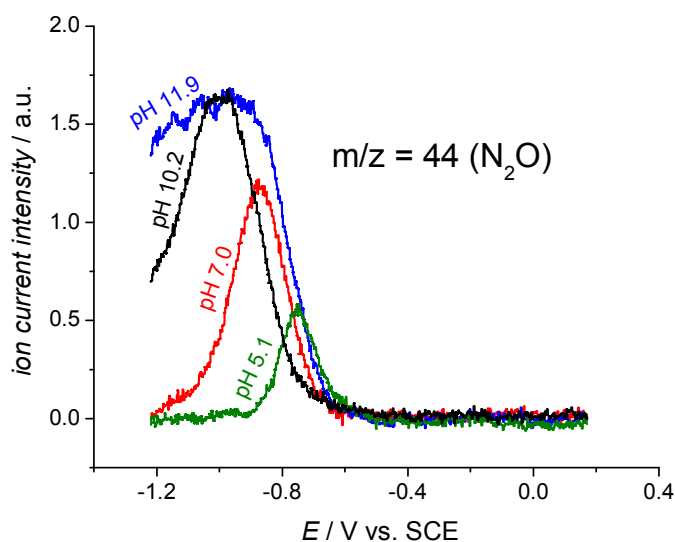


Figure 3A.7 OLEMS measurements on a heme-DDAB film in saturated NO solution at 2 mV/s. The ion current intensity for $m/z = 44$ (N_2O) in the cathodic scan is plotted as a function of potential. Films were cast on PG and measurements were performed in 0.5 M acetate, pH 5.1 (—), 0.5 M phosphate, pH 7.0 (—), 0.5 M borate, pH 10.2 (—) and 0.5 M phosphate, pH 11.9 (—). Measurements were performed under continuous NO bubbling through the solution. Recorded current and ion current intensity for $m/z = 30$ (NO) can be found in Figure S3A.5.

RRDE was employed to detect the product of the pH dependent pathway. In order to use the Pt ring for selectivity measurements, the voltammetric responses of the possible products (NH_2OH and NH_3) and of the reactant (NO) on Pt have to be determined. Figure 3A.8a shows that NH_2OH and NO can be easily distinguished by their respective oxidation and reduction waves. NH_3 oxidation on the Pt ring is negligible in comparison to NH_2OH oxidation. The voltammetric response of the Pt ring was determined during NO reduction on the heme-DDAB disk at $E_d = -0.93$ V and $E_d = -1.13$ V (Figure 3A.8b). The measurements were performed at pH 10.2, which implies that at $E_d = -0.93$ V only the pH independent pathway occurs, whereas at $E_d = -1.13$ V the pH dependent pathway also occurs. For $E_d = -0.93$ V a decrease of approximately 0.14 mA was observed in the NO reduction wave on the ring, while the current on the disk was -0.51 mA. It is known that on Pt NO is reduced via a one electron process to N_2O^4 and combined with the collection efficiency of 0.27 ± 0.03 previously reported for this electrode^{32,33} this confirms that the pH independent pathway also occurs via a one electron process. Hence N_2O is the product, which is in agreement with the OLEMS results. No NH_2OH oxidation wave was observed on the ring, which confirms that NH_2OH is not a product of the pH independent pathway. It also shows that N_2O cannot be oxidized on the Pt ring at potentials between 0 and 0.3 V versus SCE. At $E_d = -1.13$ V a clear NH_2OH oxidation wave is observed. This suggests that NH_2OH is the main product of the pH dependent pathway. Since at $E_d = -1.13$ V part of the NO is probably still reduced by the pH independent pathway, no quantitative information can be derived. RRDE measurements at different pH's strongly suggest that NH_2OH is the product of the pH dependent pathway (Figure S3A.6). At lower pH's, for which the pH dependent pathway starts at less negative potentials, an increase in the NH_2OH oxidation wave on the ring is observed already at $E_d = -0.93$ V. At high pH, for which the pH dependent mechanism is not observed in voltammetry, no NH_2OH oxidation wave is observed, even not at $E_d = -1.13$ V. A comparison to Figure 3A.6 shows that NH_2OH formation has a pH dependence similar to the pH dependent pathway, suggesting that NH_2OH is the product of the pH dependent pathway.

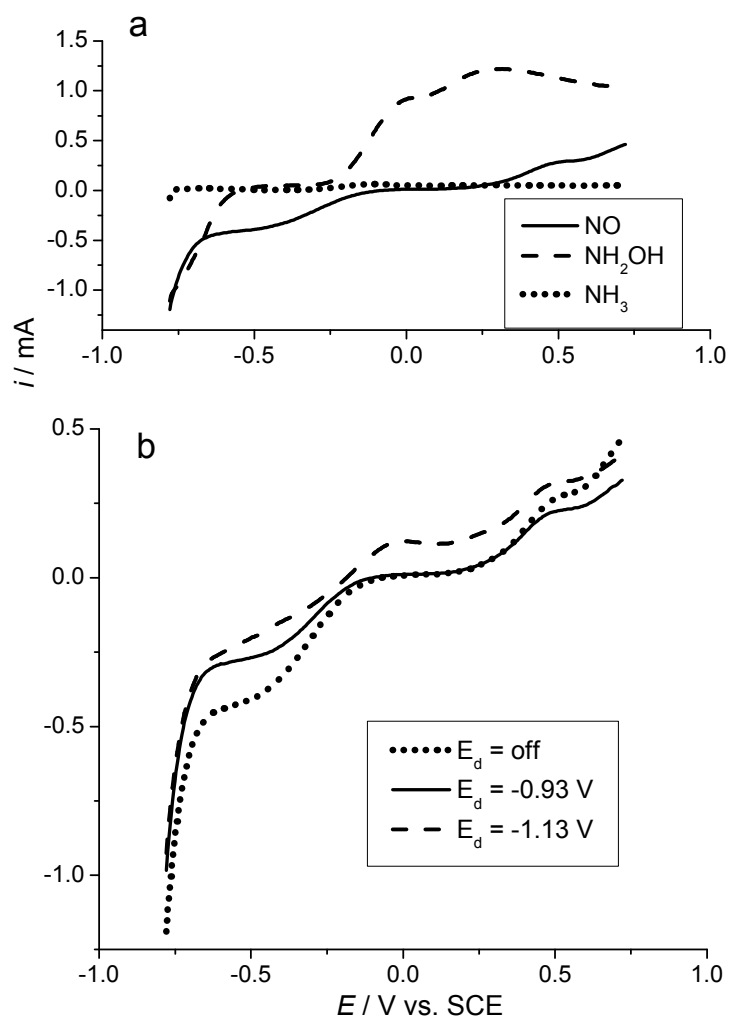


Figure 3A.8 (a) anodic scans of a Pt ring in saturated NO solution (—), 1 mM $(\text{NH}_2\text{OH})_2\text{SO}_4$ (- -), and 2 mM NH_4Cl (.....). (b) anodic scans of a Pt ring in saturated NO solution without a potential applied to the heme-DDAB disk (.....), with a potential of -0.93 V applied to the heme-DDAB disk (—) and, with a potential of -1.13 V applied to the heme-DDAB disk (- -). Measurements were performed in 0.5 M borate, pH 10.2 at a scan rate of 50 mV/s and a rotation rate of 16 rps. The recorded current on the heme-DDAB disk was -0.51 mA at $E_d = -0.93$ V and -1.1 mA at $E_d = -1.13$ V.

Neither OLEMS nor RRDE can detect the formation of NH_3 , when NH_2OH is also formed. To deduce whether NH_2OH can react further to form NH_3 , the electrochemical reduction of NH_2OH by heme-DDAB films was investigated. Since no reduction of NH_2OH was observed (Figure S3A.7), N-O bond breaking by heme-DDAB films

appears to be very sluggish, making it unlikely that NH_3 is a product in NO reduction by heme-DDAB films. This is in accordance with our previous study of NO reduction by adsorbed heme groups, in which we deduced that the selectivity toward NH_2OH was 100% for a pathway with a similar pH dependence.⁶

It is known that for NO reduction on metals, N_2O formation only occurs with NO present in solution.^{3,4} To investigate whether this is also the case for a heme-DDAB film, so-called NO “stripping” experiments were performed by reducing the Fe^{II} -NO adduct of the heme-DDAB film without NO present in solution. This Fe^{II} -NO adduct was formed by performing continuous NO reduction on the heme-DDAB film electrode for a short time (5 s), and subsequently transporting it to a buffer solution without NO. Figure 3A.9 shows that NO stripping of the heme-DDAB film starts at more negative potentials than continuous NO reduction. The area under the stripping peak is $4.7 \times 10^{-10} \text{ mol cm}^{-2}$ which corresponds to 2.6 electrons per heme group and implies that NH_2OH is the main product. The fact that NH_2OH and not N_2O is the product suggests that NO is stripped by the pH dependent pathway. Apparently the pH independent pathway does not occur without NO present in solution similar to NO stripping on Pt, in which N_2O is also not observed.⁴⁰ The absence of the pH independent pathway also explains why the NO stripping peak starts at more negative potentials than continuous NO reduction.

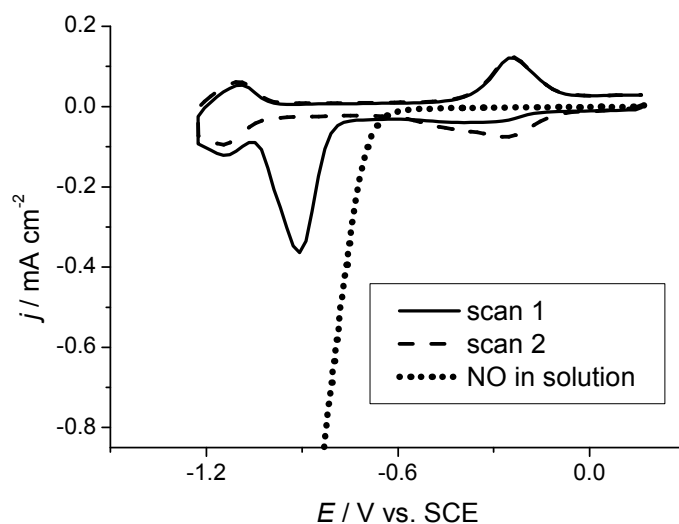


Figure 3A.9 NO stripping voltammetry of a heme-DDAB film, scan 1 (—) and scan 2 (- -), as compared to continuous NO reduction by a heme-DDAB film (.....). Measurements were performed in 0.5 M phosphate, pH 7.0 at scan rate of 500 mV/s.

The fact that the two NO reduction pathways result in the formation of two different products makes it interesting to study their respective mechanisms in more detail. Tafel slopes³⁹ were determined for both pathways by plotting the absolute currents measured in

cyclic voltammetry on a logarithmic scale (Figure 3A.10). The Tafel slope for the pH dependent pathway was determined at pH 2.5 to minimize the influence of the pH independent pathway and the Tafel slope of the pH independent pathway was determined at pH 13.7 to minimize the influence of the pH dependent pathway. Figure 3A.10 shows that the pH dependent pathway has a Tafel slope of -59 mV/dec. A similar Tafel slope was previously observed for NO reduction by heme groups directly adsorbed on PG.⁶ The Tafel slope of the pH independent pathway is -108 mV/dec, which is reasonably close to -118 mV/dec and therefore can be interpreted in terms of a mechanism in which an electrochemical step is rate-determining.⁴¹

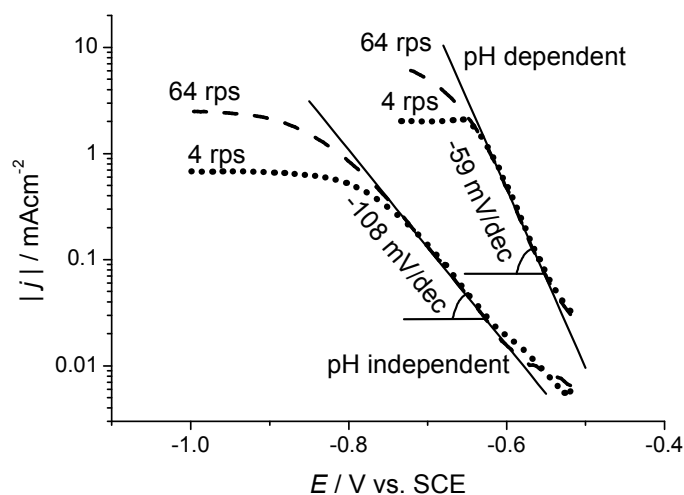


Figure 3A.10 Absolute current density plotted on a logarithmic scale as a function of potential for NO reduction by a heme-DDAB film. The Tafel slope of the pH dependent pathway (right) was determined in 0.5 M phosphate, pH 2.5, at 64 rps (---) and 4 rps (.....). The Tafel slope of the pH independent pathway (left) was determined in 0.5 M KOH, pH 13.7, at 64 rps (---) and 4 rps (.....). Plots are deduced from cathodic scans of cyclic voltammograms. Measurements were performed in saturated NO solution at a scan rate of 50 mV/s.

The Tafel slope of -59 mV/dec observed for the pH dependent pathway suggests the presence of an electrochemical equilibrium prior to the rate-determining step (EC-mechanism).⁴¹ This electrochemical equilibrium could be a redox couple involving the nitrosyl (NO) to nitroxyl (NO⁻) transformation as was observed before.⁸ We tried to detect the reversible peaks of such a redox couple by scanning at high scan rates to minimize NO reduction. At low pH we were unable to find a reversible couple for scan rates up to 50 V/s, which implies that the nitroxyl state is very unstable in acidic media. At high pH, however, a redox couple could clearly be observed for NO reduction by the heme-DDAB film (Figure S3A.8). The midpoint potential of this redox couple is

independent of pH and its value of $E = -0.91$ V versus SCE is in reasonable agreement with the value of $E = -0.87$ V reported by Bayachou et al.⁸

3A.4 Discussion and conclusions

Two main conclusions can be drawn from our study of myoglobin-DDAB and heme-DDAB films and their catalytic activity for NO reduction. Firstly, immobilization of myoglobin and hemoglobin-DDAB films on pyrolytic graphite induces the release of heme resulting in the formation of heme-DDAB vesicles. Secondly, NO reduction by these heme-DDAB vesicles can proceed via a pH dependent and a pH independent pathway, resulting in the formation of NH_2OH and N_2O , respectively.

Our conclusion that DDAB induces release of heme in myoglobin-DDAB films is based on (i) the similar voltammetric peaks observed for myoglobin-DDAB and heme-DDAB films, (ii) the similar pH dependence of the E_m of the $\text{Fe}^{\text{III}}/\text{Fe}^{\text{II}}$ couple for the heme-DDAB and myoglobin-DDAB films, (iii) the similar catalytic response in NO reduction for myoglobin-DDAB and heme-DDAB films, (iv) the shift in wavelength of the Soret band for myoglobin in a DDAB solution and the similar wavelengths observed for the Soret, Q and CT1 bands for a myoglobin-DDAB solution as compared to a heme-DDAB solution, and (v) the observation that the voltammetric peaks are much smaller for DDAB films of heme proteins such as cytochrome *c* and HRP, in which the heme group is more tightly bound to the protein.

Various other studies also showed that interactions between surfactants and myoglobin can induce the release of heme groups⁴²⁻⁴⁴ resulting in the incorporation of the heme groups in micelles.⁴³ In addition, it is known that heme groups incorporated in micelles can exhibit a strong voltammetric response.⁴⁵⁻⁴⁷ Furthermore, similar redox potentials for the $\text{Fe}^{\text{III}}/\text{Fe}^{\text{II}}$ couple have been reported for different heme proteins incorporated in DDAB films²¹ and often these potentials do not correspond to the redox potentials of the proteins in solution.²⁸ In addition, the charge under the voltammetric peaks corresponds to more than one protein monolayer, which combined with the fact that the peaks are reversible up to scan rates of more than 100 mV/s^{23,28} would suggest an almost improbably fast protein diffusion within the DDAB layer.

Our results indicate that the use of UV/Vis spectroscopy on films cast on quartz or glass can sometimes be insufficient to determine whether the voltammetric peaks observed are caused by the native protein. A valuable extra control experiment is the comparison of the voltammetric response of the protein incorporated in the film to the voltammetric response of the cofactor incorporated in the same film. This control experiment is not only useful for heme proteins in DDAB films, but might also be of value for heme proteins incorporated in other films.⁴⁸⁻⁵³

Our results show two NO reduction pathways on heme-DDAB films: a pH independent pathway resulting in the formation of N_2O and a pH dependent pathway resulting in the formation of NH_2OH . Although it is tempting to relate the pH dependent pathway to the possible $\text{Fe}^{\text{II}}/\text{Fe}^{\text{I}}$ couple, the potential of this $\text{Fe}^{\text{II}}/\text{Fe}^{\text{I}}$ couple is independent

of pH (data not shown) and therefore this is unlikely. Therefore we postulate different mechanisms for both pathways in Figure 3A.11 based on their products and the observed Tafel slopes. For the pH independent pathway the Tafel slope of -108 mV/dec suggests that the first electron transfer is rate determining. Most likely this is the reduction of the $\text{Fe}^{\text{II}}\text{-NO}$ adduct formed by reaction of $\text{Fe}^{\text{II}}\text{-heme}$ with NO. Since the pathway is pH independent, a proton transfer is not involved in this step and hence $\text{Fe}^{\text{II}}\text{-NO}^-$ must be the product. However, a change in rate-determining step might occur at lower NO concentrations and under conditions where NO mass transfer is rate limiting. In these cases the reaction of the $\text{Fe}^{\text{II}}\text{-NO}^-$ adduct with NO might become rate determining. Such a change in rate-determining step would explain why the $\text{Fe}^{\text{II}}\text{-NO}/\text{Fe}^{\text{II}}\text{-NO}^-$ couple can be observed at high scan rates at high pH. A similar change of rate-determining step with NO concentration has also been reported for the enzyme cytochrome P450nor.¹ For the pH dependent pathway the Tafel slope of -59 mV/dec suggests an electrochemical equilibrium followed by a chemical rate-determining step. The electrochemical equilibrium could be the $\text{Fe}^{\text{II}}\text{-NO}/\text{Fe}^{\text{II}}\text{-NO}^-$ couple and the chemical rate-determining step that follows might be the proton transfer that results in the formation of $\text{Fe}\text{-HNO}$. This is supported by the pH dependence of the pathway. Based on this mechanism, one would expect to be able to observe a $\text{Fe}^{\text{II}}\text{-NO}/\text{Fe}^{\text{II}}\text{-NO}^-$ couple at high scan rates. Unfortunately, our maximum scan rate (1000 V/s) was too slow to observe the couple. This suggests that even though the proton transfer is rate determining, it is still very rapid at low pHs.

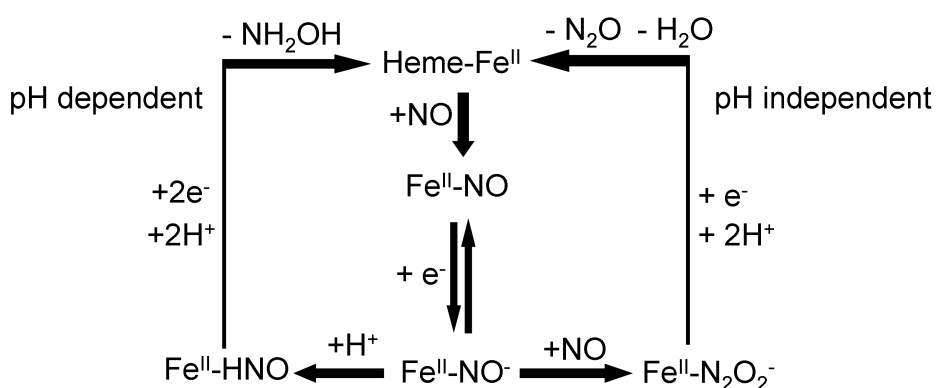


Figure 3A.11. Mechanisms of the two pathways for NO reduction observed for a heme-DDAB film casted on PG.

Figure 3A.11 suggests that there are three factors that govern which NO reduction pathway occurs. These are the pH of the solution, which determines whether a proton transfer occurs to the $\text{Fe}^{\text{II}}\text{-NO}^-$ adduct, the NO concentration in solution, which determines the rate of the reaction of the $\text{Fe}^{\text{II}}\text{-NO}^-$ adduct with NO and the potential of the electrode, which determines the concentration of the $\text{Fe}^{\text{II}}\text{-NO}^-$ adduct. Even though the $\text{Fe}^{\text{II}}\text{-NO}^-$ adduct is an intermediate in both pathways, an increase in the concentration

of the $\text{Fe}^{\text{II}}\text{-NO}^-$ adduct can result in a change from the pH independent pathway to the pH dependent pathway under conditions where the reaction is limited by NO mass transfer.

An attractive feature of the mechanisms we propose for NO reduction by heme-DDAB films is that they can explain the results for NO reduction by myoglobin-DDAB films obtained by other groups.^{8,26} We consider this as another confirmation of our conclusion that myoglobin-DDAB films and heme-DDAB films are equivalent. Previous studies on myoglobin-DDAB films show a similar interpretation of results in terms of the pH independent pathway, but they could not clearly explain certain parts of the results, which we would now ascribe to the pH dependent pathway. Firstly, it was observed in these studies that the reversible $\text{Fe}^{\text{II}}\text{-NO}/\text{Fe}^{\text{II}}\text{-NO}^-$ couple could only be found at high pHs and that the lifetime of the $\text{Fe}^{\text{II}}\text{-NO}^-$ adduct decreases with pH.⁸ We can now ascribe this to the fact that the $\text{Fe}^{\text{II}}\text{-NO}^-$ adduct reacts further to NH_2OH . Secondly, a second NO reduction wave was also observed in previous studies.²⁶ This peak was ascribed to a second electron transfer, but we can now readily ascribe it to the pH dependent pathway. The fact that NH_2OH was not previously reported as a product in NO reduction by a protein-DDAB film⁸ is probably due to the fact that the electrolysis experiments in which the selectivity of the reaction was determined were performed at a potential where the pH independent pathway dominates.

The presence of two different NO reduction pathways has also been observed for heme enzymes. The cytochrome P450nor selectively reduces NO to N_2O ¹, whereas the cytochrome *c'* nitrite reductase⁵⁴ selectively reduces nitrite to NH_3 . Although the substrate of cytochrome *c'* nitrite reductase is nitrite instead of NO, the reaction occurs via a heme-NO intermediate similar to NO reduction by the cytochrome P450nor. The different selectivity of both enzymes therefore confirms that there are at least two pathways in heme-NO reduction.

The two different pathways can also explain the remarkable difference in selectivity previously reported for NO reduction by adsorbed heme (NH_2OH) as compared to NO reduction by heme protein-DDAB films (N_2O). For the heme-DDAB film our results demonstrate that NO reduction does not necessarily result in the formation of N_2O , but can also result in the formation of NH_2OH . For adsorbed heme we previously reported NH_2OH as the main product, but we did observe N_2O as a minor byproduct.⁶ This suggests that in both systems the two NO reduction pathways presented in Figure 3A.11 can occur. However, both systems are also distinctly different. At pH 7 the amount of N_2O we observed for a heme-DDAB film is more than ten times larger than the amount of N_2O reported previously for adsorbed heme. This suggests that the specific surroundings of the heme group influence important parameters such as the potential of the $\text{Fe}^{\text{II}}\text{-NO}/\text{Fe}^{\text{II}}\text{-NO}^-$ couple, the rate of protonation of the $\text{Fe}^{\text{II}}\text{-NO}^-$ intermediate, and the local NO concentration (which has been suggested to be higher in DDAB films than in aqueous buffer solutions⁸), parameters that determine the preference for one or the other pathway.

3A.5 Supporting Information

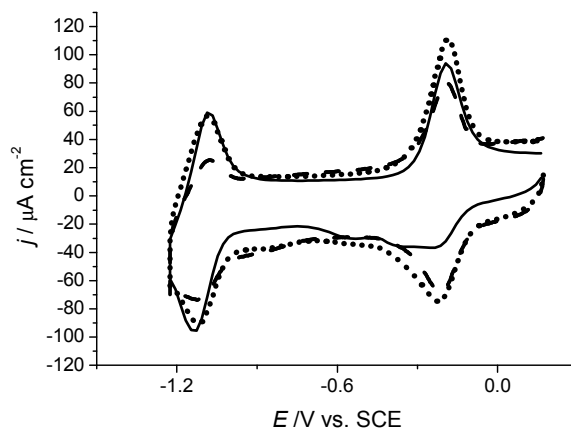


Figure S3A.1 Cyclic voltammograms of myoglobin-DDAB films prepared according to the procedure described in the experimental section (—), prepared using 25 μl of a fresh solution of DDAB and filtered myoglobin (.....) and prepared using using 25 μl of a fresh solution of DDAB and filtered myoglobin with slow overnight drying (- - -). Films were cast on PG that was abraded using 40 mm Al_2O_3 sandpaper and were measured in 0.1 M phosphate pH 7.0, at a scan rate of 500 mV/s.

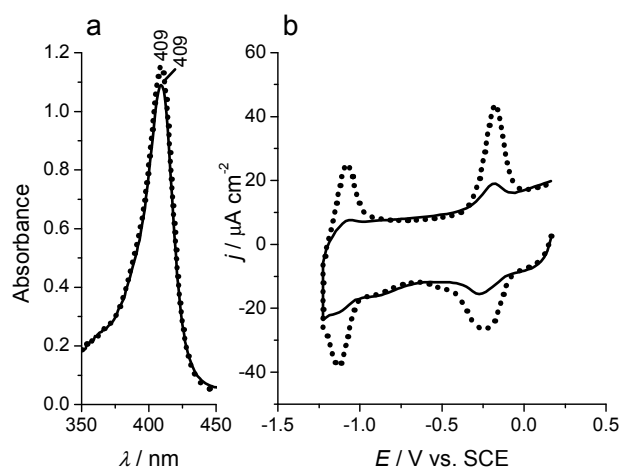


Figure S3A.2 (a): UV/Vis spectra of a myoglobin (.....) and a myoglobin-DDAB (—) solution after overnight incubation at 4 $^{\circ}\text{C}$ in 0.1 M phosphate pH 7.0, 0.25 mM myoglobin/heme, and 2 mM DDAB. Solutions were diluted 1:25 in 0.1 M sodium acetate pH 7.0 immediately before UV/Vis measurement. (b): Cyclic voltammograms of a film cast from a myoglobin-DDAB phosphate solution of pH 7 that was dried over a period of 15 min (—) as compared to a film that was dried over a period of 2 hours (.....). Films were cast on PG and were measured in 0.1 M phosphate, pH 7.0, at a scan rate of 500 mV/s.

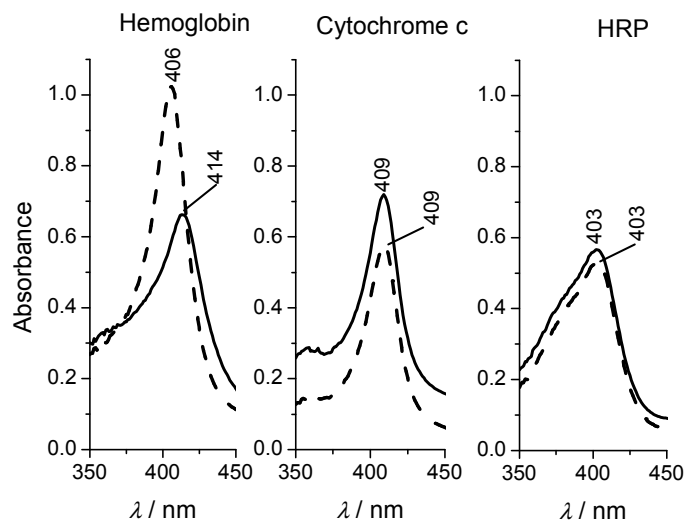


Figure S3A.3 UV/VIS spectra of hemoglobin, cytochrome *c* and horse radish peroxidase in the absence (---) and presence of 5 mM DDAB (—) after incubation overnight at 4 °C in 0.1 M sodium acetate, pH 5.0. Protein concentration: 0.25 mM. Solutions were diluted 1:25 in 0.1 M sodium acetate pH 5.0 immediately before UV/VIS measurement.

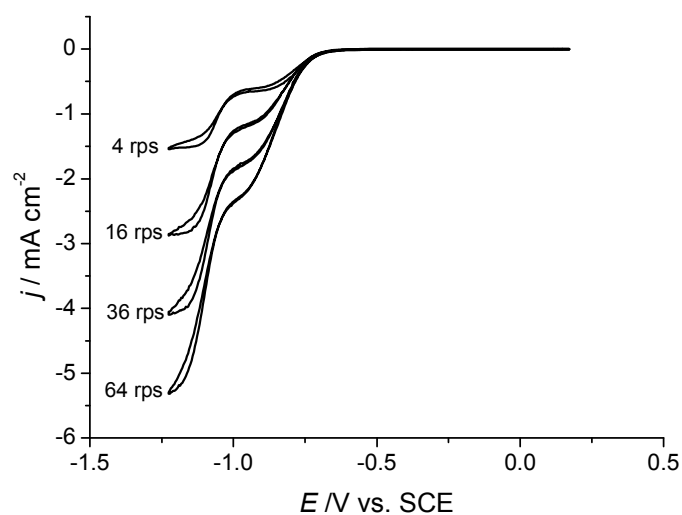


Figure S3A.4 Cyclic voltammograms of a hemin-DDAB film in 0.5 M borate, pH 10.2, at a rotation rate of 4 rps, 16 rps, 36 rps, and 64 rps. Measurements were performed in saturated NO solution at a scan rate of 50 mV/s.

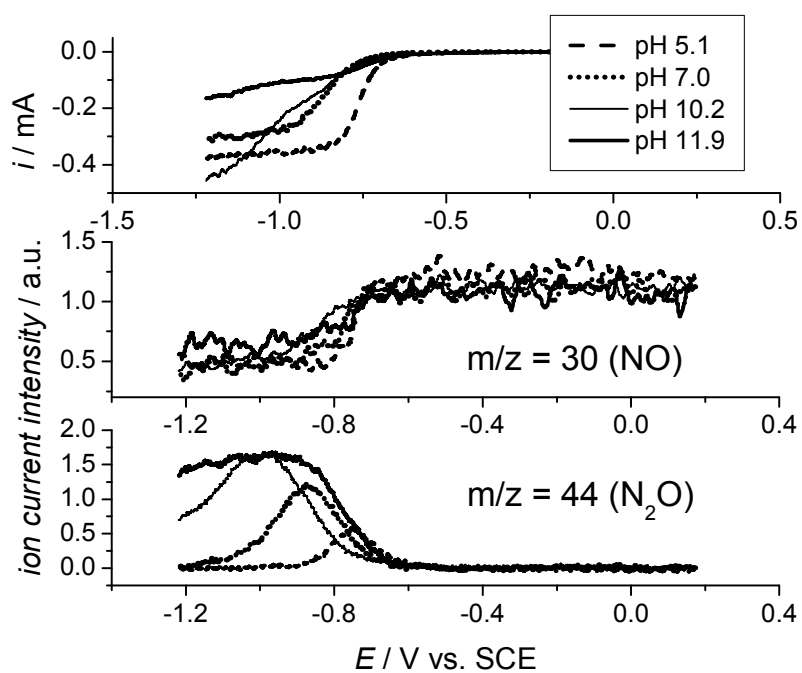


Figure S3A.5 OLEMS measurements on a heme-DDAB film in saturated NO solution at 2 mV/s. The voltammetric response, the ion current intensity for $m/z = 30$ (NO), and the ion current intensity for $m/z = 44$ (N_2O) recorded in the cathodic scan are plotted as a function of potential. Films were cast on PG and measurements were performed in 0.5 M acetate, pH 5.1 (---), 0.5 M phosphate, pH 7.0 (.....), 0.5 M borate, pH 10.2 (—) and 0.5 M phosphate, pH 11.9 (—). Measurements were performed under continuous NO bubbling through the solution.

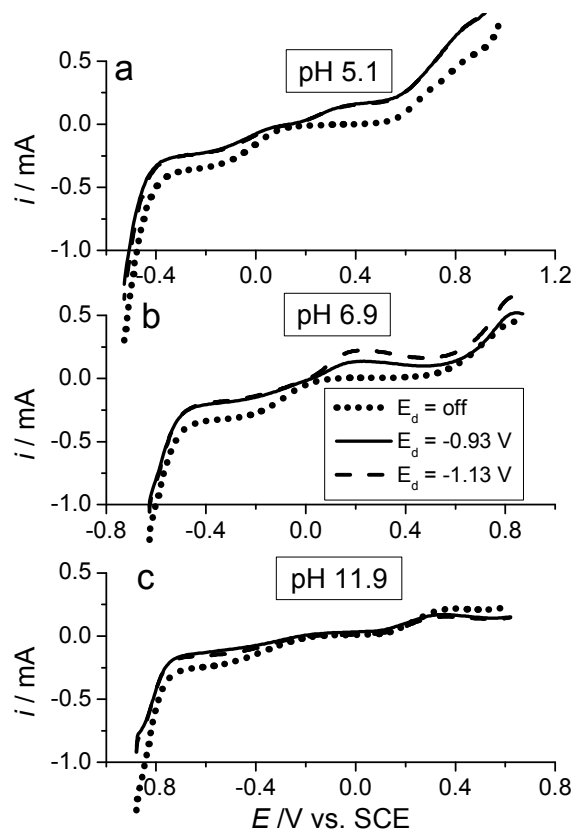


Figure S3A.6 anodic scans of a Pt ring in saturated NO solution without a potential applied to the heme-DDAB disk (.....), with a potential of -0.93 V applied to the heme-DDAB disk (—) and, with a potential of -1.13 V applied to the heme-DDAB disk (- - -) in 0.5 M acetate, pH 5.1 (a), in 0.5 M phosphate, pH 6.9 (b) and in 0.5 M phosphate pH 11.9 (c). Measurements were performed at a scan rate of 50 mV/s and a rotation rate of 16 rps. For pH 5.1 the cathodic scan was taken instead of the anodic scan, since NH_2OH oxidation is partly inhibited in the anodic scan.

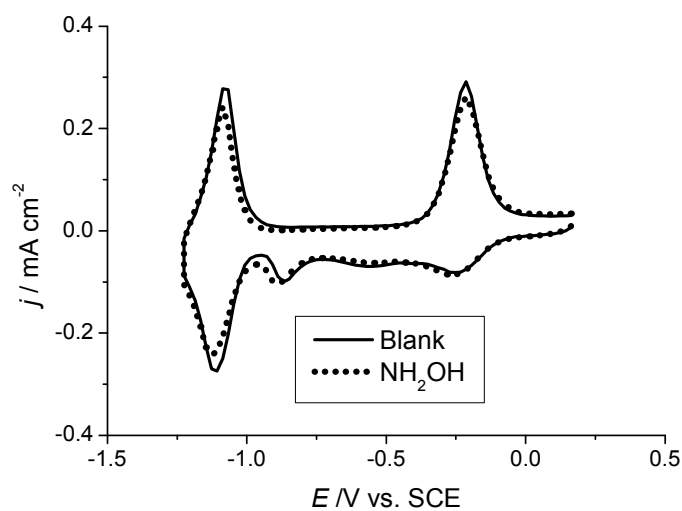


Figure S3A.7 Cyclic voltammograms of a heme-DDAB film in the absence (—) and presence of 1 mM $(\text{NH}_3\text{OH})_2\text{SO}_4$ (.....). Measurements were performed in 0.5 M phosphate, pH 7.0, at a scan rate of 500 mV/s and a rotation rate of 16 rps.

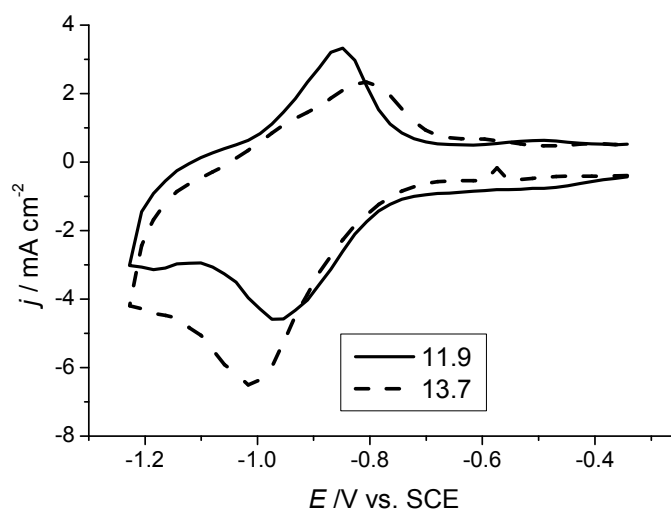


Figure S3A.8 Cyclic voltammograms of a heme-DDAB film in 0.5 M phosphate, pH 11.9 (—), and 0.5 M KOH, pH 13.7 (- - -) showing the existence of a $[\text{Fe-NO}]^{2+}/[\text{Fe-NO}]^+$ redox couple. Measurements were performed in saturated NO solution at a scan rate of 10 V/s.

3A.6 References

1. Daiber, A.; Nauser, T.; Takaya, N.; Kudo, T.; Weber, P.; Hultschig, C.; Shoun, H.; Ullrich, V., *J. Inorg. Biochem.* **2002**, *88*, 343-352.
2. Obayashi, E.; Tsukamoto, K.; Adachi, S.-i.; Takahashi, S.; Nomura, M.; Iizuka, T.; Shoun, H.; Shiro, Y., *J. Am. Chem. Soc.* **1997**, *119*, 7807-7816.
3. de Vooys, A. C. A.; Beltramo, G. L.; van Riet, B.; van Veen, J. A. R.; Koper, M. T. M., *Electrochim. Acta* **2004**, *49*, 1307-1314.
4. de Vooys, A. C. A.; Koper, M. T. M.; van Santen, R. A.; van Veen, J. A. R., *J. Catal.* **2001**, *202*, 387-394.
5. Janssen, L. J. J.; Pieterse, M. M. J.; Barendrecht, E., *Electrochim. Acta* **1977**, *22*, 27-30.
6. de Groot, M. T.; Merckx, M.; Koper, M. T. M., *J. Am. Chem. Soc.* **2005**, *127*, 7579-7586.
7. Wonders, A. H.; Housmans, T. H. M.; Rosca, V.; Koper, M. T. M., *Journal of Applied Electrochemistry* **2006**, *36*, 1215-1221.
8. Bayachou, M.; Lin, R.; Cho, W.; Farmer, P. J., *Journal of the American Chemical Society* **1998**, *120*, 9888-9893.
9. Nassar, A.-E. F.; Zhang, Z.; Hu, N.; Rusling, J. F.; Kumosinski, T. F., *J. Phys. Chem. B* **1997**, *101*, 2224-2231.
10. Nassar, A.-E. F.; Willis, W. S.; Rusling, J. F., *Anal. Chem.* **1995**, *67*, 2386-92.
11. Nassar, A.-E. F.; Zhang, Z.; Chynwat, V.; Frank, H. A.; Rusling, J. F.; Suga, K., *J. Phys. Chem.* **1995**, *99*, 11013-17.
12. Nassar, A.-E. F.; Rusling, J. F.; Kumosinski, T. F., *Biophys. Chem.* **1997**, *67*, 107-116.
13. Nassar, A.-E. F.; Narikiyo, Y.; Sagara, T.; Nakashima, N.; Rusling, J. F., *J. Chem. Soc., Faraday Trans.* **1995**, *91*, 1775-82.
14. Nassar, A.-E. F.; Bobbitt, J. M.; Stuart, J. D.; Rusling, J. F., *Journal of the American Chemical Society* **1995**, *117*, 10986-93.
15. Rusling, J. F.; Nassar, A. E. F., *J. Am. Chem. Soc.* **1993**, *115*, 11891-7.
16. Lin, R.; Bayachou, M.; Greaves, J.; Farmer, P. J., *J. Am. Chem. Soc.* **1997**, *119*, 12689-12690.
17. Boussaad, S.; Tao, N. J., *J. Am. Chem. Soc.* **1999**, *121*, 4510-4515.
18. Bayachou, M.; Elkbir, L.; Farmer, P. J., *Inorg. Chem.* **2000**, *39*, 289-293.
19. Chen, S.-M.; Tseng, C.-C., *J. Electroanal. Chem.* **2005**, *575*, 147-160.
20. Chen, S.-M.; Tseng, C.-C., *Electrochim. Acta* **2004**, *49*, 1903-1914.
21. Mimica, D.; Zagal, J. H.; Bedioui, F., *J. Electroanal. Chem.* **2001**, *497*, 106-113.
22. Alatorre Ordaz, A.; Bedioui, F., *Sens. Actuators, B* **1999**, *B59*, 128-133.
23. Lu, Z.; Huang, Q.; Rusling, J. F., *J. Electroanal. Chem.* **1997**, *423*, 59-66.
24. Chen, X.; Hu, N.; Zeng, Y.; Rusling, J. F.; Yang, J., *Langmuir* **1999**, *15*, 7022-7030.
25. Mimica, D.; Ringuede, A.; Agurto, C.; Bedioui, F.; Zagal, J., *Electroanal.* **2004**, *16*, 1632-1636.
26. Mimica, D.; Zagal, J. H.; Bedioui, F., *Electrochem. Comm.* **2001**, *3*, 435-438.

27. Chen, X.; Xie, H.; Kong, J.; Deng, J., *Biosens. Bioelectron.* **2001**, *16*, 115-120.
28. Zhang, Z.; Nassar, A.-E. F.; Lu, Z.; Schenkman, J. B.; Rusling, J. F., *J. Chem. Soc., Faraday Trans.* **1997**, *93*, 1769-1774.
29. Immoos, C. E.; Chou, J.; Bayachou, M.; Blair, E.; Greaves, J.; Farmer, P. J., *J. Am. Chem. Soc.* **2004**, *126*, 4934-4942.
30. Oku, Y.; Ohtaki, A.; Kamitori, S.; Nakamura, N.; Yohda, M.; Ohno, H.; Kawarabayasi, Y., *J. Inorg. Biochem.* **2004**, *98*, 1194-1199.
31. Fleming, B. D.; Tian, Y.; Bell, S. G.; Wong, L.-L.; Urlacher, V.; Hill, H. A. O., *Eur. J. Biochem.* **2003**, *270*, 4082-4088.
32. Van den Brink, F.; Visscher, W.; Barendrecht, E., *J. Electroanal. Chem.* **1983**, *157*, 283-304.
33. Van der Plas, J. F.; Barendrecht, E., *Rec. Trav. Chim. Pays Bas* **1977**, *96*, 133-6.
34. Dean, J. A.; Ed.; *Lange's Handbook of Chemistry*, 14 McGraw-Hill: London, 1992; p 5.6.
35. Shantha, P. K.; Saini, G. S. S.; Thanga, H. H.; Verma, A. L., *J. Raman Spectrosc.* **2001**, *32*, 159-165.
36. Shantha, P. K.; Saini, G. S. S.; Thanga, H. H.; Verma, A. L., *J. Raman Spectrosc.* **2003**, *34*, 315-321.
37. Hamachi, I.; Honda, T.; Noda, S.; Kunitake, T., *Chem. Lett.* **1991**, 1121-4.
38. Messerschmidt, A.; Huber, R.; Wieghardt, K.; Poulos, T.; *Handbook of Metalloproteins*, John Wiley & Sons: Chichester, 2001; Vol. 1; p.
39. Bard, A. J.; Faulkner, L. R., *Electrochemical Methods: Fundamentals and Applications*, 2 ed.; John Wiley & Sons: New York, 1980; pp 311-367.
40. de Vooy, A. C. A.; Koper, M. T. M.; van Santen, R. A.; van Veen, J. A. R., *Electrochimica Acta* **2001**, *46*, 923-930.
41. Vetter, K. J., *Elektrochemische Kinetik*. In *Elektrochemische Kinetik*, Springer Verlag: Berlin, 1961; pp 302-357.
42. Blauer, G.; Harmatz, D.; Zvilichovsky, B., *FEBS Lett.* **1973**, *34*, 344-6.
43. Kanti Das, T.; Mazumdar, S.; Mitra, S., *Journal of the Chemical Society, Chemical Communications* **1993**, 1447-8.
44. Tofani, L.; Feis, A.; Snoke, R. E.; Berti, D.; Baglioni, P.; Smulevich, G., *Biophys. J.* **2004**, *87*, 1186-1195.
45. Das, D. K.; Bhattaray, C.; Medhi, O. K., *J. Chem. Soc., Dalton Trans.* **1997**, 4713-4718.
46. Das, D. K.; Medhi, O. K., *J. Chem. Soc., Dalton Trans.* **1998**, 1693-1698.
47. Das, D. K.; Medhi, O. K., *J. Inorg. Biochem.* **1998**, *70*, 83-90.
48. Liu, X.; Zhang, W.; Huang, Y.; Li, G., *J. Biotechnol.* **2004**, *108*, 145-152.
49. Wang, Q.; Lu, G.; Yang, B., *Langmuir* **2004**, *20*, 1342-1347.
50. Nadzhafova, O. Y.; Zaitsev, V. N.; Drozdova, M. V.; Vaze, A.; Rusling, J. F., *Electrochem. Comm.* **2004**, *6*, 205-209.
51. Huang, H.; He, P.; Hu, N.; Zeng, Y., *Bioelectrochem.* **2003**, *61*, 29-38.
52. Shen, L.; Huang, R.; Hu, N., *Talanta* **2002**, *56*, 1131-1139.

53. Tang, J.; Jiang, J.; Song, Y.; Peng, Z.; Wu, Z.; Dong, S.; Wang, E., *Chem. Phys. Lipids* **2002**, *120*, 119-129.
54. Einsle, O.; Messerschmidt, A.; Huber, R.; Kroneck, P. M. H.; Neese, F., *J. Am. Chem. Soc.* **2002**, *124*, 11737-11745.

Chapter 3B

Additional evidence for heme release in myoglobin-DDAB films on pyrolytic graphite*

Abstract: *In Chapter IIIA¹ we claimed that heme release can occur in myoglobin-DDAB films under certain conditions. Our conclusion was based on the similar voltammetric response and electrocatalytic behavior of myoglobin-DDAB and heme-DDAB films. Our findings were challenged by Guto and Rusling,² who claim that heme release does not occur in the pH 5-7 range. In this chapter we present additional evidence for our heme release hypothesis and comment on the points put forward by Guto and Rusling. Firstly, we show that the UV/Vis spectrum of a myoglobin-DDAB solution is virtually identical to that of a heme-DDAB solution. Secondly, we show that the presence of apomyoglobin can explain the small differences in voltammetric response between a heme-DDAB and a Mb-DDAB film. Thirdly, we show that the electron transfer rate properties of Mb-DDAB and heme-DDAB films are similar. The thin layer behavior observed in these experiments cannot be rationalized for intact myoglobin. All these results are in concordance with our heme release hypothesis.*

* The contents of this chapter have been published: de Groot, M.T.; Merckx, M.; Koper, M.T.M., *Electrochem. Commun.* **2006**, 8, 999-1004

3B.1 Introduction

Over the last fifteen years DDAB films have been employed in the electrochemical study of various heme proteins.³⁻⁹ In Chapter IIIA¹ we compared myoglobin-DDAB films to heme-DDAB films on pyrolytic graphite and noticed remarkable similarities between these films. From our experiments we ultimately concluded that heme release occurs in myoglobin-DDAB films on graphite. We based this conclusion on the following arguments:

- The voltammetric responses for myoglobin-DDAB films and heme-DDAB films on PG are similar.
- The pH dependence of the midpoint potential of a myoglobin-DDAB film is identical to the pH dependence of a heme-DDAB film over a pH range of 3-10.
- The electrocatalytic properties of both films towards NO and NO₂⁻ reduction are essentially identical. In both cases, we observe selective reduction of NO to hydroxylamine at low pH and to nitrous oxide at high pH. Also, the observed potential dependencies (Tafel slope etc.) are identical for both films.
- The UV/Vis spectrum of a myoglobin-DDAB solution of pH 5.5 in the absence of NaBr is very similar to the UV/Vis spectrum of a heme-DDAB solution.
- Much smaller voltammetric signals were observed for other heme proteins such as cytochrome *c* and HRP, in which the heme group is more tightly bound to the protein. Consistent with this observation, UV/Vis experiments showed no shift in Soret bands for these proteins in DDAB solution.

The literature shows that surfactants are indeed able to induce the release of heme from myoglobin,¹⁰⁻¹² resulting in the incorporation of these heme groups in micelles.¹¹ It is also known that heme groups incorporated in micelles can exhibit a strong voltammetric response.¹³⁻¹⁵

In our view the above findings provide sufficient evidence to conclude that heme release can occur in myoglobin-DDAB films. However, our conclusions were challenged by Guto and Rusling in a recent communication.² They claim that heme release does not occur in myoglobin-DDAB films and solutions in the pH 5-7 range under any condition, substantiating their claim by providing additional evidence, on which we will comment in this chapter. To further underscore our own heme release hypothesis we present additional spectroscopic measurements on myoglobin-DDAB solutions and additional electrochemical measurements on myoglobin-DDAB films.

3B.2 Experimental

Materials. Hemin (Fluka, 98%), equine skeletal muscle myoglobin (95%-100%, Aldrich), equine skeletal muscle apomyoglobin (Sigma), horseradish peroxidase (Fluka) and didodecyldimethylammonium bromide (DDAB, 98%, Aldrich) were all used as received. All other chemicals were p.a. grade (Merck). Pyrolytic graphite (Carbone-

Lorraine) was fabricated into homemade rotating disk electrodes. The geometric surface area of the electrodes was 0.5 cm². Buffer solutions were prepared with sodium acetate (pH 4-6), sodium dihydrogen phosphate monohydrate (pH 2-3, 6-8.5, 11-12)) or boric acid (pH 8.5-10) combined with concentrated solutions of hydrochloric acid or caustic soda and Millipore MilliQ water (resistivity >18.2 MΩ cm).

Electrochemical Apparatus and Procedures. An Autolab PGstat 20 potentiostat was used for cyclic voltammetry. A homemade three-electrode cell consisting of a platinum flag counter electrode, a Hg|Hg₂SO₄ reference electrode, and a rotating ring disk electrode was used. All potentials in this chapter are relative to the standard calomel electrode (SCE). All solutions were deaerated by purging with argon for 10 min. All electrochemical experiments were performed at room temperature (21 ± 2 °C).

Preparation of protein-DDAB and heme-DDAB films. Protein-DDAB and heme-DDAB solutions were prepared by mixing 0.5 mM protein in a 0.01 M acetate solution (pH 5) or 0.5 mM hemin in a 0.01 M borate solution (pH 10) with an equal volume of 0.01 M DDAB in a 0.1 M acetate solution (pH 5). The DDAB suspension was prepared by ultrasonication for 3 hours. Prior to use, the PG electrodes were abraded using 40 μm Al₂O₃ sandpaper and ultrasonicated in Millipore MilliQ water for 5 min. The electrode was dried in a N₂ stream for 10 s. Subsequently, 5 μl of the heme/protein-DDAB solution was applied to the electrode. The electrode was dried for approximately 15 min in air, after which it was used for electrochemical experiments.

UV/Vis spectroscopy. UV/Vis spectroscopy was performed on a Shimadzu Multispec-1501. Heme-DDAB and protein-DDAB solutions were incubated for a certain time to allow equilibration of the solution. To allow accurate absorbance measurements, the solutions were diluted to a heme/protein concentration of 10 μM just before measuring.

3B.3 Results and discussion

The effect of DDAB on myoglobin in solution as evidenced by UV/Vis spectroscopy. In chapter IIIA we observed that the UV/Vis spectrum of a myoglobin-DDAB solution of pH 5.5 was practically identical to that of a heme-DDAB solutions. In our view this indicated that heme was released from myoglobin. On the other hand, Guto and Rusling claim that UV/Vis spectroscopy of myoglobin-DDAB solutions shows that the Soret band is always at 409 nm. They did observe shifts in the Q and CT1 bands of myoglobin-DDAB solutions, but these shifts were reversible upon the addition of salt. In their view such reversibility excludes the possibility of heme release from myoglobin and hence myoglobin would stay in a near-native state.

We have not been able to reproduce Guto and Rusling's observation that the Soret band always remains at 409 nm. Figure 3B.1 shows that in our experiments the Soret band of a myoglobin-DDAB solution of pH 5 shifts to a wavelength of 396 nm. The entire spectrum is essentially identical to that of a heme-DDAB solution of pH 5, which implies that the heme group in the myoglobin-DDAB solution is in the same

environment as in the heme-DDAB solution. A straightforward explanation for this observation is heme release from the protein. For a myoglobin-DDAB solution of pH 6 the situation is different. The Soret band has decreased in intensity, but can still be found at 409 nm. We also see several CT1 and Q bands. This suggests that both native and heme-released myoglobin are present in solution. Results at this pH are similar to the results published by Guto and Rusling, which were measured at the same pH.² This shows that the pH of the solution has a strong effect on the heme-release process as we already stated in chapter IIIA.¹ In Chapter IIIA measurements were performed at pH 5.5, and the Soret band was found at 406 nm, which is indicative of the presence of a small amount of native myoglobin.

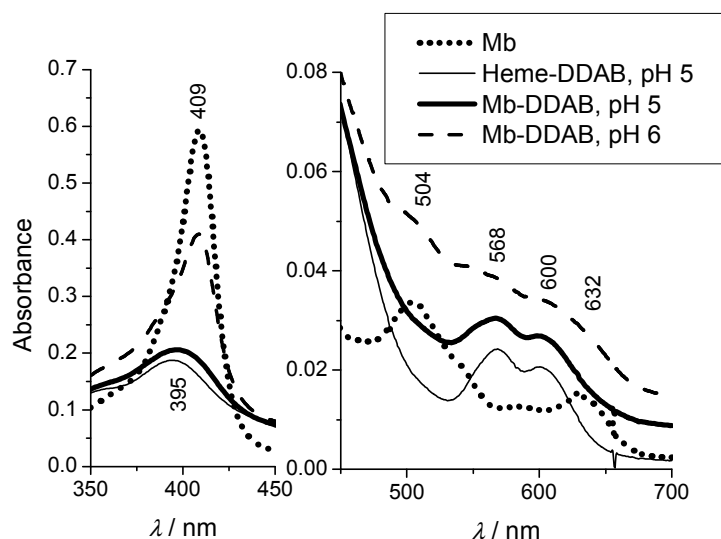


Figure 3B.1 UV/Vis spectra of myoglobin (.....), myoglobin-DDAB (—) and heme-DDAB (—) after 1.5 hour incubation at 4 °C in 0.05 M sodium acetate pH 5.0, using 0.25 mM myoglobin/hemin, and 5 mM DDAB. Another myoglobin-DDAB solution was incubated at pH 6.0 (- - -). Solutions were diluted 1:50 in 0.01 M sodium acetate pH 5.0 immediately before UV/Vis measurement.

It was argued by Guto and Rusling that the observed reversibility in the shifts of the Q and CT1 bands upon the addition of salt would exclude the possibility of heme release. However, it is known from the literature that heme can recombine with apomyoglobin to form myoglobin.¹⁶⁻¹⁹ The addition of salt can be the driving force to trigger this recombination. This is shown in Figure 3B.2 where we have added apomyoglobin to a heme-DDAB solution and subsequently added salt. For the solution without salt, the presence of apomyoglobin does not significantly change the spectrum compared to a heme-DDAB solution, which indicates that under these conditions the heme released state is thermodynamically the most stable. However, upon the addition of salt the Soret, Q and CT1 bands start to shift resulting in a spectrum that is similar to that of

myoglobin. This indicates that the addition of salt makes heme-recombined myoglobin the thermodynamically most stable state. These results confirm the observations in Chapter IIIA that salt is able to stabilize myoglobin and also show that heme release is reversible. We do not claim that myoglobin unfolds or denatures, since heme release does not have to be accompanied by unfolding of apomyoglobin.^{20,21} The presence of apomyoglobin in a native conformation can explain why circular dichroism signals were observed for myoglobin-DDAB films.²

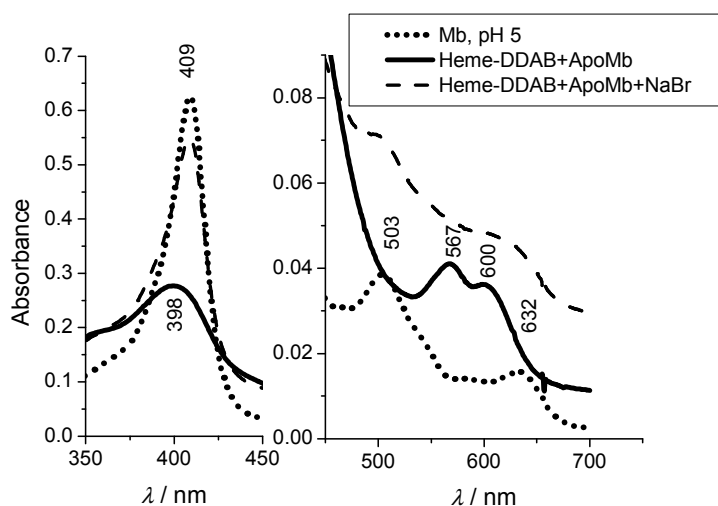


Figure 3B.2 UV/Vis spectra of myoglobin (.....), heme-DDAB with added apomyoglobin (—) and heme-DDAB with added apomyoglobin and 50 mM NaBr (—) after overnight incubation at 4 °C in 0.05 M sodium acetate pH 5.0, using 0.25 mM myoglobin/hemin, 0.25 mM apomyoglobin and 5 mM DDAB. The myoglobin-DDAB solution was also incubated at pH 6.0 (- - -). Solutions were diluted 1:50 in 0.01 M sodium acetate pH 5.0 immediately before UV/Vis measurement.

Electrochemical measurements of myoglobin in DDAB films on pyrolytic graphite. In Chapter IIIA the conclusion that heme release occurs in myoglobin-DDAB films was drawn primarily on the observation that myoglobin-DDAB films and heme-DDAB films behave similar electrochemically. Guto and Rusling challenged this conclusion by claiming that there are significant differences between the voltammetric response of myoglobin-DDAB films and heme-DDAB films.

There are indeed small differences in redox potential and peak shapes between myoglobin-DDAB and heme-DDAB films. However, these small differences can be explained by the presence of apomyoglobin in the heme-released myoglobin-DDAB films. It is known from literature that the presence of myoglobin affects the structure of aggregates of cationic surfactants,¹² and hence it might also have an influence on the midpoint potentials. Figure 3B.3 shows the voltammogram of a film cast from a heme-

DDAB solution with added apomyoglobin compared to the voltammograms of a heme-DDAB film and a myoglobin-DDAB film. The solutions from which the films were cast were pH 5 without salt and hence no heme-apomyoglobin recombination takes place (Figure 3B.2). The heme-DDAB with added apomyoglobin film gives essentially the same result as the myoglobin-DDAB film, which confirms that the differences between Mb-DDAB films and heme-DDAB films can be explained by the presence of apomyoglobin.

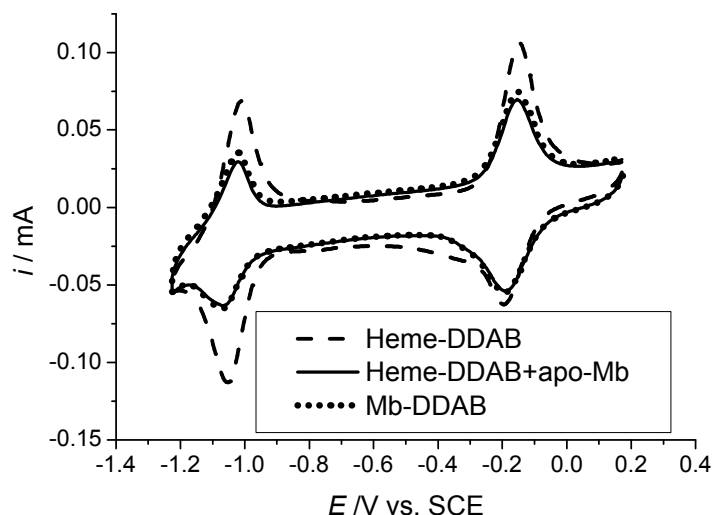


Figure 3B.3 Cyclic voltammograms for films cast from a heme-DDAB solution (---), a heme-DDAB solution with apomyoglobin (—) and a myoglobin-DDAB solution (.....). Solutions contain 0.25 mM myoglobin or hemin and 5 mM DDAB in 0.05 M sodium acetate pH 5.0 and 0.25 mM apomyoglobin where applicable. Films were dried over a period of 15 min. Films were cast on PG and were measured in 0.1 M acetate, pH 5.0, at a scan rate of 500 mV/s.

To provide additional evidence for the similarity between myoglobin-DDAB films and heme-DDAB films and hence for the heme release hypothesis we have determined the electron transfer rate constants between the electrode and the heme group for both films. This was done by measuring voltammograms at varying scan rates, as shown in Figure 3B.4. From the anodic and cathodic peak potentials of the $\text{Fe}^{\text{III}}/\text{Fe}^{\text{II}}$ redox transition of these voltammograms Trumpet plots²² were constructed (Figure 3B.5). From these plots the electron transfer rate constants between the heme group and the electrode can be extracted employing Laviron's theory.²³ The rate constants are 97 s^{-1} and 68 s^{-1} for Mb-DDAB and heme-DDAB, respectively.

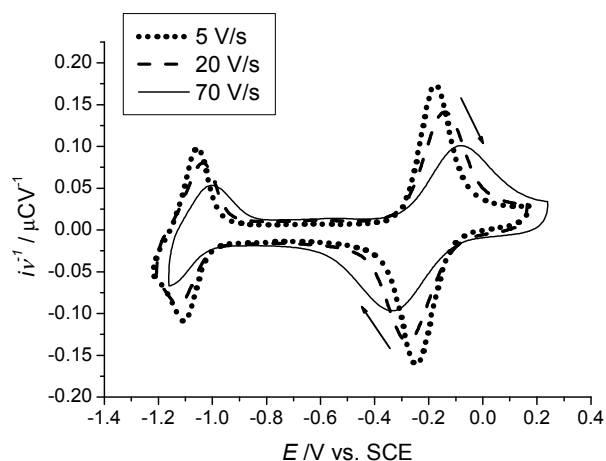


Figure 3B.4 Cyclic voltammograms for films cast from a Mb-DDAB solution at 5 V/s (.....), 20 V/s (- - -) and 70 V/s (—). The casting solution contained 0.25 mM myoglobin/hemin and 5 mM DDAB in 0.05 M sodium acetate pH 5.0. Films were cast on PG and were measured in 0.5 M acetate, pH 5.0, at a scan rate of 500 mV/s. Measured currents were divided by scan rate to allow for comparison between different scan rates.

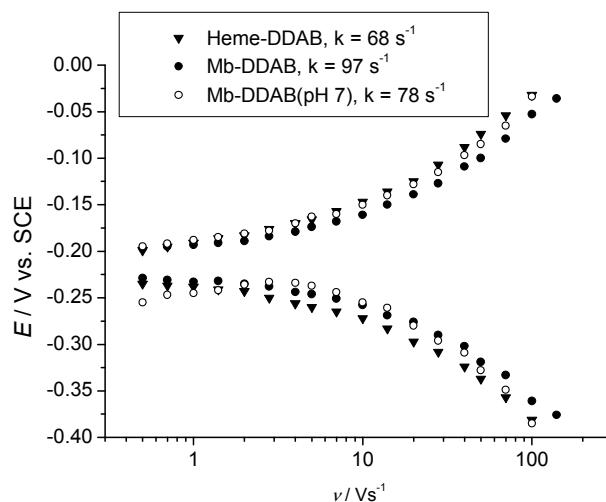


Figure 3B.5 Trumpet plots for heme-DDAB (\blacktriangledown) and Mb-DDAB (\bullet) films on pyrolytic graphite. Films were cast from solutions containing 0.25 mM myoglobin or hemin and 5 mM DDAB in 0.05 M sodium acetate, pH 5.0, and were dried over a period of 15 min. Cathodic and anodic peak potentials were determined from voltammograms that were recorded in 0.5 M acetate, pH 5.0, at a scan rate of 500 mV/s. The corresponding electron transfer rates are also reported. One of the Mb-DDAB films (\circ) was cast from a Mb-DDAB solution in 0.05 M phosphate, pH 7. This film was dried slowly over a period of 4 hours. The voltammograms for this film were recorded in 0.5 M phosphate, pH 7.0.

The similar rate constants for the myoglobin-DDAB and heme-DDAB films indicate that both films behave similarly and hence support the heme release hypothesis. Additionally, the observed behavior is typical of a thin film, as is reflected in the peak shape (Figure 3B.4) and the linear dependence of peak potential on the logarithm of scan rate (Figure 3B.5), and this behavior cannot be rationalized for a film containing native myoglobin. Thin layer behavior implies that no diffusion of protein molecules is involved. The charge under the voltammetric $\text{Fe}^{\text{III}}/\text{Fe}^{\text{II}}$ corresponds to a protein coverage of approximately 0.4 nmol cm^{-2} , consistent with results reported by Nassar.²⁴ If one takes into account that a monolayer of small protein molecules corresponds to approximately $10\text{--}15 \text{ pmol cm}^{-2}$ as has been reported for cytochrome c on gold,²⁵⁻²⁸ we can deduce that at least 30 monolayers of myoglobin with a thickness of at least 100 nm have to be in direct electronic contact with the electrode. Since electrons can only tunnel at significant rates through proteins over a distance of approximately 1.4 nm,²⁹ this seems highly unlikely. One could argue that the electrons hop from one myoglobin to the next; however this explanation can be discarded, since this behavior would be equivalent to diffusion in voltammetry.³⁰ On the other hand, heme release readily explains the high coverage and the high electron transfer rate constant. Heme is a relatively small molecule (compared to a protein) and hence much higher coverages per monolayer can be obtained. This implies that only 1-2 monolayers of heme have to be in direct contact with the electrode. This is supported by the fact that the observed total coverage is of the same order of magnitude as coverages observed for adsorbed heme.³¹ Hence the distance between the electrode and the heme groups remains below 1.4 nm, which allows for rapid electron transfer.

We have to add that the thin layer behavior we observe is different from the diffusion controlled behavior previously reported for thick Mb-DDAB films,⁸ but seems to be consistent with the behavior reported for thin Mb-DDAB films.²⁴ Currently we have no explanation for the apparent discrepancy between thin and thick films. For this a more detailed understanding about the structural properties of DDAB films on pyrolytic graphite is necessary. It has been suggested that there are potential-induced phase transitions occurring in the film,³² which could explain observations such as the irreversibility in the $\text{Fe}^{\text{III}}/\text{Fe}^{\text{II}}$ couple.¹

The discussion above concerns films, which are cast from solutions for which we are convinced that heme release occurs (pH 5, no salt). In our view the evidence that heme release occurs in these films is conclusive. However, does heme release also occur in films cast on pyrolytic graphite from solutions where myoglobin retains a native conformation (solutions of high pH (>7) or solutions containing salt)? In Chapter IIIA we concluded that heme release does indeed also occur for these films, which we based on the similar electrochemical response of films cast from solutions with or without salt. As additional evidence for this hypothesis we have determined the electron transfer rate constant for a film cast from a myoglobin-DDAB solution of pH 7 (Figure 3B.5), which is 78 s^{-1} . Based on the similarity of this rate constant to the rate constant of a heme-DDAB film we conclude that heme release also occurs in this film.

Apparently pyrolytic graphite is able to enhance the heme release process in the presence of DDAB. This can be rationalized based on the strong affinity of pyrolytic graphite to adsorb heme. Our UV/Vis measurements indicate that heme release is a reversible process, which implies that heme release occurs under all conditions. However, in solutions that are of high pH or that contain salt heme-apomyoglobin recombination keeps most of the myoglobin in its native state. On graphite the small amount of released heme can be adsorbed irreversibly to the electrode, which impedes heme-apomyoglobin recombination. Hence, heme will be slowly released from myoglobin and will adsorb on the electrode as is also reflected in the influence of film drying time on peak height (Figure 3B.6). No recombination with apomyoglobin occurs as the adsorbed heme is highly stable; heme release therefore only occurs on surfaces that have a strong affinity to adsorb heme. On surfaces such as quartz and glass spectroscopy has shown that myoglobin retains a native conformation in the DDAB films.⁸ Spectroelectrochemical results on tin-doped indium oxide (ITO) also show that native ferric myoglobin can be converted to the native ferrous form in myoglobin-DDAB films.³³ In the studies in which these experiments were performed it was assumed that the fact that myoglobin retains its native conformation in DDAB films on these surfaces would imply that myoglobin also retains its native conformation in DDAB films on pyrolytic graphite, an assumption which we consider untenable in the light of the above observations.

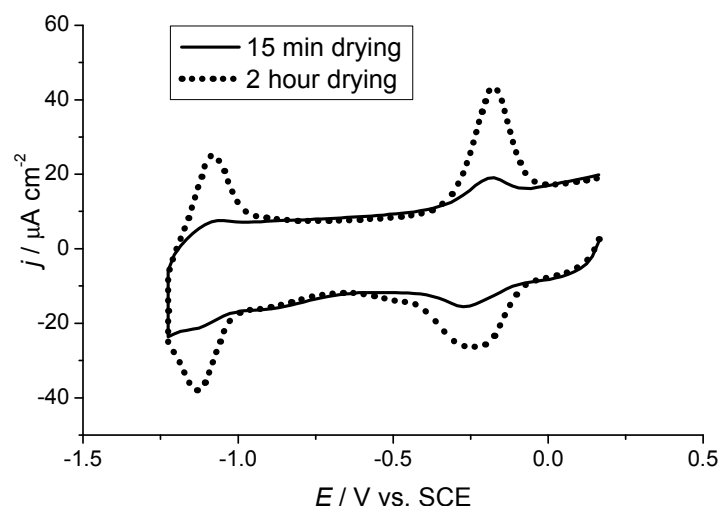


Figure 3B.6 Cyclic voltammograms of a film cast from a myoglobin-DDAB phosphate solution of pH 7 that was dried over a period of 15 min (—) as compared to a film that was dried over a period of 2 hours (·····). Films were cast on PG and were measured in 0.1 M phosphate, pH 7.0, at a scan rate of 500 mV/s.

HRP-DDAB films on pyrolytic graphite. There has been some controversy about HRP-DDAB films on pyrolytic graphite. In Chapter IIIA we reported our inability to obtain significant voltammetric peaks for HRP-DDAB films, which we ascribed to the fact that the heme is more tightly bound in HRP than in Mb. Guto and Rusling found reversible voltammetric peaks for HRP-DDAB films. In their view this new observation contradicts our heme release hypothesis.

As shown in Figure 3B.7, we have been able to obtain voltammetric peaks for HRP-DDAB films that are comparable to the peaks observed by Guto and Rusling.² Based on the similar peak potentials compared to a heme-DDAB film, we think that heme release also occurs for this HRP-DDAB film. The peaks are larger than in Chapter IIIA due to longer drying times, which is another indication that slow heme release occurs. However, compared to the peaks we observe for a myoglobin-DDAB film, the peaks for the HRP-DDAB film are almost negligible, with a heme coverage of approximately 15 pmol cm^{-2} . This is an indication that heme release from HRP is more difficult than from myoglobin.

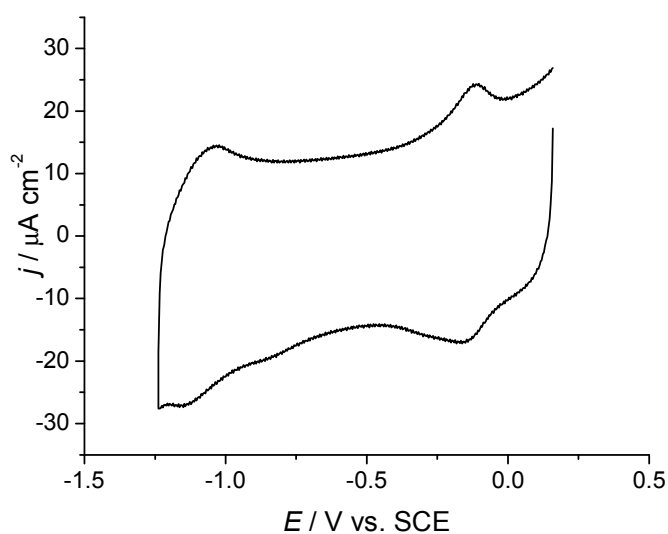


Figure 3B.7 Cyclic voltammograms of a film cast from a HRP-DDAB acetate solution of pH 5 that was slowly dried overnight. Film was cast on PG and was measured in 0.01 M phosphate, pH 5.0, at a scan rate of 500 mV/s.

3B.4 Conclusions

In conclusion, we are still convinced that heme release has occurred in all the myoglobin-DDAB films on pyrolytic graphite we investigated. We believe heme release provides a straightforward and consistent explanation for the electrochemical data in this chapter.¹ However, we do not claim that heme release occurs in all protein-DDAB films, or that only released heme can give a voltammetric response. Whether heme release occurs depends on many factors which include the protein properties, the electrode material, the pH and salt concentration of the casting solution, the drying time and possibly also the DDAB and protein concentrations. Heme release is a process that can occur and that should be reckoned with when working with heme-protein-DDAB films. Therefore the performance of control experiments is essential. In the case of pyrolytic graphite only electrochemical control experiments can be employed, since it is difficult to do spectroscopy on a strongly light absorbing surface. These control experiments include the comparison of the midpoint potentials, the electrocatalytic behavior and the electron transfer rate constant to a heme-DDAB film.

3B.5 References

1. de Groot, M. T.; Merkx, M.; Koper, M. T. M., *J. Am. Chem. Soc.* **2005**, *127*, 16224-16232.
2. Guto, P. M.; Rusling, J. F., *Electrochem. Comm.* **2006**, *8*, 455-459.
3. Chen, X.; Xie, H.; Kong, J.; Deng, J., *Biosens. Bioelectron.* **2001**, *16*, 115-120.
4. Fleming, B. D.; Tian, Y.; Bell, S. G.; Wong, L.-L.; Urlacher, V.; Hill, H. A. O., *Eur. J. Biochem.* **2003**, *270*, 4082-4088.
5. Immoos, C. E.; Chou, J.; Bayachou, M.; Blair, E.; Greaves, J.; Farmer, P. J., *J. Am. Chem. Soc.* **2004**, *126*, 4934-4942.
6. Lu, Z.; Huang, Q.; Rusling, J. F., *J. Electroanal. Chem.* **1997**, *423*, 59-66.
7. Oku, Y.; Ohtaki, A.; Kamitori, S.; Nakamura, N.; Yohda, M.; Ohno, H.; Kawarabayasi, Y., *J. Inorg. Biochem.* **2004**, *98*, 1194-1199.
8. Rusling, J. F.; Nassar, A. E. F., *J. Am. Chem. Soc.* **1993**, *115*, 11891-7.
9. Zhang, Z.; Nassar, A.-E. F.; Lu, Z.; Schenkman, J. B.; Rusling, J. F., *J. Chem. Soc., Faraday Trans.* **1997**, *93*, 1769-1774.
10. Blauer, G.; Harmatz, D.; Zvilichovsky, B., *FEBS Lett.* **1973**, *34*, 344-6.
11. Kanti Das, T.; Mazumdar, S.; Mitra, S., *Journal of the Chemical Society, Chemical Communications* **1993**, 1447-8.
12. Tofani, L.; Feis, A.; Snoke, R. E.; Berti, D.; Baglioni, P.; Smulevich, G., *Biophys. J.* **2004**, *87*, 1186-1195.
13. Das, D. K.; Bhattaray, C.; Medhi, O. K., *J. Chem. Soc., Dalton Trans.* **1997**, 4713-4718.
14. Das, D. K.; Medhi, O. K., *J. Inorg. Biochem.* **1998**, *70*, 83-90.
15. Das, D. K.; Medhi, O. K., *J. Chem. Soc., Dalton Trans.* **1998**, 1693-1698.
16. Sono, M.; Smith, P. D.; McCray, J. A.; Asakura, T., *J. Biol. Chem.* **1976**, *251*, 1418.
17. Sono, M.; Asakura, T., *J. Biol. Chem.* **1975**, *250*, 5227.

18. Smith, M. L.; Ohlsson, P. I.; Paul, K. G., *Dev. Biochem.* **1982**, *23*, 601.
19. Alston, K.; Storm, C. B., *Biochemistry* **1979**, *18*, 4292.
20. Hargrove, M. S.; Krzywda, S.; Wilkinson, A. J.; Dou, Y.; Ikeda-Saito, M.; Olson, J. S., *Biochemistry* **1994**, *33*, 11767.
21. Barrick, D.; Baldwin, R. L., *Biochemistry* **1993**, *32*, 3790.
22. Armstrong, F. A., *J. Chem. Soc., Dalton Trans.* **2002**, 661-671.
23. Laviron, E., *J. Electroanal. Chem.* **1979**, *101*, 19.
24. Nassar, A.-E. F.; Zhang, Z.; Hu, N.; Rusling, J. F.; Kumosinski, T. F., *J. Phys Chem. B* **1997**, *101*, 2224-2231.
25. Avila, A.; Gregory, B. W.; Niki, K.; Cotton, T. M., *J. Phys Chem. B* **2000**, *104*, 2759.
26. Chen, X.; Ferrigno, R.; Yang, J.; Whitesides, G. M., *Langmuir* **2002**, *18*, 7009.
27. Clark, R. A.; Bowden, E. F., *Langmuir* **1997**, *13*, 559.
28. Feng, Z. Q.; Imabayashi, S.; Kakiuchi, T.; Niki, K., *J. Chem. Soc., Faraday Trans.* **1997**, *93*, 1367.
29. Page, C. C.; Moser, C. C.; Chen, X.; Dutton, P. L., *Nature* **1999**, *402*, 47.
30. Bard, A. J.; Faulkner, L. R., *Electrochemical Methods: Fundamentals and Applications*. In *Electrochemical Methods: Fundamentals and Applications*, 2 ed.; John Wiley & Sons: New York, 1980; pp 311-367.
31. de Groot, M. T.; Merckx, M.; Koper, M. T. M., *J. Am. Chem. Soc.* **2005**, *127*, 7579-7586.
32. Boussaad, S.; Tao, N. J., *J. Am. Chem. Soc.* **1999**, *121*, 4510-4515.
33. Nassar, A.-E. F.; Bobbitt, J. M.; Stuart, J. D.; Rusling, J. F., *J. Am. Chem. Soc.* **1995**, *117*, 10986-93.

Chapter 4

Evidence for heme release in layer-by-layer assemblies of myoglobin and polystyrenesulfonate on pyrolytic graphite*

Abstract: *Layer-by-layer assemblies of myoglobin and polystyrenesulfonate (PSS) on pyrolytic graphite have been investigated with the goal of determining the origin of the voltammetric response of these films. Based on the similar midpoint potential, coverage and electron transfer behavior compared to adsorbed heme, it was concluded that the observed voltammetric peak is due to heme adsorbed at the electrode surface. This suggests that the interactions between the pyrolytic graphite electrode, PSS and myoglobin can result in heme release from the protein followed by heme adsorption on the electrode.*

* The contents of this chapter have been published: de Groot, M.T.; Merckx, M.; Koper, M.T.M., *J. Biol. Inorg. Chem.* **2007**, in press

4.1 Introduction

The immobilization of redox proteins on electrodes is a topic of active research both for obtaining a better mechanistic understanding of enzyme catalysis¹ and for the development of biosensors.² However, for the successful immobilization of a redox protein certain challenges have to be overcome. Firstly, the interactions between the protein and the electrode should be sufficient for immobilization, but should not significantly affect the tertiary structure of the protein. Secondly, in order to obtain electron transfer between the electrode and the redox group of the protein, the distance between them should not be much greater than 14 Å, the maximum observed for electron transfer between two redox centers in proteins.³ To overcome these challenges a wide variety of methods using covalent, electrostatic or hydrophobic interactions on numerous electrode materials including gold, silver, indium oxide and pyrolytic graphite have been investigated.⁴

The extent to which an immobilization method affects the protein's properties can be probed in different ways. On gold, silver and indium oxide electrodes spectroscopic techniques such as Surface-Enhanced Resonance Raman Spectroscopy (SERRS)⁵ and Surface-Enhanced Infrared Difference Adsorption Spectroscopy (SEIDAS) can be employed.⁶ With these techniques it has e.g. been shown that cytochrome *c* retains a near-native conformation on carboxylic acid-terminated self-assembled monolayers,⁷ whereas it undergoes significant conformational changes on bare metal electrodes.^{5,8,9} On "dark" materials such as graphite spectroscopic measurements are difficult and therefore one has to rely largely on indirect electrochemical evidence. This includes the comparison of properties such as midpoint potential and enzymatic activity to the protein in solution¹⁰⁻¹² and the determination whether the observed coverage and electron transfer behavior are typical of a protein.^{13,14} Using this kind of indirect evidence we have shown that myoglobin in films of didodecyldimethylammonium bromide (DDAB) on pyrolytic graphite can undergo heme release under certain conditions,^{15,16} although our conclusions were disputed by Guto and Rusling.¹⁷ Another case in which partial or complete heme removal from myoglobin has been suggested is for myoglobin in agarose hydrogel films in ionic liquids.¹⁸

In this chapter we investigate layer-by-layer assemblies¹⁹ of myoglobin and polystyrenesulfonate (PSS) on pyrolytic graphite.²⁰ It has been claimed that there is fast direct electron transfer between the electrode and the protein molecules in these assemblies and therefore these assemblies are interesting for mechanistic studies of redox enzymes and for use as biosensors. They can be made by alternately adsorbing negatively charged PSS and positively charged myoglobin.²¹⁻²⁵ Our goal was to determine whether the observed electrochemical response of these assemblies is due to the native protein or to a partially or completely denatured protein. We did this by comparing the electrochemical properties of the immobilized myoglobin to the properties of myoglobin in solution and to immobilized heme, a possible denaturation product.

4.2 Materials and Methods

Materials. Horse heart myoglobin (>90%, Aldrich), poly(sodium styrenesulfonate) (MW ~ 70,000, Aldrich), poly(diallyldimethylammoniumchloride) (MW ~ 200,000-350,000, Aldrich) and hemin (Fluka, 98%) were used as received. All other chemicals were p.a. grade. Buffer solutions were prepared with sodium acetate (pH 5.5), sodium dihydrogen phosphate monohydrate (pH 6-8) and boric acid (pH 9-10) combined with concentrated solutions of hydrochloric acid or sodium hydroxide and Millipore MilliQ water (resistivity > 18.2 M Ω cm). The concentration of the buffer was 0.1 M in all experiments, except for the electron transfer rate constant experiments where the buffer concentration was 3.0 M. Pyrolytic graphite (Carbone-Lorraine) was fabricated into homemade rotating ring-disk electrodes.^{26,27} The geometric surface area of the electrodes was 0.5 cm². In the electron transfer rate constant experiments the surface area of the electrode was reduced by taping off part of the surface, in order to reduce the ohmic drop.

Electrochemical Apparatus and Procedures. An Autolab PGstat 20 potentiostat was used for cyclic voltammetry. A homemade three-electrode cell consisting of a platinum flag counter electrode, a Hg|Hg₂SO₄ reference electrode and a pyrolytic graphite rotating disk working electrode was employed. All potentials in this paper are relative to the standard hydrogen electrode (SHE). All solutions were deaerated by purging with argon for 15 min. All electrochemical experiments were performed at room temperature.

Preparation of (Mb-PSS)_n multilayer on pyrolytic graphite. Prior to use, the pyrolytic graphite (PG) electrode was abraded using P1000 SiC sandpaper and ultrasonicated in Millipore MilliQ water for 1 min. The electrode was dried in a N₂ stream for 5 sec. Subsequently, the electrode was immersed in 120 μ M Mb in a 0.1 M acetate solution, pH 5.5, for 10 min. After being washed with water the electrode was then immersed in 3 mg/ml PSS in a 0.1 M acetate solution, pH 5.5, containing 0.5 M NaCl for 10 minutes. This cycle was repeated to make multilayer assemblies.

Preparation of adsorbed heme on pyrolytic graphite. A 0.5 mM hemin solution was prepared by dissolving 1.6 mg hemin in 5 ml of a 0.01 M borate solution, pH 11, since hemin only dissolves in alkaline solution. Prior to use, the pyrolytic graphite (PG) electrode was abraded using P1000 SiC sandpaper and ultrasonicated in Millipore MilliQ water for 1 min. The electrode was dried in a N₂ stream for 5 sec. The electrode was immersed in the hemin solution for 10 min to saturate the surface with hemin,^{28,29} after which the electrode was rinsed with water.

Preparation of a PDDA-PSS-heme-PDDA-PSS later on pyrolytic graphite. Prior to use, the pyrolytic graphite (PG) electrode was abraded using P1000 SiC sandpaper and ultrasonicated in Millipore MilliQ water for 1 min. The electrode was immersed in 3 mg/ml poly(diallyldimethylammoniumchloride) (PDDA) in 0.1 M acetate solution, pH 5.5, containing 0.5 M NaCl for 10 min.. After being washed with water the electrode was then immersed in a 3 mg/ml PSS 0.1 M acetate solution, pH 5.5, containing 0.5 M NaCl for 10 min. Subsequently, the electrode was immersed in a 0.5 mM hemin 0.01 M borate

solution, pH 11, for 30 min. This was followed by 10 min immersion in the PDDA solution and 10 min immersion in the PSS solution.

4.3 Results

Figure 4.1 shows the voltammetric response of a layer-by-layer assembly of PSS and myoglobin on pyrolytic graphite, which has been grown by alternately adsorbing negatively charged PSS and positively charged myoglobin, both buffered at pH 5.5. The voltammetric peak corresponds to the $\text{Fe}^{\text{III}}/\text{Fe}^{\text{II}}$ redox transition of the protein's heme group. The charge under the voltammetric peaks increases with the number of layers, corresponding to a coverage of approximately $2.6 \times 10^{-10} \text{ mol}\cdot\text{cm}^{-2}$ for a $\{\text{Mb-PSS}\}_6$ multilayer. The midpoint potential is $-0.04 \pm 0.01 \text{ V}$ versus SHE and the peak separation is $120 \pm 10 \text{ mV}$. All these properties are in reasonable agreement with results in the literature²⁴ and show that we have prepared similar films.

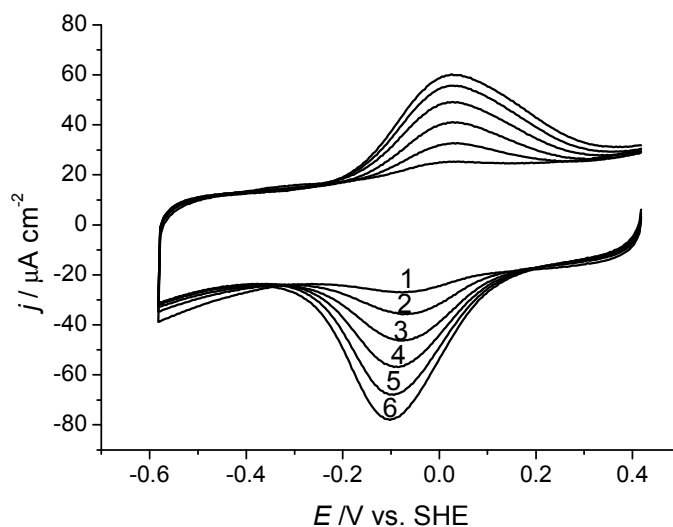


Figure 4.1 Cyclic voltammograms of a pyrolytic graphite electrode after alternate adsorption from a $120 \mu\text{M}$ Mb solution and a 3 mg/ml PSS solution, both buffered at pH 5.5. Voltammetry at a scan rate of 500 mV/s was performed in 0.1 M acetate, pH 5.5. The number of Mb-PSS layers is indicated by the number in the graph.

The determined midpoint potential significantly differs from the midpoint potential of myoglobin in solution, which is 0.06 V vs. SHE at pH 5.5.^{30,31} This could be related to either a change in the heme environment of the protein or to a local electric field, as has been reported for cytochrome *c* immobilized on carboxylic acid-terminated SAMs.³²⁻³⁵ To obtain more insight into the effect of the immobilization, we determined the midpoint potential over a broad pH range and compared it to myoglobin in solution (Figure 4.2).

The figure reveals large differences between immobilized Mb and Mb in solution of more than 250 mV above pH 9. This is significantly more than the maximum shift of 70 mV reported between immobilized cytochrome *c* and cytochrome *c* in solution. It is unlikely that such a large shift is solely due to an electric field, suggesting that at least part of the difference is due to an altered heme environment.

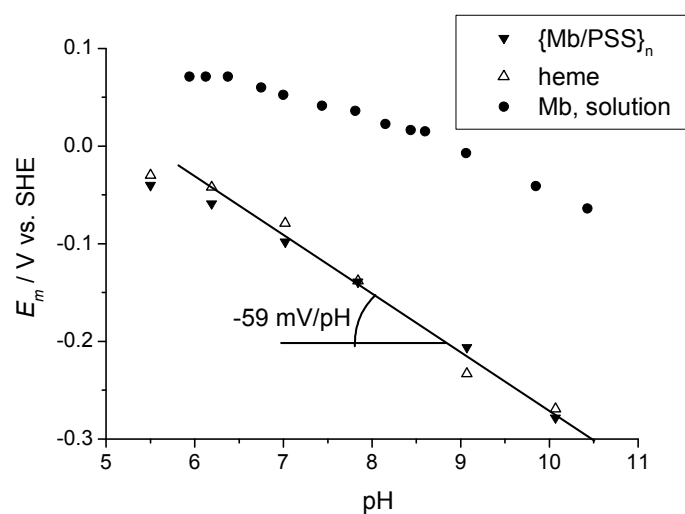


Figure 4.2 Midpoint potentials of a $\{\text{PSS}/\text{Mb}\}_6$ multilayer film on pyrolytic graphite (\blacktriangledown) as a function of pH compared to myoglobin in solution (\bullet)³⁰ and adsorbed hemin on pyrolytic graphite (Δ). Buffer: 0.1 M acetate, phosphate or borate; scan rate = 500 mV/s.

In previous studies on myoglobin-DDAB films on pyrolytic graphite we discovered that heme release can occur in these films, and that the observed electrochemical response was in fact due to isolated heme.^{15,16} To determine whether a similar process occurs in the $\{\text{Mb-PSS}\}_6$ -multilayer film we compared the voltammetric response of the multilayer film to the voltammetric response of adsorbed hemin at pH 5.5 (Figure 4.3) and to the voltammetric response of heme in a film of positively and negatively charged polymers. Direct comparison to a heme-PSS film is not possible, since the negatively charged PSS only adsorbs on the electrode when there is an electrostatic interaction with a positively charged polymer such as myoglobin. Figure 4.3 shows similarities and differences between the $\{\text{Mb-PSS}\}_6$ -multilayer and adsorbed heme. The coverage ($4.0 \times 10^{-10} \text{ mol}\cdot\text{cm}^{-2}$) and midpoint potential ($-0.03 \text{ V} \pm 0.01 \text{ vs SHE}$) of adsorbed heme are comparable to a $\{\text{Mb-PSS}\}_6$ multilayer. Especially the latter is striking, since the midpoint potential is determined by the heme environment and this is significantly different in adsorbed heme compared to myoglobin. To further investigate this similarity, we determined the midpoint potentials of both films over the pH 5-10 range (Figure 4.2). A very close correspondence was found, which suggests that the voltammetric response of the $\{\text{Mb-PSS}\}_6$ multilayer is caused by an electroactive group that closely resembles adsorbed heme. However, Figure 4.3 also shows a distinctly different peak shape and

lower peak separation (20 mV) for adsorbed heme compared to the $\{\text{Mb-PSS}\}_6$ multilayer. To determine whether this might be related to the presence of PSS in the $\{\text{Mb-PSS}\}_6$ multilayer, we incorporated heme in a multilayer of positively charged poly(diallyldimethylammoniumchloride) (PDDA) and negatively charged PSS. It appeared that the presence of both charged polymers induces a peak separation of 115 mV, which is comparable to the peak separation of 120 mV observed for a $\{\text{Mb-PSS}\}_6$ multilayer. This suggests that the presence of PSS can indeed cause an increased peak separation. The PDDA-PSS multilayer also induces a 30 mV shift in midpoint potential compared to adsorbed heme. Nevertheless, the pH dependence of the midpoint potential of heme incorporated in the PDDA-PSS multilayer is comparable to adsorbed heme (data not shown).

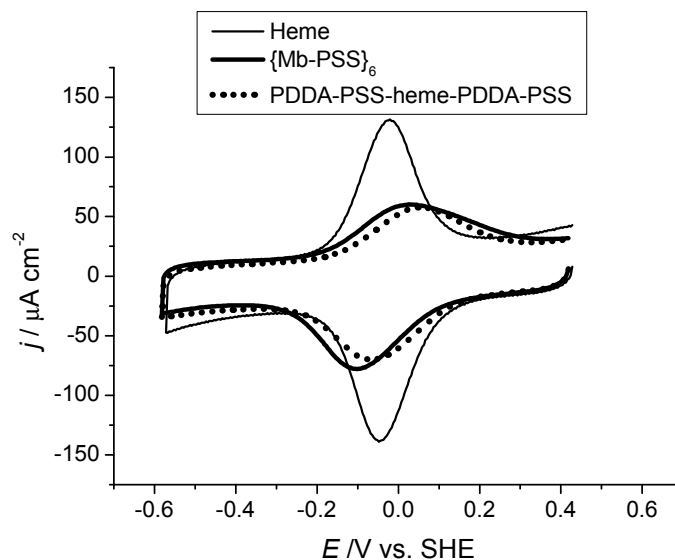


Figure 4.3 Cyclic voltammograms of adsorbed heme (—), a $\{\text{Mb-PSS}\}_6$ multilayer (—) and a PDDA-PSS-heme-PDDA-PSS layer (····) on pyrolytic graphite. Voltammetry at a scan rate of 500 mV/s was performed in 0.1 M acetate, pH 5.5.

To learn more about the properties of a $\{\text{Mb-PSS}\}_6$ multilayer, we tried to determine the electron transfer rate constant between the electrode and the heme group. This was done by measuring voltammograms at increasing scan rates. The anodic and cathodic peak potentials should start to shift with increasing scan rate, since the electron transfer cannot “keep up” with the high scan rate. From the dependence of peak separation on scan rate it is possible to calculate the electron transfer rate constants employing Laviron’s theory.³⁶ However, Figure 4.4 shows that in the case of a $\{\text{Mb-PSS}\}_6$ -multilayer, the peak separation does not shift with increasing scan rates. At 50 V s⁻¹ the peak separation is still the same as at 500 mV s⁻¹, namely 130 mV. Measuring at higher scan rates is possible, but due to a significant ohmic drop it becomes difficult to

accurately determine the peak potentials. Therefore, we were unable to determine the exact electron transfer rate constant. However, based on the fact that no significant increase in peak separation is observed at 50 V s^{-1} we can deduce that the electron transfer rate constant is at least 500 s^{-1} . Such a high electron transfer rate constant is not expected for a multilayer system where the large size of the myoglobin molecules implies that electrons have to tunnel over long distances in order to enable electron transfer between two protein molecules. Also, direct electron transfer between the electrode and the outer protein layers at this high rate seems unlikely, since the distance well exceeds 14 \AA , the maximum for fast electron transfer between two redox centers in proteins.³ Moreover, one would expect diffusion controlled behavior, similar to what has been observed for layer-by-layer assemblies of cytochrome *c* and poly(anilinesulfonic) acid (PASA).^{37,38} Therefore, it seems more likely that the electroactive response is caused by a redox-active group which is close to the electrode, possibly adsorbed heme. We tried to determine the electron transfer rate constant for adsorbed heme, but similar to the $\{\text{Mb-PSS}\}_6$ -multilayer, the peak separation did not increase with increasing scan rate up to 50 V s^{-1} (data not shown). This implies that the electron transfer rate constant again exceeds 500 s^{-1} . This agrees with a previous study for heme adsorbed on glassy carbon, in which a rate constant of $4.9 \times 10^3 \text{ s}^{-1}$ was found employing potential-modulated UV-vis reflectance spectroscopy.³⁹ The similarity between the $\{\text{Mb-PSS}\}_6$ -multilayer and adsorbed heme again suggests that part of the myoglobin in the multilayer system undergoes heme release, which is followed by subsequent heme adsorption.

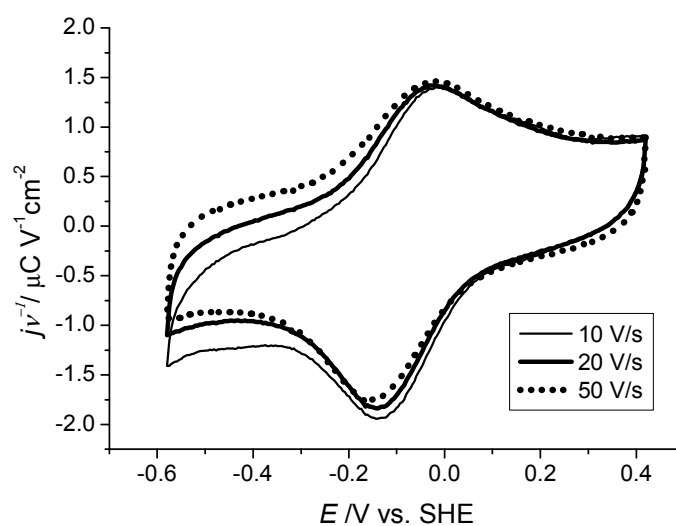


Figure 4.4 Cyclic voltammograms of a $\{\text{Mb-PSS}\}_6$ multilayer on pyrolytic graphite in 3.0 M acetate, $\text{pH } 5.5$ at 10 V/s (—), 20 V/s (—■—) and 50 V/s (.....). Measured currents were divided by scan rate to allow for comparison between different scan rates.

Although the poor reflection of the pyrolytic graphite electrode makes it difficult to do spectroscopy, one can gain interesting information by simple visible inspection. During the layer-by-layer formation, the color of the electrode becomes more brownish as can be seen in Figure 4.5. This is due to the combination of multiple myoglobin layers which adsorb visible light. The darkening can therefore be used as a crude tool to determine whether the $\{\text{Mb-PSS}\}_n$ multilayer formation indeed occurs. In contrast, no significant darkening is observed when free heme is adsorbed on the electrode, since the monolayer coverage is too low to be visually observed.

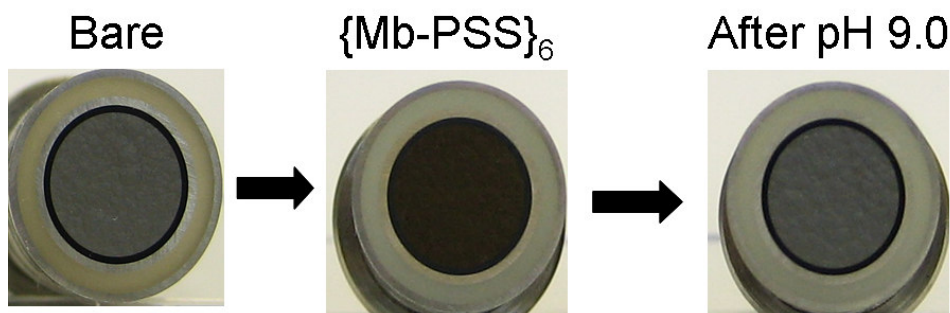


Figure 4.5 Photos of the pyrolytic graphite electrode before and after a $\{\text{Mb-PSS}\}_6$ multilayer has formed on the electrode. A photo of the electrode after a 10 minute immersion in a 0.1 M pH 9 borate solution is also given.

Interestingly, when a $\{\text{Mb-PSS}\}_6$ multilayer electrode is immersed in a 0.1 M borate solution of pH 9 for 10 minutes, the brownish color disappears from the electrode (Figure 4.5). This indicates that the multilayer is desorbed from the electrode, which can be explained by the fact that at pH 9 myoglobin becomes negatively charged ($pI = 7.35$)⁴⁰ and hence the electrostatic interaction with the negatively charged PSS becomes repulsive. If the voltammetric response were due to the myoglobin in the multilayer, one would expect that this would also result in the disappearance of the voltammetric peaks. However, Figure 4.6, which shows the voltammetric response after immersion in a pH 9.0 solution and subsequent reimmersion in a pH 5.5 solution, shows that this is not the case. The coverage decreases, but large voltammetric peaks remain. This is an indication that the voltammetric response is not due to myoglobin in the Mb-PSS multilayer, but instead due to a redox active group close to the electrode, of which only a small fraction is desorbed from the electrode when the pH is increased. Heme that is either directly adsorbed on the electrode or embedded in the first layer of PSS is the most likely candidate for this redox active group. It is interesting to see that the peak separation has decreased to 70 mV in the second measurement at pH 5.5. Probably, this is related to the fact that a large fraction of the PSS polymer has desorbed from the electrode, and hence the peak separation caused by this polymer decreases.

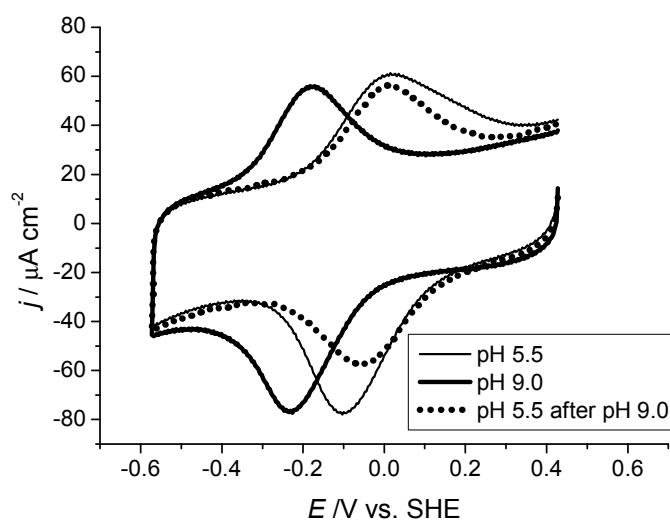


Figure 4.6 Cyclic voltammograms of a $\{\text{Mb-PSS}\}_6$ multilayer on pyrolytic graphite in a 0.1 M pH 5.5 acetate solution (—) and in a 0.1 M pH 9.0 borate solution (—). The voltammetric scan that is obtained after reimmersion in a 0.1 M pH 5.5 acetate solution is also plotted (.....). Scan rate = 500 mV/s

Our heme release hypothesis would imply that free heme is formed by interactions between PSS, myoglobin and pyrolytic graphite. This suggests that it should be possible to obtain a voltammetric response by immersing the electrode in a mixture of PSS and myoglobin, and that formation of a multilayer by alternate adsorption of PSS and myoglobin is not necessary. Figure 4.7 shows that immersion in a Mb-PSS mixture indeed results in a large voltammetric peak, which is found at the same potential as for a $\{\text{Mb-PSS}\}_6$ multilayer and also has a similar shape. Apart from the midpoint potential, the Mb-PSS-mixture film also has a coverage ($4.0 \times 10^{-10} \text{ mol}\cdot\text{cm}^{-2}$) that is comparable to the coverage of adsorbed heme. One could argue that it is possible to directly adsorb a multilayer or mixture of Mb and PSS from this solution, but this seems unlikely since there are no interactions that favor adsorption in this case. Also, the electrode does not undergo a significant darkening after immersion in the Mb-PSS mixture, whereas one would expect a darkening comparable to a $\{\text{Mb-PSS}\}_6$ multilayer (Figure 4.5), if a thick Mb-PSS film had adsorbed. Therefore, it seems more likely that the voltammetric response is due to free heme.

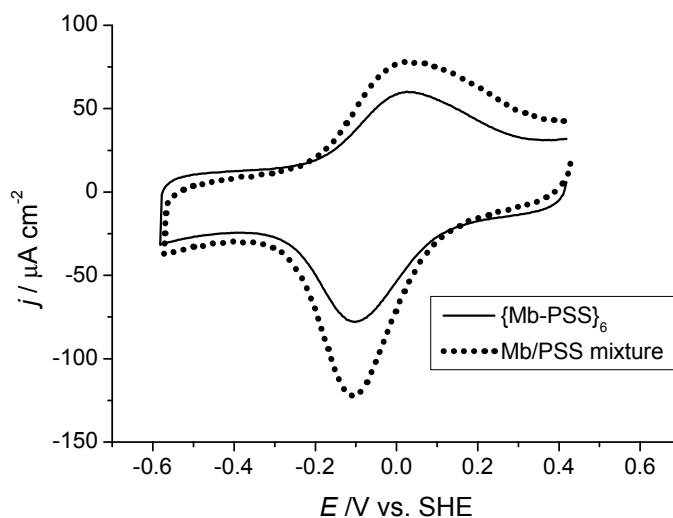


Figure 4.7 Cyclic voltammograms of a $\{\text{Mb-PSS}\}_6$ multilayer (—) and a Mb/PSS mixture (····) on pyrolytic graphite. Voltammetry at a scan rate of 500 mV/s was performed in 0.1 M acetate, pH 5.5. The Mb/PSS mixture film was made by immersing a freshly sanded pyrolytic graphite electrode in a solution of 60 μM Mb and 1.5 mg/ml PSS in 0.05 M pH 5.5 acetate solution with 0.25 M NaCl for three hours.

4.4 Discussion and conclusions

Our results indicate that the voltammetric response of a $\{\text{Mb-PSS}\}_n$ multilayer on pyrolytic graphite can be ascribed to free heme, which is either directly adsorbed on the electrode or embedded in the PSS layer. We base this on (i) the large difference in midpoint potential of a $\{\text{Mb-PSS}\}_n$ multilayer on pyrolytic graphite compared to myoglobin in solution, (ii) the similar pH dependence of the midpoint potential of a $\{\text{Mb-PSS}\}_n$ multilayer on pyrolytic graphite compared to adsorbed heme, (iii) the similar coverage of a $\{\text{Mb-PSS}\}_6$ multilayer on pyrolytic graphite compared to adsorbed heme (iv) the similar peak separation of a $\{\text{Mb-PSS}\}_6$ multilayer compared to a PDDA-PSS-heme-PDDA-PSS film (v) the high electron transfer rate constants of a $\{\text{Mb-PSS}\}_n$ multilayer, which is unlikely for electron transfer to protein molecules, but in line with the electron transfer expected for a layer of adsorbed heme, (vi) the fact that desorption of the multilayer induced by high pH does not result in a disappearance of the voltammetric peaks, and (vii) the fact that a large voltammetric response can be obtained by direct immersion in a Mb-PSS mixture showing that the formation of multilayers is not necessary.

Our conclusion is in apparent disagreement with previous studies on $\{\text{Mb-PSS}\}_n$ layer-by-layer films on pyrolytic graphite,²²⁻²⁵ in which it was concluded that myoglobin retains a near-native conformation in the layer-by-layer films. This was concluded mainly

on the basis of spectroscopic data, which consistently show that myoglobin retains a near-native conformation. However, these spectroscopic measurements were carried out on $\{\text{Mb-PSS}\}_n$ multilayers on transparent or reflective surfaces and not on pyrolytic graphite. Therefore they fail to take into account possible specific interactions between the pyrolytic graphite electrode, PSS and myoglobin. As we reported for myoglobin-DDAB films these interactions with the electrode can sometimes enhance heme release.^{15,16} The spectroscopic data therefore only show that myoglobin retains a near-native conformation in the absence of interactions with the electrode, corresponding to the myoglobin present in the layers far away from the electrode. On the other hand, our voltammetric results are a measure of the state of the protein near the electrode. Hence the spectroscopic data are not in disagreement with our conclusion that heme release followed by heme adsorption can occur in $\{\text{Mb-PSS}\}_n$ multilayers on pyrolytic graphite. We therefore emphasize that we do not claim that all myoglobin molecules in the layer-by-layer assembly undergo heme release. Only a small fraction near the pyrolytic graphite electrode may be involved, but it is this small fraction that nevertheless determines the electrochemical response of the assembly.

4.5 References

1. Armstrong, F. A., *J. Chem. Soc., Dalton. Trans.* **2002**, 661-671.
2. Schuhmann, W., *Rev. Mol. Biol.* **2002**, 82, 425.
3. Page, C. C.; Moser, C. C.; Chen, X.; Dutton, P. L., *Nature* **1999**, 402, 47.
4. Armstrong, F. A.; Wilson, G. S., *Electrochim. Acta* **2000**, 45, 2623-2645.
5. Hildebrandt, P.; Stockburger, M., *Biochemistry* **1989**, 28, 6710.
6. Ataka, K.; Heberle, J., *J. Am. Chem. Soc.* **2004**, 126, 9445.
7. Hildebrandt, P.; Murgida, D. H., *Bioelectrochemistry* **2002**, 55, 139.
8. Hobara, D.; Niki, K.; Cotton, T. M., *Biospectroscopy* **1998**, 4, 161.
9. Wackerbarth, H.; Hildebrandt, P., *ChemPhysChem* **2003**, 4, 714-724.
10. Elliott, S. J.; Hoke, K. R.; Heffron, K.; Palak, M.; Rothery, R. A.; Weiner, J. H.; Armstrong, F. A., *Biochemistry* **2004**, 43, 799.
11. Hudson, J. M.; Heffron, K.; Kotlyar, V.; Sher, Y.; Maklashina, E.; Cecchini, G.; Armstrong, F. A., *J. Am. Chem. Soc.* **2005**, 127, 6977.
12. Vincent, K. A.; Parkin, A.; Lenz, O.; Albracht, S. P. J.; Fontecilla-Camps, J. C.; Cammack, R.; Friedrich, B.; Armstrong, F. A., *J. Am. Chem. Soc.* **2005**, 127, 18179.
13. de Groot, M. T.; Evers, T. H.; Merkx, M.; Koper, M. T. M., *Langmuir* **2007**, 23, 729-736.
14. Armstrong, F. A.; Camba, R.; Heering, H. A.; Hirst, J.; Jeuken, L. J. C.; Jones, A. K.; Leger, C.; McEvoy, J. P., *Faraday Discuss.* **2000**, 116, 191.
15. de Groot, M. T.; Merkx, M.; Koper, M. T. M., *Electrochem. Commun.* **2006**, 8, 999.
16. de Groot, M. T.; Merkx, M.; Koper, M. T. M., *J. Am. Chem. Soc.* **2005**, 127, 16224.
17. Guto, P. M.; Rusling, J. F., *Electrochem. Commun.* **2006**, 8, 455-459.
18. Brusova, Z.; Gorton, L.; Magner, E., *Langmuir* **2006**, 22, 11453-11455.
19. Decher, G., *Science* **1997**, 277, 1232-1237.
20. Rusling, J. F.; Forster, R. J., *J. Colloid Interface Sci.* **2003**, 262, 1-15.

21. Lvov, Y.; Ariga, K.; Ichinose, I.; Kunitake, T., *J. Am. Chem. Soc.* **1995**, *117*, 6117-23.
22. Lvov, Y.; Ariga, K.; Kunitake, T., *Chem. Lett.* **1994**, 2323-6.
23. Lvov, Y. M.; Lu, Z.; Schenkman, J. B.; Zu, X.; Rusling, J. F., *J. Am. Chem. Soc.* **1998**, *120*, 4073-4080.
24. Ma, H.; Hu, N.; Rusling, J. F., *Langmuir* **2000**, *16*, 4969-4975.
25. Panchagnula, V.; Kumar, C. V.; Rusling, J. F., *J. Am. Chem. Soc.* **2002**, *124*, 12515-12521.
26. Van den Brink, F.; Visscher, W.; Barendrecht, E., *J. Electroanal. Chem.* **1983**, *157*, 283-304.
27. Van der Plas, J. F.; Barendrecht, E., *Rec. Trav. Chim. Pays Bas* **1977**, *96*, 133-6.
28. Brown, A. P.; Koval, C.; Anson, F. C., *J. Electroanal. Chem.* **1976**, *72*, 379-87.
29. Duong, B.; Arechabaleta, R.; Tao, N. J., *J. Electroanal. Chem.* **1998**, *447*, 63-69.
30. Behlke, J.; Scheler, W., *Naturwissenschaften* **1961**, *48*, 717.
31. Brunori, M.; Saggese, U.; Rotilio, G. C.; Antonini, E.; Wyman, J., *Biochemistry* **1971**, *10*, 1604-9.
32. Murgida, D. H.; Hildebrandt, P., *Acc. Chem. Res.* **2004**, *37*, 854-861.
33. de Groot, M. T.; Merkx, M.; Koper, M. T. M., *Langmuir*, **2007**, *23*, 3832.
34. Petrovic, J.; Clark, R. A.; Yue, H.; Waldeck, D. H.; Bowden, E. F., *Langmuir* **2005**, *21*, 6308.
35. Fedurco, M., *Coord. Chem. Rev.* **2000**, *209*, 263-331.
36. Laviron, E., *J. Electroanal. Chem.* **1979**, *101*, 19.
37. Beissenhertz, M. K.; Kafka, J.; Schaefer, D.; Wolny, M.; Lisdat, F., *Electroanalysis* **2005**, *17*, 1931-1937.
38. Beissenhertz, M. K.; Scheller, F. W.; Stocklein, W. F. M.; Kurth, D. G.; Mohwald, H.; Lisdat, F., *Angew. Chem. Int. Ed.* **2004**, *43*, 4357-4360.
39. Feng, Z. Q.; Sagara, T.; Niki, K., *Anal. Chem.* **1995**, *67*, 3564-70.
40. Radola, B. J., *Biochim. Biophys. Acta* **1973**, *295*, 412-28.

Chapter 5

Electron transfer and ligand binding to cytochrome *c'* immobilized on self-assembled monolayers*

Abstract: *We have successfully immobilized *Allochromatium vinosum* cytochrome *c'* on carboxylic acid-terminated thiol monolayers on gold and investigated its electron transfer and ligand binding properties. Immobilization could only be achieved for pH's ranging from 3.5 to 5.5, reflecting the fact that the protein is only sufficiently positively charged below pH 5.5 ($pI = 4.9$). Upon immobilization the protein retains a near-native conformation, as is suggested by the observed potential of 85 mV vs. SHE for the heme Fe^{III}/Fe^{II} transition, which is close to the value of 60 mV reported in solution. The electron-transfer rate to the immobilized protein depends on the length of the thiol spacer, displaying distance-dependent electron tunneling for long thiols and distance-independent protein reorganization for short thiols. The unique CO-induced dimer-to-monomer transition observed for cytochrome *c'* in solution also seems to occur for immobilized cytochrome *c'*. Upon saturation with CO a new anodic peak corresponding to the oxidation of a Fe^{II} -CO adduct is observed. CO binding is accompanied by a significant decrease in protein coverage, which could be due to weaker electrostatic interactions between the self-assembled monolayer and cytochrome *c'* in its monomeric form compared to its dimeric form. The observed CO binding rate of $24 M^{-1} s^{-1}$ is slightly slower than the binding rate in solution ($48 M^{-1} s^{-1}$), which could be due to electrostatic protein-electrode interactions or could be the result of protein crowding on the surface. This study shows that the use of carboxyl acid-terminated thiol monolayers as a protein friendly method to immobilize redox proteins on gold electrodes is not restricted to cytochrome *c*, but can also be used for other proteins such as cytochrome *c'*.*

* The contents of this chapter have been published: de Groot, M.T.; Evers T.H.; Merkx, M.; Koper, M.T.M., *Langmuir* **2007**, 23, 729-736

5.1 Introduction

Over the last two decades the immobilization of redox proteins on conducting surfaces has been actively pursued. Protein immobilization on electrodes allows one to probe electron-transfer mechanisms in proteins with electrochemical techniques.¹ From a more practical point of view electrodes with immobilized redox enzymes can potentially be employed as biosensors^{2,3} or as a new approach in biocatalysis, in which expensive electron donors and enzyme-product separation steps are no longer necessary.⁴ A wide variety of methods using covalent, electrostatic or hydrophobic interactions have been employed to immobilize redox proteins on both metal surfaces such as gold and silver as well as carbon surfaces such as pyrolytic graphite and glassy carbon.⁵

An important question is to what extent immobilization of a protein affects its properties. Detailed knowledge about the interactions between proteins and electrodes and the way electron transfer occurs between them is still lacking for most immobilized proteins. In some cases the proteins have been shown to retain a near-native conformation as reflected in its enzymatic activity,⁶⁻⁸ but in other systems significant conformational changes⁹⁻¹¹ or even cofactor release from the protein were observed after immobilization.^{12,13}

Probably the best characterized immobilized protein system is horse heart cytochrome *c* on gold and silver, either bare or covered with ionic or hydrophobic self-assembled monolayers (SAM).¹⁴⁻¹⁶ Surface-Enhanced Resonance Raman Spectroscopy (SERRS)¹⁷ and Surface-Enhanced Infrared Difference Absorption Spectroscopy (SEIDAS)¹⁸ have shown that cytochrome *c* undergoes significant conformational changes on bare metal electrodes,^{9,11} whereas it retains a near-native conformation on carboxylic acid-terminated SAMs.¹⁷ SEIDAS¹⁸ and protein engineering^{19,20} studies have been used to identify the residues on cytochrome *c* that bind to the negatively charged carboxyl groups of the self-assembled monolayer. Additionally, detailed electron-transfer rate studies have been presented for SAMs of different lengths showing rate limitation by electron tunneling and protein reorganization.²¹⁻²⁵ Although immobilization via hydrophobic interactions on SAMs of alkanethiols has also been shown to be suitable for certain proteins (azurin),^{26,27} the studies on cytochrome *c* suggest that electrostatic immobilization is a relatively mild method that enables direct electron transfer between protein and electrode, but does not seem to significantly affect its structure and properties. Hence it could be a suitable method for protein immobilization in general.

In this study we investigate whether electrostatic immobilization on carboxylic acid-terminated SAMs can be extended to a more complex protein system. For this purpose the protein cytochrome *c'* from *Allochromatium Vinosum* was chosen. This particular cytochrome *c'* displays a unique reversible dimer-to-monomer transition upon binding of NO, CO and CN⁻.²⁸ This monomerization has been attributed to the displacement of Tyr16 from the distal site upon ligand binding, which results in a conformational change in one of the α -helices present at the dimer interface.²⁹ This cytochrome *c'* thus provides an attractive model system to understand how binding of small diatomic ligands can induce large conformational changes.³⁰ Similar ligand induced conformational changes

are observed in heme-based sensor proteins such as guanylate cyclase (NO), CooA (CO) and FixL (O₂).³¹⁻³⁴ Here we show that cytochrome *c'* immobilized on carboxylic acid-terminated SAMs displays fast electron transfer between the protein and the electrode and discuss the orientation of the protein on the electrode. In order to test whether the ligand-induced conformational changes are impeded by the immobilization, the influence of CO and NO binding on the immobilized cytochrome *c'* was studied.

5.2 Experimental Procedures

Materials. Cytochrome *c'* (*Allochromatium vinosum*) was expressed and purified as described previously.³⁵ Horse heart cytochrome *c* (95%, Fluka), 3-mercaptopropionic acid (99%, Aldrich) (MPA), 4-mercaptobutyric acid (95%, Pfaltz & Bauer) (MBA), 6-mercaptohexanoic acid (97%, Dojindo) (MHA), 8-mercaptooctanoic acid (97%, Dojindo) (MOA), 11-mercaptoundecanoic acid (95%, Aldrich) (MUA), and 16-mercaptohexadecanoic acid (90%, Aldrich) (MHDA) were all used as received. All other chemicals were p.a. grade (Merck). Buffer solutions (pH 3.5-6) were prepared by combining sodium acetate with concentrated solutions of hydrochloric acid and Millipore MilliQ water (resistivity > 18.2 M Ω cm). The concentration of the buffer solutions ranged from 1 to 100 mM.

Electrochemical Apparatus and Procedures. An Autolab PGstat 20 potentiostat was used for cyclic voltammetry. A homemade three-electrode cell consisting of a gold working electrode, typically a wire with an attached bead, a platinum wire counter electrode and a Hg|Hg₂SO₄ reference electrode was employed. All potentials reported in this paper are relative to the standard hydrogen electrode (SHE). All solutions were deaerated by purging with argon for 15 min. For voltammograms at high scan rates (>5 V/s) that were used in the determination of electron-transfer rate constants, ohmic drop compensation was applied. Ligand binding experiments were performed in saturated solutions of carbon monoxide (purity 4.7) or nitric oxide (purity 2.5, Linde AG) by purging the solution for 10 minutes. Prior to entering the electrochemical cell, NO was bubbled through two washing flasks filled with a 3 M KOH solution, a procedure that was found to be important in order to remove NO₂.^{36,37} The saturated solutions contained 2.1 mM NO or 1.1 mM CO at 20 °C.³⁸ All electrochemical experiments were performed at room temperature.

Preparation of gold electrodes with COOH-terminated thiols. Prior to use the gold wire electrodes were flame-annealed and subsequently quenched in water. The electrodes were then immersed in a 1 mM solution of one of the COOH-terminated thiols for approximately 10 minutes. For 3-mercaptopropionic acid and 4-mercaptobutyric acid these solutions were prepared by mixing the thiol with water. The other thiol solutions were prepared by mixing with ethanol. The gold electrodes were rinsed and subsequently immersed in the electrochemical cell. The protein concentration in the cell was 100 nM. Protein adsorption was enhanced by argon or CO bubbling and continued until the voltammetric peak reached a maximum, which was after approximately 5 minutes in a solution of pH 4.5.

Determination of protein coverages. Coverages were determined by subtraction of a natural cubic splines baseline³⁹ from the anodic or cathodic scan of the voltammogram and subsequent division by area of the gold electrode. For the baseline subtraction the program “Utilities for Data Analysis” developed by Dr Dirk Heering was employed.⁴⁰ The surface area of the gold electrodes was determined from an oxygen adsorption experiment in 0.5 M H₂SO₄.⁴¹

UV-vis spectroscopy. UV-vis spectra were obtained at room temperature on a Shimadzu Multispec-1501 using a quartz cuvette with a rubber septum. Cytochrome *c*' was diluted from a concentrated stock solution to a concentration of 1 μ M in 50 mM acetate, pH 4.5. The solution was saturated with CO by flushing with CO. Cytochrome *c*' was reduced by the addition of \sim 15 mM Na₂S₂O₄. Subsequently the increase in absorption at 418 nm with time was measured.

5.3 Results

Adsorption of cytochrome *c*'. Figure 5.1 shows the adsorption of cytochrome *c*' from a 100 nM solution on a gold electrode with a SAM of mercaptohexanoic acid at pH 4.5. The peak size gradually increases with the number of scans, with full coverage being reached after approximately 100 scans, corresponding to 2000 s. The shape of the peaks is typical of an adsorbed species and does not display any diffusion limitation, which is a strong indication that the peaks are only caused by adsorbed cytochrome *c*'. When argon is bubbled through solution to enhance convection, the maximum coverage is obtained within 15 scans, corresponding to 300 s.

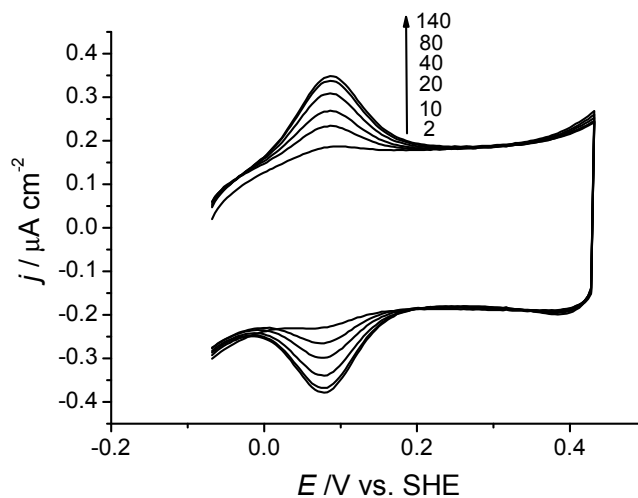


Figure 5.1 Cyclic voltammograms of a gold electrode with a SAM of mercaptohexanoic acid (MHA) after immersion in 100 nM *Allochrodatum vinosum* cytochrome *c*' in a 10 mM acetate solution, pH 4.5. Scan 2, 10, 20, 40, 80 and 140 are displayed. Scan rate = 50 mV/s.

Figure 5.2 shows baseline-subtracted voltammograms for cytochrome *c'* and cytochrome *c* adsorbed at pH 4.5. Potentials of 85 mV and 275 mV were determined for the Fe^{III}/Fe^{II} transitions of cytochrome *c'* and cytochrome *c*, respectively. The 190 mV difference between both proteins reflects the different coordination of the heme, being five coordinate mixed-spin for cytochrome *c'* and six-coordinate low-spin for cytochrome *c*.⁴²⁻⁴⁴ A difference of 190 mV has also been observed between the midpoint potentials of the two proteins in solution, which are 60 mV for cytochrome *c'*^{45,46} and 250 mV for cytochrome *c* at pH 4.5.⁴⁷ The difference of 25 mV between the midpoint potentials of the immobilized proteins compared to the proteins in solution is probably related to the negative charge of the carboxyl thiol and the electric field created by the gold electrode.²⁵

Half-height widths (δ) are 97 mV for cytochrome *c'* and 94 mV for cytochrome *c*. Both δ 's are close to the theoretical δ of 89 mV at 21 °C for Nernstian behavior⁴⁸ and are similar to δ 's observed for proteins immobilized on edge plane pyrolytic graphite.⁴⁹ This implies that the immobilized protein molecules display almost ideal electron-transfer behavior, which is also reflected in the small peak separation between the anodic and the cathodic peaks, being 4 mV for cytochrome *c'* and 2 mV for cytochrome *c*.

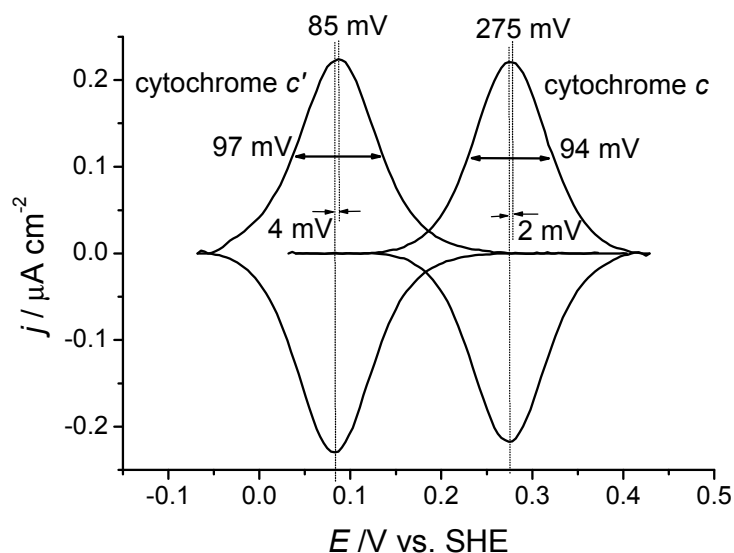


Figure 5.2 Baseline subtracted voltammograms of a gold electrode coated with mercaptohexanoic acid (MHA) after immersion in 100 nM *Allochroa matium vinosum* cytochrome *c'* or 200 nM horse heart cytochrome *c* in a 10 mM acetate solution, pH 4.5. Scan rate = 50 mV/s.

Based on the charge under the voltammetric peaks and the surface area of the gold electrodes, the heme coverage can be determined. Since cytochrome *c'* is a dimer, the

actual protein coverage is half the heme coverage. It appeared from the voltammograms that there was a strong influence of pH on heme coverage (Figure S5.1, which can be found at the end of this chapter). Therefore the maximum heme coverage for cytochrome c' and cytochrome c was determined as a function of pH. Figure 5.3 shows that there is a gradual increase in coverage up to pH 4.5 for both proteins. At pHs above 4.5, the coverage of cytochrome c' decreases and becomes zero at pH 5.5. The maximum heme coverage for cytochrome c' is 5 pmol cm^{-2} at pH 4.5. The coverage of cytochrome c keeps increasing above pH 4.5 and does not reach a maximum. The value of 8.5 pmol cm^{-2} at pH 6 is in line with previously reported values of $10\text{--}15 \text{ pmol cm}^{-2}$ at pH 7.^{14,21,22,50}

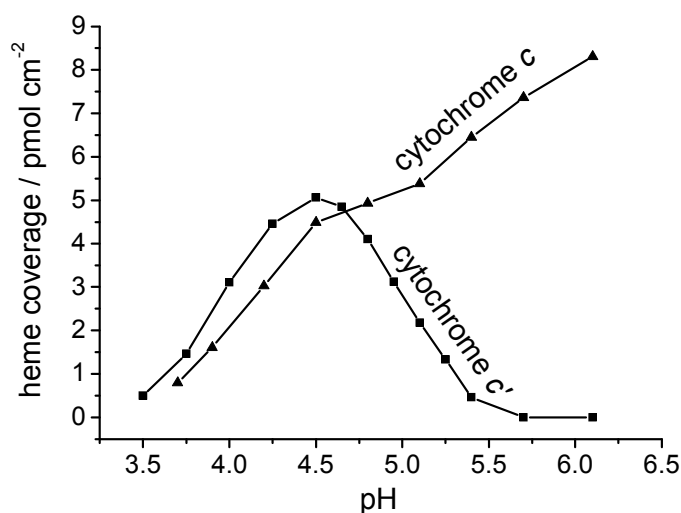


Figure 5.3 Heme coverages of cytochrome c' (■) and cytochrome c (▲) determined at different pHs on SAMs of mercaptohexanoic acid on gold. Coverages were determined from the charge under the voltammetric peaks of base-line subtracted voltammograms divided by the surface area of the gold electrodes. These surface areas were determined from oxygen adsorption experiments.⁴¹ The voltammograms were recorded in 10 mM acetate solutions containing 100 nM cytochrome c' or 200 nM cytochrome c at a scan rate of 50 mV/s. The actual protein coverage for cytochrome c' is half the heme coverage.

Our results can be rationalized, taking into account the fact that high coverages are only obtained if the thiol is sufficiently negatively charged and the protein is sufficiently positively charged. Cytochrome c has a pI of 10.0 and is therefore sufficiently positively charged over the whole pH range. Cytochrome c' has a pI of 4.9 and hence is only positively charged below pH 4.9, which explains the sharp decrease in coverage above pH 4.5. The increase in coverage observed in the pH 3.5–4.5 range for both proteins can be related to an increase in the negative charge on the carboxylic acid-terminated SAM.

Carboxylic acids have a pKa around 4.8,³⁸ but higher pKa's have been reported for SAMs of carboxylic acid-terminated thiols.^{18,51-60}

The electrostatic binding of cytochrome *c'* is also reflected in the fact that the coverage depends on both the length of the carboxylic acid-terminated thiol and the ionic strength of the solution. Figure 5.4 shows different coverages on thiols of different length, which may be related to a difference in pKa between the SAMs.⁵¹ Significantly higher coverages for all SAMs are obtained in a 1 mM buffer instead of a 10 mM buffer, which is also indicative of electrostatic binding. The binding of cytochrome *c'* is weaker than that of cytochrome *c*, since the coverage of electrostatically bound cytochrome *c* does not decrease until the buffer concentration is raised over 25 mM (Figure S5.2).^{21,50,61}

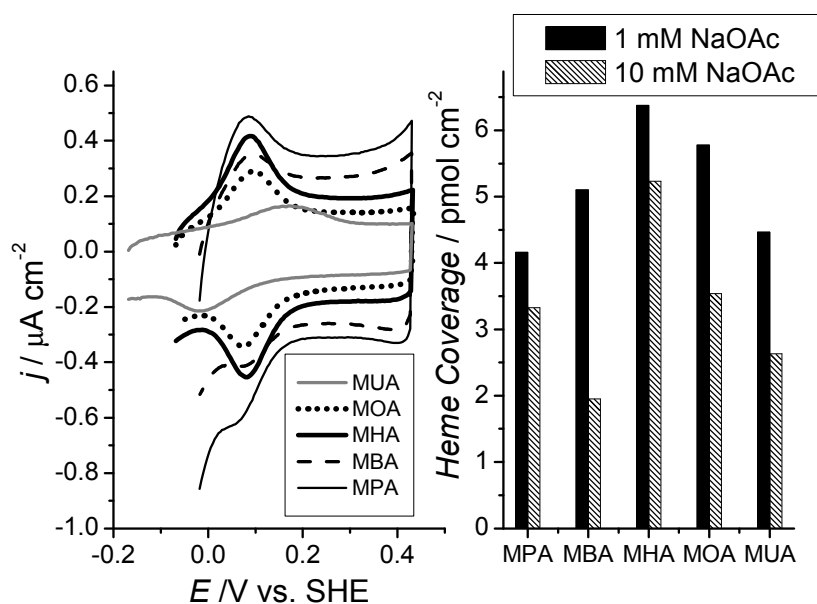


Figure 5.4 Cyclic voltammograms and heme coverages for a gold electrode coated with a SAM of 3-mercaptopropionic acid (MPA), 4-mercaptopbutyric acid (MBA), 6-mercaptophexanoic acid (MHA), 8-mercaptopoctanoic acid (MOA) or 11-mercaptopundecanoic acid (MUA) in 100 nM *Allochrodatum vinosum* cytochrome *c'* in 10 mM acetate solution of pH 4.5. Scan rate = 50 mV/s. Coverages obtained in buffer solutions of 1 mM acetate solution of pH 4.5 are also listed.

Electron transfer to immobilized cytochrome *c'*. Having established proper conditions for electrostatic immobilization of cytochrome *c'* on SAM's, we next studied the rate of electron transfer as a function of thiol length. Studies on electrostatically immobilized cytochrome *c* previously showed a distinct influence of the length of the carboxylic acid-terminated thiol on the electron-transfer rate (Figure 5.6),^{22,23} displaying

rates limited by electron tunneling for long thiols and rates limited by protein reorganization for short thiols. Electron-transfer rate constants on the different thiols were determined employing the method described by Laviron.⁶² This involves measuring the cathodic and anodic peak potentials of voltammograms at different scan rates (Figure S5.3) and subsequent plotting of these potentials in so-called Trumpet plots (Figure 5.5).⁶³ From these plots rate constants at midpoint potential of 140 s^{-1} , 140 s^{-1} , 36 s^{-1} , 3.9 s^{-1} and 0.18 s^{-1} were determined for SAMs of respectively 3-mercaptopropionic acid (MPA), 4-mercaptopbutyric acid (MBA), 6-mercaptophexanoic acid (MHA), 8-mercaptopoctanoic acid (MOA) and 11-mercapoundecanoic acid (MUA).^{62,63} The determined rate constants are plotted in Figure 5.6 as a function of chain length. For comparison electron-transfer rate constants were also determined for horse heart cytochrome *c* under the same conditions. The determined values of 845 s^{-1} , 1098 s^{-1} , 536 s^{-1} , 69.5 s^{-1} and 0.42 s^{-1} for respectively MBA, MHA, MOA, MUA and 16-mercaptophexadecanoic acid (MHDA) are in close correspondence with values previously reported for cytochrome *c* at pH 7.²²

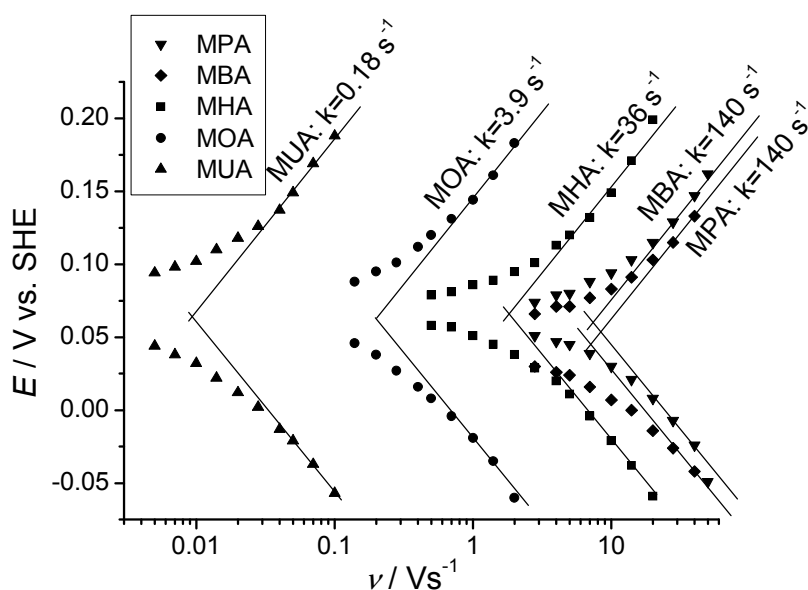


Figure 5.5 Trumpet plots for cytochrome *c*' immobilized on gold with a SAM of 3-mercaptopropionic acid (MPA), 4-mercaptopbutyric acid (MBA), 6-mercaptophexanoic acid (MHA), 8-mercaptopoctanoic acid (MOA) or 11-mercapoundecanoic acid (MUA). Cathodic and anodic peak potentials were determined from voltammograms that were recorded in 10 mM acetate, pH 4.8 containing 100 nM cytochrome *c*' at scan rates ranging from 5 mV s^{-1} to 40 V s^{-1} . Peak potentials were corrected for ohmic drop at high scan rates. The corresponding electron-transfer rate constants are also reported.

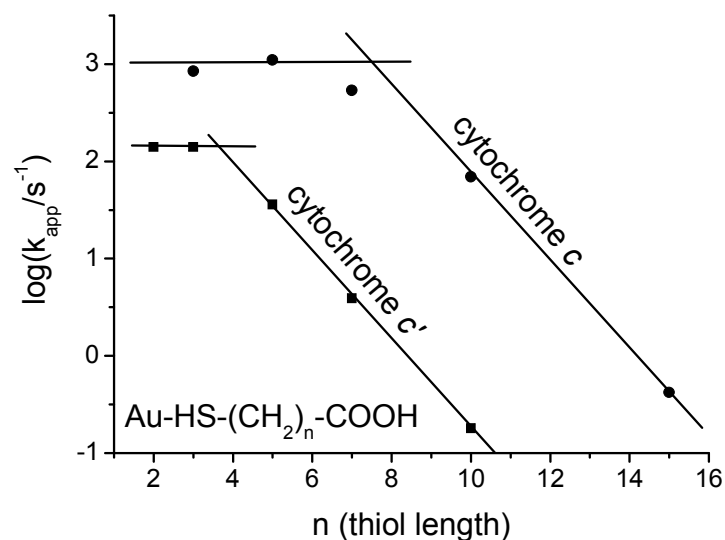


Figure 5.6 Electron-transfer rate constants for cytochrome *c*' and cytochrome *c* as a function of the number of methylene groups in the mercaptocarboxyl thiols ($\text{HS}(\text{CH}_2)_n\text{COOH}$). The electron-transfer rates were determined from Trumpet plots (Figure 5.5). The voltammograms for these Trumpet plots were recorded in 10 mM acetate, pH 4.8 containing 100 nM cytochrome *c*' or 200 nM cytochrome *c* at scan rates ranging from 5 mVs^{-1} to 300 Vs^{-1} . For cytochrome *c* on SAMs of MBA, MHA and MOA a 50 mM acetate solution was used to avoid large ohmic drops. Increasing ionic strength does not affect rate constants, as was evidenced by values of 70 s^{-1} and 75 s^{-1} for cytochrome *c* on MUA in respectively 10 mM and 50 mM acetate.

Figure 5.6 shows that cytochrome *c*' and cytochrome *c* exhibit a similar kind of electron-transfer behavior. For long thiols the electron-transfer constant decreases with increasing length of the thiol, corresponding to long range electron tunneling.⁶⁴ The slope of this decrease is the same for both cytochrome *c* and cytochrome *c*' and corresponds to an exponential decay coefficient β of 1.06 per methylene unit, in line with electron-transfer rates through alkanethiols reported for other systems.⁶⁵⁻⁶⁷ For short thiols, the electron-transfer rate constants become independent of chain length for both proteins. This has been ascribed to a rate limiting conformational change or proton transfer.⁶⁸

However, there are some distinct differences between immobilized cytochrome *c*' and immobilized cytochrome *c*. For short thiols the electron-transfer rate constant of immobilized cytochrome *c*' ($\approx 150 \text{ s}^{-1}$) is a factor 7 slower than the rate constant of immobilized cytochrome *c* ($\approx 1000 \text{ s}^{-1}$). This difference implies that the conformational change or proton transfer accompanying the electron transfer is slower for cytochrome *c*' than for cytochrome *c*, which is not surprising since cytochrome *c* is an electron transfer protein optimized to efficiently undergo redox changes, whereas the function of cytochrome *c*' is still unclear.^{42,43} For long thiols the rate constants for immobilized

cytochrome c' are even 500 fold slower than for immobilized cytochrome c . This suggests that the heme group of immobilized cytochrome c' is further away from the electrode than the heme group of immobilized cytochrome c .

Ligand binding to cytochrome c' . The efficient electron transfer between the electrode and the heme groups in cytochrome c' also allowed us to study the effects of ligand binding on cytochrome c' . CO, NO and CN⁻ have all been reported to induce protein monomerization, which is caused by a conformational change in one of the α -helices present at the dimer interface that occurs upon displacement of Tyr16 by ligand binding.²⁹ We focused on CO because this ligand is easily handled and redox inactive. CO only binds to the protein in its Fe^{II} state and was previously reported to bind relatively slowly.⁴⁴ Indeed, voltammograms recorded at high scan rates in a saturated CO solution do not show an apparent influence of CO, which is consistent with slow CO binding. However, when lowering the scan rate we observed a decrease in the intensity of the original anodic peak and the formation of a new anodic peak at potentials about 250 mV more positive (Figure 5.7). This new peak can be assigned to the oxidation of Fe^{II}-CO cytochrome c' . Since Fe^{II}-CO cytochrome c' has a six coordinated heme it has a much more positive potential. The reactions that occur are described by equations 1-4. The fact that the size of the new anodic peak strongly depends on the scan rate, implies that binding of CO to the Fe^{II} state of cytochrome c' is a relatively slow process. Since no new cathodic peak is observed at high potentials for any scan rate, we can also deduce that release of CO after oxidation of the Fe^{II}-CO cytochrome c' is fast.



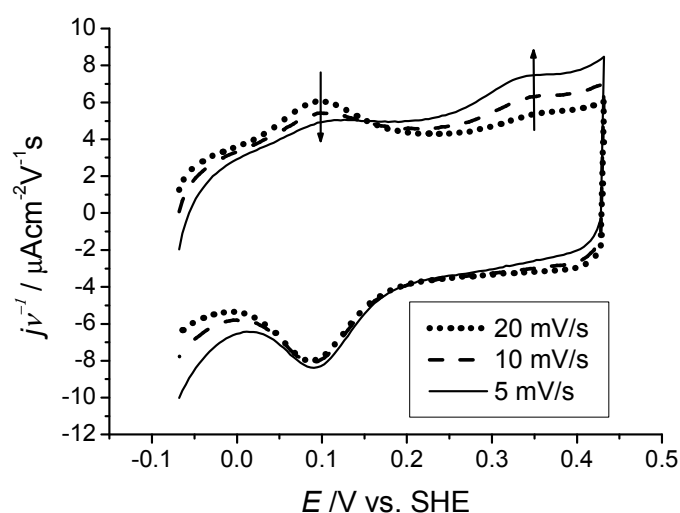


Figure 5.7 Cyclic voltammograms at 20 mV/s (—), 10 mV/s (- - -) and 5 mV/s (····) of a gold electrode with a SAM of 6-mercaptophexanoic acid in a saturated CO solution (~1.1 mM) with 100 nM cytochrome *c'* in 1 mM acetate, pH 4.5. For comparison voltammograms are divided by scan rate.

Binding of CO does not only result in a shift of the anodic peak, but also results in significant conformational changes of the protein on the surface. This can be derived from Figure 5.8, where a voltammetric scan at 100 mV/s is plotted after the electrode is held at $E = -0.02$ V vs. SHE for 100 s. At this potential the immobilized cytochrome *c'* is in its Fe^{II} state, which means that it is slowly binding CO. Accordingly, in the voltammetric scan following the incubation period the original anodic peak has largely disappeared and the new anodic peak corresponding to oxidation of $\text{Fe}^{\text{II}}\text{-CO}$ is observed at higher potentials. This peak is found at approximately 0.38 V, which given the Nernstian behavior of the protein would imply that almost all CO bound protein molecules should be oxidized by the time the voltammetric scan reaches its anodic limit of 0.53 V. However, there seems to be some tailing of the anodic peak, which could indicate limited electronic coupling between the protein and the electrode and hence suggests that part of the CO bound cytochrome *c'* has reoriented or desorbed. This is confirmed by the fact that the charge under the subsequent cathodic peak has significantly decreased, which implies that there is a decrease in coverage of electroactive protein. Experiments in the absence of CO did not show any loss in protein coverage when the electrode was held at $E = -0.02$ V vs. SHE. A plausible explanation for the decrease in protein coverage is that the interactions between cytochrome *c'* and the SAM are weaker in its monomeric form than in its dimeric form resulting in a lower protein coverage. Another explanation is that the monomerization induced by CO

binding causes the protein to reorient on the surface impeding the electron transfer between the electrode and the protein. This is also suggested by the fact that the position of the new anodic peak shifts positively with increasing scan rate, which indicates that electron transfer is relatively slow (Figure S5.4). This makes it difficult to investigate the new anodic peak of the CO bound cytochrome c' at high scan rates, since it shifts outside our potential window. Both explanations are consistent with the CO-induced monomerization observed in solution and suggest that protein monomerization is not impeded by the fact that the protein is immobilized. Denaturation of the protein does not occur, as is reflected in the fact that both the cathodic and anodic peak are recovered after continued scanning.

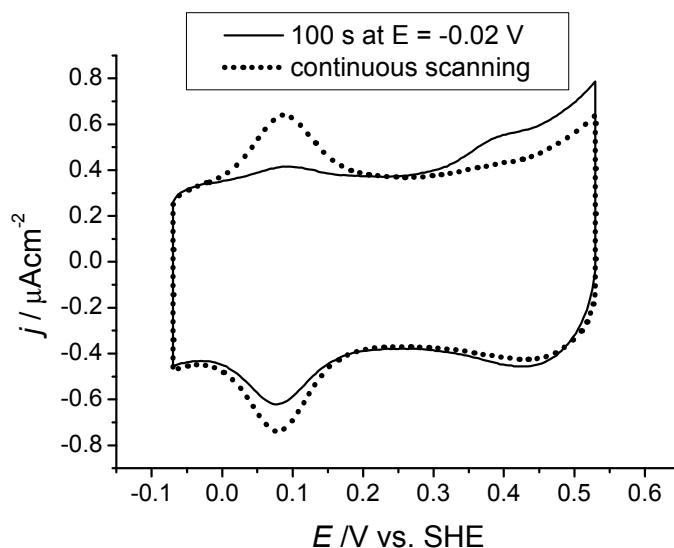


Figure 5.8 Cyclic voltammograms of a gold electrode with a SAM of 6-mercaptophexanoic acid in a saturated CO solution with 100 nM cytochrome c' in 10 mM acetate, pH 4.5. The dotted line (---) is obtained after continuous scanning at 100 mV/s. The solid line (—) is obtained in the first scan (100 mV/s) after incubation at $E = -0.02$ V vs. SHE for 100 sec.

To determine the rate of CO binding to the adsorbed cytochrome c' we measured the binding of CO as a function of time. Analogous to Figure 5.8, the potential of the electrode was held at -0.02 V vs. SHE for a certain time and subsequently a scan at 1 V/s was recorded. A high scan rate was used to avoid readsorption of cytochrome c' from solution during the scan. The voltammograms are displayed in Figure S5.5. Direct determination of CO binding employing the area under the new anodic peak is not possible, since not all CO bound cytochrome c' is oxidized within our potential window at this high scan rate. Therefore we determined the amount of adsorbed cytochrome c' that had *not* reacted with CO by integration of the low potential anodic peak. The area

under this peak was divided by the area under the anodic peak before incubation at $E = -0.02$ V resulting in the fraction of cytochrome *c'* that has *not* reacted with CO. In Figure 5.9 the natural logarithm of this fraction is plotted as a function of the incubation time. A linear relationship is observed, which means that binding of CO to cytochrome *c'* is a first-order process. Such a process can be described by equation 5. Given the saturation concentration for CO of 1.1 mM, a k of 24 ± 1 M⁻¹ s⁻¹ can be deduced.

$$\ln\left(\frac{[Fe^{II}]}{[Fe^{II}]_0}\right) = -k[CO]t \quad (5)$$

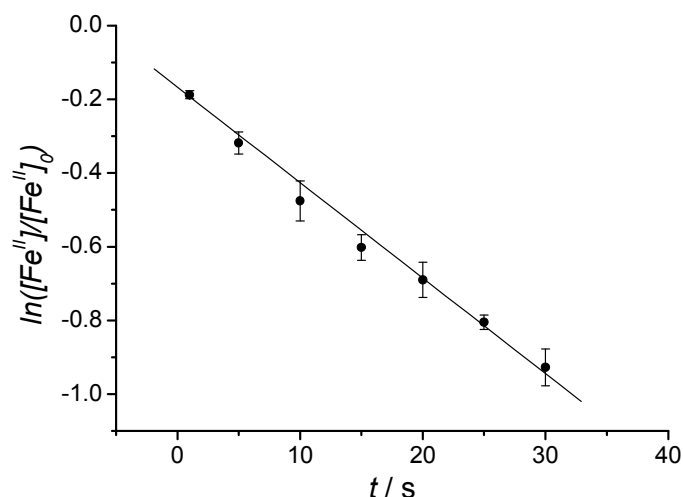


Figure 5.9 Plot of the natural logarithm of the fraction of Fe^{II} that has not reacted with CO versus the time at which the potential has been kept at $E = -20$ mV vs. SHE. Fractions were determined by dividing the low potential anodic peak area after incubation by the anodic peak area before incubation. Voltammograms were recorded at 1 V/s. The experiments were performed on cytochrome *c'* immobilized on a self-assembled monolayer of mercaptohexanoic acid in a 10 mM acetate solution, pH 4.5. All points were measured at least three times and standard deviations are indicated by bars. $T = 22$ °C.

In order to determine whether immobilization of the protein affects its CO binding rate we also measured the CO binding to cytochrome *c'* in solution under identical conditions. For this the absorption maximum at 418 nm typical of CO bound cytochrome *c'* was monitored by UV/Vis spectroscopy.³⁵ Figure 5.10 shows a gradual increase in the absorbance at this wavelength after reduction of ferric to ferrous cytochrome *c'* by dithionite in a CO saturated solution. The data can be fitted with a first order exponential

decay, which implies that the reaction is first order in cytochrome c' with a k of $48 \pm 1 \text{ M}^{-1} \text{ s}^{-1}$. The measured rate is lower than the previously reported value of $140 \text{ M}^{-1} \text{ s}^{-1}$,⁴⁴ which is probably due to the difference in pH between both measurements (pH 7.4 vs. pH 4.5). The fact that the CO binding rate in solution is of the same order as for immobilized cytochrome c' suggests that the protein retains near-native behavior on the surface.

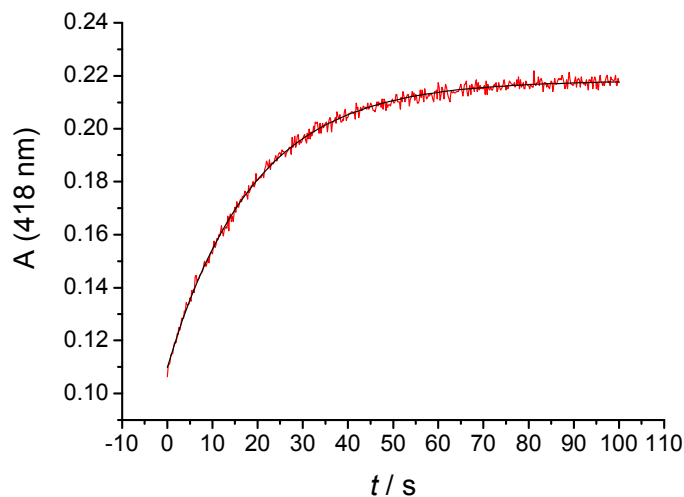


Figure 5.10 CO binding to cytochrome c' measured by UV/Vis spectroscopy. Absorption at 418 nm (typical of CO bound cytochrome c') is followed in time after ferric cytochrome c' is reduced to ferrous cytochrome c' by dithionite in a CO saturated solution. The solution contained $1 \mu\text{M}$ cytochrome c' in 50 mM acetate solution, pH 4.5. $T = 22 \text{ }^\circ\text{C}$. The data were fitted with a first order exponential decay (black line).

The NO binding properties of immobilized cytochrome c' are distinctly different from the CO binding properties. Bubbling NO through solution for just one second resulted in an immediate disappearance of the anodic and cathodic peaks (Figure 5.11). We could not detect a new anodic peak below 400 mV, but were able to recover a small fraction of the original protein peaks if we cycled at high scan rates to potentials as high as 800 mV vs. SHE (Figure S6). This is in line with the behavior of iron porphyrins, which can also only be oxidized at high potentials.^{69,70} Due to anodic oxide formation on the electrode we could not detect the location of a new anodic peak. Also the NO binding rate is too fast to determine it voltammetrically, so we can only say that NO binding is much faster than CO binding. This is consistent with data reported for *Alcaligenes xylosoxidans* cytochrome c' in solution, which is the only cytochrome c' for which NO binding rates have been reported. For this cytochrome c' NO and CO binding rates were determined to be $4400 \text{ M}^{-1} \text{ s}^{-1}$ and $92 \text{ M}^{-1} \text{ s}^{-1}$, respectively.^{44,71}

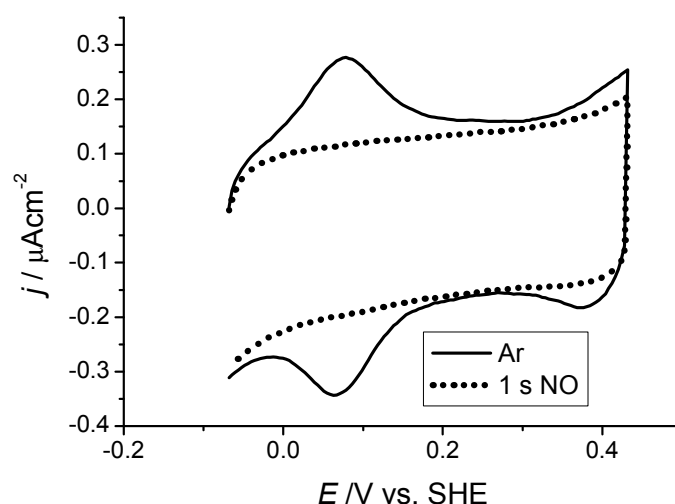


Figure 5.11 Cyclic voltammograms of cytochrome *c'* immobilized on a SAM of mercaptohexanoic acid before (—) and after 1 s of NO bubbling (····) through an 10 mM acetate solution, pH 4.8 containing 100 nM cytochrome *c'*. Scan rate = 50 mV/s.

5.4 Discussion and Conclusions

We have successfully immobilized *Allochromatium vinosum* cytochrome *c'* on carboxylic acid-terminated SAMs. The immobilization does not seem to induce large conformational changes or denaturation of the protein. We base this on the fact that (i) the potential for the Fe^{III}/Fe^{II} heme transition is in reasonable accordance with values reported for the protein in solution, (ii) the coverage is similar to the coverage of immobilized cytochrome *c* and is typical of a protein, (iii) the voltammetric peaks display almost ideal Nernstian behavior, which is typical of a protein, but uncommon for e.g. adsorbed porphyrins,^{72,73} (iv) the narrow pH range in which successful adsorption can be achieved is in accordance with the pI of the protein (v) the observed electron-transfer behavior is typical of an immobilized protein (vi) the unique ligand binding properties observed for cytochrome *c'* in solution (slow CO binding, fast NO binding) are also observed for immobilized cytochrome *c'*.

Our results on immobilized cytochrome *c'* from *Allochromatium vinosum* distinctly differ from previous immobilization studies of cytochromes *c'* from different organisms.⁷⁴⁻⁷⁶ In these studies peak separations of over 50 mV⁷⁴ and much lower electron-transfer rate constants were reported.⁷⁶ Additionally, protein adsorption rates were more than 10000 fold slower than in our work.⁷⁶ Taking into account that that no dependence of ionic strength on protein coverage was observed,⁷⁶ it seems that the binding of cytochrome *c'* in these studies was not electrostatic. This is also suggested by the fact that the measurements were reported at pH 7 (where the protein is negatively

charged) on a negatively charged SAM. It is likely that the way cytochrome c' was bound in these studies induced conformational changes to the proteins structure, which impedes the comparison with our results. Moreover, no electron transfer on thiols of different length and ligand binding kinetics were reported in these studies.

Based on our results and the structure of the protein we can make a rough estimate of the way in which cytochrome c' adsorbs on the carboxyl thiol layer. Binding of cytochrome c' to the negatively charged SAMs occurs via positively charged residues (arginine and lysine) on the surface of the protein. Given the high heme coverage observed with cytochrome c' , we can assume that both hemes in the protein are in electronic contact with the electrode. It is unlikely that direct electron transfer occurs between the two hemes in cytochrome c' due to the fact that the edge-to-edge distance between both hemes is 19 Å (the iron-to-iron distance is 23 Å), which is well above the maximum of 14 Å reported for feasible biological electron transfer.⁷⁷ Since we observe a single electron-transfer rate, we can conclude that both hemes are probably at an equal distance from the electrode. This leaves only two possible orientations by which the protein can bind to the SAM (Figure 5.12). Since the positively charged residues are mostly located on one particular side of the protein (View A), it is likely that the protein is bound to the electrode via this side. The hemes are located close to this positive surface, explaining why efficient electron transfer was observed between the electrode and the protein.

Based on the differences in electron-transfer rate constants between immobilized cytochrome c' and cytochrome c , we can roughly estimate the difference in the heme-electrode distance between both systems. For this, we assume that the difference in reorganization energy upon reduction of both proteins is reflected in the difference between the maximum electron-transfer rate constants observed at short thiols. Given the differences in electron-transfer rate constants of approximately 500 and 7 for long and short thiols, respectively, we can deduce that a 70 fold decrease is caused by the extra distance. Assuming that the exponential decay coefficient β through both proteins is approximately 1.2 \AA^{-1} ,^{78,79} we can estimate that this distance is about $3.5 \pm 1 \text{ \AA}$.⁶⁴ This agrees with the distance predicted from an analysis of the most likely orientation of both cytochrome c' and cytochrome c immobilized on an electrode (Figure 5.13).

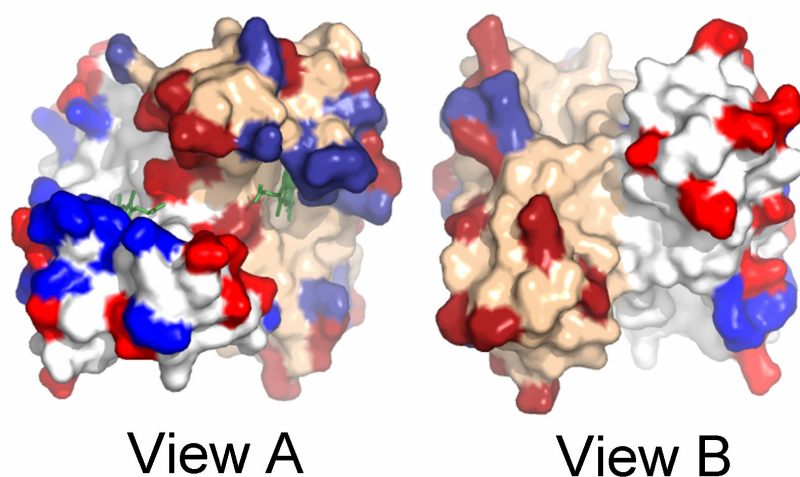


Figure 5.12 Charge distribution on cytochrome *c'* at pH 5.0, observed from opposite sides of the protein. Positive groups (lysine and arginine) are depicted in blue, whereas negative groups (aspartic acid and glutamic acid) are depicted in red. The heme groups are depicted in green. Different colors are used for the two monomers forming the dimeric protein. PDB code: 1BBH.

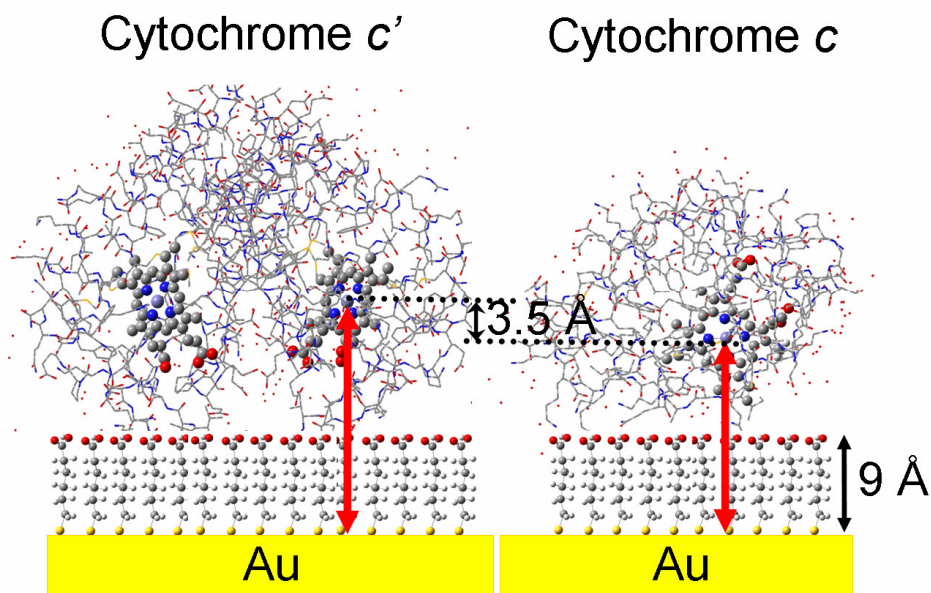


Figure 5.13 Schematic representation of *Allochromatium vinosum* cytochrome *c'* (left) and horse heart cytochrome *c* (right) immobilized on a SAM of mercaptohexanoic acid. The heme groups in both proteins have been accentuated. The representation is approximately to scale. PDB codes: 1BBH and 1HRC.

An important reason to study cytochrome *c*' was to probe whether ligand-induced conformational changes are impeded when a protein is immobilized. In the case of cytochrome *c*' these conformational changes can be induced by CO binding, which results in the monomerization of the protein. In voltammetry we observed the formation of a new anodic peak at high potentials reflecting the oxidation of a newly formed Fe^{II}-CO adduct. Additionally, we observed a decrease in the cathodic peak indicating the loss of electroactive protein. This suggests that the protein indeed undergoes monomerization, which influences the binding of the protein to the electrode. The protein either reorients on the surface with a possible temporal loss of electron transfer or desorbs. Although the difference in CO binding kinetics is relatively small, CO binding is slower for surface immobilized cytochrome *c*' by a factor 2. This could be due to either the electrostatic interactions between the electrode and the protein or due to steric hindrance on the surface hindering monomerization.

In conclusion, we have shown that cytochrome *c*' immobilized on carboxylic acid-terminated SAMs retains a near-native conformation, exhibits fast electron transfer to the electrode and probably undergoes the same conformational changes upon ligand binding as in solution. Our results suggest that carboxylic acid-terminated SAMs are suitable for the study of immobilized proteins in general, since the electrostatic interactions are sufficient to confine the protein to the surface, but do not significantly affect its properties. Successful immobilization requires that the protein is sufficiently positively charged and that the distance between the electrode and the proteins redox groups is not too long. Whether these requirements are met can be deduced from the pI of the protein and an analysis of the most likely conformation of the protein on the SAM.

5.5 Supporting Information

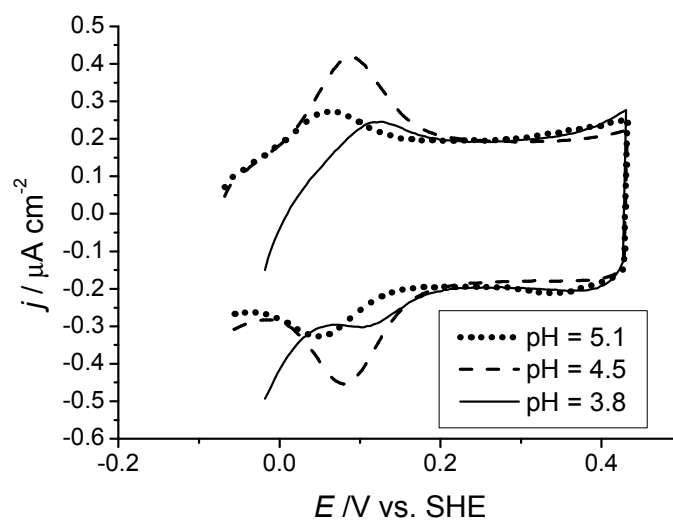


Figure S5.1 Cyclic voltammograms of an Au electrode coated with mercaptohexanoic acid (MHA) in 200 nM *Allochromatium vinosum* cytochrome *c*' in 10 mM acetate solution of pH 3.8 (—), pH 4.5 (---) and pH 5.1 (····). Scan rate = 50 mV/s.

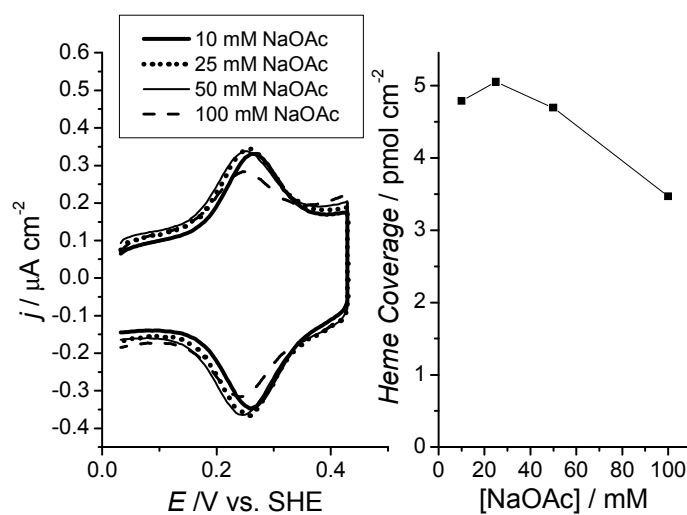


Figure S5.2 Cyclic voltammograms of adsorbed cytochrome *c* on Au with a SAM of mercaptohexanoic acid in 200 nM cytochrome *c* (a) in 10 (—), 25 (····), 50 (—) and 100 (---) mM acetate solution, pH 4.8. Scan rate = 50 mV/s.

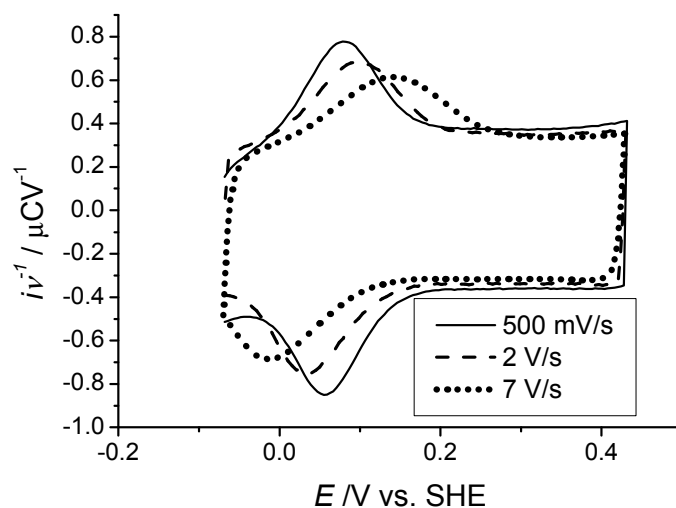


Figure S5.3 Cyclic voltammograms of an Au electrode with a 6-mercaptohexanoic acid (MHA) SAM in 200 nM *Allochromatium vinosum* cytochrome *c'* in 10 mM acetate solution of pH 4.8 at 500 mV/s (—), 2 V/s (---) and 7 V/s (····).

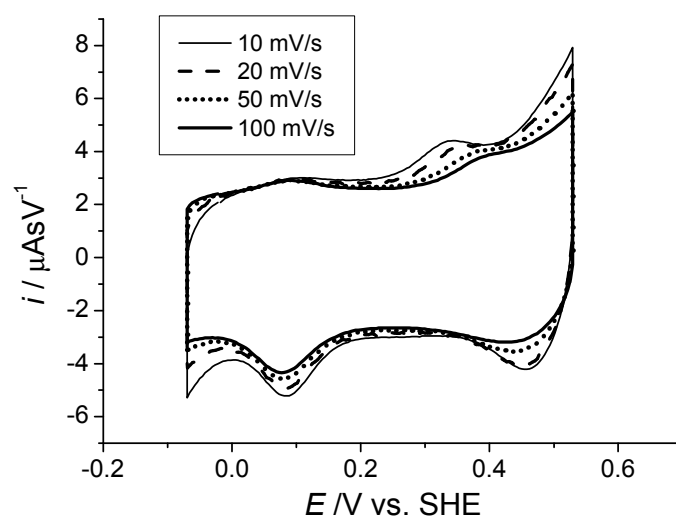


Figure S5.4 Cyclic voltammograms at 10 (—), 20 (---), 50 (····) and 100 (—) mV/s of a gold electrode with a SAM of 6-mercaptohexanoic acid in a saturated CO solution with 100 nM *Allochromatium vinosum* cytochrome *c'* in 10 mM acetate, pH 4.5 after incubation at $E = -0.02 \text{ V vs. SHE}$ for 100 sec.

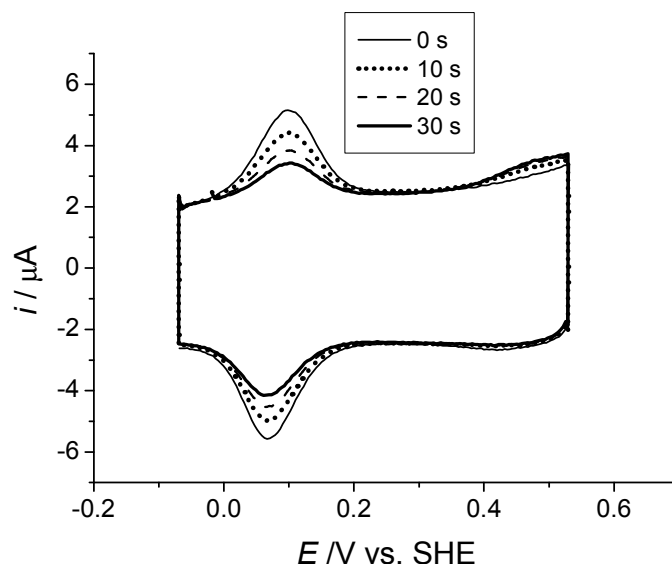


Figure S5.5 Cyclic voltammograms at 1 V/s of a gold electrode with a SAM of 6-mercaptohexanoic acid in a saturated CO solution with 100 nM *Allochromatium vinosum* cytochrome *c'* in 10 mM acetate, pH 4.5 after incubation at $E = -0.02$ V vs. SHE for 0 (—), 10 (⋯), 20 (---), or 30 (—) sec.

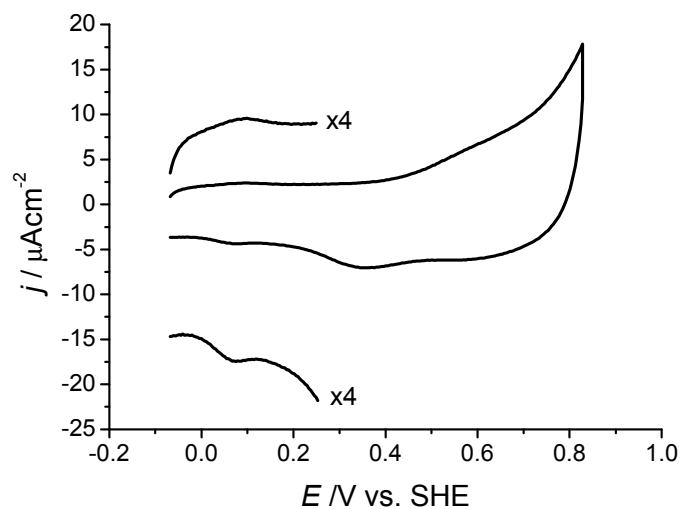


Figure S5.6 Cyclic voltammograms of an Au-MHA-cytochrome *c'* electrode after one second of NO bubbling through a 10 mM acetate solution, pH 4.8 with 200 nM cytochrome *c'*. Scan rate = 500 mV/s. Part of the voltammogram (between -0.07 V and 0.23 V) is enlarged four times to show the presence of the protein's redox couple.

5.6 References

1. Armstrong, F. A. *Curr. Opin. Chem. Biol.* **2005**, *9*, 110-117.
2. Schuhmann, W. *Rev. Mol. Biotech.* **2002**, *82*, 425-441.
3. Scheller, F. W.; Wollenberger, U.; Lei, C.; Jin, W.; Ge, B.; Lehmann, C.; Lisdat, F.; Fridman, V. *Rev. Mol. Biotech.* **2002**, *82*, 411-424.
4. Ikeda, T.; Kano, K. *Biochim. Biophys. Acta* **2003**, *1647*, 121-126.
5. Armstrong, F. A.; Wilson, G. S. *Electrochim. Acta* **2000**, *45*, 2623-2645.
6. Elliott, S. J.; Hoke, K. R.; Heffron, K.; Palak, M.; Rothery, R. A.; Weiner, J. H.; Armstrong, F. A. *Biochemistry* **2004**, *43*, 799-807.
7. Hudson, J. M.; Heffron, K.; Kotlyar, V.; Sher, Y.; Maklashina, E.; Cecchini, G.; Armstrong, F. A. *J. Am. Chem. Soc.* **2005**, *127*, 6977-6989.
8. Vincent, K. A.; Parkin, A.; Lenz, O.; Albracht, S. P. J.; Fontecilla-Camps, J. C.; Cammack, R.; Friedrich, B.; Armstrong, F. A. *J. Am. Chem. Soc.* **2005**, *127*, 18179-18189.
9. Hobara, D.; Niki, K.; Cotton, T. M. *Biospectroscopy* **1998**, *4*, 161-170.
10. Wackerbarth, H.; Hildebrandt, P. *ChemPhysChem* **2003**, *4*, 714-724.
11. Hildebrandt, P.; Stockburger, M. *Biochemistry* **1989**, *28*, 6710-6721.
12. de Groot, M. T.; Merckx, M.; Koper, M. T. M. *J. Am. Chem. Soc.* **2005**, *127*, 16224-16232.
13. de Groot, M. T.; Merckx, M.; Koper, M. T. M. *Electrochem. Commun.* **2006**, *8*, 999-1004.
14. Chen, X.; Ferrigno, R.; Yang, J.; Whitesides, G. M. *Langmuir* **2002**, *18*, 7009-7015.
15. Haas, A. S.; Pilloud, D. L.; Reddy, K. S.; Babcock, G. T.; Moser, C. C.; Blasie, J. K.; Dutton, P. L. *J. Phys. Chem. B* **2001**, *105*, 11351-11362.
16. Tarlov, M. J.; Bowden, E. F. *J. Am. Chem. Soc.* **1991**, *113*, 1847-1849.
17. Hildebrandt, P.; Murgida, D. H. *Bioelectrochemistry* **2002**, *55*, 139-143.
18. Ataka, K.; Heberle, J. *J. Am. Chem. Soc.* **2004**, *126*, 9445-9457.
19. Niki, K.; Hardy, W. R.; Hill, M. G.; Li, H.; Sprinkle, J. R.; Margoliash, E.; Fujita, K.; Tanimura, R.; Nakamura, N.; Ohno, H.; Richards, J. H.; Gray, H. B. *J. Phys. Chem. B* **2003**, *107*, 9947-9949.
20. Niki, K.; Pressler, K. R.; Sprinkle, J. R.; Li, H.; Margoliash, E. *Russ. J. Electrochem.* **2002**, *38*, 63-67.
21. Avila, A.; Gregory, B. W.; Niki, K.; Cotton, T. M. *J. Phys. Chem. B* **2000**, *104*, 2759-2766.
22. Feng, Z. Q.; Imabayashi, S.; Kakiuchi, T.; Niki, K. *J. Chem. Soc., Faraday Trans.* **1997**, *93*, 1367-1370.
23. Murgida, D. H.; Hildebrandt, P. *J. Am. Chem. Soc.* **2001**, *123*, 4062-4068.
24. Nahir, T. M.; Bowden, E. F. *J. Electroanal. Chem.* **1996**, *410*, 9-13.
25. Murgida, D. H.; Hildebrandt, P. *Acc. Chem. Res.* **2004**, *37*, 854-861.
26. Chi, Q.; Zhang, J.; Andersen, J. E. T.; Ulstrup, J. *J. Phys. Chem. B* **2001**, *105*, 4669-4679.
27. Jeuken, L. J. C.; McEvoy, J. P.; Armstrong, F. A. *J. Phys. Chem. B* **2002**, *106*, 2304-2313.
28. Doyle, M. L.; Gill, S. J.; Cusanovich, M. A. *Biochemistry* **1986**, *25*, 2509-2516.
29. Ren, Z.; Meyer, T.; McRee, D. E. *J. Mol. Biol.* **1993**, *234*, 433-445.
30. Mizoue, L. S.; Chazin, W. J. *Curr. Opin. Struct. Biol.* **2002**, *12*, 459-463.

31. Akiyama, S.; Fujisawa, T.; Ishimori, K.; Morishima, I.; Aono, S. *J. Mol. Biol.* **2004**, *341*, 651-668.
32. Gilles-Gonzalez, M. A.; Gonzalez, G. *J. Applied Physiology* **2004**, *96*, 774-783.
33. Jain, R.; Chan, M. K. *J. Biol. Inorg. Chem.* **2003**, *8*, 1-11.
34. Padayatti, P. S.; Pattanaik, P.; Ma, X.; van den Akker, F. *Pharmacol. Ther.* **2004**, *104*, 83-99.
35. Evers, T. H.; Merckx, M. *Biochem. Biophys. Res. Commun.* **2005**, *327*, 668-674.
36. Van den Brink, F.; Visscher, W.; Barendrecht, E. *J. Electroanal. Chem.* **1983**, *157*, 283-304.
37. de Vooy, A. C. A.; Koper, M. T. M.; van Santen, R. A.; van Veen, J. A. R. *Electrochim. Acta* **2001**, *46*, 923-930.
38. Lide, D. R. *CRC Handbook of Chemistry and Physics, 83rd Edition*; CRC press: Cleveland: 2002.
39. Press, W. H.; Flannery, B. P.; Teukolsky, S. A.; Vetterling, W. T. *Numerical Recipes in Pascal*; Cambridge University Press: New York, 1989.
40. Heering, H. A.; Wiertz, F. G. M.; Dekker, C.; De Vries, S. *J. Am. Chem. Soc.* **2004**, *126*, 11103-11112.
41. Trasatti, S.; Petrii, O. A. *Pure Appl. Chem.* **1991**, *63*, 711-734.
42. Romao, M. J.; Archer, M. Handbook of Metalloproteins, Volume 1. Messerschmidt, A., Huber, R., Wieghardt, K., Poulos, T., Eds.; John Wiley & Sons: Chichester, 2001; pp 44-54.
43. Weiss, R.; Gold, A.; Terner, J. *Chem. Rev.* **2006**, *106*, 2550-2579.
44. Cusanovich, M. A.; Gibson, Q. H. *J. Biol. Chem.* **1973**, *248*, 822-834.
45. Erabi, T.; Yamashita, Y.; Nishimura, K.; Wada, M. *Bull. Chem. Soc. Jpn.* **1987**, *60*, 2251-2252.
46. Barakat, R.; Streckas, T. C. *Biochim. Biophys. Acta* **1982**, *679*, 393-399.
47. Rodkey, F. L.; Ball, E. G. *J. Biol. Chem.* **1950**, *182*, 17-28.
48. Laviron, E. In *Electroanalytical Chemistry*, Bard, A. J., Ed.; Marcel Dekker: New York, 1982; p 53.
49. Armstrong, F. A.; Camba, R.; Heering, H. A.; Hirst, J.; Jeuken, L. J. C.; Jones, A. K.; Leger, C.; McEvoy, J. P. *Faraday Discuss.* **2000**, *116*, 191-203.
50. Clark, R. A.; Bowden, E. F. *Langmuir* **1997**, *13*, 559-565.
51. Aoki, K.; Kakiuchi, T. *J. Electroanal. Chem.* **1999**, *478*, 101-107.
52. Fawcett, W. R.; Fedurco, M.; Kovacova, Z. *Langmuir* **1994**, *10*, 2403-2408.
53. Sugihara, K.; Teranishi, T.; Shimazu, K.; Uosaki, K. *Electrochemistry* **1999**, *67*, 1172-1174.
54. Smalley, J. F.; Chalfant, K.; Feldberg, S. W.; Nahir, T. M.; Bowden, E. F. *J. Phys. Chem. B* **1999**, *103*, 1676-1685.
55. Sugihara, K.; Shimazu, K.; Uosaki, K. *Langmuir* **2000**, *16*, 7101-7105.
56. Dai, Z.; Ju, H. *Phys. Chem. Chem. Phys.* **2001**, *3*, 3769-3773.
57. Zhao, J.; Luo, L.; Yang, X.; Wang, E.; Dong, S. *Electroanalysis* **1999**, *11*, 1108-1111.
58. Hu, K.; Bard, A. J. *Langmuir* **1997**, *13*, 5114-5119.
59. Munakata, H.; Kuwabata, S. *Chem. Commun.* **2001**, 1338-1339.
60. Shimazu, K.; Teranishi, T.; Sugihara, K.; Uosaki, K. *Chem. Lett.* **1998**, 669-670.
61. Petrovic, J.; Clark, R. A.; Yue, H.; Waldeck, D. H.; Bowden, E. F. *Langmuir* **2005**, *21*, 6308-6316.
62. Laviron, E. *J. Electroanal. Chem.* **1979**, *101*, 19-28.

63. Armstrong, F. A. *J. Chem. Soc., Dalton Trans.* **2002**, 661-671.
64. Marcus, R. A.; Sutin, N. *Biochim. Biophys. Acta* **1985**, 811, 265-322.
65. Finklea, H. O.; Hanshew, D. D. *J. Am. Chem. Soc.* **1992**, 114, 3173-3181.
66. Xu, J.; Li, H.; Zhang, Y. *J. Phys. Chem.* **1993**, 97, 11497-11500.
67. Smalley, J. F.; Feldberg, S. W.; Chidsey, C. E. D.; Linford, M. R.; Newton, M. D.; Liu, Y. P. *J. Phys. Chem.* **1995**, 99, 13141-13149.
68. Jeuken, L. J. C. *Biochim. Biophys. Acta* **2003**, 1604, 67-76.
69. Chi, Y.; Chen, J.; Aoki, K. *Inorg. Chem.* **2004**, 43, 8437-8446.
70. Trofimova, N. S.; Safronov, A. Y.; Ikeda, O. *Inorg. Chem.* **2003**, 42, 1945-1951.
71. Andrew, C. R.; George, S. J.; Lawson, D. M.; Eady, R. R. *Biochemistry* **2002**, 41, 2353-2360.
72. Pilloud, D. L.; Chen, X.; Dutton, P. L.; Moser, C. C. *J. Phys. Chem. B* **2000**, 104, 2868-2877.
73. Sagara, T.; Fukuda, M.; Nakashima, N. *J. Phys. Chem. B* **1998**, 102, 521-527.
74. Ge, B.; Meyer, T.; Schoning, M. J.; Wollenberger, U.; Lisdat, F. *Electrochem. Commun.* **2000**, 2, 557-561.
75. Erabi, T.; Ozawa, S.; Hayase, S.; Wada, M. *Chem. Lett.* **1992**, 2115-2118.
76. Lisdat, F.; Ge, B.; Stocklein, W.; Scheller, F. W.; Meyer, T. *Electroanalysis* **2000**, 12, 946-951.
77. Page, C. C.; Moser, C. C.; Chen, X.; Dutton, P. L. *Nature* **1999**, 402, 47-52.
78. Moser, C. C.; Keske, J. M.; Warncke, K.; Farid, R. S.; Dutton, P. L. *Nature* **1992**, 355, 796-802.
79. Langen, R.; Chang, I. J.; Germanas, J. P.; Richards, J. H.; Winkler, J. R.; Gray, H. B. *Science* **1995**, 268, 1733-1735.

Chapter 6

Reorganization of immobilized horse and yeast cytochrome *c* induced by pH changes or nitric oxide binding*

Abstract: *The redox properties of horse and yeast cytochrome *c* electrostatically immobilized on carboxylic acid-terminated self-assembled monolayers (SAMs) have been determined over a broad pH range (pH 3.5–8) in the absence and presence of nitric oxide. Below pH 6, both proteins exhibit comparable midpoint potentials, coverages, and electron-transfer rate constants, which suggests that they are adsorbed on the SAM in a similar fashion. Above pH 6, a sharp decrease in electron-transfer rate constants is observed for immobilized yeast cytochrome *c*, which is indicative of a change in the electron tunneling pathway between the heme and the electrode and hence suggests that the protein reorients on the surface. Such a decrease is not observed for horse cytochrome *c*, and therefore must be related to the specific charge distribution on yeast cytochrome *c*. Apart from the charge distribution on the protein, the reorientation also seems to be related to the charge on the SAM surface. The presence of nitric oxide causes a decrease in electron-transfer rate constants of both yeast and horse cytochrome *c* at low pH. This is probably due to the fact that nitric oxide induces a conformational change of the protein and also changes the reorganization energy for electron transfer.*

* The contents of this chapter have been published: de Groot, M.T.; Merckx, M.; Koper, M.T.M., *Langmuir* **2007**, 23, 3832-3839

6.1 Introduction

The number of papers devoted to the electrochemical investigation of redox proteins has rapidly increased over the past few decades. Experiments can be performed with the protein in solution or with the protein immobilized on an electrode surface. The latter method is most informative, if direct electron transfer between the electrode and the protein's redox centers is possible. This enables the probing of fast processes that occur upon a redox transition in the protein.¹⁻⁴ To derive valuable conclusions from these experiments, one has to ensure that immobilization of the protein does not significantly affect its conformation. This can be determined directly by spectroscopic methods⁵⁻⁷ or indirectly by checking its electrochemical properties such as enzymatic activity, redox potential, Nernstian behavior, and electron-transfer rates.⁸⁻¹¹

The most widely studied immobilized protein is horse cytochrome *c*. When electrostatically immobilized on carboxylic acid-terminated self-assembled monolayers (SAMs), rapid electron transfer is observed between cytochrome *c* and the electrode.^{12,13} Surface spectroscopy methods have shown that the electrostatic immobilization does not significantly affect the conformation of the protein.⁵⁻⁷ This is in contrast to immobilization on bare gold or silver electrodes or hydrophobic SAMs, on which horse cytochrome *c* undergoes significant conformation changes.¹⁴⁻¹⁶ Using a combination of spectroscopy, and protein engineering the protein residues that interact with the negatively charged SAM have been identified, and from this the most probable orientation of horse cytochrome *c* on these carboxylic acid-terminated SAMs at pH 7 has been determined.^{5,17-19} The electrode coverage of immobilized cytochrome *c* has been determined with STM.²⁰

The extensive characterization of immobilized horse cytochrome *c* on carboxylic acid-terminated SAMs makes it a good model system to gain a more fundamental understanding of the properties of immobilized proteins. The system was, e.g., used to study long-distance electron transfer between the protein and electrode,^{6,21-23} and the influence of interfacial electric fields and the ionic strength of the solution on the properties of the protein.^{24,25}

Although the studies mentioned above have yielded a detailed understanding of the properties of immobilized horse cytochrome *c* on these SAMs, some observations remain poorly understood. One of these is the large difference in electron-transfer rate constants between horse and yeast cytochrome *c*,²⁶ which is striking given the 64% sequence identity and similar function of both proteins.²⁷ Another unresolved issue is the more than 50 mV difference in midpoint potential between immobilized horse cytochrome *c* and horse cytochrome *c* in solution at pH 7.^{24,28} This difference has been tentatively ascribed to the influence of an electric field and the charge on the SAM. A third interesting observation is the decrease in the electron-transfer rate constant between immobilized horse cytochrome *c* and the electrode with increasing pH, which suggests a change in the electron transfer mechanism.²⁹

This study aims to provide explanations for these observations based on a careful experimental study of the properties of immobilized horse and yeast cytochrome *c* as a

function of pH. The properties we investigate include midpoint potential, electroactive coverage, and electron-transfer rate. The results will be related to the structural properties of horse and yeast cytochrome *c*, and the probable orientations of both proteins on the electrodes will be discussed.

In addition, we also present the first nitric oxide binding study to immobilized horse and yeast cytochrome *c*. Nitric oxide is a biologically important signaling molecule that binds to heme proteins in both ferrous and ferric states.³⁰ The binding of NO to cytochrome *c* results in structural changes of the protein, since NO replaces either methionine or histidine in the heme pocket.^{31,32} In this study we determine the influence of NO binding on the midpoint potential and electron-transfer rate constants for both horse and yeast cytochrome *c*.

6.2 Experimental Procedures

Materials. Horse *heart* cytochrome *c* (95%, Fluka) and yeast (*Saccharomyces cerevisiae*) cytochrome *c* (>85%, Fluka), 3-mercaptopropionic acid (99%, Aldrich) (MPA), 4-mercaptopropionic acid (95%, Pfaltz & Bauer) (MBA), 6-mercaptopropionic acid (97%, Dojindo) (MHA), 8-mercaptopropionic acid (97%, Dojindo) (MOA), 11-mercaptopropionic acid (95%, Aldrich) (MUA), and 16-mercaptopropionic acid (90%, Aldrich) (MHDA) were all used as received. All other chemicals were p.a. grade (Merck). Buffer solutions were prepared with sodium acetate (pH 3.5-6) or sodium dihydrogen phosphate monohydrate (pH 6-8) combined with concentrated solutions of hydrochloric acid or caustic soda and Millipore MilliQ water (resistivity >18.2 MΩ cm). The concentration of the buffer solutions was either 10 or 50 mM.

Electrochemical Apparatus and Procedures. An Autolab PGstat 20 potentiostat was used for cyclic voltammetry. A homemade three-electrode cell consisting of a gold working electrode, typically a wire with an attached bead, a platinum wire counter electrode and a Hg|Hg₂SO₄ reference electrode was employed. All potentials reported in this paper are relative to the standard hydrogen electrode (SHE). All solutions were deaerated by purging with argon for 15 min. Voltammograms at high scan rates (>5 V/s) that were used in the determination of electron-transfer rate constants were corrected for ohmic drop. Nitric oxide binding experiments were performed in saturated solutions of nitric oxide (purity 2.5, Linde AG) by purging the solution for 10 min. Prior to entering the electrochemical cell, NO was bubbled through two washing flasks filled with a 3 M KOH solution, a procedure that was found to be important to remove NO₂.^{33,34} Since NO readily reacts with oxygen, the cell was purged with argon for 20 min prior to bubbling of NO and was kept closed during the experiments. The saturated solutions contained 2.1 mM NO at 20 °C.³⁵ All electrochemical experiments were performed at room temperature.

Preparation of Gold Electrodes with COOH-Terminated Thiols. Prior to use the gold wire electrodes were flame-annealed and subsequently quenched in water. The electrodes were then immersed in a 1 mM solution of one of the COOH-terminated thiols for approximately 10 min. For 3-mercaptopropionic acid and 4-mercaptopropionic acid

these solutions were prepared by mixing the thiol with water. The other thiol solutions were prepared by mixing with ethanol. The gold electrodes were rinsed and subsequently immersed in the electrochemical cell. The protein concentration in the cell was 400 nM. Protein adsorption was enhanced by argon bubbling and continued until the voltammetric peak reached a maximum, which was after approximately 5 min in a solution of pH 4.5.

Determination of Protein Coverages. Coverages were determined by subtraction of a natural cubic splines baseline³⁶ from the anodic or cathodic scan of the voltammogram and subsequent division by area of the gold electrode. For the baseline subtraction the program “Utilities for Data Analysis” developed by Heering was employed.³⁷ The area of the gold electrodes was determined from an oxygen adsorption experiment in 0.5 M H₂SO₄.³⁸

6.3 Results

Figure 6.1 shows typical voltammograms for immobilized horse and yeast cytochrome *c* at pH 5.4, pH 7.0, and pH 8.0. Clear peaks for the heme Fe^{III}/Fe^{II} transition in cytochrome *c* are observed at all three pH values for both proteins, but there are distinct differences in midpoint potential, coverage, and peak separation between the voltammograms recorded at different pH values. Additionally, there are significant differences between horse and yeast cytochrome *c*, especially in peak separation. To accurately determine the influence of pH on the properties of immobilized cytochrome *c*, voltammograms were recorded over a broad pH range (3.5–8) for both horse and yeast cytochrome *c*. The midpoint potentials and coverages determined from these voltammograms are plotted in Figures 6.2 and 6.3. We focus on the pH 3.5–8 region, where both cytochromes *c* retain the same conformation as at neutral pH. The behavior at higher pH values, where both cytochromes *c* undergo a conformational change to an alkaline form,^{39–41} was not investigated, since this change would significantly complicate the interpretation of the results. The values determined at pH 7 are in line with previous studies.^{21,25,28,29,42}

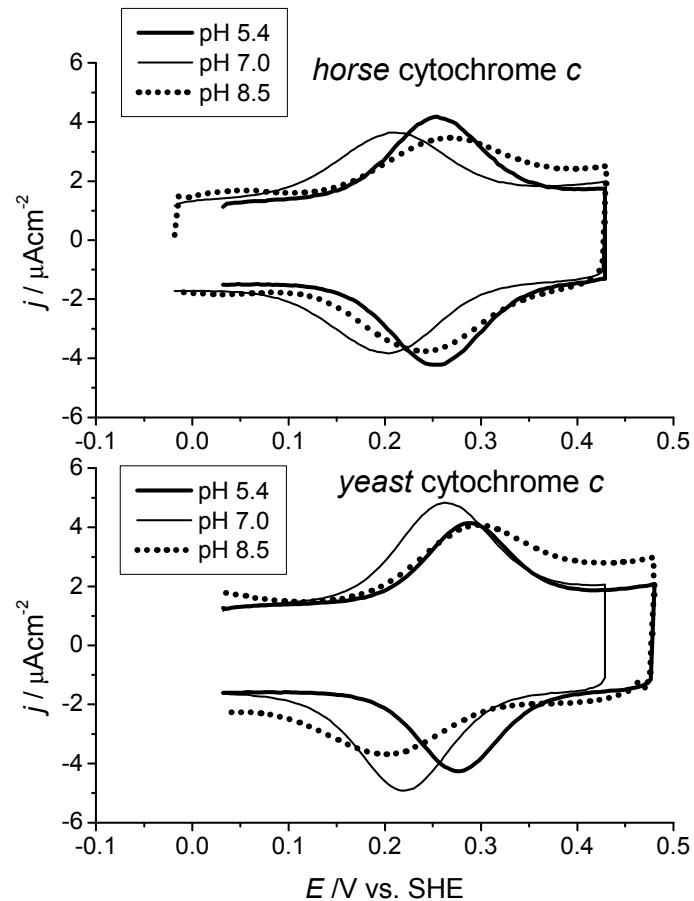


Figure 6.1 Cyclic voltammograms of a gold electrode with a SAM of mercaptohexanoic acid (MHA) in 400 nM horse or yeast cytochrome *c* in a 10 mM acetate solution, pH 5.4 (—), a 10 mM phosphate solution, pH 7.0 (—), or a 10 mM phosphate solution, pH 8.0 (····). Scan rate = 500 mV/s.

Figure 6.2 shows that the dependence of the midpoint potential on pH is similar for horse and yeast cytochrome *c* between pH 3.5 and pH 7. For both proteins there is a gradual decrease in midpoint potential of about 100 mV over this pH range. The small difference of approximately 20 mV between the proteins is consistent with the difference in midpoint potential in solution, being 270 mV for horse cytochrome *c*^{41,43-46} and 290 mV for yeast cytochrome *c*.^{37,40,46,47}

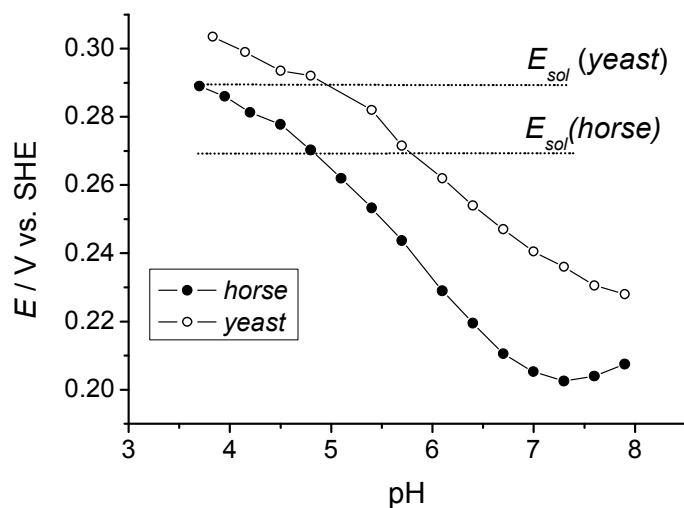


Figure 6.2 Midpoint potentials of horse (●) or yeast (○) cytochrome *c* immobilized on a gold electrode with a SAM of mercaptohexanoic acid (MHA) as a function of pH. Midpoint potentials were determined from baseline-subtracted voltammograms recorded in 10 mM buffer solutions containing 400 nM protein at a scan rate of 500 mV/s. Acetate (pH 3.5-6.1) and phosphate (pH 6.1-8.0) buffers were employed. The midpoint potentials of horse and yeast cytochrome *c* in solution are indicated by dotted lines.⁴⁰

The observed pH dependence of the immobilized proteins is significantly different from the pH dependence of the proteins in solution. In solution the midpoint potentials of both horse and yeast cytochrome *c* do not depend on pH between pH 4 and pH 7.^{40,41,45,48} Therefore, the decrease in midpoint potential we observe must be related to the fact that cytochrome *c* is immobilized. Since horse cytochrome *c* does not reorient on the surface in this pH range (which we will discuss later), the change in midpoint potential is most likely caused by a change in the interfacial electric field.²⁴ This change is probably related to the increasing negative charge on the carboxylic acid-terminated SAM with increasing pH. This is consistent with the finding that the midpoint potential of cytochrome *c* immobilized on a positively charged SAM is 90 mV higher than on a negatively charged SAM.²⁸

Figure 6.3 shows the electroactive coverage of both proteins as a function of pH. Both proteins display a comparable increase in coverage between pH 3.5 and pH 6. This increase in coverage can be related to an increased electrostatic interaction between the protein and the SAM due to increased negative charge on the carboxylic acid-terminated SAM, which has a pKa around 5-7.⁴⁹⁻⁵³ On the other hand, there is a distinct difference in the coverages of both proteins between pH 6 and pH 8, which suggests some intrinsic differences in binding to the SAM.

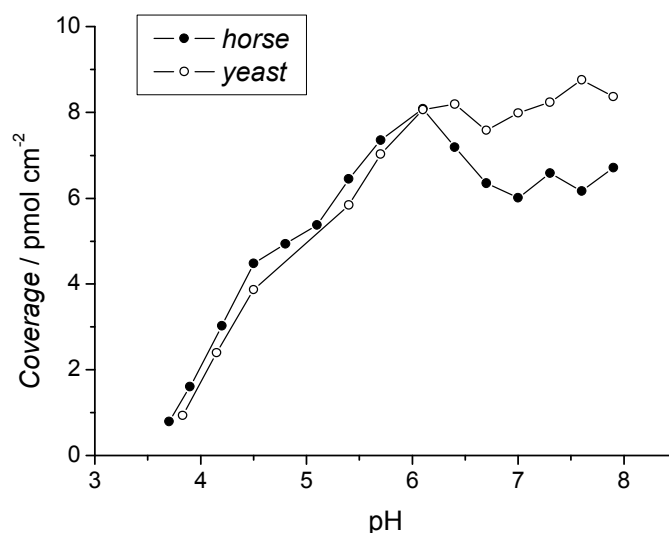


Figure 6.3 Maximum coverages of horse (●) or yeast (○) cytochrome *c* immobilized on a gold electrode with a SAM of mercaptohexanoic acid (MHA) as a function of pH. Coverages were determined from the charge under the voltammetric peaks of baseline-subtracted voltammograms divided by the surface area of the gold electrodes. The voltammograms were recorded in 10 mM buffer solutions containing 400 nM protein at a scan rate of 500 mV/s. Acetate (pH 3.5-6.1) and phosphate (pH 6.1-8.0) buffers were employed.

A third property that can be determined from the voltammograms is the electron-transfer rate constant between immobilized cytochrome *c* and the electrode. This rate constant is related to the dependence of the peak separation between the anodic and the cathodic peaks in the voltammograms on the scan rate. Figure 6.4 shows voltammograms for yeast and horse cytochrome *c* at different pH values and at different scan rates. Both proteins display similar behavior at pH 5. This suggests that both proteins are immobilized on the electrode in a very similar way. However, at pH 7 yeast cytochrome *c* displays significant peak separations at much lower scan rates, indicative of a lower electron-transfer rate constant, whereas horse cytochrome *c* behaves the same as at pH 5. This decrease in rate constant for yeast cytochrome *c* can be related to a change in the length and nature of the electron-tunneling pathway and hence a reorientation of the protein on the electrode or to a change in the reorganization energy of the protein to accommodate electron transfer. Changes in the electron-transfer behavior also occur for horse cytochrome *c* as is shown by the measurement at pH 8, but these changes occur at much higher pH values than for yeast cytochrome *c*.

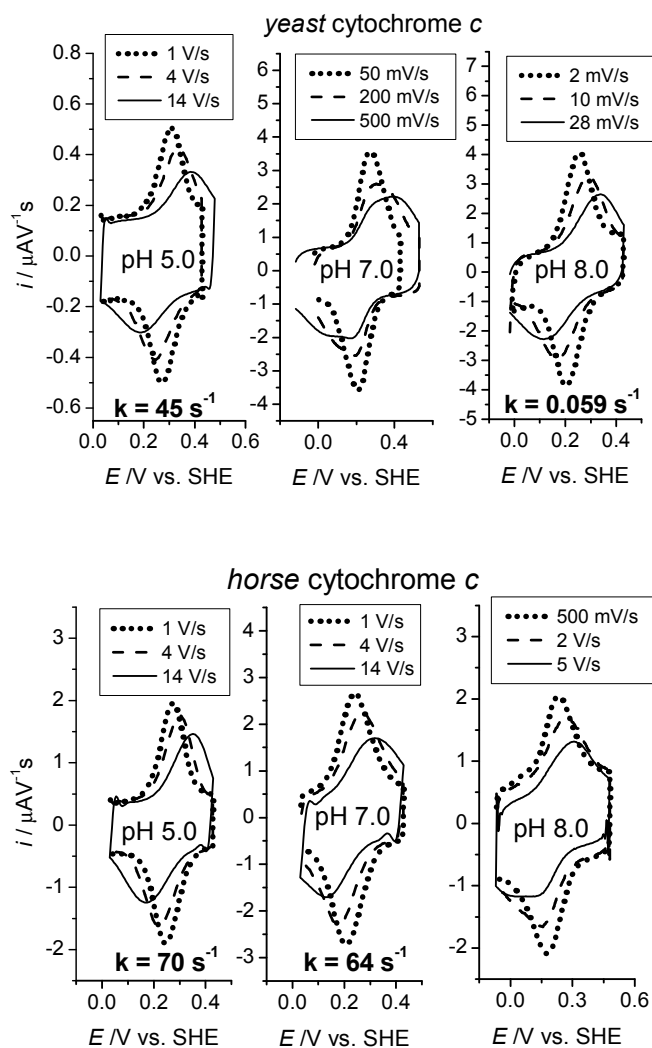


Figure 6.4 Cyclic voltammograms at different scan rates of a gold electrode with a SAM of mercaptoundecanoic acid (MUA) in 400 nM yeast or horse cytochrome *c* in a 10 mM acetate solution, pH 5.0, a 10 mM phosphate solution, pH 7.0, or a 10 mM phosphate solution, pH 8.0.

Electron-transfer rate constants can be determined employing Laviron's method,⁵⁴ which involves plotting the cathodic and anodic peak potentials of voltammograms as a function of the scan rate in so-called Trumpet plots.¹ For horse cytochrome *c* at pH 5 and pH 7 and yeast cytochrome *c* at pH 5 and pH 8 this has been done in Figure 6.5. Employing Laviron's method, the corresponding electron-transfer rate constants can be deduced from these plots. These are given in both Figures 6.4 and Figure 6.5. The rate

constants could not be determined for yeast cytochrome *c* at pH 7 and horse cytochrome *c* at pH 8, due to difficulties in peak potential determination. In these cases the peaks seem to consist of two overlapping peaks, which is indicative of two different peak separations and hence of two different protein orientations on the surface.

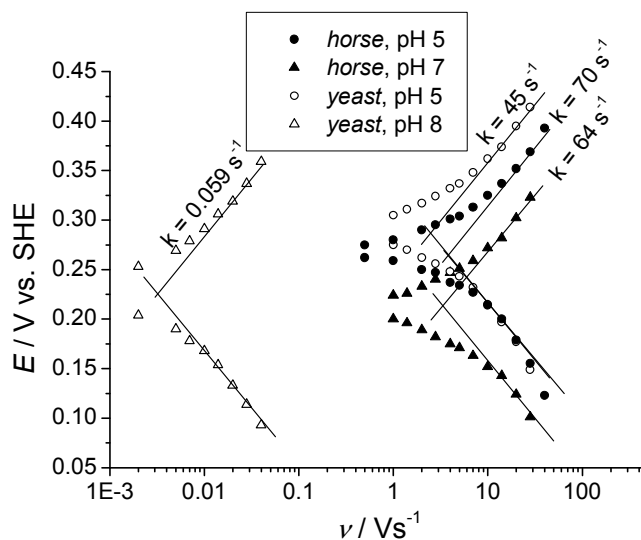


Figure 6.5 Trumpet plots for horse and yeast cytochrome *c* on a SAM of mercaptoundecanoic acid (MUA). Cathodic and anodic peak potentials were determined from voltammograms that were recorded in 400 nM yeast or horse cytochrome *c* in a 10 mM acetate solution, pH 5.0, a 10 mM phosphate solution, pH 7.0, or a 10 mM phosphate solution, pH 8.0. Scan rates ranging from 2 mV s^{-1} to 40 V s^{-1} were employed. Voltammograms at high scan rates were corrected for ohmic drop.

A more complete understanding of the electron-transfer behavior between the electrode and cytochrome *c* can be obtained by determining the electron-transfer rate constants with varying SAM thickness. This thickness can be varied by changing the length of the carboxylic acid-terminated thiol. Figure 6.6 shows the electron-transfer constants as a function of SAM thickness for yeast cytochrome *c* at pH 5.0 and pH 8.0 and for horse cytochrome *c* at pH 5.0 and pH 7.0. The rate constants have been determined employing Trumpet plots (Figure S6.1, which can be found at the end of this chapter) and are also given in Table 1. The figure shows very similar behavior of horse cytochrome *c* at pH 5 and pH 7 and of yeast cytochrome *c* at pH 5, and the results are in close agreement with results reported previously for horse cytochrome *c* at pH 7.²¹ The results show that for long thiols ($n > 8$) the rate constants decrease with increasing length of the thiol, which corresponds to long-range electron tunneling through alkanethiols.⁵⁵⁻⁵⁷ For short thiols ($n < 8$) the rates become independent of the thiol length, which is due to the fact that electron transfer becomes limited by protein reorganization. For horse and yeast cytochrome *c* these reorganization-limited electron-transfer rate constants are

respectively approximately 1000 and 600 s⁻¹. For yeast cytochrome *c* at pH 8, lower rate constants are observed for both short and long thiols. However, compared to pH 5 the general behavior is still the same. Decreasing rate constants reflecting electron tunneling are observed for long thiols (in this case $n > 4$) and approximately constant rate constants reflecting limitation by reorganization are observed for very short thiols ($n < 4$). A word of caution has to be expressed about the measurements on these very short thiols, since it is known that short thiols ($n < 5$) do not form monolayers that are as well organized as longer thiols.⁵⁸ Therefore, the value of 40 s⁻¹ for the reorganization-limited electron-transfer rate constant is only a rough estimate. From the measurements we can deduce that there is an approximately 10-fold decrease in the reorganization energy of immobilized yeast cytochrome *c* on going from pH 5 to pH 8. The approximately 1000-fold decrease observed for long thiols ($n > 8$) must be caused by both a change in reorganization energy and a change in the nature and length of the electron tunneling pathway. Since the change in reorganization energy is responsible for a 10-fold decrease, we can deduce that the change in electron tunneling pathway is responsible for a 100-fold decrease.

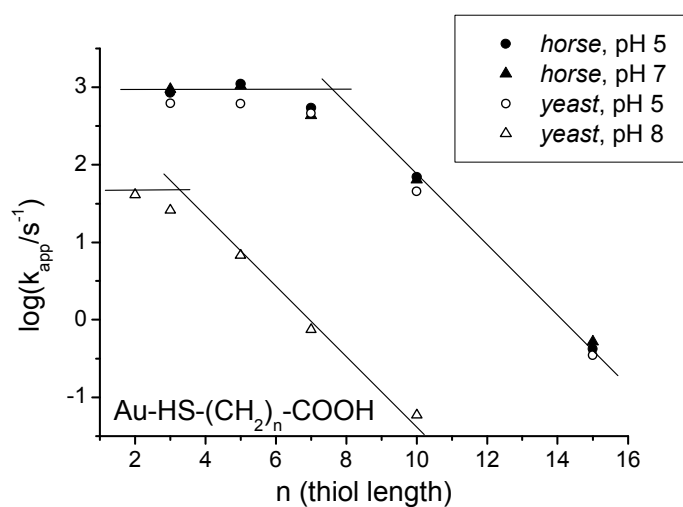


Figure 6.6 Electron-transfer rate constants for yeast cytochrome *c* at pH 5.0 (○) and pH 8.0 (△) and horse cytochrome *c* at pH 5.0 (●) and pH 7.0 (▲) as a function of the number of methylene groups in the mercapto carboxyl thiols (HS(CH₂)_nCOOH) at different pH values. The electron-transfer rates were determined from Trumpet plots. The voltammograms for these Trumpet plots were recorded in 10 or 50 mM acetate, pH 5.0, 10 or 50 mM phosphate, pH 7.0, or 10 mM phosphate, pH 8.0, and contain 400 nM cytochrome *c*. Scan rates ranging from 2 mV s⁻¹ to 300 V s⁻¹ were used. High scan rate measurements of cytochrome *c* on SAMs of MOA, MHA, MBA, and MPA were performed in a 50 mM acetate or 50 mM phosphate solution to avoid large ohmic drops. This does not affect the rate constants, as was evidenced by values of 70 s⁻¹ and 75 s⁻¹ for horse cytochrome *c* on MUA in respectively 10 and 50 mM acetate.

Table 6.1 Electron-transfer rate constants (s^{-1}) determined for horse and yeast cytochrome *c* immobilized on carboxylic acid-terminated SAMs under different conditions^a

Thiol	horse cytochrome <i>c</i>				yeast cytochrome <i>c</i>					
	pH 5	pH 5, NO	pH 7	pH 7, NO	pH 5	pH 5, NO	pH 7	pH 7, NO	pH 8	pH 8, NO
MPA		9.9					46		41	
MBA	850	7.2	940	5.2	620		49	1.2	26	0.044
MHA	1100	1.0	1040	0.67	610	0.42	16	0.25	6.8	
MOA	540	0.15	430	0.081	460	0.079	^b	0.031	0.75	
MUA	70	0.0079	64	0.006	46	0.0035	^b		0.059	
MHDA	0.42		0.52		0.35					
E_m (mV)	259	251	213	206	284	298	239	249	228 ^c	238 ^c

^a Midpoint potentials (vs SHE) under the same conditions on a SAM of MOA are also given.

^b could not be determined due to presence of more than one peak.

^c values determined on MBA.

The electron-transfer rate constants between the electrode and the immobilized protein can also be affected by ligand-induced conformational changes in the protein. A ligand that can bind to both yeast and horse cytochrome *c* is nitric oxide.^{59,60} Since binding of NO to cytochrome *c* requires replacement of either methionine or histidine,^{31,32} it results in conformational changes of the protein. Figure 6.7 shows voltammograms of horse cytochrome *c* immobilized on a SAM of mercaptooctanoic acid in the absence and presence of NO. The figure shows a large increase in peak separation upon NO binding, which is indicative of a decrease in the electron-transfer rate constant between the protein and electrode. Employing Trumpet plots (Figure S6.2) rate constants were determined for thiols of different lengths, and these are plotted in Figure 6.8. The figure shows that upon NO binding the electron-transfer rate constants decrease by a factor of 100 for very short thiols ($n < 3$) and a factor of 10000 for long thiols ($n > 8$). Again we have to remark that, due to the poor organization of the short thiols, the reorganization-limited electron-transfer rate constant of 10 s^{-1} is only a rough estimate. The results suggest that the conformational changes induced by NO binding affect both the reorganization energy and the electron tunneling pathway between the protein and the electrode. On the other hand, nitric oxide binding does not result in a large change in midpoint potential of the $\text{Fe}^{\text{III}}/\text{Fe}^{\text{II}}$ redox couple. Only an 8 mV negative shift in midpoint potential is observed (Figure S6.2). This behavior is significantly different from that of soluble iron porphyrins, where NO binding results in a 400 mV positive potential shift,^{61,62} which is due to a stabilization of the Fe^{II} state by NO. The absence of a large shift for horse cytochrome *c* implies that binding constants of NO to immobilized cytochrome *c* in its Fe^{III} and Fe^{II} state must be comparable. This observation is in slight disagreement with the literature, where binding constants of $1.63 \times 10^4\text{ M}^{-1}$ and $3.0 \times 10^5\text{ M}^{-1}$ have been reported for respectively the Fe^{III} and Fe^{II} states,^{31,32} which would correspond to a 75 mV positive potential shift. This suggests that protein immobilization does affect NO binding

constants. Changes in pH do not seem to affect NO binding, as was deduced from the comparable results obtained at pH 5 and pH 7 (Figure S6.2).

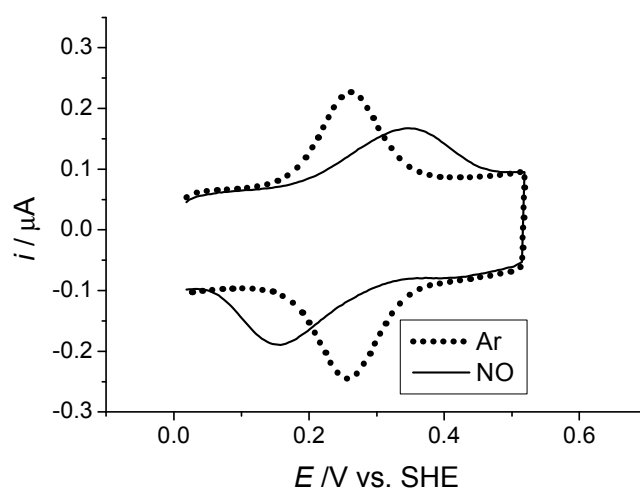


Figure 6.7 Cyclic voltammograms of immobilized horse cytochrome *c* on a SAM of mercaptooctanoic acid (MOA) in a saturated Ar solution (····) or in a saturated NO solution (—) in 400 nM horse cytochrome *c* in 10 mM acetate, pH 5.0. Scan rate = 50 mV/s.

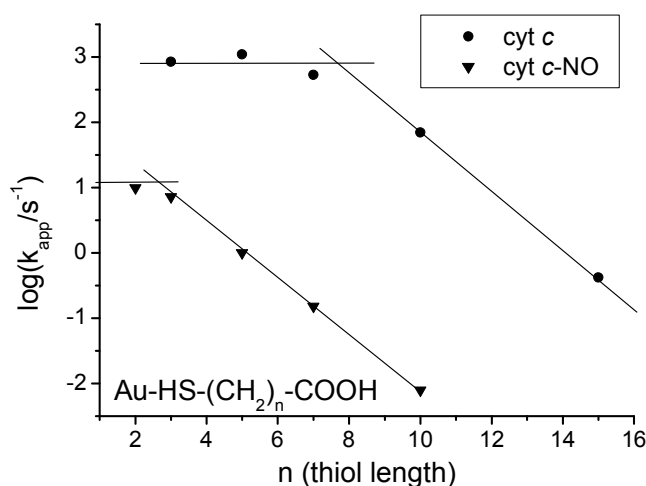


Figure 6.8 Electron-transfer rate constants for horse cytochrome *c* in an Ar solution (●) or saturated NO solution (▼) as a function of the number of methylene groups in the mercapto carboxyl thiols ($\text{HS}(\text{CH}_2)_n\text{COOH}$). The electron-transfer rate constants were determined from Trumpet plots (Figure S6.2). The voltammograms for these Trumpet plots were recorded in 10 mM acetate, pH 5.0, and contain 400 nM cytochrome *c*. Scan rates ranging from 2 mV s^{-1} to 300 V s^{-1} were used.

Similar results were obtained for yeast cytochrome *c* at pH 5 (Table 6.1), but there are some differences. Analogous to horse cytochrome *c*, a 10000-fold decrease in rate constants was observed for long thiols. Again the rate constants for yeast cytochrome *c* are somewhat lower than for horse cytochrome *c*, analogous to the behavior in the absence of NO. Yeast cytochrome *c* displays a 14 mV positive shift in midpoint potential upon NO binding, which differs from the 8 mV negative shift for horse cytochrome *c*. This indicates that both cytochromes *c* have slightly different NO binding affinities in their Fe^{II} and Fe^{III}-states. We also determined rate constants for NO-bound yeast cytochrome *c* at pH 7 and pH 8 (Table 6.1). These are much lower than for NO-bound horse cytochrome *c* at pH 7 and yeast cytochrome *c* at pH 5, which suggests that yeast cytochrome *c* reorients on the surface, analogous to its behavior in the absence of NO.

6.4 Discussion and Conclusions

Before analysis of our results, it is important to establish that the conditions we employ do not induce significant conformational changes or denaturation of either cytochrome *c*. On the basis of (i) the fact that cytochrome *c* in solution does not undergo denaturation under the same conditions, (ii) the fact that the potential always stays reasonably close to the potential in solution (<70 mV difference), (iii) the fact that the voltammetric peaks display Nernstian behavior, (iv) the fact that the coverage is typical of a protein, and (v) the fact that the observed electron-transfer behavior is typical of a protein, we can conclude that both horse and yeast cytochrome *c* retain a near-native conformation over the whole pH range. For the same reasons NO binding to immobilized cytochrome *c* seems to result in the same conformational changes that occur when NO binds to cytochrome *c* in solution.

Below pH 6 immobilized horse and yeast cytochrome *c* display similar dependencies of the midpoint potential on pH, similar coverages, and comparable electron-transfer rate constants. This suggests that, up to pH 6, horse and yeast cytochrome *c* adsorb on the electrode in a comparable orientation, creating a similar electron tunneling pathway between the electrode and the protein. A previous surface spectroscopy study has shown that the binding of horse cytochrome *c* to the carboxylic acid-terminated SAMs likely occurs via certain lysine residues, namely, Lys13, Lys72, and Lys86.⁵ This previous study was performed at pH 7.0, but since there is no apparent change in electron-transfer rate constants between pH 5.0 and pH 7.0, horse cytochrome *c* does not seem to reorient in this pH range. A representation of the side of horse cytochrome *c* containing the particular lysine residues is shown in Figure 6.9, which also shows the homologous side of yeast cytochrome *c*. The figure shows that horse and yeast cytochrome *c* closely resemble each other. This explains why both proteins adsorb on the electrode in a similar fashion and display similar properties. This particular side of cytochrome *c* is known to interact with enzymes such as cytochrome *c* oxidase and cytochrome *c* peroxidase and is closely conserved throughout the cytochromes *c*.^{27,63}

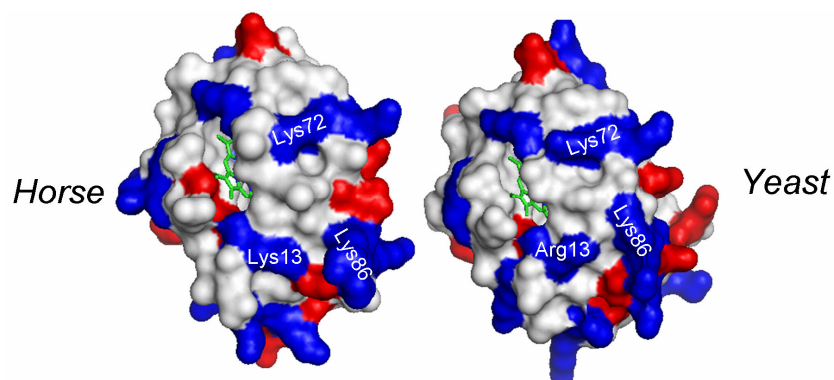


Figure 6.9 Charge distribution on horse and yeast cytochrome *c* at pH 5 on the side that binds to the carboxyl acid-terminated SAM. Positively charged groups (lysine, arginine and histidine) are depicted in blue, whereas negatively charged groups (aspartic acid and glutamic acid) are depicted in red. The heme groups are depicted as sticks in green. Prepared with PyMOL.⁶⁴ PDB codes: 1HRC and 1YCC.

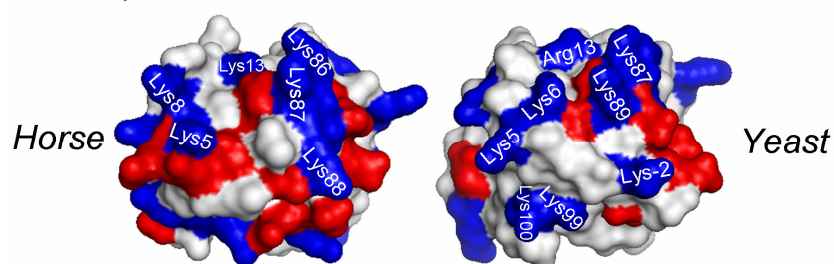


Figure 6.10 Charge distribution on horse and yeast cytochrome *c* of the side of the protein that is likely to bind to the SAM at pH 8 for yeast cytochrome *c*. Positively charged groups are depicted in blue, whereas negatively charged groups are depicted in red. Prepared with PyMOL.⁶⁴ PDB codes: 1HRC and 1YCC.

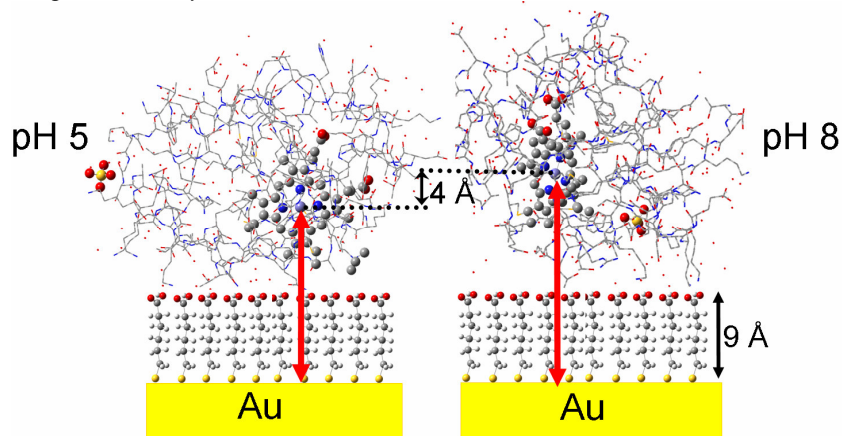


Figure 6.11 Plausible orientations of yeast cytochrome *c* on the SAM at pH 5 and pH 8. The representation is approximately to scale. The heme groups have been accentuated. Prepared with Gaussview.⁶⁶ PDB code: 1YCC.

Whereas horse cytochrome *c* retains the same orientation at the electrode at both pH 5 and pH 7, immobilized yeast cytochrome *c* seems to reorient with increasing pH. This is suggested by the large decrease in the electron-transfer rate constant of yeast cytochrome *c* at pH 8. This decrease is due to changes in the reorganization energy and the electron tunneling pathway of yeast cytochrome *c* and hence suggests that the protein has another orientation compared to that at pH 5. On the basis of the decrease in the electron-transfer rate constant and the crystal structure of yeast cytochrome *c*, we can make a rough estimate of the new orientation of the protein. Assuming an exponential decay coefficient β through cytochrome *c* of approximately 1.2 \AA^{-1} ,⁶⁵ we can estimate that the 100-fold decrease, which we ascribe to a change in the electron tunneling pathway, is caused by an increase in the electrode–heme distance of approximately 4 \AA . From the positions of the positively charged residues in the crystal structure of yeast cytochrome *c* we can deduce sides of the protein that are likely to interact with the negatively charged SAM. In combination with the extra heme–electrode distance we can estimate which side of the protein, is most likely to bind to the SAM at pH 8. This particular side is depicted in Figure 6.10, and the resulting orientation of the protein on the electrode is depicted in Figure 6.11.

The cause of the reorientation must be either a change in the conformation of the protein, the charge distribution on the protein, or the charge distribution on the carboxylic acid-terminated SAM with increasing pH. The first explanation seems unlikely, since yeast cytochrome *c* does not undergo a conformational change between pH 5 and pH 8 in solution.⁴⁰ The second explanation is also unlikely, since there are no large changes in the charges on the protein between pH 5 and pH 8. Only histidine changes its charge over this pH range, and no histidine is present on the side of cytochrome *c* that binds to the SAM. Therefore, the most probable explanation is that the reorientation is caused by a change in the charge distribution on the SAM. Over the pH 5–8 range the density of negative charges increases significantly, since the SAM has a pKa of around 5–7.^{49–53} The hypothesis that such an increase in the density of negative charges can affect the orientation of yeast cytochrome *c* is supported by a previous study, in which mixed SAMs consisting of carboxylic acid-terminated thiols and hydroxyl-terminated thiols were employed.²⁶ In this study it was shown that higher electron-transfer rates were obtained for mixed SAMs than for pure carboxylic acid-terminated SAMs. Possibly the higher density of negative charges on the SAM makes it more favorable to bind to a side of yeast cytochrome *c* that has a higher density of positive charges. Figure 6.10 indeed shows more positively charged residues than Figure 6.9.

The difference in orientation of horse and yeast cytochrome *c* in the pH 6–8 region must be related to a different charge distribution on both proteins. Figure 6.10 indeed shows significant differences between horse and yeast cytochrome *c* for the side by which yeast cytochrome *c* is likely to bind to the SAM at pH 8. Apparently these differences in charge distribution make it favorable to reorient for yeast cytochrome *c*, but not so for horse cytochrome *c*. Nevertheless, Figure 6.4 suggests that at pH 8 horse cytochrome *c* also starts to change its orientation. This is in line with results from a previous study, which showed decreasing electron-transfer rate constants with increasing

pH.²⁹ However, it is also possible that the decrease in rate constants is caused by a conformational change of the protein that occurs at high pH.⁴¹

The electron tunneling pathway can be influenced not only by a reorientation of the protein, but also by a conformational change of the protein, as occurs in the case of NO binding. The physiological function of NO binding to cytochrome *c* is still unclear, but it might play a role in the inhibition of mitochondrial cytochrome *c* oxidase by NO.⁶⁷ Upon binding of NO, the electron-transfer rate constants for both horse and yeast cytochrome *c* on long thiols ($n > 8$) decrease by a factor of 10000. Our results on short thiols suggest that a factor of 100 of this decrease is related to a change in reorganization energy for electron transfer and hence the other factor of 100 may be related to a change in the electron tunneling pathway. The relatively large decrease in reorganization energy is probably related to the strength of the NO binding. This binding deepens the potential energy wells of cytochrome *c* in both its Fe^{II} and Fe^{III} states, but also the reorganization energy for electron transfer (λ) is increased, and correspondingly the electron-transfer rate constants decrease (Figure 6.12).⁶⁸

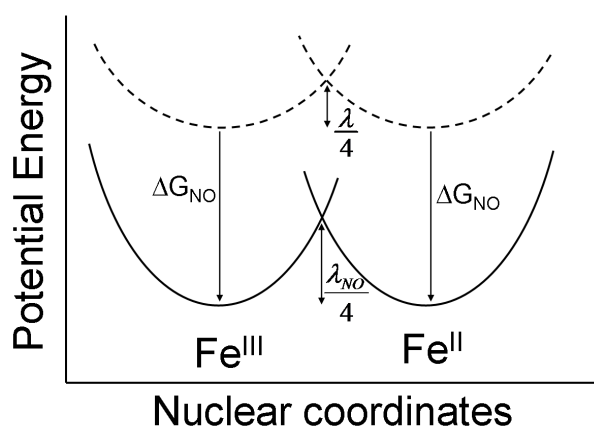


Figure 6.12 Profile of the potential energy surface of immobilized cytochrome *c* with (—) and without (---) bound nitric oxide. The reorganization energies are $\lambda_{NO}/4$ and $\lambda/4$, respectively.

The factor of 100 decrease related to the change in the electron tunneling pathway can be translated into an extra heme–electrode distance of 4 Å. No crystal structure for nitric oxide-bound cytochrome *c* is available, and therefore, we do not know what exact conformational changes are caused by NO binding. However, a crystal structure is available for cyanide-bound cytochrome *c*, and since cyanide and nitric oxide are both strongly binding diatomic ligands, they probably induce similar conformational changes. The cyanide-bound crystal structure shows that cyanide coordinates to the heme by replacing methionine 80, which as a result is moved from the heme pocket to the surface of the protein (Figure 6.13).⁶⁹ This happens on the side of the protein that binds to the SAM at low pH, and therefore this methionine 80 is likely to change the way the protein

binds to the SAM. Apparently this results in an increase of the electron tunneling pathway. On the basis of the similar behavior of yeast and horse cytochrome *c* at pH 5, we can deduce that both proteins have a comparable orientation on the electrode, similar to their behavior in the absence of NO. Since the side of the protein depicted in Figure 6.9 is the only side where the proteins closely resemble each other, it seems that nitric oxide binding does not change the side by which both proteins bind to the electrode, as does increasing the pH in the case of yeast cytochrome *c*.

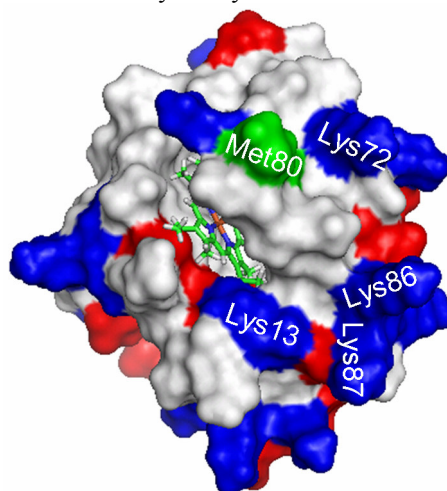
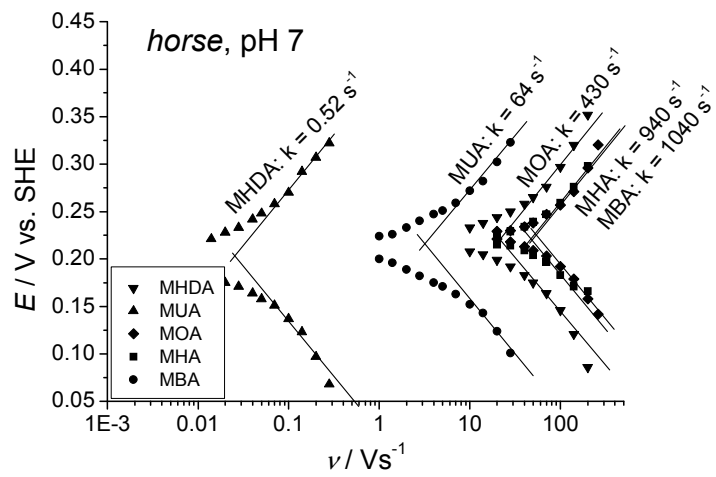
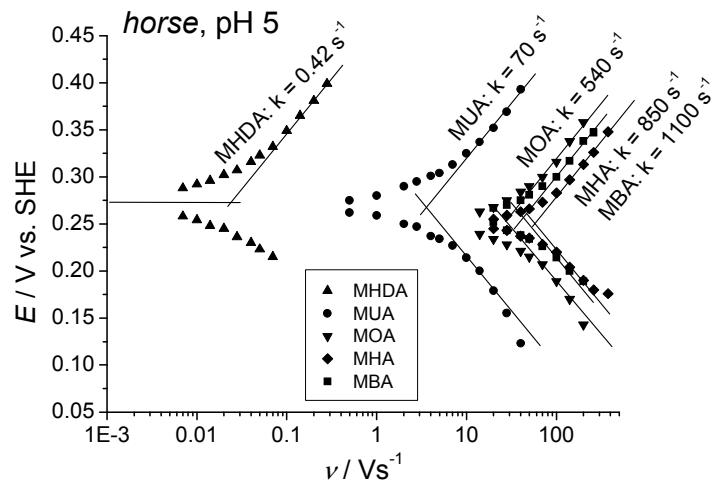


Figure 6.13 Charge distribution on cyanide bound horse cytochrome *c* at pH 7. Positive groups (lysine and arginine) are depicted in blue, whereas negative groups (aspartic acid and glutamic acid) are depicted in red. Methionine 80 has been depicted in green for accentuation. The heme groups are depicted as sticks in green. Prepared with PyMOL. PDB codes: 1I5T

In conclusion, we have shown that several electrochemical properties of immobilized horse and yeast cytochrome *c* can be influenced by changing the pH and binding of nitric oxide. The pH-induced changes seem to be related to the charging of the self-assembled monolayer, since both proteins do not undergo large changes in surface charge or conformation in the investigated pH range. In the case of yeast cytochrome *c* increasing the pH causes a large decrease in electron-transfer rate constants, which is indicative of a reorientation of the protein on the electrode. Such a reorientation is not observed for horse cytochrome *c*, which is probably related to a different charge distribution on both proteins. Binding of nitric oxide causes decreases in electron-transfer rate constants for both cytochromes *c*. This is probably related to changes in the reorganization energy for electron transfer and changes in the conformation for NO-bound cytochrome *c* compared to cytochrome *c*.

6.5 Supporting information



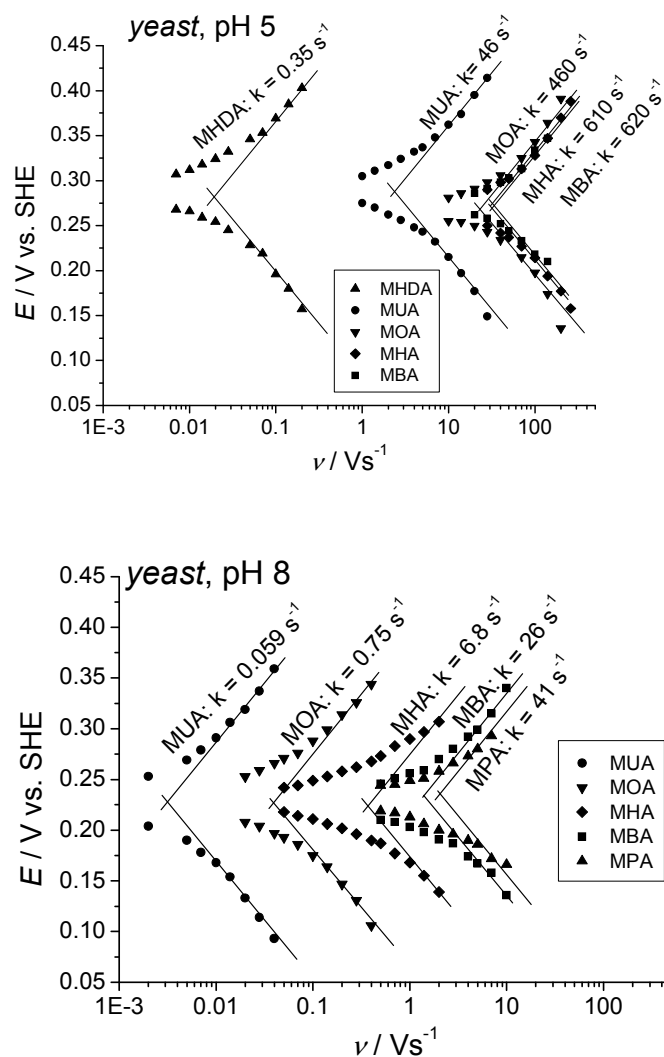


Figure S6.1 Trumpet plots for horse and yeast cytochrome *c* immobilized on gold with a SAM of 3-mercaptopropionic acid (MPA), 4-mercaptopbutyric acid (MBA), 6-mercaptophexanoic acid (MHA), 8-mercaptopoctanoic acid (MOA), 11-mercaptopundecanoic acid (MUA) or 16-mercaptophexadecanoic acid (MHDA). Cathodic and anodic peak potentials were determined from voltammograms that were recorded in either 10 or 50 mM acetate, pH 5.0 or 10 or 50 mM phosphate, pH 7.0 containing 400 nM cytochrome *c* at scan rates ranging from 2 mV s^{-1} to 300 V s^{-1} . Peak potentials were corrected for ohmic drop at high scan rates. High scan rate measurements of cytochrome *c* on SAMs of MOA, MHA, MBA and MPA were performed in a 50 mM acetate or 50 mM phosphate solution to avoid large ohmic drops. This does not affect the rate constants, as was evidenced by values of 70 s^{-1} and 75 s^{-1} for horse cytochrome *c* on MUA in respectively 10 mM and 50 mM acetate.

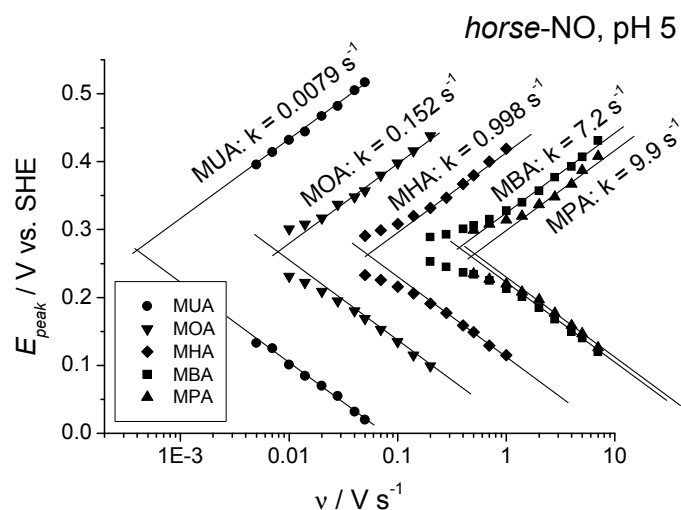


Figure S6.2 Trumpet plots for horse cytochrome *c* immobilized on gold with a SAM of MPA, MBA, MHA, MOA, MUA or MHA in saturated NO solution. Cathodic and anodic peak potentials were determined from voltammograms that were recorded in 10 mM acetate, pH 5.0 containing 200 nM cytochrome *c* at scan rates ranging from 2 mV s^{-1} to 300 V s^{-1} . Peak potentials were corrected for ohmic drop at high scan rates. The corresponding electron transfer rate constants, which were calculated using Laviron's theory are also reported.

6.6 References

1. Armstrong, F. A., *J. Chem. Soc., Dalton Trans.* **2002**, 661.
2. Armstrong, F. A.; Camba, R.; Heering, H. A.; Hirst, J.; Jeuken, L. J. C.; Jones, A. K.; Leger, C.; McEvoy, J. P., *Faraday Discuss.* **2000**, *116*, 191.
3. Jeuken, L. J. C., *Biochim. Biophys. Acta* **2003**, *1604*, 67.
4. Leger, C.; Elliott, S. J.; Hoke, K. R.; Jeuken, L. J. C.; Jones, A. K.; Armstrong, F. A., *Biochemistry* **2003**, *42*, 8653.
5. Ataka, K.; Heberle, J., *J. Am. Chem. Soc.* **2004**, *126*, 9445.
6. Hildebrandt, P.; Murgida, D. H., *Bioelectrochemistry* **2002**, *55*, 139.
7. Zheng, J.; Zhou, Q.; Zhou, Y.; Lu, T.; Cotton, T. M.; Chumanov, G., *J. Electroanal. Chem.* **2002**, *530*, 75.
8. Elliott, S. J.; Hoke, K. R.; Heffron, K.; Palak, M.; Rothery, R. A.; Weiner, J. H.; Armstrong, F. A., *Biochemistry* **2004**, *43*, 799.
9. Hudson, J. M.; Heffron, K.; Kotlyar, V.; Sher, Y.; Maklashina, E.; Cecchini, G.; *J. Am. Chem. Soc.* **2005**, *127*, 6977.
10. Vincent, K. A.; Parkin, A.; Lenz, O.; Albracht, S. P. J.; Fontecilla-Camps, J. C.; Cammack, R.; Friedrich, B.; Armstrong, F. A., *J. Am. Chem. Soc.* **2005**, *127*, 18179.

11. de Groot, M. T.; Evers, T. H.; Merckx, M.; Koper, M. T. M., *Langmuir* **2007**, *23*, 729-736.
12. Song, S.; Clark, R. A.; Bowden, E. F.; Tarlov, M. J., *J. Phys. Chem.* **1993**, *97*, 6564.
13. Tarlov, M. J.; Bowden, E. F., *J. Am. Chem. Soc.* **1991**, *113*, 1847.
14. Hildebrandt, P.; Stockburger, M., *Biochemistry* **1989**, *28*, 6710.
15. Murgida, D. H.; Hildebrandt, P.; Wei, J.; He, Y. F.; Liu, H.; Waldeck, D. H., *J. Phys. Chem. B* **2004**, *108*, 2261.
16. Wackerbarth, H.; Hildebrandt, P., *ChemPhysChem* **2003**, *4*, 714.
17. Niki, K.; Hardy, W. R.; Hill, M. G.; Li, H.; Sprinkle, J. R.; Margoliash, E.; Fujita, K.; Tanimura, R.; Nakamura, N.; Ohno, H.; Richards, J. H.; Gray, H. B., *J. Phys. Chem. B* **2003**, *107*, 9947.
18. Niki, K.; Pressler, K. R.; Sprinkle, J. R.; Li, H.; Margoliash, E., *Russ. J. Electrochem.* **2002**, *38*, 63.
19. Xu, J.; Bowden, E. F., *J. Am. Chem. Soc.* **2006**, *128*, 6813-6822.
20. Hobara, D.; Imabayashi, S.; Kakiuchi, T., *Nano Lett.* **2002**, *2*, 1021.
21. Feng, Z. Q.; Imabayashi, S.; Kakiuchi, T.; Niki, K., *J. Chem. Soc., Faraday Trans.* **1997**, *93*, 1367.
22. Murgida, D. H.; Hildebrandt, P., *J. Am. Chem. Soc.* **2001**, *123*, 4062.
23. Yue, H.; Khoshtariya, D.; Waldeck, D. H.; Grochol, J.; Hildebrandt, P.; Murgida, D. H., *J. Phys. Chem. B* **2006**, *110*, 19906-19913.
24. Murgida, D. H.; Hildebrandt, P., *Acc. Chem. Res.* **2004**, *37*, 854.
25. Petrovic, J.; Clark, R. A.; Yue, H.; Waldeck, D. H.; Bowden, E. F., *Langmuir* **2005**, *21*, 6308.
26. Kasmi, A. E.; Wallace, J. M.; Bowden, E. F.; Binet, S. M.; Linderman, R. J., *J. Am. Chem. Soc.* **1998**, *120*, 225.
27. Bushnell, G. W.; Louie, G. V.; Brayer, G. D., *J. Mol. Biol.* **1990**, *214*, 585.
28. Chen, X.; Ferrigno, R.; Yang, J.; Whitesides, G. M., *Langmuir* **2002**, *18*, 7009.
29. Avila, A.; Gregory, B. W.; Niki, K.; Cotton, T. M., *J. Phys. Chem. B* **2000**, *104*, 2759.
30. Henry, Y.; Guissani, A., *Cell. Mol. Life Sci.* **1999**, *55*, 1003.
31. Hoshino, M.; Maeda, M.; Konishi, R.; Seki, H.; Ford, P. C., *J. Am. Chem. Soc.* **1996**, *118*, 5702.
32. Hoshino, M.; Ozawa, K.; Seki, H.; Ford, P. C., *J. Am. Chem. Soc.* **1993**, *115*, 9568.
33. de Vooy, A. C. A.; Koper, M. T. M.; van Santen, R. A.; van Veen, J. A. R., *Electrochim. Acta* **2001**, *46*, 923.
34. Van den Brink, F.; Visscher, W.; Barendrecht, E., *J. Electroanal. Chem.* **1983**, *157*, 283.
35. Lide, D. R.; *CRC Handbook of Chemistry and Physics, 83rd Edition*, CRC press: Cleveland: 2002; p 2664 pp.
36. Press, W. H.; Flannery, B. P.; Teukolsky, S. A.; Vetterling, W. T.; *Numerical Recipes in Pascal*, Cambridge University Press: New York, 1989; p.

37. Heering, H. A.; Wiertz, F. G. M.; Dekker, C.; De Vries, S., *J. Am. Chem. Soc.* **2004**, *126*, 11103.
38. Trasatti, S.; Petrii, O. A., *Pure Appl. Chem.* **1991**, *63*, 711.
39. Assfalg, M.; Bertini, I.; Dolfi, A.; Turano, P.; Mauk, A. G.; Rosell, F. I.; Gray, H. B., *J. Am. Chem. Soc.* **2003**, *125*, 2913.
40. Barker, P. D.; Mauk, A. G., *J. Am. Chem. Soc.* **1992**, *114*, 3619.
41. Ikeshoji, T.; Taniguchi, I.; Hawkridge, F. M., *J. Electroanal. Chem.* **1989**, *270*, 297.
42. Clark, R. A.; Bowden, E. F., *Langmuir* **1997**, *13*, 559.
43. Eddowes, M. J.; Hill, H. A., *J. Am. Chem. Soc.* **1979**, *101*, 4461.
44. Gopal, D.; Wilson, G. S.; Earl, R. A.; Cusanovich, M. A., *J. Biol. Chem.* **1988**, *263*, 11652.
45. Haladjian, J.; Bianco, P., *Bioelectrochem. Bioenerg.* **1983**, *11*, 319.
46. Terrettaz, S.; Cheng, J.; Miller, C. J.; Guiles, R. D., *J. Am. Chem. Soc.* **1996**, *118*, 7857.
47. Lett, C. M.; Guillemette, J. G., *Biochem. J.* **2002**, *362*, 281.
48. Rodkey, F. L.; Ball, E. G., *J. Biol. Chem.* **1950**, *182*, 17.
49. Aoki, K.; Kakiuchi, T., *J. Electroanal. Chem.* **1999**, *478*, 101.
50. Dai, Z.; Ju, H., *Phys. Chem. Chem. Phys.* **2001**, *3*, 3769.
51. Munakata, H.; Kuwabata, S., *Chem. Commun.* **2001**, 1338.
52. Sugihara, K.; Shimazu, K.; Uosaki, K., *Langmuir* **2000**, *16*, 7101.
53. Sugihara, K.; Teranishi, T.; Shimazu, K.; Uosaki, K., *Electrochemistry* **1999**, *67*, 1172.
54. Laviron, E., *J. Electroanal. Chem.* **1979**, *101*, 19.
55. Finklea, H. O.; Hanshew, D. D., *J. Am. Chem. Soc.* **1992**, *114*, 3173.
56. Smalley, J. F.; Feldberg, S. W.; Chidsey, C. E. D.; Linford, M. R.; Newton, M. D.; Liu, Y. P., *J. Phys. Chem.* **1995**, *99*, 13141.
57. Xu, J.; Li, H.; Zhang, Y., *J. Phys. Chem.* **1993**, *97*, 11497.
58. Porter, M. D.; Bright, T. B.; Allara, D. L.; Chidsey, C. E. D., *J. Am. Chem. Soc.* **1987**, *109*, 3559-68.
59. Kon, H.; Kataoba, N., *Biochemistry* **1969**, *8*, 4757.
60. Stevens, T. H.; Bocian, D. F.; Chan, S. I., *FEBS Lett.* **1979**, *97*, 314.
61. Chi, Y.; Chen, J.; Aoki, K., *Inorg. Chem.* **2004**, *43*, 8437.
62. Trofimova, N. S.; Safronov, A. Y.; Ikeda, O., *Inorg. Chem.* **2003**, *42*, 1945.
63. Kang, S. A.; Marjavaara, P. J.; Crane, B. R., *J. Am. Chem. Soc.* **2004**, *126*, 10836.
64. DeLano, W. L. *PyMOL*, DeLano Scientific LLC: San Carlos, CA, 2003.
65. Langen, R.; Chang, I. J.; Germanas, J. P.; Richards, J. H.; Winkler, J. R.; Gray, H. B., *Science* **1995**, *268*, 1733.
66. Frisch, M. J.; et al. *Gaussian 03*, Gaussian, Inc.: Wallingford CT, 2004.
67. Sharpe, M. A.; Cooper, C. E., *Biochem. J.* **1998**, *332*, 9.
68. Marcus, R. A.; Sutin, N., *Biochim. Biophys. Acta* **1985**, *811*, 265.
69. Yao, Y.; Qian, C.; Ye, K.; Wang, J.; Bai, Z.; Tang, W., *J. Biol. Inorg. Chem.* **2002**, *7*, 539.

Chapter 7

Redox transitions of chromium, manganese, iron, cobalt and nickel protoporphyrins in aqueous solution*

Abstract: *The electrochemical redox behavior of immobilized chromium, manganese, iron, cobalt, and nickel protoporphyrins IX has been investigated over the pH 0-14 range. In the investigated potential domain the metalloporphyrins were observed in four different oxidation states (M^I , M^{II} , M^{III} and M^{IV}). The metalloporphyrins differ in the potentials at which the redox transitions occur, but the observed pH dependence of the redox transitions was similar for the different metalloporphyrins and revealed that the M^{II}/M^{III} and M^{III}/M^{IV} transitions were accompanied by a hydroxide transfer at high pH. The fact that the metalloporphyrins are immobilized on graphite does not seem to have a large influence on their redox behavior, as can be deduced from the comparable behavior of immobilized metalloporphyrins on gold and of water soluble metalloporphyrins in solution. We also performed Density Functional Theory (DFT) calculations on the metalloporphyrins in different oxidation states. The geometries and spin states predicted by these calculations agree well with experimentally determined values and suggest that there is a correlation between the spin states and the metal nitrogen bond distances; the calculations were also employed to predict the electrochemical potentials of the redox transitions, with mixed success. Relative potential differences between the different metalloporphyrins were reasonably predicted for the M^{II}/M^{III} and M^{III}/M^{IV} transitions, whereas prediction of the actual electrochemical potentials, which requires certain assumptions regarding solvation, was only reasonably successful for the M^{II}/M^{III} redox transition.*

* The contents of this chapter have been submitted: de Groot, M.T.; Koper, M.T.M., *Inorganic Chemistry* **2007**

7.1 Introduction

Metalloporphyrins (Figure 7.1) are versatile organometallic molecules that are incorporated in many proteins. The most widely occurring metalloporphyrin is iron protoporphyrin IX, better known as heme. Heme proteins perform a wide variety of functions, including oxygen transport, oxygen reduction and electron transport.¹ Porphyrins and porphyrin derivatives with other metals than iron also occur. Examples include magnesium in chlorophyll and cobalt in vitamin B₁₂.²

Metalloporphyrins are actively being investigated to better understand how they perform their functions in proteins.¹ Apart from this, they can potentially be employed as biomimicking catalysts and biosensors³ and therefore it is also interesting to study them in their isolated form. A number of experimental techniques have been employed to characterize metalloporphyrins. These include X-ray diffraction to determine bond distances,⁴ ESR and NMR to determine spin states,⁵ Infrared and Raman spectroscopy to determine vibrational properties,⁶ and electrochemistry to determine the potentials of the redox transitions.⁷ Over the past two decades Density Functional Theory (DFT) calculations have also greatly helped in gaining a better understanding of the electronic and ligand binding properties of porphyrins.⁸⁻¹⁰

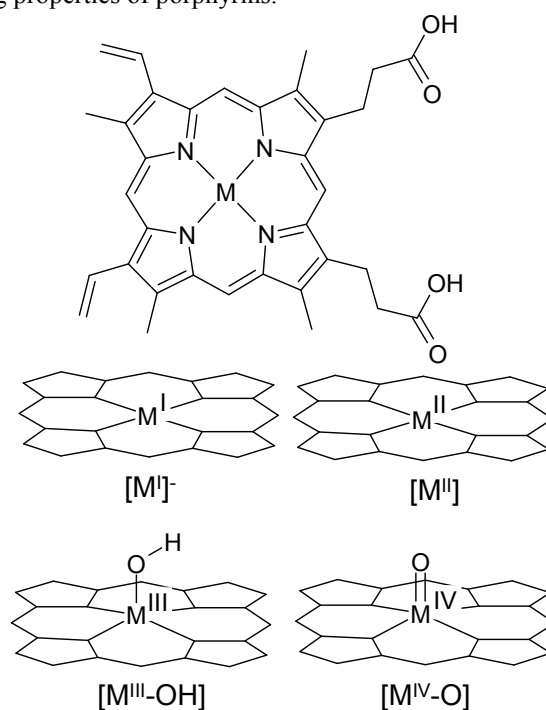


Figure 7.1 Structures of metalloprotoporphyrin IX (top) and of the metalloporphyrins in different oxidation states (bottom). The OH and O²⁻ substituents for the metalloporphyrins in their M^{III} and M^{IV} oxidation are likely to occur when adsorbed on a pyrolytic graphite electrode in an aqueous solution (discussed in text). All complexes are neutral except for the metalloporphyrins in their M^I oxidation state. The notations we use for the different porphyrins are depicted under the structures.

In this paper we investigate the properties of chromium, manganese, iron, cobalt and nickel porphyrins in different oxidation states. Our goal is to determine the similarities and differences between these porphyrins, especially with regard to their redox transitions in an aqueous environment. We have done this by electrochemically determining the midpoint potentials of the redox transitions over a wide pH range (0-14). From the pH dependence of these midpoint potentials, it becomes possible to determine whether the redox transitions are accompanied by a proton or hydroxide transfer. In this way the nature of the redox transitions can be determined and a comparison between the different metalloprotoporphyrins can be made.

We have deliberately chosen not to perform our electrochemical measurements on metalloprotoporphyrins in solution, but instead on metalloprotoporphyrins immobilized on pyrolytic graphite. The reason is that the investigation of metalloprotoporphyrins in solution has some disadvantages. Firstly, there is a solubility issue, since the biochemically relevant metalloprotoporphyrins IX (Figure 7.1) are not soluble at low pH values.^{11,12} Secondly, metalloprotoporphyrins that are soluble in water tend to form dimers and trimers. This results in complicated electrochemical behavior,¹³⁻¹⁵ which makes it difficult to correctly assign the redox transitions. In contrast, immobilized porphyrins have the advantage that reversible well-defined peaks are obtained over the whole pH range.^{16,17} Also, since the immobilization blocks one coordination site, the electrochemical behavior is not so complicated and can be relatively easily interpreted. However, an important question is whether the proximity of the immobilized metalloprotoporphyrins to the electrode affects their properties compared to the metalloprotoporphyrins in solution. In this paper we will show that there does not seem to be a significant “electrode” effect on the redox potentials. We do this by comparing different immobilization methods and by comparing the redox potentials to the redox potentials of water soluble metalloprotoporphyrins.

Apart from the electrochemical measurements, we have also performed DFT calculations on the metalloprotoporphyrins in their different oxidation states. These DFT calculations have a dual purpose. Firstly, they are used to determine possible relationships between particular characteristics of the metalloprotoporphyrins such as nature of metal, oxidation state, geometry, spin state, symmetry and ligand. Since it has been reported that DFT sometimes has difficulties at correctly describing some metalloprotoporphyrins,^{18,19} we compare the results of the calculations to experimentally determined geometries and spin states. Secondly, the calculated differences in energies between the different metalloprotoporphyrins can be employed to calculate the differences in redox potentials between the metalloprotoporphyrins. In this way the ability of the calculations to correctly predict energy differences between different metalloprotoporphyrins can be assessed. The calculations can even be employed to calculate the actual electrochemical potentials of the redox transitions, although certain assumptions that have to be made with regard to the solvation of the metalloprotoporphyrins become more stringent in this case.

7.2 Experimental procedures

Materials. Hemin (Fluka, 98%), Cr(III) Protoporphyrin IX chloride (Frontier Scientific), Mn(III) Protoporphyrin IX chloride (Frontier Scientific), Co(III) Protoporphyrin IX chloride (Frontier Scientific), Ni(II) Protoporphyrin IX (Frontier Scientific), and didodecyldimethylammonium bromide (DDAB, 98%, Aldrich) were all used as received. All other chemicals were p.a. grade. Buffer solutions were prepared with sodium acetate (pH 4-6), sodium dihydrogen phosphate monohydrate (pH 2-3, 6-8, 11-12) and boric acid (pH 9-10) combined with concentrated solutions of hydrochloric acid or caustic soda and Millipore MilliQ water (resistivity > 18.2 M Ω cm). The concentration of the buffer was 0.1 M in all experiments. Solutions of sulfuric acid (pH 0-1) and caustic soda (pH 13-14) were used for low and high pHs. Pyrolytic graphite (Carbone-Lorraine) was fabricated into homemade rotating ring-disk electrodes.^{20,21} The geometric surface area of the electrodes was 0.5 cm².

Electrochemical Apparatus and Procedures. An Autolab PGstat 20 potentiostat was used for cyclic voltammetry. A homemade three-electrode cell consisting of a platinum flag counter electrode, a Hg|Hg₂SO₄ reference electrode and a pyrolytic graphite rotating disk working electrode was employed. All potentials in this paper are relative to the standard hydrogen electrode (SHE). All solutions were deaerated by purging with argon for 15 min. All electrochemical experiments were performed at room temperature.

Preparation of adsorbed metalloprotoporphyrin on pyrolytic graphite. 0.5 mM chromium, manganese, iron, cobalt and nickel protoporphyrin solutions were prepared by dissolving 1.6 mg of the particular metalloprotoporphyrin in 5 ml of a 0.01 M borate solution, pH 10. Prior to use, the pyrolytic graphite (PG) electrode was abraded using P500 and P1000 SiC sandpaper and ultrasonicated in Millipore MilliQ water for 1 min. The electrode was dried in a N₂ stream for 5 sec. It was then immersed in the desired metalloprotoporphyrin solution for 5 min to saturate the surface with the protoporphyrin,^{22,23} after which the electrode was rinsed with water.

Preparation of metalloprotoporphyrin-DDAB films on pyrolytic graphite. Protoporphyrin-DDAB solutions were prepared by mixing 0.5 mM metalloprotoporphyrin in 0.01 M borate solution, pH 10, with an equal volume of a 0.01 M DDAB suspension in 0.1 M acetate, pH 5. The DDAB suspension was prepared by ultrasonication for 1 hour. Prior to use, the PG electrodes were abraded using P500 and P1000 SiC sandpaper and ultrasonicated in Millipore MilliQ water for 1 min. The electrode was dried in a N₂ stream for 5 s. Subsequently, 5 μ l of the protoporphyrin-DDAB solution was put on the electrode. The electrode was dried for approximately 15 min in air, after which it was used for electrochemical experiments.

Computational details. Calculations were performed with the Amsterdam Density Functional (ADF) program.^{24,25} The atomic orbitals on all atoms were described by an uncontracted triple- ζ valence plus polarization STO basis set (TZP). The inner cores of carbon, nitrogen, and oxygen (1s²) and that of iron (1s²-2s²2p²) were kept frozen. The exchange-correlation potential is based on the newly developed GGA exchange functional OPTX²⁶ in combination with the nonempirical PBE correlation functional

(OPBE).²⁷ This functional is generally known to be good at calculating the correct spin states of iron complexes and has low computational costs.²⁸ The calculations were performed on simple metalloprotoporphyrins, which means that the substituents present on the metalloprotoporphyrins were replaced by hydrogens. Geometries of all metal porphyrins were optimized with symmetry constraints for different oxidation states of the metalloprotoporphyrin, namely $[M^I]$, $[M^{II}]$, $[M^{III}-OH]$ and $[M^{IV}-O]$ (Figure 7.1), for low, intermediate and high spin states using the OPBE functional. The correct symmetry of the ground state was determined by also performing geometry optimizations without symmetry constraints. If the energy of the optimization with symmetry constraints was found to lie within 10 meV of the optimization without symmetry constraints, the symmetry was assigned to the geometry. Otherwise the calculations were repeated with a lower symmetry. Based on the energies of the different spin states the ground state for the metal porphyrins for different oxidation states was determined. All reported energies in this manuscript are formation energies from the atoms. These formation energies were determined from the calculated energies for the complexes minus the calculated energies of the individual atoms in their lowest spin state. In case of charged molecules such as $[M^I]$ and OH^- , the energies of neutral individual atoms were deduced. Therefore for these charged molecules the reported energies correspond to the formation energy plus their electron affinity. In order to determine the influence of functional on our calculated ground state energies, we also determined the ground state energies with the hybrid B3LYP functional. For this we used the geometry that was calculated with the OPBE functional. The calculated B3LYP energies are post-SCF.

7.3 Experimental Results

Figure 7.2 shows the electrochemical response of chromium, manganese, iron, cobalt and nickel protoporphyrins IX at pH 7, immobilized via direct adsorption from an alkaline solution. Based on previous electrochemical measurements for different metalloprotoporphyrins in organic solvents and aqueous solution,^{7,13,14,29-31} it is possible to assign the redox peaks to different metal redox transitions, as is shown in the figure. It can be seen that the M^{III}/M^{II} redox potential shifts to more positive potentials in the order chromium, manganese, iron and cobalt, the same order as these metals occur in the periodic table. For chromium, apart from the M^{III}/M^{II} transition, also a M^{IV}/M^{III} redox transition can be observed. No peaks were observed for the nickel protoporphyrin.

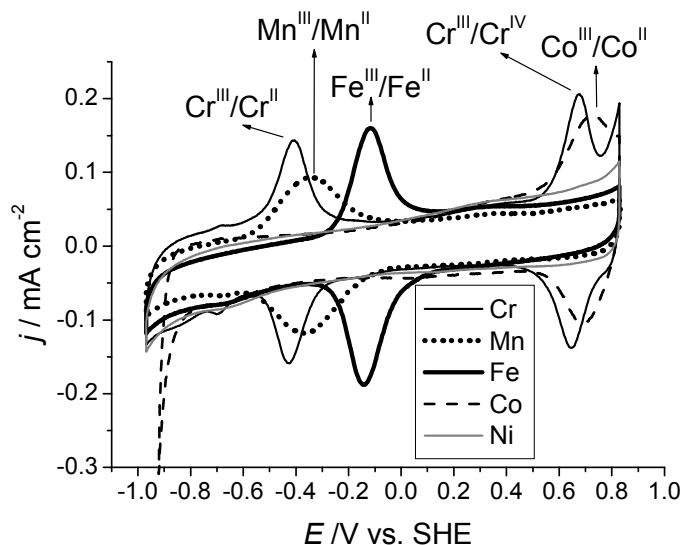


Figure 7.2 Cyclic voltammograms of a pyrolytic graphite electrode, with adsorbed Cr protoporphyrin IX (—), Mn protoporphyrin IX (····), Fe protoporphyrin IX (=heme) (—), Co protoporphyrin IX (- - -) and Ni protoporphyrins IX (- · -). Voltammograms were measured in 0.1 M phosphate, pH 7.0, at a scan rate of 500 mV/s.

To learn more about the properties of the different metalloporphyrins we investigated the dependence of the midpoint potentials of the different redox transitions as a function of pH (Figure 7.3). These potentials were determined from voltammograms measured in the pH 0-14 range. As an example the voltammograms recorded for chromium are depicted in Figure S7.1. Figure 7.3 shows similar behavior as a function of pH for the M^{III}/M^{II} redox transitions of the chromium, iron and cobalt protoporphyrins. This consists of a pH independent midpoint potential at low pH, and a pH dependent midpoint potential (59 mV/pH) at high pH. The value of 59 mV/pH corresponds to a hydroxide transfer accompanying the M^{III}/M^{II} transition. This behavior has been previously observed for iron porphyrins and has been ascribed to reactions 1 (low pH) and 2 (high pH).^{16,32,33} In these previous studies it has been suggested that the $[Fe^{II}]$ complex is coordinated by a water molecule ($[Fe^{II}-H_2O]$), but we have deliberately omitted the water molecule, since a XANES study has suggested that the $[Fe^{II}]$ remains four-coordinate, when adsorbed on a graphite electrode.³⁴ As can be deduced from reaction 1 and 2, the pH at which transition from the pH independent to the pH dependent midpoint potential occurs is equivalent to the pKa of the $[M^{III}]^+$ complex (reaction 3). From Figure 7.3 it can be seen that all metalloporphyrins have a pKa around 4. This is an indication that this pKa is mainly determined by the charge on the metal, and not by the specific electronic properties of the metal in the porphyrin. Figure 7.3 also shows that as a result of the similar behavior of the different metalloporphyrins, the observed difference in midpoint potential between the porphyrins remains similar over the whole pH range. This constant

difference is apparently related to the electronic properties of the different metalloprotoporphyrins. Only the manganese porphyrin behaves different from the other metalloprotoporphyrins, since it also displays a pH independent region between pH 7 and 11. A possible explanation could be that the manganese porphyrin adsorbs on the electrode as a dimer,³⁵ which would affect its redox transitions.

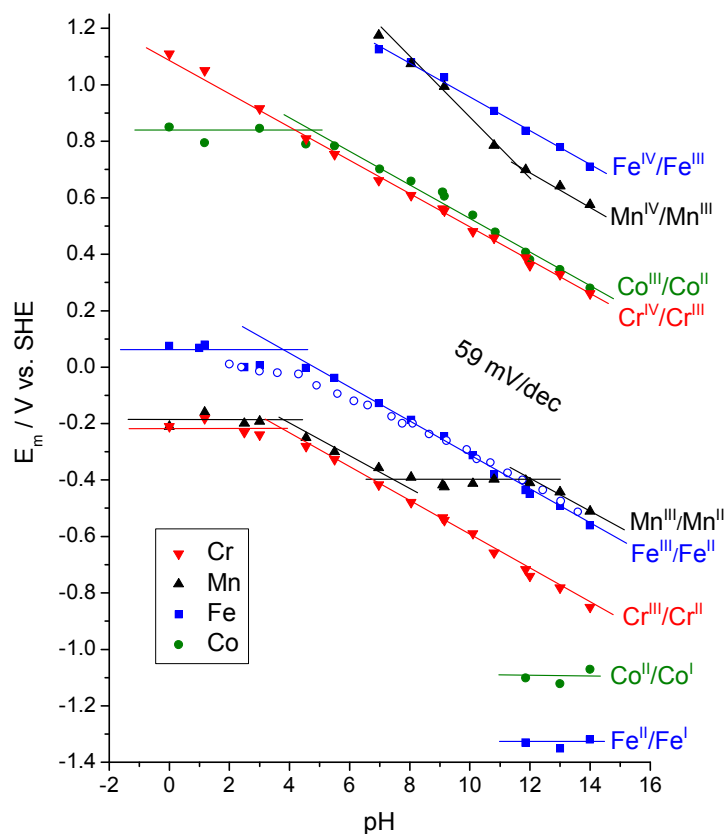
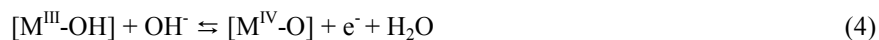


Figure 7.3 pH dependence of midpoint potentials of adsorbed Cr protoporphyrin IX (\blacktriangledown), Mn protoporphyrin IX (\blacktriangle), Fe protoporphyrin IX (=heme) (\blacksquare) and Co protoporphyrin IX (\bullet). Apart from the M^{III}/M^{II} transitions, also the observed M^{IV}/M^{III} and M^{II}/M^I transitions have been plotted. Measurements were performed in sulfuric acid (pH 0-1), 0.1 M acetate (pH 4-6), 0.1 M phosphate (2-3, 6-8, 11-12), 0.1 M borate (9-10) and caustic soda (pH 13-14) at a scan rate of 500 mV/s. For comparison the pH dependence of Fe protoporphyrin IX immobilized on a self-assembled monolayer on gold has been plotted (\circ).³²

Figure 7.3 also displays the pH dependence of some M^{IV}/M^{III} and M^{II}/M^I redox transitions. Similar to the behavior of the M^{III}/M^{II} redox transition at high pH, the M^{IV}/M^{III} redox transitions of chromium and iron also display a pH dependence of 59 mV/pH. This again indicates that a hydroxide transfer accompanies the electron transfer. Given the fact that the reduced species is $[M^{III}-OH]$ and the fact that only one coordination site is available when the porphyrin is adsorbed, the most likely reaction that occurs is reaction 4. Again the behavior for the manganese porphyrin is more complicated, and it seems that the electron transfer is accompanied by two hydroxide transfers between pH 7 and 11. M^{II}/M^I redox transitions are observed for iron and cobalt. Since this redox transition is independent of pH, reaction 5 is most likely to occur. The fact that this transition is not accompanied by a hydroxide or proton transfer, such as for example the binding of H_3O^+ to the negatively charged metalloporphyrin, is not too surprising, since it is unlikely that a positively charged cation can coordinate to the iron center, which still has a positive charge even though the overall complex is negatively charged. We have to remark that it is not completely clear whether the M^{II}/M^I electron transfer occurs on the metal for all metalloporphyrins. It is also possible that the electron transfer occurs on the porphyrin ring and that the metal remains in its 2+ oxidation state. Only in the case of iron and cobalt there is proof that the electron transfer occurs on the metal.^{7,36,37} Lastly, we would like to remark that we are not able to locate redox transitions at higher or lower potentials than approximately +1.3 or -1.3 V vs. SHE due to water decomposition on the metalloporphyrin or graphite electrode, resulting in decomposition of the porphyrin.



To determine whether there is a specific influence of our immobilization method on the redox behavior of the metalloporphyrins, we compared our results to the previously determined redox behavior of iron protoporphyrin IX immobilized on a self-assembled monolayer on gold (Figure 7.3).³² Direct comparison to metalloprotoporphyrins IX in solution was not possible, since they are not soluble in neutral solution and form complexes in alkaline solution.^{11,12} Figure 7.3 shows that the pH dependence of the midpoint potential of the M^{II}/M^{III} transition of the iron protoporphyrin IX immobilized on gold corresponds very well to our results on graphite. This suggests that the surface on which the metalloporphyrins are immobilized does not have a strong influence on their electrochemical behavior. Hence, it also suggests that the behavior on the electrode would be similar to that in solution, if the formation of dimers was left out of consideration. This is indeed suggested by a pH dependence study of a watersoluble metalloporphyrins.¹³

To further investigate the possible influences of immobilization methods on the redox behavior, we also immobilized the metalloprotoporphyrins by a different method, namely by incorporating them in films of the surfactant didodecyldimethylammoniumbromide

(DDAB). In aqueous solutions this surfactant forms vesicles,³⁸ and in the bilayers of these vesicles the relatively hydrophobic metalloprotoporphyrins can be dissolved. Films can then be formed by casting a small amount of this solution on a pyrolytic graphite electrode and evaporating the water. Since the porphyrins are now immobilized in a hydrophobic environment and not in an aqueous environment, we expect a significantly different voltammetric response. Figure 7.4 indeed shows some differences compared to Figure 7.2. Most striking is the fact that we now observe the M^{II}/M^I redox transition for all metalloporphyrins except manganese at pH 7. When comparing the potentials of the M^{II}/M^I transitions for cobalt and iron in the DDAB film compared to the adsorbed case we notice that they are about 500 mV more positive. We do not have a clear explanation for this difference, but apparently the vesicles are able to stabilize the $[M^I]^-$ adduct. Another difference compared to Figure 7.2 is that the peaks, corresponding to the M^{III}/M^{II} transition of Cr and Fe, display irreversible behavior. This has been tentatively ascribed to a potential-induced phase transition in the DDAB film,^{39,40} but might also be related to the irreversible formation of porphyrindimers in the vesicles. A last difference is that the redox peaks, which can be ascribed to the M^{III}/M^{II} transitions of Cr, Mn and Fe are found at higher potentials than in the adsorbed case.

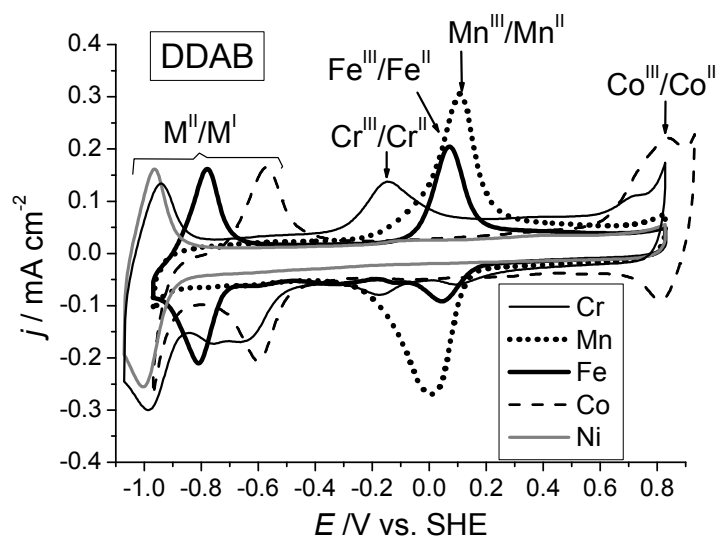


Figure 7.4 Cyclic voltammograms of a DDAB film with incorporated Cr protoporphyrin IX (—), Mn protoporphyrin IX (···), Fe protoporphyrin IX (=heme) (—), Co protoporphyrin IX (- - -) and Ni protoporphyrin IX (- · -) on a pyrolytic graphite electrode. Voltammograms were measured in 0.1 M phosphate, pH 7.0, at a scan rate of 500 mV/s.

Apart from these differences, large similarities between the adsorbed metalloprotoporphyrins and the metalloprotoporphyrins incorporated in the DDAB film can be found. This can especially be seen from Figure 7.5, which shows the pH dependence of the redox transitions of the porphyrins in the DDAB film. The potentials were again

determined from voltammograms in the pH 1-14 range, and an example for the iron protoporphyrin is shown in Figure S7.2. Figure 7.5 shows that similar to the adsorbed porphyrins, the midpoint potentials of the M^{III}/M^{II} transitions also display a pH independent midpoint potential region at low pH and a pH dependent region at high pH. This suggests that the same reactions occur as for the adsorbed metalloprotoporphyrins. Interestingly, the potential of the pH independent region is about the same as for the adsorbed porphyrins, which suggests that the hydrophobic environment has no significant influence on the M^{III}/M^{II} redox transition (in apparent contrast to the M^{II}/M^I redox transition). A difference is that the pH dependent region starts at a more positive pH value (around 8) for the DDAB films and as a result the midpoint potentials at high pH are higher. Apparently, reaction 3 is shifted to the left in the DDAB vesicles. Most likely this is related to the fact that the porphyrin is incorporated in a hydrophobic environment, where the water concentration is similar to the water concentration in an organic solvent such as hexane, namely approximately 0.01 weight percent.⁴¹ Consequently, the OH^- concentration is also a factor 10000 lower, corresponding to a potential change of 0.24 V or 4 pH units, which is in line with our results. Another similarity between the adsorbed porphyrins and the porphyrins incorporated in the DDAB vesicles is the comparable difference in potential between the M^{III}/M^{II} redox transitions and the M^{IV}/M^{III} redox transitions of chromium and iron. This suggests that the differences in potential between the different redox transitions are also largely independent of the solvent environment.

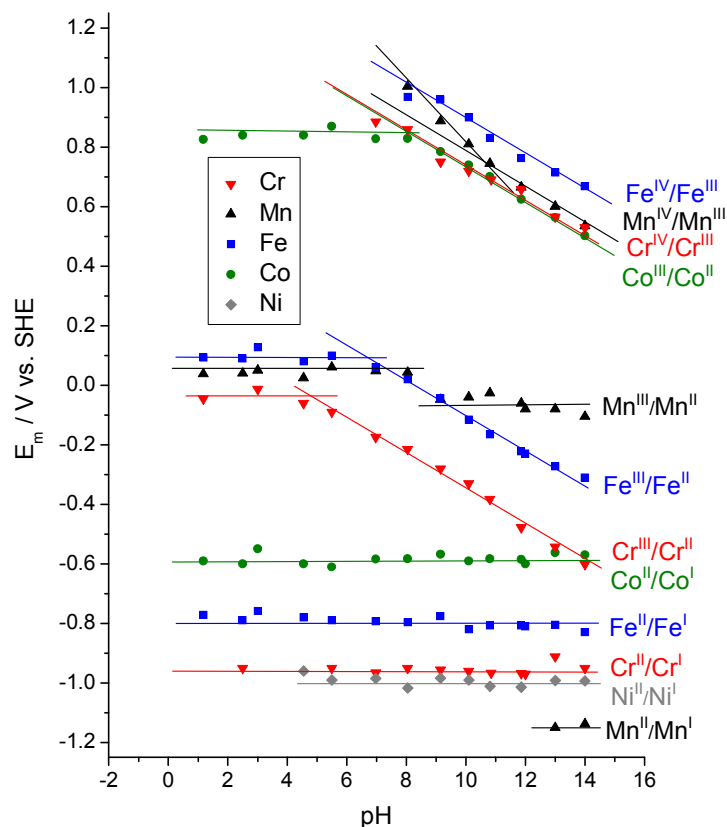


Figure 7.5 pH dependence of midpoint potentials of a DDAB film with incorporated Cr protoporphyrin IX (\blacktriangledown), Mn protoporphyrin IX (\blacktriangle), Fe protoporphyrin IX (=heme) (\blacksquare) and Co protoporphyrin IX (\bullet) and Ni protoporphyrin IX (\blacklozenge) on pyrolytic graphite. Apart from the M^{III}/M^{II} transitions, also the observed M^{IV}/M^{III} and M^{II}/M^I transitions have been plotted. Measurements were performed in sulfuric acid (pH 0-1), 0.1 M acetate (pH 4-6), 0.1 M phosphate (2-3, 6-8, 11-12), 0.1 M borate (9-10) and caustic soda (pH 13-14) at a scan rate of 500 mV/s. Due to the irreversible nature of the Cr^{II}/Cr^{III} redox transitions many peaks are present in the voltammogram and therefore it is hard to determine the potentials. For clarity, only the potentials of the peaks that are most likely to correspond to the reversible Cr^{II}/Cr^{III} transition have been plotted.

Based on our electrochemical measurements, we can conclude that some of the properties of the metalloprotoporphyrins are independent of immobilization method and pH and are hence only related to the specific electronic properties of the metalloprotoporphyrin. This includes the relative differences in potential between the different metalloprotoporphyrins. For example, the difference in the M^{II}/M^{III} redox transition between iron and cobalt is approximately 0.80 V, independent of the immobilization method and

pH. Also, largely independent of immobilization method are the differences in potential between the M^{IV}/M^{III} and M^{III}/M^{II} redox transitions. The fact that these properties are apparently only related to the specific electronic properties of the metalloporphyrin should make it possible to calculate these differences in potential, even based on calculations performed without a solvent. This will be attempted in the next section. For ease of comparison Table 7.1 lists the redox transitions at pH 14 for the porphyrins immobilized in different ways.

Table 7.1 Midpoint potentials at pH 14 of the different redox transitions in Cr, Mn, Fe, Co and Ni protoporphyrins. Potentials are given in V vs. SHE.

	M^I/M^{II}		M^{II}/M^{III}		M^{III}/M^{IV}	
	Ads.	DDAB	Ads.	DDAB	Ads.	DDAB
Cr		-0.95	-0.85	-0.60	0.26	0.53
Mn		-1.14	-0.41	-0.11	0.58	0.54
Fe	-1.32	-0.82	-0.56	-0.31	0.71	0.67
Co	-1.07	-0.58	0.28	0.50		
Ni		-0.99				

7.4 Calculations

We calculated the geometries and formation energies of the different metalloporphyrins in different oxidation states, namely $[M^I]$, $[M^{II}]$, $[M^{III}-OH]$ and $[M^{IV}-O]$ (Figure 7.1). We deliberately chose to perform calculations on $[M^{III}-OH]$ and $[M^{IV}-O]$, instead of $[M^{III}]^+$ and $[M^{IV}]^{2+}$, since these are the experimentally observed complexes. Additionally, DFT is known to perform better on neutral than on charged complexes. An important factor that we have to take into account in the calculations is the spin state of the metalloporphyrins. Metalloporphyrins are known to occur in many different spin states, depending on metal, ligand and oxidation state. Therefore, we have to do our calculations for high, intermediate and low spin states. The ground spin state can then be assigned to the spin state with the lowest energy. The results of our calculations are listed in Table 7.2. In this table the lowest energy and the corresponding spin state are given. The energies of the other spin states are listed in Table S7.1. Table 7.2 also lists the metal-nitrogen distance and point group that describe the geometry of the metalloporphyrins. The orbital occupations of the orbitals that have mainly d-orbital character are listed in Table S7.2. With regard to the $[M^{II}]$ complex, we would like to remark that we also did some calculations on a $[M^{II}-H_2O]$ complex, but these calculations resulted in dissociation of the water molecule from the metalloporphyrins, indicating that the H_2O ligand does not bind to the metalloporphyrins.

Table 7.2 The calculated formation energies from the atoms (in eV) of the metalloprotoporphyrins in different oxidation states and their corresponding spin states, metal-nitrogen distance (\AA) and point group (P.G.). The energies and geometries were calculated with the OPBE functional. Single point energy calculations of the determined geometries were also performed with the B3LYP functional.

Oxidation state	Metal	Energy (OPBE)	Spin	M-N	P.G.	Energy (B3LYP)
[M ^I]	Cr	-206.73	3/2	2.047	D _{2h}	-218.01
	Mn	-205.15	1	2.011	D _{4h}	-215.80
	Fe	-206.43	1/2	1.981	D _{4h}	-218.10 ^b
	Co	-206.49	0	1.961	D _{4h}	-219.55 ^c
	Ni	-205.56	1/2	2.026	D _{4h}	-217.82
[M ^{II}]	Cr	-205.33	2	2.038	D _{4h}	-216.63
	Mn	-203.55 ^a	5/2	2.088	D _{4h}	-214.60
	Fe	-204.75	1	1.980	D _{2h}	-216.95
	Co	-204.80	1/2	1.971	D _{4h}	-218.34
	Ni	-204.11	0	1.962	D _{4h}	-216.86
[M ^{III} -OH]	Cr	-212.72	3/2	2.048	C _s	-225.11
	Mn	-210.48	1	2.017	C _s	-222.56
	Fe	-212.09	5/2	2.113	C _s	-225.22
	Co	-211.37	0	1.977	C _s	-225.69
	Ni	-209.84	1/2	1.985	C _s	-223.54
[M ^{IV} -O]	Cr	-209.48	0	2.057	C _{4v}	-221.41
	Mn	-207.39	3/2	2.028	C _{4v}	-218.84
	Fe	-208.56	1	2.004	C _{4v}	-221.02
	Co	-207.51	3/2	2.073	C _{4v}	-221.32
	Ni	-205.80	2	2.074	C _{4v}	-219.07

^a the $s = 3/2$ spin state of the [Mn^{II}] complex has the same energy (see Table S7.1).

^b This energy corresponds to the $s = 5/2$ spin state of [Fe^I], which is 0.02 eV lower in energy than the $s = 1/2$ spin state.

^c This energy corresponds to the $s = 1$ spin state of [Co^I], which is 0.19 eV lower in energy than the $s = 1$ spin state.

The results of the calculations can be compared with experimentally determined values (Table 7.3), which have been determined with X-ray crystallography and NMR spectroscopy. Although the experimentally determined metal-nitrogen distances are for porphyrins with different substituents, the influence of these substituents on the metal-nitrogen bond length is generally not larger than 0.01 \AA ,^{42,43} and therefore the values can be compared meaningfully. In case of the [M^{II}] complexes all listed metal-nitrogen bond lengths are for crystals with planar metalloprotoporphyrins. For iron, cobalt and nickel porphyrins also distorted crystal structures have been reported (so-called ruffled and saddled structures).⁴³⁻⁴⁵ However, these structures have metal-nitrogen bond lengths that differ up to 0.03 \AA compared to the planar porphyrins and are therefore less suitable for comparison.

Table 7.3 Experimentally determined metal-nitrogen bond lengths (Å) and spin states of the metal porphyrins.

Oxidation state	Metal	M-N	Spin
[M ^I]	Fe	1.980 ³⁶	(1/2) ³⁶
	Co	1.942 ⁴⁶	
[M ^{II}]	Cr	2.033 ⁴⁷	(2) ⁴⁸
	Mn	2.082 ⁴⁹	(5/2) ⁴⁸
	Fe	1.986 ⁴³	(1) ⁵
	Co	1.971 ⁴⁴	(1/2) ⁴⁴
	Ni	1.958 ⁵⁰	(0) ⁵⁰
[M ^{III} -OH]	Fe	2.044 ^{51,52}	
[M ^{IV} -O]	Cr	2.032 ⁵³	(0) ⁵³
	Mn	2.00 ⁵⁴	(3/2) ⁵⁵
	Fe	2.005 ⁵⁶	(1) ⁵⁶

The calculated metal-nitrogen distances and spin states are in good agreement with experimentally determined values. Most distances are correctly predicted to within 0.01 Å and the listed spin states are the same. Therefore, we can conclude that the OPBE functional is generally good at predicting spin states and geometries of metalloporphyrins. Only the metal-nitrogen distance in the [Fe^{III}-OH] porphyrin is clearly not correctly predicted (2.113 Å vs. 2.044 Å experimentally), which is probably due to the fact that a wrong spin state ($s=5/2$) is calculated to be the ground state. Most likely the $s=3/2$ state is the actual ground state, which we base on the fact that this spin state has a calculated M-N bond length of 2.023 Å, which is much closer to the experimental value. However, according to the calculations this state is about 0.25 eV higher in energy. The fact that our calculations have difficulties in determining the correct ground state for this compound is not too surprising,¹⁹ since Fe^{III}-porphyrins occur in both $s=3/2$ and $s=5/2$ spin states. Even mixed spin states do exist.^{57,58} We cannot determine whether the calculations for the other [M^{III}-OH] are also incorrect, since no data for other [M^{III}-OH] complexes are available. The reason for this is that the [M^{III}-OH] complexes tend to form oxo-bridged dimers in solution and hence no monomeric crystals can be formed.^{35,59,60}

Since the calculations give a reasonably accurate description of the metalloporphyrins, we can use Table 7.2 to deduce some general trends for the metalloporphyrins. A first observation is that for the [M^I] and [M^{II}] porphyrins, decreasing spin states are observed when going from chromium to nickel. This is related to the filling up of partially filled orbitals, when increasing the number of electrons in the system (Table S7.2). These orbitals mainly have metal d orbital character, but also have some porphyrin character. A detailed discussion about how the orbitals of porphyrin and metal interact can be found in the literature.⁵⁸ Interestingly, for the [M^{III}-OH] and [M^{IV}-O] porphyrins the trend of decreasing spin state when going from Cr to Ni no longer exists. For the [M^{IV}-O] porphyrin it even seems reversed. When comparing the calculated energies of the

different spin states it appears that they are relatively close to each other (Table S7.1), which suggests that the hydroxide and oxygen ligands are able to stabilize the spin states relative to each other. This would then also explain the observation of mixed spin states for $[\text{Fe}^{\text{III}}]$ porphyrins with different ligands.^{57,58} A second observation is that the metal-nitrogen distance seems to depend mostly on the spin state of the metal (Figure 7.6), instead of on the particular metal. High spin states have relatively long metal-nitrogen bonds, whereas low spin states have short metal-nitrogen bonds. The short distances for low spin states can be rationalized in light of the fact that the isolated metals are naturally high spin and therefore a strong interaction between the porphyrin and metal orbitals is necessary to stabilize the low spin state. The long distances for high spin states imply that there is less overlap between the metal orbitals and the porphyrin orbitals, thereby stabilizing the high spin states. A third observation is that almost all reported porphyrins are of the highest point group possible, namely D_{4h} for the $[\text{M}^{\text{I}}]$ and $[\text{M}^{\text{II}}]$ complexes, C_s for the $[\text{M}^{\text{III}}\text{-OH}]$ complex and C_{4v} for the $[\text{M}^{\text{IV}}\text{-O}]$ complex. Only the $[\text{Fe}^{\text{II}}]$ porphyrin and the $[\text{Cr}^{\text{I}}]$ porphyrin are of a lower point group, namely D_{2h} , which is caused by a Jahn-Teller effect. Three electrons have to fill two degenerate e_g orbitals (dxz and dyx) (Supporting information S4), and hence the geometry is distorted so that these orbitals are no longer degenerate. The distortion does not affect the planarity of the metalloprotoporphyrins and can therefore not explain experimentally observed distortions. A fourth observation is that all redox transitions seem to occur on the metal centers of the metalloprotoporphyrins, as is suggested by the number of d electrons (Supporting information S4).

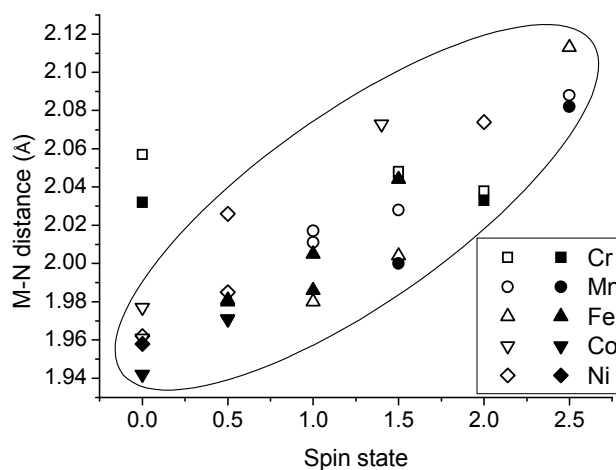


Figure 7.6 Correlation between spin states of chromium (\blacksquare \square), manganese (\bullet \circ), iron (\blacktriangle \triangle), cobalt (\blacktriangledown \triangledown) and nickel (\blacklozenge \lozenge) metalloprotoporphyrins in different oxidation states and metal nitrogen distances in \AA . Filled symbols represent experimental data, whereas open symbols represent calculated data. Since the spin states of the $[\text{Co}^{\text{I}}]$ and $[\text{Fe}^{\text{III}}\text{-OH}]$ complexes have not been experimentally determined, these are assumed to be respectively 0 and 3/2. We base this on the correspondence of metal nitrogen distances compared to the calculations.

Since it has been recently reported that the OPBE functional has some difficulties at predicting the energetics of the intermediate spin-states of iron porphyrins,⁶¹ we also calculated the formation energies and spin states of the metalloporphyrins using the hybrid B3LYP functional. This functional has been reported to provide a satisfactory description of the energies of low, intermediate and high spin states.⁶¹ Since B3LYP is a “more expensive” functional, and since the geometries predicted by the OPBE functional agree well with experimental data, we only performed a single point energy calculation, the results of which are listed in Table 7.2 (for the spin states with the lowest energies) and Table S7.3 (all spin states). When comparing the calculated energies we observe that B3LYP predicts lower energies (between -214 and -226 eV) than OPBE (between -203 and -213 eV). This discrepancy suggests that both functionals are unable to accurately predict the formation energy of the metalloporphyrins. However, for the calculation of electrochemical potentials we are not interested in the absolute formation energies, but in the differences in energies between the different metals and oxidation states. Comparing the energies of the different spin states it appears that B3LYP generally predicts the same ground states as OPBE, which suggests that both functionals are able to make a reasonable prediction of the relative energy differences. The functional also predicts that the ground state of the [Fe^{III}-OH] porphyrin is $s=5/2$, and hence seems to make the same mistake as OPBE. Only in the case of the [M^I] porphyrin it predicts different spin states for iron and cobalt, which is not in agreement with the experimental data and therefore OPBE outperforms B3LYP. In the case of the [Mn^{II}] porphyrin, B3LYP outperforms OPBE, as can be deduced from the fact that it predicts a lower energy for the experimentally observed $s=5/2$ over the $s=3/2$ ground state, whereas OPBE predicted the same energies for both spin states. A further comparison of the functionals will follow in the discussion on electrochemical potentials.

From the calculated formation energies we can now determine the potentials of the redox transitions. These redox potentials are directly related to the differences in energy between the different oxidation states. The relative differences in potential between the different metalloporphyrins can therefore be predicted by simply comparing the energy differences between the different oxidation states for the different metals. However, to determine the “real” redox potentials, we also have to take into account that the redox transitions occur in aqueous solution and that some of the transitions involve ligands such as hydroxide. Equation 6 gives the equation to calculate the “real” potential of the [M^{II}]/[M^{III}-OH] redox transition, in which $\Delta G^{\text{form}}[\text{M}^{\text{II}}]$ and $\Delta G^{\text{form}}[\text{M}^{\text{III}}\text{-OH}]$ are the free formation energies of the complexes, $\Delta G^{\text{solv}}[\text{M}^{\text{II}}]$ and $\Delta G^{\text{solv}}[\text{M}^{\text{III}}\text{-OH}]$ their solvation energies, $\Delta G^{\text{form}}[\text{OH}^-]$ and $\Delta G^{\text{solv}}[\text{OH}^-]$ the free formation energy and solvation energy of OH⁻, and Φ_{m} the absolute potential of the standard hydrogen electrode in water. To determine the “real” potential from equation 6, we have to make some assumptions. These assumptions are the same for the different metals and will therefore not affect the calculated differences in energy and hence potential between the different metalloporphyrins. For convenience, we will put the discussion on the capability of the calculations to predict the relative potential differences together with the discussion on the “real” potentials. Therefore we will first discuss the assumptions.

$$e_0 E^0 = \Delta G^{form} [M^{III} - OH] - \Delta G^{form} [M^{II}] - \Delta G^{form} [OH^-] \\ + \Delta G^{solv} [M^{III} - OH] - \Delta G^{solv} [M^{II}] - \Delta G^{solv} [OH^-] - \Phi_m \quad (6)$$

Since we want to use our calculated formation energies to predict the potentials, we must assume that these are approximately equal to the free energies as given in equation 6. In principal, these energies are not the same, since contrary to the calculated energies the free energies also have an entropy contribution. Therefore we have to assume that the entropic contribution to the free energy is negligible or that the entropies of the different reactants approximately cancel.

Since experimentally determined solvation energies for the $[M^{II}]$ and $[M^{III}-OH]$ complexes are not available, we have to either calculate them or assume that the solvation energies of both complexes are equal. Since calculations using solvation models are less accurate than calculations in the gas phase, the use of a solvation model would increase the error in the electrochemical potential and this is not desirable. Therefore it seems more logical to make the assumption that both complexes have approximately the same solvation energy, which also seems justified. We base this on the fact that both complexes are neutral and have a low solubility in water and therefore they should both have a low solvation energy. Also, there does not seem to be a particular reason why one of the complexes should have a significantly higher solvation energy than the other.

Equation 6 also requires values for the free energy and solvation energy of the OH^- ligand. Therefore we calculated the formation energy of the OH^- ligand employing the same functionals as used previously for the metalloprotoporphyrins. A value of -6.33 eV was determined with the OPBE functional and a value of -7.37 eV was determined with the B3LYP functional. We deliberately chose to use calculated values instead of experimental values, since in this way the same systematic errors are made as for the metalloprotoporphyrins. Hence, when calculating the potential, the systematic errors made in the calculation of the energy of $[M^{II}]$ and OH^- should cancel out against the systematic errors made in the calculation of the energy of the $[M^{III}-OH]$ complex. On the other hand, for the solvation energy $\Delta G^{solv}[OH^-]$ we chose to use the experimentally determined value of -4.553 eV.⁶²⁻⁶⁴ In this case it seems more appropriate to use the experimental value, since there is no cancelling out of systematic errors on the calculations due to the fact that $\Delta G^{solv}[M^{II}]$ and $\Delta G^{solv}[M^{III}-OH]$ are assumed equal. For comparison we also calculated the solvation energies with the conductor-like screening model (COSMO).⁶⁵ A value of -4.26 eV was found with both functionals, which is in reasonable agreement with the experimental value.

With these assumptions the potentials for the $[M^{II}]/[M^{III}-OH]$ redox transitions can be calculated. Since the calculated differences in energy result in absolute potentials, it is necessary to deduct the absolute potential of the standard hydrogen electrode in water Φ_m in order to relate our results to electrochemical potentials. Φ_m has been estimated to be

4.44 ± 0.02 V at 298.15 K.⁶⁶ The resulting potentials are listed in Table 7.4. Since we have not taken into account any concentration effect of the OH⁻ ligand, the calculated potentials correspond to [OH⁻] = 1 M, i.e. pH 14. This is also a convenient pH for comparison to the experimental data, since all redox transitions observed in the pH 0-14 range, can be observed at this pH. Also, at this pH the [M^{II}]/[M^{III}-OH] redox transition is accompanied by a hydroxide transfer.

Table 7.4 Calculated redox potentials (vs. SHE) for the redox transitions of the different metalloporphyrins at pH 14 as determined from the energies calculated with the OPBE and B3LYP functionals.

	[M ^I]/[M ^{II}]		[M ^{II}]/[M ^{III} -OH]		[M ^{III} -OH]/[M ^{IV} -O]	
	OPBE	B3LYP	OPBE	B3LYP	OPBE	B3LYP
Cr	-3.04	-3.06	-0.95	-0.99	-0.97	-0.35
Mn	-2.84	-3.23	-0.49	-0.49	-1.12	-0.31
Fe	-2.76	-3.29	-0.90	-0.79	-0.68	0.15
Co	-2.75	-3.23	-0.13	0.13	-0.33	0.32
Ni	-2.99	-3.49	0.71	0.81	-0.15	0.42

Potentials for the [M^I]/[M^{II}] and [M^{III}-OH]/[M^{IV}-O] redox transitions were calculated in a similar way as for the [M^{II}]/[M^{III}-OH] redox transition and are also listed in Table 7.4. Since a water molecule is involved in the [M^{III}-OH]/[M^{IV}-O] redox transition (reaction 4), we also required values for $\Delta G^{\text{form}}[\text{H}_2\text{O}]$ and $\Delta G^{\text{sol}}[\text{H}_2\text{O}]$. As we did for the OH⁻ ligand, we calculated the formation energy of the water molecule and used the experimentally determined solvation energy. The calculated values for the formation energy were -10.37 eV with the OPBE functional and -11.25 eV with the B3LYP functional. The experimentally determined value for the solvation energy is -0.278 eV.⁶²⁻⁶⁴

Figure 7.7 shows a graphical comparison of the experimental and calculated midpoint potentials. It shows that the correspondence of calculated and experimental values strongly varies between the different redox transitions. The best predictions are made for the [M^{II}]/[M^{III}-OH] redox transition. Firstly, the calculated values reasonably accurately predict the differences in potential between the different metalloporphyrins. These relative differences are largely independent of the assumptions made, and are therefore a direct measure of the quality of our calculations. A closer look reveals that the results for B3LYP are somewhat better than for OPBE, since the maximum error for B3LYP is 150 mV, whereas it is 260 mV for OPBE. Secondly, the calculated potentials are close to the measured potentials. This suggests that the assumptions made are reasonable in the case of the [M^{II}]/[M^{III}-OH] redox transition.

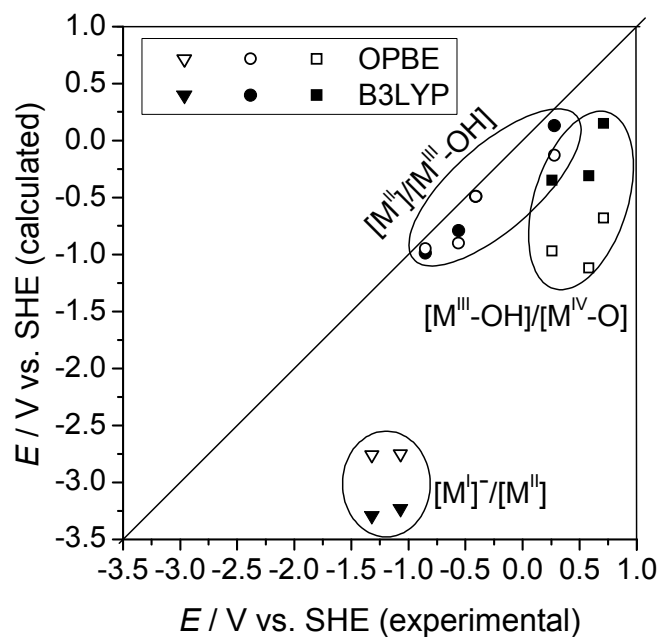


Figure 7.7 Comparison of experimentally determined and calculated midpoint potentials.

For the $[M^{III}\text{-OH}]/[M^{IV}\text{-O}]$ redox transitions the predictions are less satisfactory. With regard to the relative differences between the metalloporphyrins, the predictions are still reasonable. The B3LYP functional accurately predicts the difference in potential between the chromium and iron porphyrin and also correctly predicts that the potential of the manganese porphyrin is in between the chromium and iron porphyrins. The OPBE functional gives less accurate results, especially for the manganese porphyrin. When comparing to the experimental values, both functionals predict potentials that are significantly lower. In the case of OPBE the deviation is about 1.2 V, whereas it is about 500 mV for B3LYP. OPBE even predicts that the $[M^{III}\text{-OH}]/[M^{IV}\text{-O}]$ transition is lower in potential than the $[M^{II}]/[M^{III}\text{-OH}]$ transition. The difference with the experimental results could have two causes. Either a systematic error in the calculations results in overestimation of the energies of the $[M^{IV}\text{-O}]$ adducts or an incorrect assumption has been made. Since the differences between the OPBE functional and the B3LYP functional are independent of the assumptions, we can conclude that in case of the OPBE functional at least 700 mV is caused by a systematic error in the calculations. The 500 mV for the B3LYP functional could be due to a similar systematic error or due to for example different solvation energies of both complexes.

For the $[M^I]/[M^{II}]$ redox transitions the predicted potentials are much lower than the recorded potentials. This is not too surprising, since the assumption that the $[M^I]$

complex has the same solvation energy as the $[M^{II}]$ complex is clearly incorrect, given the fact that a charged complex has a much higher solvation energy. As a result the calculated values for the potentials are approximately 2-2.5 eV too low. Assuming a relatively low solvation energy of the $[M^{II}]$ adduct, this suggests that the $[M^I]^-$ adduct has a solvation energy of approximately 2-2.5 eV, which is in line with the range of 2.4-3.0 eV expected for large anions.⁶² With regard to the relative differences between the metalloporphyrins, we observe that both functionals are unable to predict these differences and are also unable to determine the right peak order. This suggests that both functionals have more difficulties with this redox transition than the other redox transitions. This is probably related to the fact that the $[M^I]^-$ complex is charged and DFT is known to perform worse on charged complexes than on neutral complexes. In principle we could convert the negatively charged complex into a neutral complex by adding a cation, but since the iron atom in the porphyrin is positively charged, it is unlikely that the cation would form a bond with the porphyrin. Therefore the porphyrin would in fact remain positively charged. On the other hand, the calculations do correctly predict the fact that the potentials of the $[M^{II}]/[M^I]^-$ redox transitions for the different metalloporphyrins are relatively close to each other, which is in contrast to the other redox transitions.

7.5 Discussion and conclusions

From our electrochemical data we can conclude that the different metalloporphyrins generally display similar redox behavior. This behavior as a function of pH and potential is displayed in the phase diagram of Figure 7.8. Only in case of the manganese porphyrin the redox behavior is more complicated, which might be due to interactions between the porphyrin molecules. The most striking feature in the phase diagram is the different redox behavior for the M^{II}/M^{III} redox transition at low and high pH. At high pH this transition is accompanied by a hydroxide transfer, whereas this is not the case at low pH. This is probably due to the low hydroxide concentration at low pH. The pH at which the transition from $[M^{III}]^+$ to $[M^{III}-OH]$ occurs corresponds to the pKa of the $[M^{III}]^+$ complex. For all metalloporphyrins this pKa is around 4.

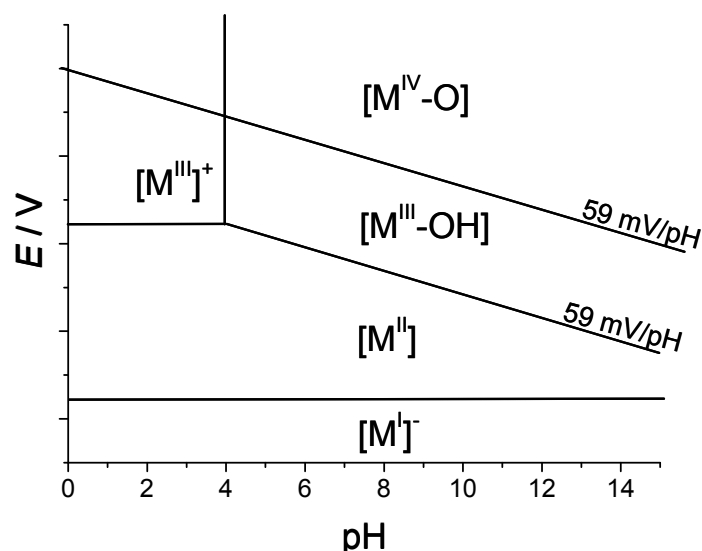


Figure 7.8. Phase diagram for the redox transitions of the metalloprotoporphyrins.

Although the metalloprotoporphyrins display similar redox behavior, they differ in the potentials at which the redox transitions occur. These differences in potential are largely independent of pH and are therefore almost solely related to the specific electronic properties of the metalloprotoporphyrins. For example, the difference between the $M^{\text{II}}/M^{\text{III}}$ transitions for chromium and iron remains approximately 0.25 V over the whole pH range. The potential differences between the different metalloprotoporphyrins depend on the specific redox transition. It is interesting to see that for the $M^{\text{I}}/M^{\text{II}}$ transition, the order in which the peaks are observed is manganese, nickel, chromium, iron and cobalt. This is in contrast to the order observed for the $M^{\text{II}}/M^{\text{III}}$ and $M^{\text{III}}/M^{\text{IV}}$ transitions, which is chromium, manganese/iron, cobalt and nickel as expected from the periodic table. Also, the peaks of the $M^{\text{I}}/M^{\text{II}}$ transition are relatively close to each other in potential, in contrast to the other transitions. An explanation for this behavior is not straightforward and would require a more detailed investigation of the orbitals of the porphyrins, which is outside the scope of this paper.

We can also conclude that the way in which the porphyrins are immobilized does not have a large influence on the overall redox behavior of the metalloprotoporphyrins. This is reflected in the fact that the voltammetric response of immobilized iron protoporphyrins is approximately the same on graphite as on gold.³² Increasing the hydrophobicity of the surrounding medium does also not result in large changes in the phase diagram, as can be seen from the measurements on the metalloprotoporphyrins incorporated in the DDAB vesicles. Only the potentials of the $M^{\text{I}}/M^{\text{II}}$ transitions are shifted positively and the pKa of the $[M^{\text{III}}]^+$ complex is increased. The latter is probably a result of the lower OH^- concentration in the hydrophobic vesicles. The observed electrochemical behavior is also

similar to the behavior of water soluble porphyrins in solution.¹³ This suggests that the studied metalloporphyrins would display similar redox behavior in solution, if they were soluble. However, we have to remark that in case of the adsorbed metalloporphyrins one of the coordination sites is blocked and also that the metalloporphyrins are unable to form dimers. Therefore the electrochemical behavior in solution is probably more complicated than the behavior depicted in Figure 7.8. However, the phase diagram might be of particular relevance to heme proteins, in which porphyrindimers cannot be formed and in which the sixth coordination site is mostly occupied, leaving only one site for ligand changes.

From a comparison of our DFT calculations with experimental data we can conclude that good predictions of metal-nitrogen bond lengths and spin states of metalloporphyrins can be made. This has enabled us to deduce some general conclusions on the metalloporphyrins, namely that there is a correlation between spin state and metal-nitrogen distances, that hydroxide or oxo ligands stabilize the higher and lower spin states relative to each other, and that the metalloporphyrins are highly symmetric and do mostly not undergo deformations. The prediction of electrochemical potentials employing DFT calculations gives more mixed results. The relative potential differences between metalloporphyrins are reasonably predicted for the M^{II}/M^{III} and M^{III}/M^{IV} transitions, but not for the M^I/M^{II} transition. This is probably related to the inability of the DFT calculations to correctly predict the energies of the charged $[M^I]$ complexes. We also have to take into account that the calculation of electrochemical potentials requires accurate calculation of energy differences (to within about 0.2 eV, which corresponds to 4 kcal/mol). With regard to the calculation of the “real” potentials, these are remarkably well predicted for the M^{III}/M^{II} transitions, but not for the other transitions. This is an indication that it is possible to determine electrochemical potentials from gas phase calculations, even when ligand changes are involved. Therefore assumptions required with regard to solvation and entropy seem tenable. Nevertheless, great care should be taken as indicated by the results for the M^I/M^{II} and M^{III}/M^{IV} redox transitions. With regard to the calculation of electrochemical potentials we can also conclude that the B3LYP functional outperforms the OPBE functional.

7.6 Supporting Information

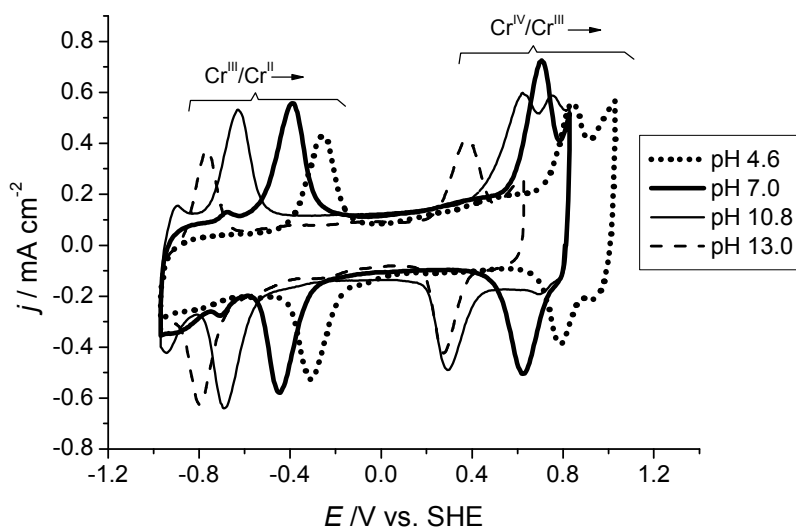


Figure S7.1 Cyclic voltammograms of a pyrolytic graphite electrode with adsorbed Cr protoporphyrin IX, in 0.1 M acetate pH 4.6 (····), 0.1 M phosphate pH 7.0 (—▲—), 0.1 M phosphate pH 10.8 (—●—) and 0.1 M sodium hydroxide, pH 13.0 (---). Voltammograms were measured at a scan rate of 2 V/s.

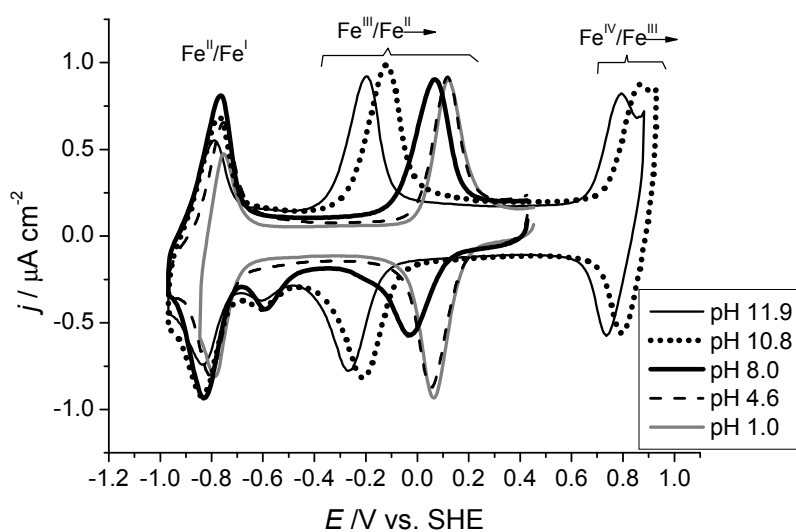


Figure S7.2 Cyclic voltammograms of a DDAB film with incorporated Fe protoporphyrin IX on a pyrolytic graphite electrode, in 0.1 M HCl pH 1.0 (—■—), 0.1 M acetate pH 4.6 (---), 0.1 M phosphate pH 8.0 (—●—), 0.1 M phosphate, pH 10.8 (····) and 0.1 M phosphate, pH 11.9 (—▲—). Voltammograms were measured at a scan rate of 2 V/s.

Table S7.1 The calculated formation energies of the different metal porphyrins, for different spin states and different oxidation states (in eV). The corresponding symmetry is also given. The energies of the optimized geometries were calculated with the OPBE functional.

[M ^I]						
S	Cr	Mn	Fe	Co	Ni	
0		-203.79 ^a D _{4h}		-206.50 D _{4h}		
½	-205.28 ^a D _{2h}		-206.43 ^a D _{4h}		-205.56 ^a D _{4h}	
1		-205.15 D _{4h}		-205.97 D _{2h}		
3/2	-206.73 D _{2h}		-206.20 ^a D _{4h}		-204.41 D _{2h}	
2		<i>b</i>		-205.22 D _{2h}		
5/2	-206.50 D _{2h}		-205.71 D _{2h}			

[M ^{II}]						
S	Cr	Mn	Fe	Co	Ni	
0			-203.99 D _{2h}		-240.11 D _{4h}	
½		-201.97 ^a D _{4h}		-204.80 D _{4h}		
1	-203.84 ^a D _{2h}		-204.75 D _{2h}		-203.21 D _{4h}	
3/2		-203.55 ^a D _{2h}		-203.95 D _{4h}		
2	-205.33 D _{4h}		-204.40 D _{2h}			
5/2		-203.55 D _{4h}				

[M ^{III} -OH]						
S	Cr	Mn	Fe	Co	Ni	
0		-209.93 ^a C _s		-211.38 C _s		
½	-211.72 ^a C _s		-211.68 C _s		-209.84 C _s	
1		-210.48 C _s		-211.30 C _s		
3/2	-212.72 C _s		-211.82 C _s		-209.77 C _s	
2		<i>b</i>		-211.19 C _s		
5/2	-210.82 C _s		-212.09 C _s		<i>b</i>	

[M ^{IV} -O]						
S	Cr	Mn	Fe	Co	Ni	
0	-209.48 C _{4v}		<i>b</i>		-205.03 C _{2v}	
½		-207.20 C _{2v}		-206.74 C _{4v}		
1	-209.35 C _{2v}		-208.57 C _{4v}		-205.19 C _{2v}	
3/2		-207.40 C _{4v}		-207.51 C _{4v}		
2	-207.70 C _{4v}		-208.15 C _{4v}		-205.80 C _{4v}	
5/2		-205.44 C _{2v}		<i>b</i>		

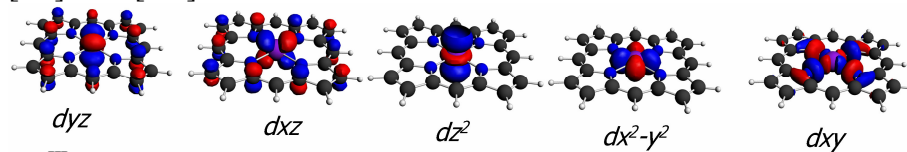
^a Spin contaminated value (Wittbrodt et al., *J. Chem. Phys.* 1995, 99, 3465). Energies have not been corrected for this spin contamination. However, correction would not affect the designation of ground state spin states. Only in the case of [M^I] there would be some influence of spin contamination on the ground state energies.

^b SCF does not converge.

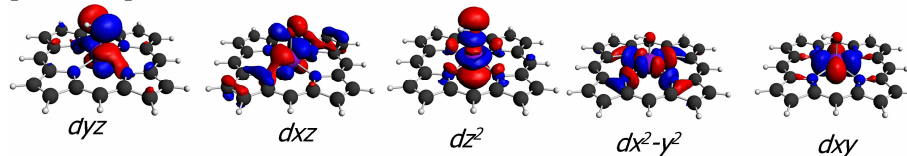
Table S7.2 Occupations of metalloporphyrin orbitals that have mainly metal *d*-orbital character for the different metalloporphyrins in different oxidation states. The total number of *d* electrons and the spin states are also given. Representations of these orbitals and the names of the corresponding *d*-orbitals are shown below the table.

Oxidation state	Metal	<i>dyz</i>	<i>dxz</i>	<i>dz²</i>	<i>dx²-y²</i>	<i>dxy</i>	nr. of d electrons	Spin
[M ^I]	Cr	2	1	1	1	0	5	3/2
	Mn	2	2	1	1	0	6	1
	Fe	2	2	1	2	0	7	1/2
	Co	2	2	2	2	0	8	0
	Ni	2	2	2	2	1	9	1/2
[M ^{II}]	Cr	1	1	1	1	0	4	2
	Mn	1	1	1	1	1	5	5/2
	Fe	2	1	1	2	0	6	1
	Co	2	2	1	2	0	7	1/2
	Ni	2	2	2	2	0	8	0
[M ^{III} -OH]	Cr	1	1	0	0	1	3	3/2
	Mn	1	1	0	0	2	4	1
	Fe	1	1	1	1	1	5	5/2
	Co	2	2	0	0	2	6	0
	Ni	2	2	1	0	2	7	1/2
[M ^{IV} -O]	Cr	0	0	0	0	2	2	0
	Mn	1	1	0	0	1	3	3/2
	Fe	1	1	0	0	2	4	1
	Co	1	1	0	1	2	5	3/2
	Ni	1	1	1	1	2	6	2

[M^I] and [M^{II}]



[M^{III}-OH]



[M^{IV}-O]

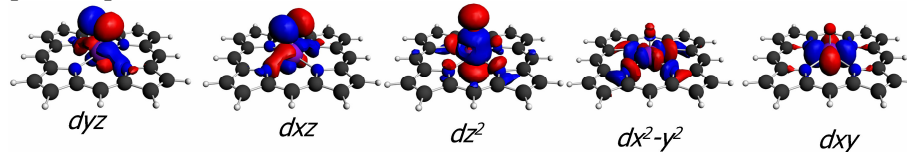


Table S7.3 The calculated formation energies of the different metal porphyrins, for different spin states and different oxidation states (in eV). The corresponding symmetry is also given. The energies were calculated with the B3LYP functional.

[M ^I]					
S	Cr	Mn	Fe	Co	Ni
0		-214.32 ^a		-219.36	
½	-216.68 ^a		-218.11 ^a		-217.82
1		-215.80 ^a		-219.55	
3/2	-218.01 ^a		-218.03 ^a		-217.72
2		<i>b</i>			
5/2	-217.81		-218.12		

[M ^{II}]					
S	Cr	Mn	Fe	Co	Ni
0			-215.04		-216.87
½		-212.63 ^a		-218.34	
1	-215.38 ^a		-216.95		-216.50
3/2		-214.30		-217.81	
2	-216.64		-216.84		
5/2		-214.60			

[M ^{III} -OH]					
S	Cr	Mn	Fe	Co	Ni
0		-221.58 ^a		-225.68	
½	-224.23 ^a		-224.67		-223.54
1		-222.57		-225.57	
3/2	-225.10		-224.95		-223.53
2		<i>b</i>		-225.63	<i>b</i>
5/2	-223.00		-225.22		

[M ^{IV} -O]					
S	Cr	Mn	Fe	Co	Ni
0	-221.41		<i>b</i>		-217.69
½		-218.64		-220.49 ^a	
1	-221.17		-221.02		-218.76
3/2		-218.84		-221.32	
2	-219.10		-220.73		-219.07
5/2		-216.88		<i>b</i>	

^a Spin contaminated value (Wittbrodt et al., J. Chem. Phys. 1995, 99, 3465). Energies have not been corrected for this spin contamination. However, correction would not affect the designation of ground state spin states. Only in the case of [M^I] there would be some influence of spin contamination on the ground state energies.

^b SCF does not converge.

7.7 References

1. Messerschmidt, A.; Huber, R.; Wieghardt, K.; Poulos, T.; *Handbook of Metalloproteins, Volume 1*, John Wiley & Sons: Chichester, 2001; p.
2. Messerschmidt, A.; Huber, R.; Wieghardt, K.; Poulos, T.; *Handbook of Metalloproteins, Volume 2*, John Wiley & Sons: Chichester, 2001; p.
3. Collman, J. P.; Boulatov, R.; Sunderland, C. J.; Fu, L., *Chem. Rev.* **2004**, *104*, 561-588.
4. Wyllie, G. R. A.; Scheidt, W. R., *Chem. Rev.* **2002**, *102*, 1067-1089.
5. Goff, H.; La Mar, G. N.; Reed, C. A., *J. Am. Chem. Soc.* **1977**, *99*, 3641-6.
6. Vogel, K. M.; Kozlowski, P. M.; Zgierski, M. Z.; Spiro, T. G., *J. Am. Chem. Soc.* **1999**, *121*, 9915.
7. Davis, D. G.; Dolphin, D., Electrochemistry of Porphyrins. In *The Porphyrins, Vol. 5: Physical Chemistry, Pt. C.*, Academic press: New York, 1978; Vol. 1, p 137.
8. Spiro, T. G.; Zgierski, M. Z.; Kozlowski, P. M., *Coord. Chem. Rev.* **2001**, *219-221*, 923.
9. Rovira, C.; Kunc, K.; Hutter, J.; Ballone, P.; Parrinello, M., *J. Phys. Chem. A* **1997**, *101*, 8914.
10. Ghosh, A., *Acc. Chem. Res.* **1998**, *31*, 189-198.
11. Brown, S. B.; Dean, T. C.; Jones, P., *Biochem. J.* **1970**, *117*, 733-9.
12. Medhi, O. K.; Silver, J., *Inorg. Chim. Acta* **1988**, *153*, 133-4.
13. Chen, S. M.; Sun, P. J.; Su, Y. O., *J. Electroanal. Chem.* **1990**, *294*, 151-64.
14. Jeon, S.; Bruice, T. C., *Inorg. Chem.* **1992**, *31*, 4843-8.
15. Chen, S. M.; Su, Y. O., *J. Chem. Soc., Chem. Commun.* **1990**, 491-3.
16. de Groot, M. T.; Merkx, M.; Koper, M. T. M., *J. Am. Chem. Soc.* **2005**, *127*, 7579-7586.
17. Sagara, T.; Fukuda, M.; Nakashima, N., *J. Phys. Chem. B* **1998**, *102*, 521-527.
18. Ghosh, A., *J. Biol. Inorg. Chem.* **2006**, *11*, 671-673.
19. Ghosh, A., *J. Biol. Inorg. Chem.* **2006**, *11*, 712-724.
20. Van den Brink, F.; Visscher, W.; Barendrecht, E., *J. Electroanal. Chem.* **1983**, *157*, 283-304.
21. Van der Plas, J. F.; Barendrecht, E., *Recl. Trav. Chim. Pays-Bas* **1977**, *96*, 133-6.
22. Brown, A. P.; Koval, C.; Anson, F. C., *J. Electroanal. Chem.* **1976**, *72*, 379-87.
23. Duong, B.; Arechabaleta, R.; Tao, N. J., *J. Electroanal. Chem.* **1998**, *447*, 63-69.
24. SCM ADF 2006.01, Theoretical Chemistry, Vrije Universiteit: Amsterdam, the Netherlands, <http://www.scm.com>.
25. Te Velde, G.; Bickelhaupt, F. M.; Baerends, E. J.; Fonseca Guerra, C.; Van Gisbergen, S. J. A.; Snijders, J. G.; Ziegler, T., *J. Comp. Chem.* **2001**, *22*, 931-967.
26. Handy, N. C.; Cohen, A. J., *Mol. Phys.* **2001**, *99*, 403-412.
27. Perdew, J. P.; Burke, K.; Ernzerhof, M., *Phys. Rev. Lett.* **1996**, *77*, 3865-3868.
28. Swart, M.; Groenhof, A. R.; Ehlers, A. W.; Lammertsma, K., *J. Phys. Chem. A* **2004**, *108*, 5479-5483.
29. Kellett, R. M.; Spiro, T. G., *Inorg. Chem.* **1985**, *24*, 2373-7.
30. Song, E.; Shi, C.; Anson, F. C., *Langmuir* **1998**, *14*, 4315-4321.
31. Boucher, L. J., *Coord. Chem. Rev.* **1972**, *7*, 289-329.
32. Pilloud, D. L.; Chen, X.; Dutton, P. L.; Moser, C. C., *J. Phys. Chem. B* **2000**, *104*, 2868-2877.

33. Shigehara, K.; Anson, F. C., *J. Phys. Chem.* **1982**, *86*, 2776-83.
34. Kim, S.; Bae, I. T.; Sandifer, M.; Ross, P. N.; Carr, R.; Woicik, J.; Antonio, M. R.; Scherson, D. A., *J. Am. Chem. Soc.* **1991**, *113*, 9063-6.
35. Cheng, B.; Cukiernik, F.; Fries, P. H.; Marchon, J.-C.; Scheidt, W. R., *Inorg. Chem.* **1995**, *34*, 4627-39.
36. Mashiko, T.; Reed, C. A.; Haller, K. J.; Scheidt, W. R., *Inorg. Chem.* **1984**, *23*, 3192-6.
37. Rodgers, K. R.; Reed, R. A.; Su, Y. O.; Spiro, T. G., *Inorg. Chem.* **1992**, *31*, 2688-700.
38. Warr, G. G.; Sen, R.; Evans, D. F.; Trend, J. E., *J. Phys. Chem.* **1988**, *92*, 774-83.
39. Boussaad, S.; Tao, N. J., *J. Am. Chem. Soc.* **1999**, *121*, 4510-4515.
40. de Groot, M. T.; Merckx, M.; Koper, M. T. M., *J. Am. Chem. Soc.* **2005**, *127*, 16224-16232.
41. Black, C.; Joris, G. G.; Taylor, H. S., *J. Chem. Phys.* **1948**, *16*, 537-43.
42. Liao, M.-S.; Scheiner, S., *J. Chem. Phys.* **2002**, *117*, 205-219.
43. Hu, C.; Noll, B. C.; Schulz, C. E.; Scheidt, W. R., *Inorg. Chem.* **2007**, *46*, 619-621.
44. Scheidt, W. R.; Turowska-Tyrk, I., *Inorg. Chem.* **1994**, *33*, 1314-18.
45. Scheidt, W. R., *J. Biol. Inorg. Chem.* **2001**, *6*, 727-732.
46. Doppelt, P.; Fischer, J.; Weiss, R., *Inorg. Chem.* **1984**, *23*, 2958-62.
47. Scheidt, W. R.; Reed, C. A., *Inorg. Chem.* **1978**, *17*, 710-14.
48. Reed, C. A.; Kouba, J. K.; Grimes, C. J.; Cheung, S. K., *Inorg. Chem.* **1978**, *17*, 2666-70.
49. Gonzalez, B.; Kouba, J.; Yee, S.; Reed, C. A.; Kirner, J. F.; Scheidt, W. R., *J. Am. Chem. Soc.* **1975**, *97*, 3247-9.
50. Cullen, D. L.; Meyer, E. F., Jr., *J. Am. Chem. Soc.* **1974**, *96*, 2095-102.
51. Buchler, J. W.; Lay, K. L.; Lee, Y. J.; Scheidt, W. R., *Angew. Chem.* **1982**, *94*, 456-7.
52. Fleischer, E. B.; Miller, C. K.; Webb, L. E., *J. Am. Chem. Soc.* **1964**, *86*, 2342-7.
53. Groves, J. T.; Kruper, W. J., Jr.; Haushalter, R. C.; Butler, W. M., *Inorg. Chem.* **1982**, *21*, 1363-8.
54. Ayougou, K.; Bill, E.; Charnick, J. M.; Garner, C. D.; Mandon, D.; Trautwein, A. X.; Weiss, R.; Winkler, H., *Angew. Chem. Int. Ed.* **1995**, *34*, 343-6.
55. Schappacher, M.; Weiss, R., *Inorg. Chem.* **1987**, *26*, 1189-90.
56. Schappacher, M.; Weiss, R.; Montiel-Montoya, R.; Trautwein, A.; Tabard, A., *J. Am. Chem. Soc.* **1985**, *107*, 3736-8.
57. Reed, C. A.; Guiset, F., *J. Am. Chem. Soc.* **1996**, *118*, 3281-2.
58. Cheng, R.-J.; Chen, P.-Y.; Lovell, T.; Liu, T.; Noodleman, L.; Case, D. A., *J. Am. Chem. Soc.* **2003**, *125*, 6774-6783.
59. Hoffman, A. B.; Collins, D. M.; Day, V. W.; Fleischer, E. B.; Srivastava, T. S.; Hoard, J. L., *J. Am. Chem. Soc.* **1972**, *94*, 3620-6.
60. Gold, A.; Jayaraj, K.; Doppelt, P.; Fischer, J.; Weiss, R., *Inorg. Chim. Acta* **1988**, *150*, 177-81.
61. Liao, M.-S.; Watts, J. D.; Huang, M.-J., *J. Comp. Chem.* **2006**, *27*, 1577-1592.
62. Kelly, C. P.; Cramer, C. J.; Truhlar, D. G., *J. Phys. Chem. B* **2006**, *110*, 16066-16081.
63. Pliego, J. R., Jr.; Riveros, J. M., *Phys. Chem. Chem. Phys.* **2002**, *4*, 1622-1627.

-
64. Tissandier, M. D.; Cowen, K. A.; Feng, W. Y.; Gundlach, E.; Cohen, M. H.; Earhart, A. D.; Coe, J. V.; Tuttle, T. R., Jr., *J. Phys. Chem. A* **1998**, *102*, 7787-7794.
 65. Pye, C. C.; Ziegler, T., *Theor. Chem. Acc.* **1999**, *101*, 396-408.
 66. Trasatti, S., *Pure Appl. Chem.* **1986**, *58*, 955-66.

Chapter 8

Conclusions and future prospects

8.1 Immobilization of heme proteins

In this thesis different methods for the immobilization of heme proteins on electrode surfaces have been investigated. The goals were to determine the extent to which each immobilization method affects the native properties of the protein, to study the electron transfer process between the protein and electrode and to determine how the protein is immobilized on the electrode. To this purpose the electrochemical properties of the immobilized proteins were investigated and compared to the properties of the native proteins in solution. The results greatly differed for the studied immobilization methods. For myoglobin incorporated in films of the surfactant didodecyldimethylammonium bromide (DDAB) on pyrolytic graphite, it was found that the hydrophobic interactions between the protein and the surfactant can cause heme release from the protein (Chapter 3). Heme release can also occur in layer-by-layer films of myoglobin and polystyrenesulfonate (PSS) on pyrolytic graphite, probably as a result of interactions between the pyrolytic graphite electrode, myoglobin and PSS (Chapter 4). Therefore these two methods can be regarded as generally unsuitable for the immobilization of soluble heme proteins. On the other hand, electrostatic immobilization on carboxylic acid-terminated self-assembled monolayers (SAM) seems to be a suitable heme protein immobilization method, as is reflected in the fact that immobilized cytochrome *c* and cytochrome *c'* retain properties that are similar to the properties of both proteins in solution (Chapter 5 and 6). Nevertheless, also for this immobilization method small differences between the properties of the immobilized protein and the protein in solution remain. These can be explained in light of the local electric fields and the binding interactions between the protein and the SAM.

Although our results suggest that electrostatic immobilization is a suitable method for the immobilization of heme proteins, it is not necessarily successful for every heme protein. This also depends on some specific properties of the protein. These include the position of the heme group relative to the surface of the protein and the distribution of charges on the protein surface. Success is only achieved if the electrostatic interactions between the protein and the electrode are attractive, enabling its immobilization, and if the distance between the heme group and the electrode is not too long, enabling electron transfer. For example, one cannot expect that proteins with deeply buried heme groups such as the cytochromes P450 display fast electron transfer with an electrode. In certain cases varying the solution conditions can enable successful immobilization. A good example is cytochrome *c'*, for which immobilization was only possible between pH 3.5

and pH 5.5 due to the fact that only in this pH range the protein is sufficiently positively charged to bind to the negatively charged SAM (Chapter 5).

A question that remains after this thesis is whether it is possible to immobilize myoglobin, the protein for which the immobilization methods described in Chapter 3 and 4 were unsuccessful. Although not described in this thesis, we also attempted to electrostatically immobilize myoglobin on positively as well as negatively charged SAMs under different conditions. However, we were unable to obtain any voltammetric response corresponding to its heme group. An explanation might be that myoglobin adsorbs in an orientation, in which the distance between the heme group and the electrode is too long. It might also be of relevance that contrary to cytochrome *c* (and possibly also cytochrome *c*') myoglobin is not an electron transfer protein.

For a successful further development of the research into immobilized redox proteins, it is necessary to extensively study the properties of immobilized proteins both by electrochemical methods as well as by spectroscopic methods. Also, a larger number of redox proteins should be immobilized. This should lead to the development of a detailed understanding of protein-electrode interactions and long range electron transfer. Currently, the field of protein immobilization is still in a state where new immobilization methods are developed regularly. Not all of these methods are well-evaluated. This sometimes leads to speculative conclusions, which go against our common understanding of protein stability and long range electron transfer. Examples include claims to the occurrence of native myoglobin and hemoglobin under extreme conditions (pH 1)¹ and claims to fast electron transfer to immobilized cytochromes P450, which have deeply buried hemes.²⁻⁴ This kind of conclusions shows that the understanding of protein-electrode interactions and long range electron transfer is still limited.

Ultimately, an increased understanding of protein-electrode interactions and long range electron transfer should lead to the development of computer models that should be able to predict the orientation of a protein on an electrode, the rate of electron transfer between the protein's redox group and the electrode and the effect of the immobilization process on the protein's properties. These models will stimulate the use of immobilized enzymes in industrial processes and will also be of great value in the development of biosensors.

8.2 Nitric oxide reduction by immobilized hemes

In this thesis we have shown that immobilized hemes can selectively reduce nitric oxide (NO) to either hydroxylamine (NH₂OH) or nitrous oxide (N₂O). By optimizing the conditions (pH, immobilization method, potential and NO concentration) 100% selectivity toward either of these products can be obtained (Chapter 2 and 3). Especially the high selectivity toward NH₂OH is striking, since NO reduction by enzymes and metal catalysts generally results in the formation of N₂O and NH₃. The reason that NH₂OH and not NH₃ is the product of the reduction probably lies in the fact that the nitric oxide molecule is only coordinated to the heme via its nitrogen atom, and this is

not sufficient to break the N-O bond. In the NO reducing enzymes, the NO molecule also interacts with the amino acids of the enzyme enabling NO bond breaking. From a fundamental point of view, this shows the weakness of using model complexes for enzymatic reactions, since a model complex remains only a model and therefore its catalytic properties can significantly differ from the corresponding enzyme. In this case the discrepancy is not too surprising, since the heme group is just a very simple model for a heme enzyme. It could be further “improved” to more closely resemble the catalytic site of a heme enzyme by adding additional groups to the heme, which could mimic the enzyme’s amino acids. However, from an industrial point of view, the formation of NH_2OH can be regarded as advantageous, since NH_2OH is a much more valuable material than NH_3 .

To really understand the reactivity of heme groups and heme proteins toward different substrates, it is necessary to make a more detailed investigation of the electronic properties of a heme group. A first step has been made in Chapter 7, in which electrochemical measurements on different metalloporphyrins have been combined with density functional theory (DFT) calculations. This has led to an improved understanding of the redox transitions of metalloporphyrins. The potentials of some of these redox transitions can even be predicted with DFT calculations to within a reasonable accuracy. In the future, calculations in the presence of substrate molecules should be able to predict the reactivity of heme and heme enzymes in catalytic reactions such as NO reduction.

The work described in this thesis has focused on hemes, but for future work one can also think about the immobilization of other biomimetic complexes. Based on the desired reaction, one can study the corresponding enzyme, construct a model complex, immobilize it on a conducting surface, and do catalysis. An interesting challenge would be nitrate reduction, which is catalyzed by molybdenum complexes.

8.3 References

1. Chen, S.-M.; Tseng, C.-C., *J. Electroanal. Chem.* **2005**, *575*, 147-160.
2. Udit, A. K.; Hagen, K. D.; Goldman, P. J.; Star, A.; Gillan, J. M.; Gray, H. B.; Hill, M. G., *J. Am. Chem. Soc.* **2006**, *128*, 10320-10325.
3. Immoos, C. E.; Chou, J.; Bayachou, M.; Blair, E.; Greaves, J.; Farmer, P. J., *J. Am. Chem. Soc.* **2004**, *126*, 4934-4942.
4. Estavillo, C.; Lu, Z.; Jansson, I.; Schenkman, J. B.; Rusling, J. F., *Biophys. Chem.* **2003**, *104*, 291-296.

Summary

Electrochemistry of Immobilized Hemes and Heme Proteins

Enzymes, nature's catalysts, have always been a source of inspiration for research in the field of catalysis. The reason is that their activities and selectivities are generally much better than those of industrial metal catalysts. People have been trying to use enzymes in industrial processes, but until now their use remains relatively limited due to their low stability and the difficulties involved in separating them from the reaction products.

A possibility to improve the ease of use of enzymes in industrial processes is by immobilizing them on supports. This enables an easy separation of the enzymes from the products and also enables an easy replacement of deactivated enzymes. In the case of redox enzymes, immobilization on a conducting support has the additional advantage that it removes the need to use expensive electron donors. However, in order to successfully immobilize an enzyme, certain challenges have to be overcome. Firstly, the immobilization process should not have a large influence on the structure and properties of the enzyme. Secondly, in the case of immobilized redox enzymes, direct electron transfer between the enzyme and the conducting surface should be possible. Since electrons can only tunnel through a protein over a limited distance ($\pm 20 \text{ \AA}$), this means that the enzyme has to be immobilized in such a way that its redox centre is relatively close to the electrode. Until now, a considerable number of protein and enzyme immobilization methods have been developed. However, for most methods relatively little is known on the effect of the immobilization process on the protein's properties and also long range electron transfer is still poorly understood. Therefore it is still unclear which methods can be regarded as suitable for enzyme immobilization.

In part of this thesis (Chapter 3-6) we have studied different immobilization methods, aiming to determine to what extent each immobilization process affects the protein's properties, to obtain a better understanding of the electron transfer process between the electrode and the protein's redox group, and to determine the orientation of the immobilized protein. We have done this by studying the electrochemical properties of the immobilized proteins. The class of proteins we have investigated are the heme proteins, a class known to be involved in diverse reactions such as oxygen transport, oxygen reduction and electron transport.

In chapter 3 and 4 we have investigated the immobilization of the protein myoglobin in films on pyrolytic graphite. One of the films was made of the surfactant didodecyltrimethylammonium bromide (DDAB), in which myoglobin was incorporated using hydrophobic interactions (Chapter 3). The other film was made of negatively charged polystyrenesulfonate (PSS), which electrostatically interacts with positively charged myoglobin (Chapter 4). For both films it was concluded that the interactions

with the film and the electrode can result in the dissociation of the heme groups from the myoglobin, and therefore both methods are unsuitable for protein immobilization. This was based on experiments, which showed that heme immobilized in the films gave almost the same electrochemical response as myoglobin immobilized in the films. It was also supported by UV/Vis experiments, which showed that the spectrum of myoglobin incorporated in DDAB vesicles is almost the same as the spectrum of heme incorporated in DDAB vesicles.

In chapter 5 and 6 we have investigated the immobilization of the proteins cytochrome *c'*, horse cytochrome *c*, and yeast cytochrome *c* via electrostatic interactions on self-assembled monolayers (SAM) on gold. It was concluded that this method is suitable for the immobilization of these proteins, based on the similar properties of the immobilized proteins compared to the proteins in solution. Nevertheless, relatively small differences with regard to midpoint potential and ligand binding properties remain, which are probably related to the electric field created by the negatively charged SAM and the interactions between the proteins and the SAM. Based on the electron transfer properties we estimated the orientation of the proteins on the electrode, and determined how this orientation can be influenced by the protein's surface charge distribution and pH. Also, the influence of ligands such as carbon monoxide (CO) and nitric oxide (NO) on the conformation and orientation of the proteins was determined.

Another possibility to tackle the disadvantages of using enzymes in industrial processes is by making use of catalysts that mimic the active site of an enzyme. These synthetic complexes have the advantage that they are generally more stable and easier to immobilize than enzymes. However, they remain models, and therefore their catalytic activity and selectivity can significantly differ from the corresponding enzymes.

In Chapter 2 and part of Chapter 3A of this thesis we have investigated the nitric oxide (NO) reduction by immobilized heme groups on pyrolytic graphite. A heme group can be regarded as a simple model complex for the NO reducing enzymes. It appeared that depending on the conditions (pH, immobilization method, potential and NO concentration) the reduction was selective to either NH_2OH or N_2O . This was determined by combining electrochemical measurements with the Rotating Ring disk Electrode (RRDE) and the newly developed On-Line Electrochemical Mass Spectroscopy (OLEMS). The high selectivity toward NH_2OH distinguishes immobilized heme from metal catalysts and enzymes, on which NO reduction generally yields N_2O or NH_3 . The reason for this difference in selectivity compared to NO reducing enzymes is probably that NO can only coordinate to immobilized heme via its nitrogen atom, which is insufficient to break the N-O bond. On the other hand, in the enzymes the amino acids of the enzyme can interact with the oxygen atom, which enables N-O bond breaking. The different selectivity confirms that simple model complexes can have catalytic properties that significantly differ from the corresponding enzymes. Nevertheless, from an industrial point of view the selectivity toward NH_2OH is interesting.

In relation to understanding the electrocatalytic behavior of immobilized heme, it is useful to obtain a more fundamental understanding of the nature of its redox transitions.

This was the aim of Chapter 7, in which the heme group, which is an iron porphyrin, is compared to other metalloporphyrins (chromium, manganese, cobalt and nickel). This was done by performing electrochemical measurements over the pH 1-14 range, as well as by performing density functional theory (DFT) calculations. The results show that the metalloporphyrins display comparable redox behavior and occur in four different oxidation states. It was found that most redox transitions are accompanied by a hydroxide transfer. Interestingly, it appeared possible to predict the electrochemical potentials of certain redox transitions from the calculated differences in energies between the redox states.

Samenvatting*

Elektrochemie van geïmmobiliseerde hemen en heemeiwitten

Als u een willekeurige voorbijganger op straat zou vragen wat een katalysator is, zal deze u waarschijnlijk iets zeggen als “Zo’n ding heb ik onder mijn auto, en volgens mij is het goed voor het milieu.”. Hoe de katalysator precies werkt weten de meeste mensen echter niet. Welnu, de autokatalysator zorgt ervoor dat schadelijke gassen zoals stikstofmonoxide en koolstofmonoxide, die in de motor worden gevormd, worden omgezet in relatief onschadelijke gassen zoals stikstof en koolstofdioxide. Zonder de autokatalysator zouden de schadelijke gassen in de atmosfeer komen, wat vooral in steden heel slecht zou zijn voor de volksgezondheid. De autokatalysator is echter niet de enige katalysator. Katalysatoren worden namelijk ook veel in industriële processen gebruikt, onder andere in de olieraffinage, kunstmestproductie en de productie van medicijnen. Net zoals de autokatalysator bestaan deze katalysatoren meestal uit kleine metaaldeeltjes die op een drager zitten. Het principe achter al deze katalysatoren is dat ze ervoor zorgen dat belangrijke reacties plaatsvinden, maar zelf niet opgebruikt worden. Daarom kan een katalysator vaak heel lang mee en hoeft deze in een auto bijvoorbeeld nooit vervangen te worden.

Naast in door de mens bedachte processen komen katalysatoren ook heel veel voor in natuurlijke processen. Deze natuurlijke katalysatoren worden enzymen genoemd en het hele menselijke lichaam zit er vol mee. Ze zorgen onder andere voor de omzetting van zuurstof en voedsel naar koolstofdioxide, de reactie waaruit de mens al zijn energie haalt. Deze enzymen zijn eiwitten, wat relatief grote organische moleculen zijn. Ze zien er dus anders uit dan de door de mens gemaakte katalysatoren en daardoor hebben ze ook andere eigenschappen. Zo zijn ze erg actief, wat betekent dat ze reacties erg snel kunnen laten verlopen. Ook kunnen ze heel ingewikkelde reacties goed laten verlopen. Als nadeel hebben ze echter dat ze wat sneller stukgaan (‘deactiveren’).

Omdat een katalysator vaak bepalend is voor de economische haalbaarheid van een industrieel proces, valt er met het ontwikkelen van nieuwe en betere katalysatoren veel geld te verdienen. Vanwege hun goede eigenschappen zijn enzymen hiervoor altijd een bron van inspiratie geweest. Ze worden echter nog relatief weinig in industriële processen gebruikt vanwege hun lage stabiliteit en het feit dat ze na afloop van de reactie gescheiden moeten worden van de producten.

Een oplossing waarmee een gedeelte van deze nadelen kan worden ondervangen is het vastzetten van de enzymen op een drager. Deze drager kan eenvoudig uit het reactiemengsel worden gehaald en daardoor kunnen de enzymen eenvoudig worden vervangen als ze gedeactiveerd zijn. Omdat ze vastzitten, hoeven de enzymen na afloop ook niet meer uit het productmengsel te worden gehaald. Het vastzetten van een enzym

* Deze Nederlandstalige samenvatting geeft slechts een algemeen beeld van het werk verricht in dit proefschrift. Voor een meer gedetailleerde samenvatting dient u de Engelstalige samenvatting te lezen.

op het oppervlak is echter niet zo gemakkelijk en brengt de nodige risico's met zich mee. Het voornaamste risico is dat de krachten die nodig zijn om het enzym vast te zetten, de structuur van het enzym en daarmee zijn gunstige katalytische eigenschappen veranderen. Een probleem is dat het op het moment niet echt bekend is wat 'goede' en 'slechte' methoden zijn om enzymen vast te zetten.

In een gedeelte van dit proefschrift (Hoofdstuk 3 - 6) zijn verschillende methodes onderzocht om eiwitten vast te zetten, met als doel te begrijpen wat voor invloed het vastzetten heeft op de eigenschappen van de eiwitten. Dit bleek sterk te verschillen voor de verschillende methodes. Zo leidt het inbedden van eiwitten in bepaalde films ertoe dat de eiwitten uit elkaar vallen (Hoofdstuk 3 en 4). Het vastzetten door middel van elektrostatische krachten leidt echter nauwelijks tot veranderingen in de eigenschappen. (Hoofdstuk 5 en 6). Voor deze laatste methode is ook bepaald welke oriëntatie de eiwitten op het oppervlak hebben. Door dit betere begrip van de eigenschappen van vastgezette eiwitten zou het in de toekomst mogelijk moeten zijn om allerlei enzymen vast te zetten en deze te gebruiken in industriële processen.

Naast het directe gebruik van enzymen in industriële processen kunnen enzymen ook als een bron van inspiratie dienen in de ontwikkeling van nieuwe katalysatoren. Zo kan op basis van de structuur van het enzym een synthetische katalysator worden ontwikkeld, die ongeveer dezelfde katalytische eigenschappen zou moeten hebben als een enzym. Zo'n synthetisch complex blijft echter een model, en daarom kan niet verwacht worden dat de katalytische eigenschappen van het complex net zo goed zijn als van het enzym. Synthetische complexen hebben echter wel als voordeel dat ze over het algemeen stabiel zijn dan eiwitten en bovendien kunnen ze makkelijker worden vastgezet op een drager.

In hoofdstuk 2 en 3 van dit proefschrift hebben we de katalytische eigenschappen van heemgroepen in de omzetting van stikstofmonoxide (NO) onderzocht. Heemgroepen zijn ijzercomplexen, die ook voorkomen in enzymen die stikstofmonoxide kunnen omzetten. Het bleek dat de reactie met de heemgroepen als katalysator niet hetzelfde product opleverde als de reactie met het enzym als katalysator. Dit toonde eens te meer aan dat een complex niet dezelfde eigenschappen heeft als een enzym. Het complex bleek echter wel een interessante katalysator, omdat het stikstofmonoxide omzet in hydroxylamine, wat een belangrijke grondstof is voor de productie van nylon. Tenslotte zijn in hoofdstuk 7 van dit proefschrift nog theoretische berekeningen aan heemgroepen uitgevoerd, met als doel de eigenschappen van deze complexen beter te begrijpen.

List of publications

M.T. de Groot, M. Merkx, M.T.M. Koper, "Reorganization of immobilized *horse* and *yeast* cytochrome *c* induced by pH changes or nitric oxide binding", *Langmuir*, **2007**, *23*, 3832-3839

M.T. de Groot, T.H. Evers, M. Merkx, M.T.M. Koper, "Electron transfer and ligand binding to cytochrome *c*' on self-assembled monolayers", *Langmuir*, **2007**, *23*, 729-736

M.T. de Groot, M. Merkx, M.T.M. Koper, "Evidence for heme release in layer-by-layer assemblies of myoglobin and polystyrenesulfonate on pyrolytic graphite", *Journal of Biological Inorganic Chemistry*, **2007**, *In Press*

M.T. de Groot, M. Merkx, M.T.M. Koper, "Bioinspired electrocatalytic reduction of nitric oxide by immobilized heme groups", *Comptes Rendus Chimie*, **2007**, *In Press*

M.T. de Groot, M.T.M. Koper, "Redox transitions of chromium, manganese, iron, cobalt and nickel protoporphyrins in aqueous solution", *Inorganic Chemistry*, **2007**, submitted

M.T. de Groot, M. Merkx., M.T.M. Koper, "Additional evidence for heme release in myoglobin-DDAB films on pyrolytic graphite", *Electrochemistry Communications*, **2006**, *8*, 999-1004

M.T. de Groot, M. Merkx, M.T.M. Koper, "Heme release in myoglobin-DDAB films and its role in electrochemical NO reduction", *Journal of the American Chemical Society*, **2005**, *127*, 16224-16234

M.T. de Groot, M. Merkx, A.H. Wonders, M.T.M. Koper, "Electrochemical reduction of NO by hemin adsorbed at pyrolytic graphite" *Journal of the American Chemical Society*, **2005**, *127*, 7579-7586

M.T. de Groot, M.T.M. Koper, "The influence of nitrate concentration and acidity on the electrocatalytic reduction of nitrate on platinum", *Journal of Electroanalytical Chemistry*, **2004**, *562*, 81-94

Curriculum vitae

Thijs de Groot werd op 12 augustus 1979 in Deurne geboren en groeide op in het nabijgelegen Helmond. In 1991 ging hij naar het St.-Willibrord Gymnasium in Deurne, waar hij in 1997 zijn diploma behaalde. In hetzelfde jaar begon hij met zijn studie Chemische Technologie aan de Technische Universiteit Eindhoven. Tijdens zijn studie liep hij vier maanden stage bij GE Plastics in Bergen op Zoom. Thijs' fascinatie voor onderzoek begon met zijn afstudeerproject, waarin hij werkte aan de elektrochemische reductie van nitraat op platina. Nadat hij in 2002 cum laude afstudeerde, wilde hij wat meer van de wereld zien en daarom ging hij vier maanden stage lopen in de groep van Nenad Markovic en Philip Ross in Berkeley, waar hij onderzoek deed naar protonreductie aan zilver. Hierna keerde hij terug naar Eindhoven, waar hij in 2003 zijn promotieonderzoek begon onder begeleiding van Marc Koper. Onderwerp van dit onderzoek was de elektrochemie van geïmmobiliseerde hemen en heemeiwitten, zoals beschreven in dit proefschrift. Als onderdeel van zijn promotie heeft Thijs drie maanden in de groep van Fraser Armstrong in Oxford gewerkt. In 2006 verhuisde hij van de Universiteit Eindhoven naar de Universiteit Leiden, omdat Marc Koper daar professor was geworden. In juni 2007 ronde hij zijn promotie af met dit proefschrift als resultaat. Naast het doen van onderzoek houdt Thijs ervan de mooiste plekjes op deze aardbol te bezoeken en daar rond te wandelen. Daarnaast houdt hij van schaken en andere gezelschapsspelen en vindt hij het leuk om te borrelen met vrienden en collega's.



Thijs de Groot was born in Deurne on 12 August 1979 and grew up in Helmond in the south of the Netherlands. In 1997 he started studying Chemical Engineering at the Eindhoven University of Technology. During his studies he did a four-month internship at GE Plastics in Bergen op Zoom, where he synthesized and studied polycarbonate. His fascination with research started when working on his Master's thesis, which was on the electrocatalytic reduction of nitrate on platinum. After he graduated cum laude in 2002, he did a four-month internship in the group of Nenad Markovic and Philip Ross in Berkeley working on electrocatalytic proton reduction on silver. Thijs returned to Eindhoven in 2003 where he became a PhD student under supervision of Marc Koper, studying the electrochemistry of immobilized hemes and heme proteins. As part of this project he worked in the group of Fraser Armstrong in Oxford for three months to gain experience in the field of protein film voltammetry. In 2006 he moved to Leiden together with Marc Koper, where he finished his PhD in June 2007. Apart from scientific research Thijs loves travelling around the globe, playing games and having a beer with friends and colleagues.

Dankwoord

Promoveren is geweldig! Het is heerlijk om vier jaar lang ‘onbezorgd’ aan een onderzoek te werken. Het is een combinatie van ‘klussen’ op het lab, resultaten analyseren, en artikelen of presentaties in elkaar zetten om de rest van de wereld te laten horen wat voor moois je doet. Als je een keer een avondje gedronken hebt, blijf je gewoon lekker in bed liggen. Geen deadlines, geen managers die zeggen wat jij moet doen en nauwelijks vergaderingen, wat een leven! Bovenal zijn er de momenten waarop het gewenste piekje eindelijk op het beeldscherm verschijnt. Wat je dan voelt, is pure extase! Dit alles betekent overigens niet dat je een beetje kunt flierefluiten. Het is namelijk jouw onderzoek en jij moet ervoor zorgen dat er na vier jaar een topresultaat ligt.

Promoveren is een tamelijk individualistische bezigheid, maar toch zijn de mensen om je heen erg belangrijk. Soms dragen ze direct bij aan je onderzoek, maar bovenal zorgen ze voor een goede sfeer. Die sfeer zorgt ervoor dat je lekker in je vel zit en dat is erg belangrijk bij het doen van onderzoek. In dit dankwoord wil ik iedereen bedanken, die voor mijn gevoel direct of indirect heeft bijgedragen aan mijn promotieonderzoek.

Allereerst wil ik de mensen bedanken die een wetenschappelijk steentje hebben bijgedragen aan dit proefschrift. Natuurlijk begin ik met Marc, die niet alleen een leuk project uit de hoge hoed wist te toveren, maar ook een uitstekende begeleider was. Wat me vooral goed is bevallen, is de grote vrijheid die hij me gaf, waardoor ik mijn onderzoek grotendeels zelf richting kon geven. Hierdoor heb ik me tot zelfstandig onderzoeker kunnen ontwikkelen. Als tweede wil ik Maarten bedanken en wel in het bijzonder voor zijn kritische blik op mijn artikelen. Hij wist altijd de vinger op de zwakke plek te leggen. Dit heeft mijn schrijfstijl aanzienlijk verbeterd. Verder wil ik Ad bedanken, die met kunst- en vliegwerk de OLEMS-opstelling aan de praat heeft gekregen en daarmee de weg heeft geplaveid voor mijn eerste JACS-publicatie. Daarnaast wil ik Toon bedanken, zonder wiens cytochrome *c* ik het in mijn ogen mooiste hoofdstuk van dit proefschrift (hoofdstuk 5) nooit had kunnen schrijven. Ook de studenten die mij op het spoor zetten van de heme release hypothese verdienen een bedankje. Tenslotte bedank ik nog Rutger van Santen, zonder wiens financiële steun dit hele onderzoek niet mogelijk zou zijn geweest.

Since I was one of the few persons working in the field of immobilized proteins in the Netherlands, I had to go abroad. I would like to thank Fraser Armstrong and all his group members (especially my cheerful glove box partner Alison) for giving me the opportunity to learn how enzymes are immobilized on graphite electrodes. I would also like to thank Abhik Ghosh for willing to be part of my promotion committee and for his good company at the Gordon Conference in Ventura. Finally, I would like to thank all open-minded scientists in the field who believe in my heme release hypothesis (chapter 3) and all scientists with whom I had interesting discussions.

Nu kom ik bij de mensen die hebben gezorgd voor een goede sfeer. Allereerst begin ik met de groep in Eindhoven. SKA was erg gezellig door zijn borrels, koffiepauzes, promoties en groepsuitjes. Mede dankzij 'Mr. Borrel' Jos, 'onze vrouw' Michèle, 'retourtje Maastricht' Jarno, 'Landhorst' Tiny, 'biertje' Gilbère, 'onze Rus' Evgeny, 'ik ben als een broer voor vrouwen' Barry, 'de skiënde Indiër' Dilip, 'de badkamerklusser' Paul, 'elf Hoegaarden in twee uur' Joost, 'Mr. Hybrid' Erik, 'blote voeten' Gijsbert, 'Cola' Hans, 'de nog niet uitgehuwelijkte Indiër' Neelesh en 'de sympathieke Duitser' Christian. Ook Pieter, Bouke, Frans, Astrid, Peter, Jarl, Arjan, Patrick, Laura, Robert, Cristina, Ton, Emiel, Davy, Daniel, Annelies, Denzil, Bart, Leandra, Katharina, Han, Ramona, Dieter en Hans verdienen vermelding, maar voor hen heb ik niet direct bijnamen voorhanden. De oude garde bestaande uit Ruben, Maria, Nollaig, Niek, Michiel, Mabel, Vincent, Sander, Eric en Chretien vergeet ik natuurlijk niet. Een speciale vermelding verdient Wout, die mijn geesteskind het brandstofcelautootje tot een indrukwekkende bolide maakte. Ook wil ik mijn elektrocollega's bedanken: Gabi en Paul voor de gemakkelijke gesprekken over 'projecten' tijdens de lunch en natuurlijk ook Tom en Victor, waarmee ik bijna drie jaar een kamer heb gedeeld. Verder hebben Afifa, Alexander, Dennis, Frank, Freek, Guillermo, Martin, Martine, Peter N., Peter V. en Van-Ahn allemaal bijgedragen aan de goede sfeer op het lab.

In het laatste jaar van mijn promotie heb ik het warme Eindhoven achter mij gelaten en ben ik noordwaarts getrokken de grote rivieren over. Voor een zuiderling was dat natuurlijk niet gemakkelijk. Ik had toch het beeld dat het noordelijk deel van dit land wordt bevolkt door een ander slag volk. De Romeinen zijn natuurlijk niet voor niets bij de rivieren gestopt. Toch viel het leven boven de rivieren mij honderd procent mee en dat kwam met name door de goede sfeer in de groep. Het was erg gezellig, mede dankzij 'sterf!' Janneke, 'daar wil ik niets over zeggen' Stanley, 'directer dan een Nederlander' Alex, 'werkt wel erg hard' Irene, 'de ene Amerikaan is de andere niet' Otto, 'de Brabanders' Meindert en Ludo, François, Ben en alle andere groepsleden. Ook de pokeravonden waren erg gezellig. Absolute hoogtepunten waren natuurlijk de 'This week's discoveries lunches'. Het concept van gratis lunch bij een praatje is briljant. Frans Saris, bedankt!

Wetenschap bedrijven vereist een frisse geest en daarvoor is ontspanning erg belangrijk. Er is voor mij geen betere plek op deze wereld om te ontspannen dan Weyerbeemd 2 in Helmond. Bij deze wil ik mijn moeder en vader bedanken voor de heerlijke zorg in de weekenden. Zonder het concept "als je studeert, hoef je geen karweitjes te doen" was ik nooit zo ver gekomen. Natuurlijk was de tuin ook erg belangrijk. Het lezen van artikelen is gewoon pure ontspanning, wanneer je het doet onder een stralend zonnetje liggend op een comfortabele tuinstoel.

Naast ontspanning zijn ook creatieve ideeën van het grootste belang in het doen van wetenschappelijk onderzoek. Voor het ontstaan van creatieve ideeën is natuurlijk een inspirerende omgeving nodig. Met alle respect, dat zijn de scheikundegebouwen in Eindhoven en Leiden bepaald niet. Daarom is het belangrijk om af en toe eens wat pittoreskere plekje op te zoeken. Het Sary Chelek meer, Icefields Parkway, Walls of Jeruzalem, Yellowstone, Freycinet, Ordesa, la Caldera de Taburiente, the Grand Canyon

en het noorderlicht waren adembenemend. Daarom verdient moeder aarde een bedankje. Ook bedank ik mijn reisgenoten voor het gezelschap en dan met name Koos, met wie ik schitterende reizen heb gemaakt naar Australië en de Rocky Mountains onder het veelzeggende motto: "We hebben nooit gezegd dat het makkelijk zou worden."

Naast mijn ouders hebben mijn overige familieleden mij ook altijd na aan het hart gelegen. Allereerst mijn broertje Willem, waarmee ik een schitterende broer-broer-band heb. Het feit dat hij sociaal altijd iets verder was dan ik, heeft mij altijd weten te stimuleren. Dan is er de familie Vissers met haar gezellige kerstdiners en buitenhuseetprojecten. Een speciaal bedankje verdient ome Jacques voor zijn mooie speeches, die mij ook hebben geïnspireerd tot het geven van speeches. Ook de familie De Groot mag er wezen. Ik zou ze willen typeren als gezellig (eigen)wijs. Wat ik er nog speciaal even uit wil pakken zijn de mooie trips naar Jan en Susanne in Denemarken.

Ook mijn vrienden vergeet ik natuurlijk niet. Allereerst de echte jeugdvrienden, Thijs, Joris en Martijn, die ik al zo ongeveer vanaf de wieg ken. Daar heb ik zo veel mooie activiteiten mee ondernomen, waaronder een oneindig aantal riskpotjes en een memorabele trip naar Schotland. Dan zijn er mijn studievrienden Arno, Bas, Jaap, Jason en Tim, waarmee ik menig gezelschapspelletje heb gespeeld en vele 'hoogwaardige' discussies heb gevoerd. Het is mooi dat we zelfs vier jaar na ons afstuderen nog zo'n goede band hebben en ik ben er dan ook van overtuigd dat we vrienden voor het leven zijn geworden.

De mensen van de mondharmonicaclub en de schaakclub verdienen ook nog een bedankje. Zoals gezegd is een stukje ontspanning voor een wetenschapper heel belangrijk en daar zorgden deze hobby's doordeweeks altijd goed voor. Maar het mooiste was eigenlijk nog wel dat telkens wanneer ik er een tijdje niet was, ik altijd weer als een verloren zoon werd ontvangen.

Ik wil afsluiten met degene die het laatst mijn leven is binnengestapt en toch al een belangrijke plek heeft veroverd. Eva, wat ik vooral waardeer in onze relatie is dat we zo goed en open met elkaar kunnen praten. Dat je ook nog knap bent is mooi meegenomen. Daarnaast zijn onze dagtochtjes naar allerlei plaatsen mij erg goed bevallen en ik hoop dat we die nog vele zullen maken.

Voor mensen die niet in een van bovenstaande rijtjes staan en dat wel verwacht hadden, jullie kunnen er vanuit gaan dat dit komt doordat mijn geheugen mij in de steek heeft gelaten. Ook voor jullie geldt:

Bedankt!

Thijs